THE UNIVERSITY
of EDINBURGH

THE UNIVERSITY of EDINBURGH

The role of PDGF-B/PDGFRβ signalling in definitive haematopoiesis

Diana Sá da Bandeira

PhD in Regenerative Medicine

The University of Edinburgh

2019

Declaration

I, Diana Sá da Bandeira, declare that this dissertation is the result of my own work, except where explicitly indicated in the text.

The data presented in this thesis has not been submitted for any other degree or professional qualification.

Abstract

The first haematopoietic stem cells (HSCs) are generated in the dorsal aorta (DA) of the midgestation mouse embryo. Signals from the microenvironment are required for HSC generation. However, the signals and identity of cells releasing them *in vivo* remain unknown. In the present work, we identified at least three populations of perivascular cells surrounding the DA based on the expression of the perivascular cell markers NG2, PDGFRβ and αSMA. NG2+ PDGFRβ+ αSMA+ pericytes/vascular smooth muscle cells (PCs/vSMCs) and NG2- PDGFRβ+ αSMA- sub-pericytes (Sub-PCs) were found to be enriched in HSC-supportive genes described in the adult bone marrow (BM). As both populations express PDGFRβ, which has recently been shown to mediate HSC specification in zebrafish, and PDGF-B/PDGFRβ signalling is also required for the recruitment of pericytes to the developing blood vessel wall, we hypothesised that PDGF-B/PDGFRβ signalling is required to generate the first HSCs *in vivo*. To answer this question, we used PDGFRβ knock-out (KO) and PDGF-B^{ret} KO mice, both of which have a defective pericyte recruitment to blood vessels and defective or absent PDGF-B/PDGFRβ signalling. Results from our haematopoietic progenitor assays (CFU-Cs) and transplantations show that the germline deletion of PDGFRβ affects both haematopoietic progenitor numbers and HSC activity in the E11 AGM. HSPCs in other haematopoietic organs are not affected at this stage. PDGF-B^{ret} KO mice showed no defects in midgestation HSPCs, but AGM HSCs failed to reconstitute secondary recipients. Together, these data suggest that PDGF-B/PDGFRβ signalling is required for AGM haematopoiesis. We found that perivascular stromal cells surrounding the DA are not affected by these mutations, nor the integrity of the blood vessel, suggesting that PDGF-B/PDGFRβ signalling is not required for PC/vSMCs recruitment to the DA. We therefore hypothesised that PDGF-B/PDGFRβ signalling is either required in the niche for HSC specification and/or generation, and/or that PDGFRβ+ cells are precursors of HSCs. Tracing experiments using PDGFRβ-Cre;TdTomato mice found that a subset of AGM HSPCs derive from PDGFRβ-Cre precursors and that both Tomato- and Tomato+ E14 foetal liver (FL) and BM cells

reconstitute irradiated recipients. Together these data suggest that adult HSCs have distinct developmental origins, one of them deriving from PDGFRβ+ cells. In conclusion, our results define PDGFRβ signalling as a key component of the HSC generating niche in the mouse embryo, and that a subset of HSCs derive from PDGFRβ+ precursors.

Lay summary

Blood stem cells (HSCs) have a high therapeutic value as they give rise to all the blood cells in the body. They are used to treat leukaemias and other diseases, but their use is limited to the availability of compatible donors. Understanding the mechanisms by which blood stem cells are generated during embryonic development will enable scientists to grow and expand them in a dish, decreasing the need for donors, and making blood stem cell-based therapies available to more patients. In the present work, we looked at the environment in which blood cells are first made in the mouse embryo and found that there are different populations of cells surrounding the dorsal aorta (DA) where HSCs are made, that express genes that were shown to support HSCs in the adult bone marrow. Two of these populations were shown to express a receptor called PDGFRβ. We found that the deletion of this receptor impairs the generation of HSCs in the DA. We also found that HSCs generated in the DA derive from PDGFRβ-expressing precursors and persist into adulthood, but not all HSCs derive from these precursors. In summary, we better characterised the HSC-generating “niche”, which can provide additional information on factors that are required to make HSCs in a dish, and found that there are at least two separate origins of HSCs in the mouse embryo.

Acknowledgements

I would firstly like to thank my supervisor Mihaela Crisan for her amazing teaching and guidance, as well as for giving me the great opportunity to pursue a PhD with her (especially after I said no once…). I have learned and grown so much as a scientist and as a person ever since I joined her group in Rotterdam. It has been overall a wonderful experience. I am particularly thankful to her patience and "positiveness" (I shall never forget her saying: "Don't panicate, life is beautiful!"), even when I hit my lowest motivation. I really appreciate it. I am also very grateful to everyone in the lab, in particular to Zaniah, David and Telma, for always being there during this crazy journey. I will miss working and spending time with all of you. I would also like to thank the most recent additions to the Crisan lab, Madalena Marques and Ana Beatriz Barbosa, who have shown great potential as scientists (and who will do the revisions of the papers when I'm gone) and have brought me a piece of home (Telma also!) to Scotland.

I would also like to thank Bruno Péault, my second supervisor, for his insight during lab and review meetings, as well as everyone in his lab, especially to Mario "Papi", Isaac "Tigre", Bianca "come on guys!" and Joan "sisisisisi" (please read the previous sentence with Mario's voice) for making my days at SCRM and sometimes outside of work so much fun. Thank you also to Ege Özkaya, Graham Anderson, Jonathan Mason and Amelia Hallas-Potts from Pierre's lab for all the good time, coffee and nice dinners. Amelia, thank you so much for building InterSci with me and teaching me so much about leadership. I am proud of what we have achieved in such a short time and that our legacy continues. I would also like to thank everyone in my thesis committee: Mihaela, Bruno, Lesley Forrester, Paul Travers (and Kamil Kranc during my first year of the PhD) for their guidance and insight. Thank you also to the core facilities at SCRM for being always so helpful and patient, in particular to Fiona Rossi, Claire Cryer, Bindy Heer, Bertrand Vernay and Matthieu Vermeren.

Outside of the lab, I would like to thank my best friends from Lisbon (Sara, Ana, Ary and Maggy), and Rotterdam (Tânia, Bianca, Rodrigo and Pablo) for being there during my journey. I was also incredibly lucky with my amazing flatmate Yorgos Berdos, who has made my last year and a half in Edinburgh better than I could have ever imagined. I had the most amazing neighbours anyone could have ever wished for: Hannah Grayson, Alasdair Thomson and Hans Wilke. I don't think any neighbours can beat you in your awesomeness and support (and cake!). I feel blessed for having met all of you, and it gives me great hope for what comes next (although I think you are all unbeatable).

Last but not least, I would like to thank the best parents and sister in the world for their life-long support, for always pushing me to the best of my abilities, and believing in me even when I didn't. None of this could have been possible without you. A big thank you to my whole Sala and Sá da Bandeira families for their support and enthusiasm about what I do, (even when some seemed disappointed that I cannot cure human macular degeneration with murine blood stem cells) and for giving me something to look forward to every time I come home for Christmas.

I have probably missed many people that have participated in my journey one way or the other, but if I had to write down every single name, this section would take over my whole thesis.

Looking forward to the next adventure, and I hope to keep you all close to my heart. Thank you!!!

Publications and presentations related to this work

Publications:

- **Sá da Bandeira D.**, Ventura T., González Z.N., Marques, M., Vink C.S., van de Werken H. J. G., van IJcken W., Downing J.R., Betsholtz C., Cuervo Grajal, H., Crisan M. PDGFRβ signalling is essential for hematopoietic stem cell generation *in vivo*. *In preparation.*
- Gonzalez Z.N., Kilpatrick A.M, **Sá da Bandeira D.**, Ventura T., Bouilleau L., Rossi F., Henderson B.E.P, Henderson N.C., van de Werken H.J.G, van IJcken W., Ash S., Tomlinson S., Downing J.R., Isacke C., Crisan M. Vascular smooth muscle cells are required to generate hematopoietic stem cells in vivo. *In preparation.*
- **Sá da Bandeira D.**, Betsholtz C., Crisan. M. PDGF-B^{ret} mutation affects the self-renewal capacity of aortic HSCs in the mouse embryo. *In preparation.*
- **Sá da Bandeira D***, Casamitjana J*, Crisan M., Pericytes, integral components of adult hematopoietic stem cell niches, Pharmacol Ther. 2017 Mar;171:104-113. doi: 10.1016/j.pharmthera.2016.11.006. Epub 2016 Nov 28. *Contributed equally

Poster presentations at conferences:

- **Diana Sá da Bandeira**, Zaniah González, Telma Ventura, Harmen van de Werken, Wilfred van IJcken, Christer Betsholtz, Mihaela Crisan, PDGFRβ Signaling is Required to Generate Aortic Haematopoietic Cells *in Vivo* – presented at the ISEH meeting 2019, Brisbane, AU.
- **Sá da Bandeira D.**, Ventura T., van de Werken H. J. G., van Ijcken W., Betsholtz C., Crisan M., PDGFRβ Is Required in Perivascular Cells to Generate Aortic Hematopoietic Stem Cells *in Vivo* – presented at the ESM-EVBO meeting 2019, Maastricht, NL.

Contents

List of figures

List of tables

Abbreviations

AGM	Aorta gonad mesonephros
BL6	C57BL/6J
CV	Cardinal vein
DA	Dorsal aorta
DEG	Differentially expressed gene
Ee	Embryo equivalents
EHT	Endothelial to haematopoietic transition
EMP	Erythroid-myeloid progenitor
ESC	Embryonic stem cell
FACS	Fluorescence activated cell sorting
FCS	Foetal calf serum
FL	Foetal liver
FPKM	Fragments Per Kilobase of transcript per Million mapped reads
FSC-A	Forward scatter area
FSC-H	Forward scatter height
HET	Heterozygous
HP	Haematopoietic progenitor
HSC	Haematopoietic stem cell
HSCT	Haematopoietic stem cell transplantation
HSPC	Haematopoietic stem and progenitor cell

IAHC	Intra-aortic haematopoietic cluster
iPSC	Induced pluripotent stem cell
ISH	*In situ* hybridisation
ISV	Intersomitic vessel
KO	Knock-out
LTR-HSC	Long-term reconstituting HSC
NC	Notochord
NT	Neural tube
O/N	Overnight
PB	Peripheral blood
PBS	Phosphate buffered saline
PC	Pericyte
PFA	Paraformaldehyde
PL	Placenta
PS	Penicillin-Streptomycin
P-Sp	Para-aortic splanchnopleura
RT	Room temperature
SSC-A	Side scatter area
Sub-PC	Sub-pericyte
vSMC	Vascular smooth muscle cell

WT	Wild-type
YS	Yolk sac

Chapter 1 General Introduction

1.1 Haematopoietic stem cells

1.1.1 Discovery and definition

In the early 60's, while James Till and Ernst McCulloch were conducting experiments on bone marrow (BM) sensitivity to radiation, they discovered that the transplantation of healthy murine BM cells into lethally irradiated recipients could regenerate the entire haematopoietic system (erythroid, myeloid and lymphoid lineages) [1,2], and rescue the mice from certain death. They found that the BM contained haematopoietic stem cells (HSCs), that were defined by their ability to repopulate all blood lineages upon transplantation into irradiated recipients and self-renew [2]. In more recent years, several studies suggest that HSCs are a more heterogeneous population of cells than initially thought [3–5]. Different subtypes of HSCs have been described with different properties such as lineage differentiation output (myeloid biased or lymphoid biased) [4,6,7], cell cycle status (cycling or quiescent) [8], repopulation kinetics and self-renewal (short-, intermediate- and long-term reconstituting HSCs) [5–7,9]. HSCs can be enriched from a heterogeneous population of haematopoietic cells using different combinations of cell surface markers. However, this is not sufficient to identify functional HSCs. For this reason, transplantations are necessary to prove their presence.

1.1.2 Clinical applications

Because HSCs have the ability to give rise to the entire haematopoietic system upon transplantation and self-renew, they have a high therapeutic value. Haematopoietic stem cell transplantation (HSCT) of either autologous or allogeneic HSCs has been widely used to treat haematological malignancies, such as leukaemia, haemoglobinopathies and congenital blood disorders over the past 60 years [10]. It has so far been the only successful cellular therapy used on a large scale worldwide [11,12]. Transplantable HSCs are either derived from the BM, peripheral blood (PB) or umbilical cord blood of patients or donors. There are, however, issues associated with HSCT, such as infections and graft-versus-host disease that cause high mortality and

morbidity among patients [13]. Another limitation of HSCT is the lack of compatible donor cells.

Generating functional haematopoietic stem and progenitor cells *in vitro*, either from induced pluripotent stem cells (iPSCs) or embryonic stem cells (ESCs), has therefore been a long-term goal of haematologists for the past decades, as it would provide an unlimited source of blood cells for different therapies, drug studies, etc. For instance, HSCs could be used as vectors for gene therapy, as they could be genetically modified and transplanted back into patients. This would allow to not only treat haematological and autoimmune disorders such as sickle cell anaemia or SCID-X1 [14], but also to treat other genetic disorders, such as lysosomal storage disorders [15], providing an inexhaustible source of enzymes throughout the body. Although considerable progress has been made in recent years [16,17], the production of fully functional HSCs *in vitro* has not yet been achieved.

Understanding the mechanisms underlying HSC specification, generation and maintenance *in vivo* can provide additional information required to replicate this process *in vitro*. One way to study these mechanisms is to look at the generation of the first adult-type HSCs during embryonic development in mice, as most of the processes are highly conserved between mouse and human [18].

1.2 Murine haematopoiesis

Although HSCs were first discovered in the adult BM, they are first generated during embryonic development, in the aorta-gonad-mesonephros region (AGM) of mammals that comprises the dorsal aorta, genital ridges and mesonephros.

Murine embryonic haematopoiesis is a complex process that gives rise to different types of blood stem and progenitor cells at different stages and involves several organs, including the yolk sac (YS), placenta (PL), foetal liver (FL), AGM region and head. Haematopoietic cells are generated in three

different waves. The first two waves occur in the YS, while the third, where definitive HSCs are born, first occurs in the AGM region.

1.2.1 Primitive haematopoiesis

It is believed that the first haematopoietic cells derive from a mesodermal precursor called the haemangioblast, that can give rise to both endothelial and haematopoietic lineages [19,20]. Haemangioblasts are thought to emigrate from the primitive streak [21] into the YS, where they become committed to endothelial and haematopoietic fates and contribute to blood island formation [22,23]. Endothelial cells (ECs) within these blood islands give rise to primitive erythrocytes, macrophages and megakaryocyte progenitors from embryonic day 7 (E7) [24–27]. Primitive erythrocytes are nucleated, express embryonic haemoglobins (ε and βH1), and disappear by E9 [24,26]. These primitive erythrocytes are most likely required to provide the growing embryo with oxygen, and the macrophages for phagocytosis during tissue remodelling [28].

1.2.2 Definitive haematopoiesis

1.2.2.1 Second wave of haematopoiesis

Partially overlapping with the first wave of haematopoiesis, a second wave occurs in the YS, giving rise to erythroid-myeloid progenitors (EMPs) at E8.25, right before the onset of circulation [29,30]. This second wave marks the beginning of definitive haematopoiesis, as EMP-derived erythrocytes undergo enucleation and express the adult β-major globin, unlike their primitive counterpart that express embryonic βH1 globin and are nucleated [24]. Once circulation is established, EMPs quickly migrate to other organs. They can be detected in the placenta at E9 [31] and colonise the embryonic liver from E9.5 [24] that becomes a major site for haematopoiesis at E11-E12 [32]. When circulation starts at E8.25, EMP-derived macrophages migrate to other tissues, where they become tissue resident macrophages that persist into adulthood [33]. Some lymphoid progenitors, immune-restricted lympho-myeloid progenitors and mast cells are also generated during the second wave in the YS. These lymphoid progenitors can be detected in the YS and aorta at E8.5 [34–36], while lympho-myeloid progenitors and mast cells are found in the YS

from E9.5 [37,38]. It was also demonstrated that both the E9 YS and the E8.5 para-aortic splanchnopleura (P-Sp) which evolves into the AGM, contain HSCs capable of long-term multilineage reconstitution of newborn mice, but fail to reconstitute adult recipients [34,39]. Haematopoietic progenitors (HPs) generated in the first waves of haematopoiesis also play a role in HSC generation in the AGM through the release of pro-inflammatory signals [40–43].

1.2.2.2 HSC generation

In the third wave of haematopoiesis, starting at E10.5, the first adult-type HSCs are generated in the AGM region of the embryo [44,45]. They are defined by their ability to repopulate the entire blood system of adult irradiated recipients and to self-renew. AGM explant cultures showed that HSCs are autonomously generated in the AGM region [44], more specifically, in the ventral aspect of the dorsal aorta (DA) [46–48] through a process called endothelial to haematopoietic transition (EHT). HPs are found in the whole DA, while HSCs are localised on the ventral aspect, in haematopoietic clusters in close contact with the endothelium [46–48]. HSCs in these clusters express CD34, CD45 and cKit [47,49,50]. Such clusters have also been described in human, chick, zebrafish and amphibian embryos [49–52].

Up until recently, it was believed that the AGM region only produces 1-2 functional HSCs [53,54]. Although this quantification was defined based on limiting dilution experiments, this conclusion relied on the disruption, dissociation and transplantation of AGM cells, which could lead to an underestimation of the real number of HSCs. Two recent studies conducted on the zebrafish zebrabow model [55] as well as in confetti mice [56] used live imaging and multicolour lineage tracing without disrupting the DA to better quantify HSCs generated in the DA. With these models, at least 30 HSC clones were found in zebrafish at the peak of aortic haematopoiesis [55], and between 600 and 700 developmental precursors at E10.5-E11.5 contributed to adult haematopoiesis in the mouse [56]. AGM HSCs express CD45 [47], Ly6A (Sca1) [47,48], cKit, CD34 [32], SCL [57] and GATA2 [58,59], however,

expression of these markers is not exclusive to HSCs, making it impossible to isolate them and detect them without resorting to transplantations.

Following HSC generation in the AGM, HSCs can also be found in the umbilical and vitelline arteries [60], head [61], placenta, YS and FL as well as in circulation [44,45,62,63]. The FL is colonised from late E9 by HPs made in other haematopoietic organs [64,65], and from E11, by HSCs. In the FL HSCs are believed to mature and expand [53,66], before definitively migrating into the foetal BM from E15.5 onwards, where they reside for the whole life-span of the mouse [67]. Several studies have proposed that the PL autonomously generates HSCs, [31,68]. The E8 YS and P-Sp have also been shown to harbour HSC precursors that can maturate into definitive HSCs when co-cultured with AGM stromal cells [69]. As these studies have mainly relied on explant cultures or co-cultures with OP-9 cell lines, it remains unclear whether adult-type HSCs are normally produced by these organs during development *in vivo.* In addition, circulation is established around E8.25 [70], from which point, haematopoietic cells enter circulation, making it difficult to determine whether HSCs found in the YS and PL are generated *in situ*, as they are detected after the generation of HSCs by the AGM [71].

1.2.2.3 Endothelial to haematopoietic transition

The observations that haematopoietic clusters and the aortic endothelium are closely associated, and that HSCs share common markers with ECs such as CD31, CD34, VE-Cadherin, Tie-2 and Flk-1 and are morphologically similar [21,50,72–74], led to the hypothesis of an endothelial origin for HSCs.

Endothelial to haematopoietic transition is the process where specialised ECs called haemogenic endothelial cells (HECs) [75] transdifferentiate into adult-type HSCs [52,76–79]. This process has been well described in the dorsal aorta and is conserved across vertebrates [52,80,81]. More recently, EHT has also been described in the BM of chickens and mice [82], as well as in the midgestation mouse head [61,83]. It is unclear whether it occurs in other organs, although the presence of HECs and budding haematopoietic cells from HECs have also been described in the PL and YS [84].

During aortic EHT, HSCs become part of a cluster of haematopoietic cells, where they maturate through different stages (pro-HSC, pre-HSC type I and pre-HSC type II) [85–87]. Haematopoietic cells in these clusters are heterogeneous [88], and many are thought to come from other haematopoietic organs such as the YS and PL through circulation [40].

Two main transcription factors are required for EHT: Gata2 [58,89–91] and Runx1 [76,79,92,93]. Mice deficient for Gata2 and Runx1 die at E10.5 and E12.5, respectively, with foetal liver anaemia, haemorrhages and the lack of definitive haematopoiesis [93]. Both are required for HSC generation from HECs, but Gata2 expression is also essential for HSC survival [91], while Runx1 appears to only be necessary for EHT [79]. Both factors are expressed in the YS at E8, and from E8.5 to E11.5 they are expressed by some ECs of the aorta, umbilical and vitelline arteries, placenta and head, as well as in HSPCs [47,50,61,68,94,95]. Runx1 expression is also found in some mesenchymal stromal cells in the murine DA [47], but is restricted to the endothelium and HSPCs in zebrafish [96] and chick embryos [97]. These transcription factors were shown to be regulated by signalling pathways such as Notch and Bmp4/TGFβ [97–100].

1.2.2.4 Foetal liver and foetal BM haematopoiesis

At around E9, the FL starts being colonised by circulating HPs (and by HSCs from E11 on) and becomes a major haematopoietic organ between E11-E12, but is not capable of *de novo* generation of HSCs [32]. Co-cultures of AGM-derived HSCs with E14.5 FL non-haematopoietic cells, showed that the FL microenvironment supports HSC expansion and engraftment [66], suggesting that it promotes the maturation and expansion of HSPCs generated in other organs. In addition, there are more HSCs in the FL than the ones produced in the AGM alone [53], but it is likely that they come from the additive production by the AGM, placenta and YS [62] and subsequent expansion in the FL. However, *ex-vivo* experiments have provided evidence that a pre-HSCs population produced from E9.5 to E11.5 in the AGM (undetectable by transplantation assays) can explain the larger number of mature HSCs found

in the E12.5 FL through a quick maturation process [101]. This evidence was recently supported by lineage tracing data and clonogenic analyses using confetti mice that suggest that the FL is more likely a place for HSC maturation rather than expansion [102]. Only a three-fold expansion in HSPCs that contribute to adult peripheral blood was observed in the FL between E11.5 and E15.5 [102]. The foetal thymus and spleen also become colonised by HSCs from E12 onwards, to differentiate into T and B cells, respectively [103]. From E15.5 onward, HSPC numbers sharply decrease in the FL and start migrating to the foetal BM [104,105].

1.2.3 Adult bone marrow haematopoiesis

Following FL haematopoiesis, HSCs migrate to the BM, where they reside and provide a constant pool of blood cells and progenitors throughout adulthood. The main difference between HSCs found in the adult BM and their foetal counterpart is that foetal HSCs are highly proliferative while BM HSCs are mostly quiescent. The BM functions as a “niche” that regulates HSC maintenance, self-renewal and differentiation. The concept of niche was first defined in 1978 by Raymond Schofield, as a specialised microenvironment in a specific anatomical location that regulates stem cell proliferation, quiescence, self-renewal and differentiation [106]. In the BM, HSCs are found in the endosteal surface of trabecular bone, as well as in vascular sinusoids [107]. Both locations act as distinct niches for HSCs within the same organ, and contain distinct cell populations that have been shown or suggested to have a role in HSC homeostasis. Osteoblasts for example, have been implicated in HSC support in the BM [108]. LTR-HSCs have been reported to localise in close proximity to osteoblasts that respond to BMPR1A. An increase in the number of these osteoblasts was shown to correlate with an increase in HSC numbers in the murine BM [108]. Another study found that mouse BM osteoblasts are activated by the parathyroid hormone upregulate Jagged-1 (Notch signalling), which consequently leads to an increase in the number of HSCs in the BM [109]. BM mesenchymal stem/stromal cell (MSC) lines were also shown to support BM HSPCs in culture [110,111], and HSC engraftment potential was increased after co-culture with BM MSCs [112] or when co-

transplanted with BM-derived MSCs [113]. Other types of MSC-like cells are located in perivascular locations in the BM, namely pericytes (PCs), that were shown to support BM haematopoiesis [114–118]. In the human BM sinusoids for example, a population of perivascular cells expressing CD146, when transplanted into immunodeficient mice, was shown to form ossicles containing donor-derived bone and sinusoids, and host-derived ECs and HCs [118]. These data suggest that CD146+ BM cells have the ability to create a haematopoietic cell supportive microenvironment. These cells were also shown to express other pericyte/vascular smooth muscle cell (vSMC) markers such as αSMA, NG2 and PDGFRβ, as well as HSC niche related transcripts, such as *JAG1* (Jagged-1), *CDH2* (N-Cadherin), *CXCL12* (C-X-C motif chemokine 12) and *SCF* (Stem cell factor or Kit ligand) [118] that have been implicated in HSC maintenance in the adult BM [119–121]. CD146+ perivascular cells were also described in the human foetal BM and white adipose tissue, and have the ability to support human cord blood HSCs in co-culture experiments [117]. These cells were shown to have the capacity to engraft primary and secondary recipients, suggesting that they support HSC maintenance and self-renewal [117]. These CD146+ foetal BM and white adipose tissue perivascular cells were also shown to express *NES* (Nestin), *CXCL12* and *LEPR* (Leptin receptor) [117], also described in BM perivascular cells with HSC-niche activity [115,120,122].

Nestin+ perivascular cells with MSC potential and closely associated with adrenergic nerve fibres and HSCs were identified within the murine BM parenchyma [122]. They were shown to highly express HSC maintenance genes such as *Cxcl12*, *Adrb3* (beta-3 adrenergic receptor) and *Angpt1* (Angiopoietin-1). Depletion of Nestin+ cells with diphtheria toxin using Nes-Cre^{ERT2} mice led to a decrease of BM HSC numbers, due to a reduction in HSC homing ability, suggesting a putative role for Nestin+ perivascular cells in HSC trafficking [122]. These Nestin+ cells were further purified into a Nes+CD51+PDGFRα+ subset, that express higher levels of HSC regulatory genes such as Cxcl12, Angpt1 and Scf [123]. They also found that PDGFRα+ CD51+ cells in the human foetal BM correspond to a subset of CD146+ cells

that also express Nestin, and are enriched in HSC niche activity. When cultured as mesenspheres (MSC spheroid cultures), these cells were shown to have the potential to self-renew and transfer the hematopoietic microenvironment in ectopic grafts [123], similar to CD146+ perivascular cells [118]. Nestin-expressing cells that also express CD105 were also described in the human foetal and adult BM and were shown to support HSC maintenance and self-renewal upon transplantation after co-culture with CD34+ human cord blood cells [124]. Additional heterogeneity among Nestin-expressing cells was found in the murine BM. A subset of Nes-GFP+ cells surrounding arterioles was also shown to express NG2, and HSCs located in these vessels were shown to be quiescent [114]. Conditional depletion of NG2+ cells using NG2-creERTM/iDTR mice led to a change in location of HSCs further from the arterioles and a switch to a non-quiescent state [114]. These data suggest that NG2+ Nes-GFP+ cells surrounding arterioles are important for HSC quiescence. This study also showed that there are Nes-GFP+ cells surrounding the sinusoids, but unlike arteriolar Nes-GFP+ cells, GFP expression is much dimmer, and they do not express NG2 [114]. These sinusoidal cells mostly overlap with SCF-expressing LepR+ cells identified by Ding et al. in 2012 [115]. Deletion of *Scf* in LepR+ cells led to a reduction in the number of BM HSCs [115]. In addition, conditional deletion of Cxcl12 from LepR+ cells also led to a reduction of HSPCs in the BM, in parallel to an increase in their frequency in circulation [116], suggesting that LepR+ cells might also be part of an HSC-maintenance niche in the BM.

Overall, different perivascular cell populations, some of which partially overlap, were shown to differentially regulate HSCs in the BM of both mice and humans. In addition, the BM was recently shown to generate HSCs *de novo* from HECs [82].

1.3 The HSC-generating microenvironment

1.3.1 The AGM

In the mouse embryo, the P-Sp mesoderm develops at the beginning of E9 into the AGM region, which is composed of the dorsal aorta, genital ridges and

mesonephros. The AGM was shown to have the potential to expand HSCs in explant cultures [44]. In addition, AGM-derived mesenchymal stromal cell lines were established from midgestation embryos, and several of these lines were shown to support haematopoiesis [125], suggesting that AGM stromal cells are heterogeneous. These data led to the hypothesis that the AGM contains some stromal cells that function as a niche and/or are necessary for proper HSC specification. In addition, like many cell populations in the BM that support haematopoiesis, several AGM stromal clones and cell lines have the ability to differentiate into several mesenchymal lineages, while other haematopoietic tissues cannot [126,127]. The differentiation potential of some of the supportive cell lines was shown, however, to not be correlated with their ability to support HSCs, but rather to their site of origin [126]. Further analyses of the HSC-supportive stromal clones revealed that BMP4 is a regulator of AGM HSCs, which express BMP receptors [128]. BMP4 expression is mainly detected in mesenchymal cells located on the ventral aspect of the DA, many of which are in close proximity to nascent Ly6A-GFP+ cells in E11 intra-aortic haematopoietic clusters (IAHCs) [128]. A similar pattern of BMP4 expression was also observed in humans [129]. Inhibition of the Bmp4 pathway in E11 murine explant cultures was found to impair HSC activity [128]. However, BMP activation might only be required for HSC maintenance after E11. BMP inhibition with Noggin, which is expressed by the ventral mesenchyme and IAHCs at E10.5 was shown to be crucial for HSC maturation in the E10.5 AGM [130]. Another player in the Bmp4 pathway is BMPER, which is expressed on the ventral side of the AGM [131]. It was shown to have agonistic effects on BMP4 at low concentrations and antagonistic effects at high concentrations. BMPER was shown to increase between E9.5 and E10.5 and to be required from E9.5 in the maturation of pro-HSCs [131].

The polarisation of HSC emergence to the ventral aspect of the DA was shown to be due to inhibitory signals from the dorsal aspect of the DA and dorsal tissues, and activating signals from the ventral aspect of the DA and ventral tissues. The gut, located ventrally from the DA was proposed to be a source of Hedgehog proteins that lead to early HSC induction in AGM explant cultures

with surrounding tissues [132]. More recently, a more complex interplay of signalling pathways from three different compartments of the AGM (ventral aspect, dorsal aspect and urogenital ridges) was proposed to be required for HSC generation [130]. Explant cultures of only the ventral part of the aorta at E10.5 produce less HSCs than explants containing both the ventral and dorsal parts. This increase in definitive HSCs was shown to be mediated by Sonic Hedgehog (*Shh*) which is secreted dorsally [130]. SCF was also shown to be a positive regulator for HSCs, and is produced by the ventral mesenchyme as well as the urogenital ridges, lateral to the DA [130]. Notch expression was also found in ECs and HCs of the chick and mouse aortas, and the downregulation of Notch ligands was shown to be required for the onset of Runx1 expression and initiation of aortic haematopoiesis [97]. Like in the adult BM [133], the sympathetic nervous system (SNS) was found to play a role in AGM haematopoiesis. *Gata3*, a transcription factor highly expressed in the AGM at the time of HSC generation, was shown to be crucial for the production of catecholamines by the SNS which in turn are required for HSC generation [134].

In conclusion, a complex spatiotemporal interplay between different embryonic regions, cell types and signalling pathways is required for HSC generation in the AGM.

1.3.2 Dorsal aorta formation

At E8, a pair of dorsal aortae starts developing. They fuse together from E9.5 onwards from the anterior to the posterior part of the embryo [135]. Aortic endothelial cells have two separate origins. The roof and sides of the DA derive from the somites (paraxial mesoderm), while the aortic floor derives from the splanchnopleura (lateral plate mesoderm) [136]. In the chick embryo, endothelial cells in the aortic floor are replaced by paraxial mesoderm following HSC generation. This replacement has been proposed to explain the transient nature of HSC generation in the AGM [136–138]. However, lineage tracing data suggest that this replacement does not occur on ventral ECs in the murine DA, as they still express the lateral plate mesoderm reporter Hoxb6-cre [139].

As the DA develops, the aortic endothelium is surrounded by several layers of mesenchymal stem/stromal cells. At E10.5, a layer of PCs or vSMCs expressing αSMA and NG2 is found in close contact to the endothelium [140,141]. Similar to DA endothelial cells, stromal cells and vSMCs on the lateral and dorsal aspects of the DA derive from the somites, while the ones on the aortic floor derive from the lateral plate mesoderm [139]. Interestingly, stromal cells of the aortic floor were shown to be replaced by paraxial mesoderm-derived cells at E11.5 [139]. Experiments impairing the migration of the splanchnopleual mesoderm to the ventral aspect of the DA in the chick embryo found that this tissue is required for the onset of Runx1 expression and subsequent formation of IAHCs [97]. These data support the idea that signals from the subaortic mesenchyme are required for HSC emergence.

1.4 PDGF-B/PDGFRβ signalling

Platelet-derived growth factors (PDGFs) are growth factors that control cell growth and proliferation through the binding to the tyrosine kinase receptors PDGFRα and PDGFRβ. Binding of PDGFs to these receptors leads to their dimerization and initiation of their downstream signalling cascades. PDGFs are secreted by platelets, ECs, monocytes/macrophages, SMCs, fibroblasts, placenta cytotrophoblasts, neurons, and some glial cells [142,143]. In addition, they have been shown to affect the *in vitro* growth, migration and function of MSCs. They modulate cell functions such as the production of extracellular matrix components [144,145], and contraction [146,147]. Not much is known about the role of PDGF-B/PDGFRβ signalling in haematopoiesis, but a few recent studies have shed some light on its role during haematopoietic development in different species.

For instance, in zebrafish, it was shown that trunk neural crest cells need to associate with the DA in order to initiate aortic haematopoiesis [148]. Morpholino knock down of *pdgfra* and *pdgfrb* halted neural crest cell migration to the ventrolateral sides of the DA. Consequently, the haematopoietic programme failed to initiate in the DA of these morphants, seen by the absence of *runx1* and *cmyb* expression [148]. *Pdgfrb* was also found to be a

downstream target of Hif1α [149], which was shown to be required for HSC development in zebrafish [150,151]. Lim et al., also found that morpholino knock down as well as dominant negative *pdgfrb* expression led to the reduction in HSPC formation in the DA, and *pdgfb* overexpression led to their increase [149].

In Drosophila, a different role for PDGF/VEGF receptor (a homolog of vertebrate PDGFRs) was described. Deletion of PDGF/VEGF was found to lead to the apoptosis of haemocytes (cells of the immune system of invertebrates), followed by their phagocytosis by other blood cells [152].

In the mouse, E9 YS and embryoid bodies were found to contain haemangioblasts expressing PDGFRβ, CD31, Flk1 and CD41 [153]. Constitutive activation of PDGFRβ or ubiquitous expression of PDGF-B in recombinant mouse models was shown to promote a decrease in CD41+ expressing cells in E9.5 YS, and an increase in vascular remodelling [153], suggesting that in the YS, PDGF-B/PDGFRβ signalling acts as an “on” switch for endothelial cell development, and an “off” switch for haematopoietic cell development. However, it remains unknown whether the deletion or downregulation of PDGF-B or PDGFRβ would lead to an increase in YS haematopoiesis. PDGFRβ expression was also observed in placenta trophoblasts, which communicate with placental ECs via PDGF-B/PDGFRβ signalling [154]. The deletion of PDGFRβ, or PDGF-B, was shown to lead to the premature differentiation of erythroblasts into mature erythroid cells [154], suggesting that PDGFRβ signalling plays a role in the maintenance of erythroblasts in a more undifferentiated state.

In the AGM, PDGFRβ was recently found to be expressed in a few cell layers underneath the endothelium of the E10.5 DA [155], and is upregulated in some HSC-supportive embryonic stromal cell lines [156]. However, whether it plays a role in murine haematopoiesis is still unknown.

To study murine PDGF-B/PDGFRβ signalling *in vivo*, several mouse models have been made, namely PDGFRβ KO mice and PDGF-B^{ret} KO mice

[157,158], which were used in this study. PDGFRβ KO embryos have a normal development until around E16, after which they show severe defects in the kidney due to the absence of mesangial cells, they are thrombocytopenic and anaemic, and have severe haemorrhages. These embryos die around birth, possibly caused by oxygenation defects due to the haematological disorders and haemorrhaging [157]. PDGF-B^{ret} KO mice have a mutation in the PDGF-B retention motif, which is required for the binding of PDGF-B to the extracellular matrix surrounding ECs and forming a PDGF-B gradient necessary for pericyte and vSMC recruitment to the blood vessel wall. Deletion of this retention motif leads to a disruption of this gradient, and pericytes/vSMCs are defectively recruited to the endothelium [158,159]. Unlike PDGFRβ KO mice, PDGF-B^{ret} mice mice survive into adulthood, but are slightly growth retarded, and have reduced female fertility. PDGF-B^{ret} embryos also show defects in kidney glomeruli and proteinuria, but milder compared to PDGFRβ KO embryos [158]. In addition, they also have a progressive and severe deterioration of the retina during adulthood [158].

1.5 Summary

The first adult-type HSCs are generated in the dorsal aorta of the mid-gestation mouse embryo. Stromal cells surrounding the DA play a role in HSC specification and/or generation. However, the identity of these cells and the signals involved remain poorly understood. The present work aims to address this by better characterising the stromal cells surrounding the DA at the time of HSC generation, and the signals required for HSC generation.

Chapter 2 Materials and methods

2.1 Mice

Mice were bred and housed at the MRC Centre for Regenerative Medicine, Edinburgh, UK. PDGFRβ KO mice [157] were maintained heterozygous (PDGFRβ$^{+/-}$) in a C57BL/6J background; PDGF-B^{ret} mice [158] were maintained either as heterozygous (PDGF-B$^{ret/+}$) or homozygous (PDGF-B$^{ret/ret}$) in a C57BL/6J background; PDGFRβ-Cre (Tg(Pdgfrb-cre)1Rha) [160], TdTomato mice (JAX stock #007914) [161], Runx1-IRES-GFP mice (Runx1^{tm4Dow}) [162] and mTmG mice (JAX stock #007576) [163] were maintained homozygous in a C57BL/6J background. The day of vaginal plug detection is designated as E0.5. All experiments were performed under a Project Licence granted by the Home Office (UK), approved by the University of Edinburgh Ethical Review Committee, and conducted in accordance to local guidelines.

PDGFRβ KO mice [157] were generated by electroporation of a targeting vector into mouse ES cells and subsequent injection of positively selected ES cells into blastocysts. The targeting vector contained a neomycin phosphotransferase expression cassette (striped box, Figure 1A) inserted between the SmaI and EcoRV restriction sites, replacing a 1.8kb sequence of the *pdgfrb* locus by homologous recombination (Figure *1*A). PDGFRβ KO mice die at birth or slightly before, and embryos are haemorrhagic, thrombocytopenic, anaemic and lack mesangial cells in the kidneys leading to defective kidney glomeruli (glomerulosclerosis) [157].

PDGF-B^{ret} KO mice [158] were generated by targeting a loxP-flanked PGK-neomycin cassette into intron 5, and a premature translation stop codon with a *Hind*III restriction site into exon 6 of the *pdgfb* gene in mouse ES cells (Figure 1B). Heterozygous mice were produced and crossed with protamine-Cre mice in order to delete the PGK-neomycin cassette and generate the pdgf-b^{ret} allele. In PDGF-B^{ret} KO mice, PDGF-B lacks the C-terminal retention motif that allows its binding to heparan sulphate proteoglycans located in the extracellular

matrix surrounding ECs. Recombinant PDGF-B lacking the C-terminal retention motif is still functional [164]. KO mice survive into adulthood, but exhibit a severe deterioration of the retina, glomerulosclerosis, and proteinuria. vSMCs and pericytes have an abnormal organisation, where they partially detach from the endothelium due to the lack of a PDGF-B gradient around the endothelium required for their normal recruitment [158].

Runx1-IRES-GFP mice [162] were generated by knocking in *Runx1* cDNA in frame into exon 4 of the endogenous Runx1 allele (from exon 4), followed by an IRES-GFP sequence and polyadenylation cassette into E14 mouse ES cells. This led to the creation of an artificial exon 4 containing the full 3' coding region of the gene (Figure 1C). Successfully targeted ES cell clones were injected into C57BL6 blastocysts. As the new allele is under the endogenous *Runx1* promoter, *Runx1* expression level remains physiological, overcoming any potential issues in haematopoietic cells, which are sensitive to *Runx1* dosage [165,166]. In addition, the IRES-GFP sequence allows for normal biological activity of RUNX1. Unfortunately, GFP expression was only detectable by flow cytometry, but not by eye under a fluorescence microscope, nor by immunohistochemistry. Several immunostaining protocols with and without anti-GFP staining were tested, but no GFP was ever detected (not shown).

PDGFRβ-Cre mice were generated by pronuclear injection of fertilised 129/C57BL6 oocytes with a vector containing a fragment of the *Pdgfrb* promoter fused to a Cre recombinase followed by an SV40 polyadenylation signal. No additional information regarding the construct was reported on this mouse model. This mouse has been used in the study of pericytes and vSMCs, as PDGFRβ-Cre is exclusively expressed in these cell types in adult mice [160,167–170].

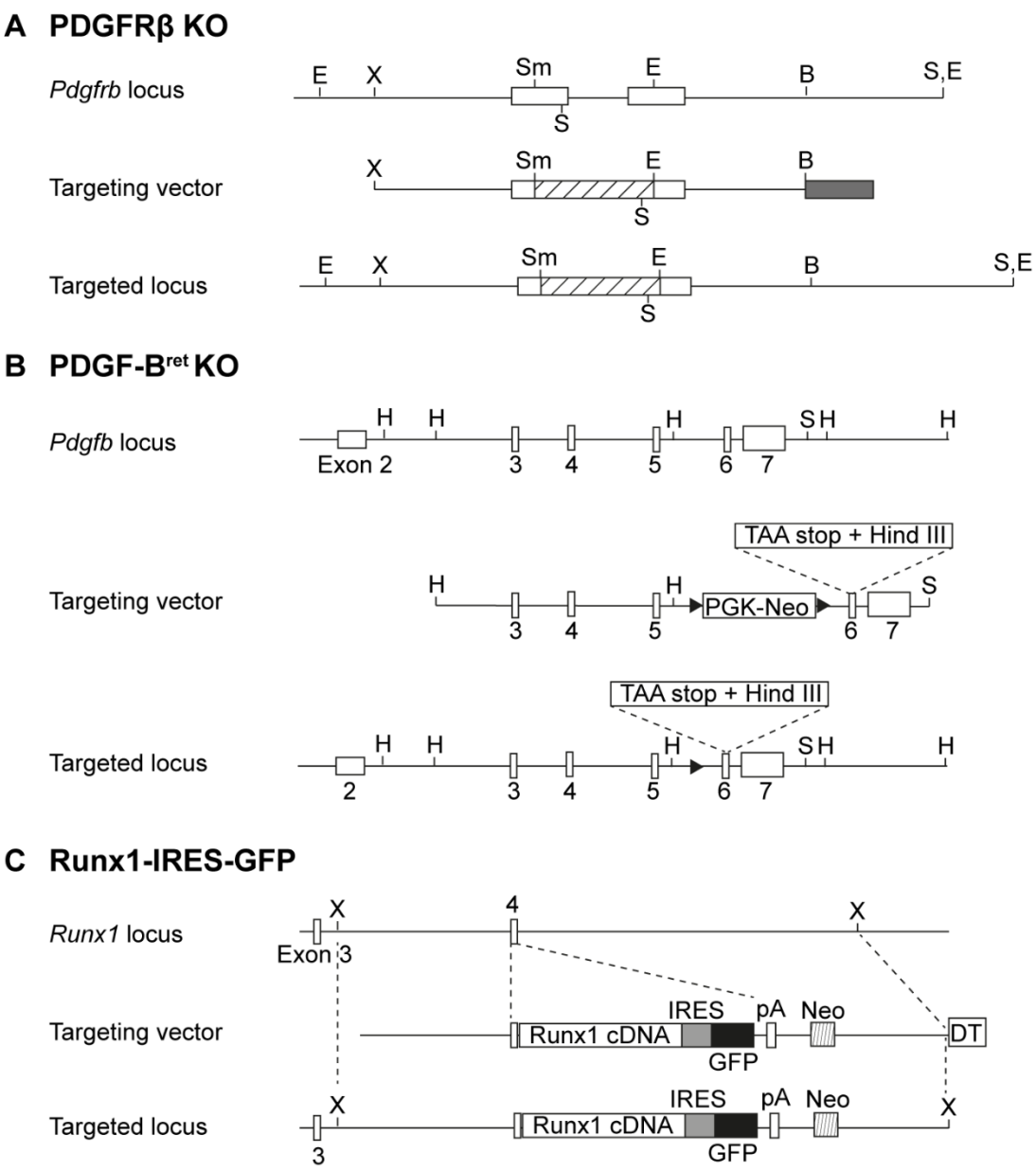

Figure 1. Generation of PDGFRβ KO, PDGF-B^{ret} KO and Runx1-IRES-GFP mice

Representative scheme of the restriction maps of the loci (original and targeted) of the PDGFRβ KO, PDGF-B^{ret} KO and Runx1-IRES-GFP transgenic mouse strains used in this study, and their respective targeting vectors. This figure was based on maps provided in the original publications. Some exons are represented as white solid boxes. Restriction enzyme abbreviations: (E) *Eco*RV, (X) *Xba*I, (Sm) *Sma*I, (S) *Sac*I. (A) Generation of the PDGFRβ KO allele. Striped box: PGKneobpA expression cassette. (B) *Bgl*II. (B) Generation of the PDGF-B^{ret} KO allele. Arrowheads: loxP sites (C) Generation of the Runx1-IRES-GFP allele.

2.2 Genotyping

2.2.1 DNA extraction

Ear clips or small pieces of embryonic tissue (YS or body wall) were placed in a solution containing 100µl of Extraction Solution (Sigma, E7526) and 25µl of Tissue Preparation Solution (Sigma, T3073). Samples were incubated in a shaker at 55ºC for 10min, and DNA denatured for 3min at 95ºC. After denaturation, 100µl of Neutralization Solution B (Sigma, N3910) was added to each sample.

2.2.2 Polymerase chain reaction (PCR) and electrophoresis

Different PCR reactions were performed for each mouse line as described below. PCR products were run at 115V for 1h30 on a 1.5% agarose gel in 1xTAE buffer (Invitrogen; 15558-026). A molecular weight ladder (EasyLadder I; BIO-33046) was added together with the PCR products to determine amplicon sizes. From bottom to top, the bands weigh 100, 250, 500, 1000 and 2000bp.

2.2.2.1 PDGFRβ KO

Following DNA extraction, PDGFRβ KO tissues were genotyped to detect both the *wt* and *ko* sequences, using the primers, PCR reagents and programme described below (Table 1-Table *3*). WT (114bp) and KO (320bp) bands were detected, as shown in Figure 2.

Table 1. Primers

Primer	Sequence	Amplicon size
Fw	ACA ATT CCG TGC CGA GTG ACA G	WT: 114bp KO:320bp
Pdgfrb$^{+/+}$ Rv	AAA AGT ACC AGT GAA ACC TCG CTG	
Pdgfrb$^{-/-}$ Rv	ATC AGC CTC GAC TGT GCC TTC TAG	

Table 2. **PCR reaction mix**
(Qiagen, 203605)

Volume/sample	Reagent
2 µl	10x Coral Load Buffer
1 µl	$MgCl_2$
0.3 µl	HotStarTaqPlus DNA polymerase
0.1 µl	Each primer
0.5 µl	dNTPs (10mM)
13.9 µl	dH_2O
2 µl	DNA

Table 3. PCR programme

Number of cycles	Duration	Temperature
1	5min	95 °C
35	1min	95 °C
	1min	58 °C
	1min	72 °C
1	10min	72 °C
1	+∞	10 °C

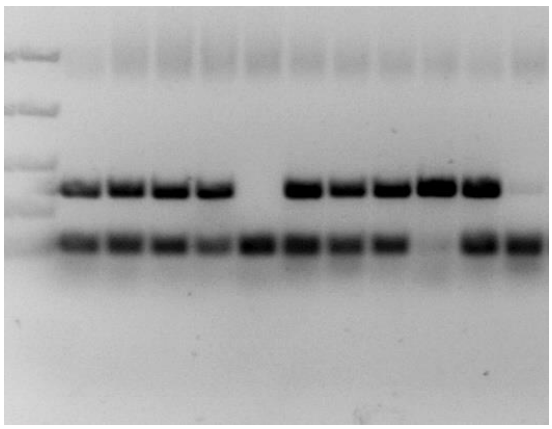

Figure 2. PDGFRβ KO genotyping example.
The upper band represents the *ko* allele (320bp), while the lower band represents the *wt* allele (114bp).

2.2.2.2 Runx1-IRES-GFP

Following DNA extraction, Runx1-IRES-GFP tissues were genotyped using the primers, PCR reagents and programme described below (Table 4). Separate PCRs had to be done to detect the *wt* and *gfp* sequences, as shown in Figure 3.

Table 4. Primers

Primer	Sequence	Amplicon size
Runx1 WT Fw	CACCTGTCTCTGCATCGCAGGACT	WT: 400bp
Runx1 WT Rv	CCATCCGTGACAGATACGCACCTC	
Runx1-GFP Fw	GTC CAG GAG CGC ACC ATC TTC TTC	GFP: 424bp
Runx1-GFP Rv	GTA CAG CTC GTC CAT GCC GAG AGT	

Table 5. PCR reaction mix

Volume/sample	Reagent
10 µl	REDExtract-N-Amp PCR Reaction Mix (Sigma, R4775)
1 µl	Each primer
4 µl	dH_2O
4 µl	DNA

Table 6. PCR programme

Number of cycles	Duration	Temperature
1	3min	94 °C
30	30 sec	94 °C
	45 sec	60 °C
	1min	72 °C
1	10min	72 °C
1	+∞	4 °C

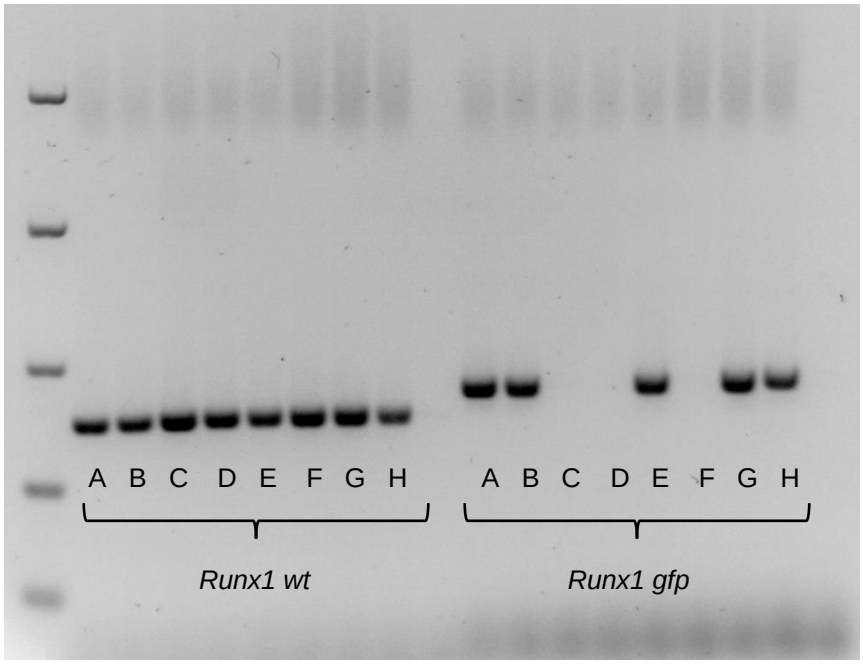

Figure 3. Runx1-IRES-GFP genotyping example.
Samples (A-H) were run separately to detect the presence of the *wt* (400bp) and the *gfp* alleles (424bp).

2.2.2.3 PDGFRβ-Cre

Following DNA extraction, PDGFRβ-Cre tissues were genotyped to detect the *cre* sequence (Figure 4) using the primers, PCR reagents and programme described below (Table 7-Table *9*).

Table 7. Primers used to genotype PDGFRβ-Cre tissues

Primer	Sequence	Amplicon size
PDGFRβ-Cre Fw	TGC CAC GAC CAA GTG ACA GCA	Cre: 324bp
PDGFRβ-Cre Rv	AGA GAC GGA AAT CCA TCG CTC	

Table 8. PCR mix used to genotype PDGFRβ-Cre tissues

Volume/sample	Reagent
5 µl	5x Q Solution
2.5 µl	10x Coral Load Buffer

0.5 µl	dNTPs (10mM)
0.4 µl	Each primer
0.2 µl	Taq DNA Polymerase
14.5 µl	dH_2O
1.5 µl	DNA

Table 9. PCR programme used to genotype PDGFRβ-Cre tissues

Number of cycles	Duration	Temperature
1	5min	94 °C
29	30 sec	94 °C
	45 sec	57 °C
	2min	72 °C
1	10min	72 °C
1	+∞	12 °C

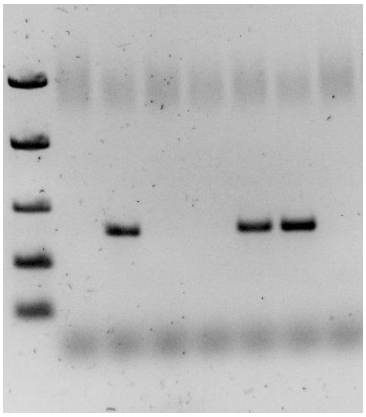

Figure 4. PDGFRβ-Cre genotyping example.
The presence of a 324bp band corresponds to the presence of *Cre*.

2.2.2.4 TdTomato

Following DNA extraction, TdTomato tissues were genotyped to detect both the *R26* and *tdtomato* sequences (Figure 5) using the primers, PCR reagents and programme described below (Table 10-Table *12*).

Table 10. Primers used to genotype R26;TdTomato tissues

Primer	Sequence	Amplicon size
R26 Fw	AAG GGA GCT GCA GTG GAG TA	R26: 297bp
R26 Rv	CCG AAA ATC TGT GGG AAG TC	
TdTomato Fw	CTG TTC CTG TAC GGC ATG G	TdTom: 196bp
TdTomato Rv	GGC ATT AAA GCA GCG TAT CC	

Table 11. PCR mix used to genotype R26;TdTomato tissues

Volume/sample	Reagent
10 µl	REDExtract-N-Amp PCR Reaction Mix (Sigma, R4775)
1 µl	Each primer
4 µl	dH_2O
4 µl	DNA

Table 12. PCR programme used to genotype R26;TdTomato tissues

Number of cycles	Duration	Temperature
1	3min	95 °C
45	30 sec	95 °C
	30 sec	60 °C
	1min 30sec	72 °C
1	10min	72 °C
1	+∞	4 °C

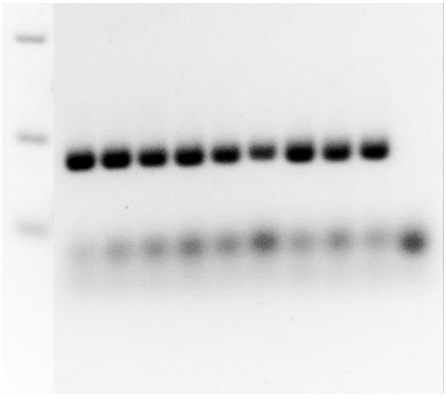

Figure 5. R26;TdTomato genotyping example.
The presence of a 196bp band corresponds to the presence of the *tdtomato* allele, and the absence of the *wt* band (297bp) suggests that these samples come from R26;TdTomato^{+} homozygous mice. Note: Other bands corresponding to a different genotyping were removed from between the DNA ladder and the R26;TdTomato samples in this figure.

2.2.2.5 mTmG

Following DNA extraction, R26;mTmG tissues were genotyped to detect both the *R26* and *mTmG* sequences (Figure 6) using the primers, PCR reagents and programme described below (Table 13-Table *15*).

Table 13. Primers used to genotype R26;mTmG tissues

Primer	Sequence	Amplicon size
R26 Fw	CTCTGCTGCCTCCTGGCTTCT	R26: 330bp mTmG: 250bp
R26 wt Rv	CGAGGCGGATCACAAGCAATA	
mTmG Rv	TCAATGGGCGGGGGTCGTT	

Table 14. PCR mix used to genotype R26;mTmG tissues

Volume/sample	Reagent
10 µl	REDExtract-N-Amp PCR Reaction Mix (Sigma, R4775)
1 µl	Each primer
4 µl	dH_2O
4 µl	DNA

Table 15. PCR programme used to genotype R26;mTmG tissues

Number of cycles	Duration	Temperature
1	3min	94 °C
35	30 sec	94 °C
	1min	61 °C
	1min	72 °C
1	5min	72 °C
1	+∞	10 °C

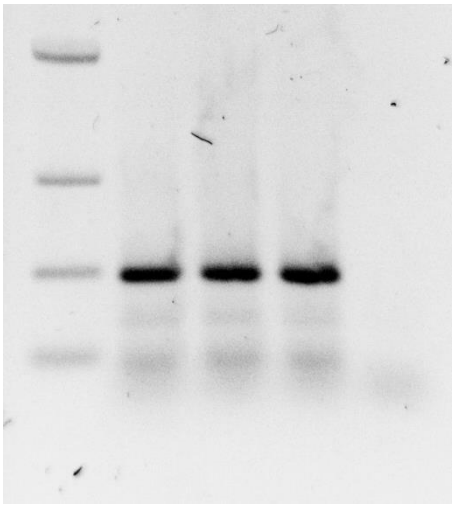

Figure 6. R26;mTmG genotyping example.
The presence of a 250bp band corresponds to the presence of the *mTmG* allele, and the absence of the *wt* band (330bp) suggests that these samples come from R26;mTmG homozygous mice.

2.2.2.6 PDGF-B^{ret}

Following DNA extraction, PDGF-B^{ret} tissues were genotyped to detect both the *wt pdgfb* and *pdgfb^{ret}* sequences using the primers, PCR reagents and programme described below (Table 16-Table *18*). Separate PCRs had to be done to detect the *wt* and *pdgfb^{ret}* sequences, as shown in Figure 7.

Table 16. Primers

Primer	Sequence	Amplicon size
Pdgfb WT Fw	CATGCTGCCTTGTAATCCGTT C	WT: 340bp
Pdgfb WT Rv	CGGCGGATTCTCACCGT	
Pdgfb Ret Fw	CTCGGGTGACCATTCGGTAA	RET:212bp
Pdgfb Ret Rv	TCTAAGTCACAGCCAGGGAGTAGC	

Table 17. PCR mix

Volume/sample	Reagent
10 µl	REDExtract-N-Amp PCR Reaction Mix (Sigma, R4775)
1 µl	Each primer
4 µl	dH_2O
4 µl	DNA

Table 18. PCR programme

Number of cycles	Duration	Temperature
1	5min	94 ºC
35	30sec	94 ºC
	40sec	63 ºC
	1min	72 ºC
1	4min	72 ºC
1	+∞	10 ºC

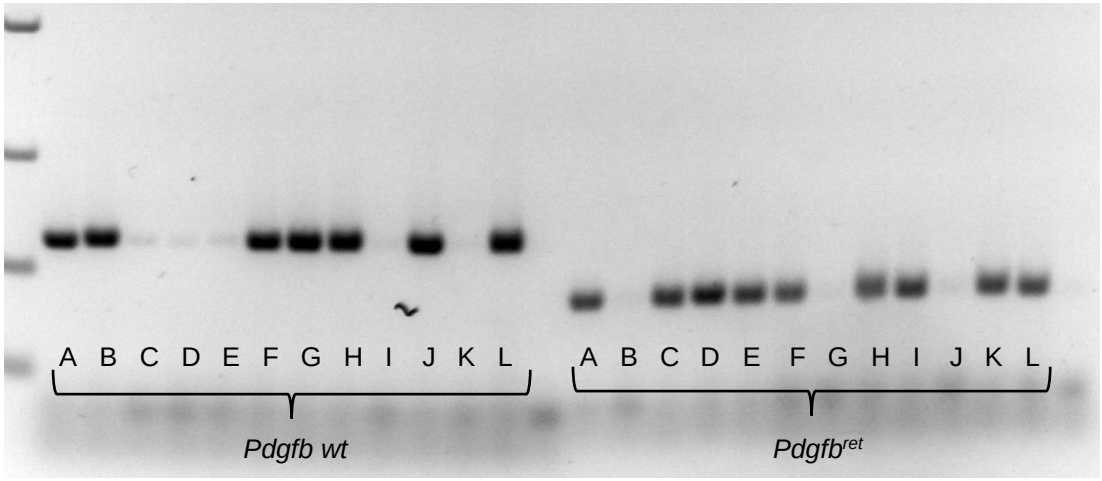

Figure 7. PDGF-B^{ret} genotyping example.
Samples (A-L) were run separately to detect the presence of the *wt* (340bp) and the *pdgfb^{ret}* alleles (212bp).

2.3 Immunohistochemistry

2.3.1 Fixation and freezing

Embryos were dissected, somites counted, and a piece of tissue was taken for genotyping. Embryos with their respective placenta and yolk sac were next fixed in 2% paraformaldehyde (PFA) for 20-30min on ice, and washed three times for 10min with PBS. They were next dehydrated in 20% sucrose/PBS and incubated overnight (O/N) at 4^{o}C. On the following day, embryos were embedded in OCT, frozen in 100% ethanol cold vapours in dry ice, and stored in -20^{o}C until used. Sections 7-10µm thick were cut using a Bright OTF5000 cryostat and caught onto SuperFrost Ultra Plus slides (Thermo Scientific; 631-0099).

2.3.2 Post-fixation and blocking

On the first day of immunohistochemistry, slides were post-fixed with 100% cold methanol for 5-7min at RT and washed three times 5min with PBS.

2.3.2.1 Avidin/biotin blocking

Sections to be stained with biotinylated antibodies were blocked with a biotin/avidin blocking kit (ThermoFisher Scientific; 004303). Sections were incubated with an avidin solution for 15min at RT, washed with PBS for 5min,

incubated with a biotin solution for 15 at RT, and washed three times 5min with PBS.

2.3.2.2 Protein block

All sections were next blocked with 5% goat serum in PBS for 1h or a ready-to-use protein blocking solution (Spring Bioscience; DPB-125) in a humidified container.

2.3.3 Antibody staining

Immediately after blocking, sections were incubated with a primary antibody (Table 19) O/N at 4^{o}C. On the second day, slides were washed three times with PBS and a secondary antibody (Table 20) was added for 1h at room temperature (RT) in a dark, humidified chamber. Slides were next washed three times for 5min with PBS, and a directly conjugated second primary antibody was added for 2h at RT. This antibody was either directly conjugated with a fluorochrome or biotinylated (Table 19). Slides were washed again three times for 5min in PBS and the sections stained with a biotinylated antibody were incubated with streptavidin (FITC or Cy3) (Table 20) for 30min at RT. Slides were washed again three times for 5min in PBS, and sections stained with DAPI (1:500; Thermofisher Scientific, D1306) for 15min at RT in a dark, humidified chamber. Slides were washed again three times 5min in PBS and mounted using Fluoromount-G (Southern Biotech, 0100-01). Stained sections were imaged using an inverted widefield fluorescence microscope (Zeiss Observer) or a Leica SP8 confocal microscope, and pictures analysed with Fiji/ImageJ software.

In certain cases, the second primary antibody used was also unconjugated, but raised in different species than the first primary antibody. In these cases, the incubation times were the same as for the first primary unconjugated antibodies.

Table 19. Primary antibodies used in immunohistochemistry staining.

Antibody	Species raised	Reactivity	Clone	Supplier	Catalogue Number	Dilution

NG2	Rabbit	Cross-species	-	Millipore	ab5320	1:100
NG2	Rat	Mouse	546930	R&D Systems	MAB6689	1:100
PDGFRβ	Rabbit	Mouse	28E1	Cell Signaling	3169S	1:250
Collagen IV	Rabbit	Mouse	-	Bioconnect	2150-1470	1:150
CD146 488	Rat	Mouse	ME-9F1	Biolegend	134707	1:100
αSMA FITC	Mouse	Mouse	1A4	Sigma	F3777	1:100
αSMA Cy3	Mouse	Mouse	1A4	Sigma	C6198	1:100
CD31 biotinylated	Rat	Mouse	MEC13-3	BD Pharmingen	553371	1:50

Table 20. Secondary antibodies used in immunohistochemistry staining.

Antibody	Species raised	Reactivity	Supplier	Catalogue Number	Dilution
AF594	Goat	Rat	Invitrogen	A-11007	1:500
AF594	Goat	Rabbit	Life Technologies	A11012	1:500
AF488	Goat	Rabbit	Invitrogen	A11008	1:500
Streptavidin-Cy3	-	-	Sigma	S6402-1ml	1:250

2.3.4 Imaging

All fluorescent imaging with the exception of PDGFRβ-Cre;mTmG sections was performed using an inverted wide field microscope (Axio Observer, Zeiss). Pictures were acquired with the Zen Pro blue edition (v2.3) software. PDGFRβ-Cre;mTmG sections were imaged using a confocal microscope (Leica TCS SP8 5 detectors and 3 detectors) and pictures were acquired using the Leica LasX software. All pictures were deconvoluted using Huygens Professional (version 19.04) deconvolution wizard, and tiled images (taken with a 63x oil objective) were further stitched either simultaneously with Huygens deconvolution, or after deconvolution, with FIJI/ImageJ software.

Maximum intensity projections were made from 1-10 z-stacks using FIJI/ImageJ. All immunohistochemistry and whole-mount pictures are oriented with the dorsal aspect of the DA at the top, unless stated otherwise.

2.4 RNA sequencing and analysis

All RNA sequencing and analyses used in this thesis were done by our collaborators Wilfred van IJcken (Center for Biomics, Department of Cell Biology, Erasmus MC University Medical Center, Rotterdam, The Netherlands) and Harmen van de Werken (Erasmus Medical Center, Cancer Computational Biology Center and Department of Urology, Rotterdam, The Netherlands).

2.4.1 Sequencing

Cells were sorted and collected directly into 20µl of lysis buffer containing Nuclease-free water (Ambion AM9930) 0.2% Triton and 1/20 RNAse inhibitor (Thermo Scientific; 10777019). Full-length cDNA was generated from 3.4 ul of this cell lysate using the Smarter2 procedure as described (Picelli et al. 2013). Sequencing libraries were generated from 500pg of cDNA with Illumina's Nextera XT sample prep kit (Illumina Inc., U.S.A) and sequenced for single-read 43bp on Illumina HiSeq2000 using the Truseq v3 sequencing chemistry (Illumina Inc., U.S.A). Reads were aligned against the mouse reference genome (mm10) with tophat2 version 2.0.10 [171]. Gene expression values were called using Cufflinks (version 2.1.1).

2.4.2 Analysis

Raw reads were counted with the summarizeOverlaps function with the GENCODE M19 gene annotation [172] using the union mode from the Bioconductor [173] Genomic Alignments package (v1.18.1). Genes were called differentially expressed after regularized-logarithm transformation using DESeq2 (v1.22.2) [174] and setting an absolute fold change of 2. Mean centered values were clustered hierarchically with complete linkage using Euclidean distances and plotted in a heat map with pheatmap package (v1.0.12). Gene Ontology (GO) and Kyoto Encyclopedia of Genes and

Genomes (KEGG) gene enrichment analyses were carried out as described previously [175] and Reactome Pathway Database analyses were carried out with the ReactomePA package (v 1.26.0) [176]. We used R(v 3.5.3) [177] for statistical analysis and visualization of the data.

2.5 Haematopoietic progenitor assays

E10 and 11 AGM, PL, head, YS and FL were dissected, dissociated with collagenase type I (Sigma, C0130, 0.12% v/v) in PBS (Table 21 and*Table 22*). E10 FL were not taken, as they are too small to dissect, and E11 FL were manually dissociated. After digestion, cells were plated as described in Table 21 and Table 22, in a methylcellulose medium (Methocult GF M3434, Stem Cell Technologies Inc.) supplemented with 1%PS, in 35mm petri dishes (Falcon 1008). Cells were next incubated at 37^{o}C in an incubator with 5% CO2, inside a humidified glass chamber. After 10-12 days, colony-forming units cells (CFU-Cs) were counted and distinguished based on their morphology. The number of colonies counted was then re-calculated for the total tissue, and the Gaussian distribution assessed using the Shapiro-Wilk test. Based on the data distribution, a 1-way ANOVA (parametric) followed by a Tukey's post hoc test, or a Kruskal-Wallis (non-parametric) followed by a Dunn's post hoc test were used.

Table 21. Summary of E10 haematopoietic tissues digestion and seeding conditions. This table shows the embryo equivalents (ee) to be seeded in Methocult, the number of dishes, as well as the volumes and time used for collagenase digestion for each tissue.

Tissue	ee	PBS/10%FCS volume/tube	Collagenase I volume/tube	Time in collagenase	Dishes seeded
AGM	1	190 µl	10 µl	45min	2
Head	0.5	475 µl	25 µl	45min	1
PL	0.5	475 µl	25 µl	1h15	1

YS	0.5	475 µl	25 µl	1h15	1

Table 22. Summary of E11 haematopoietic tissues digestion and seeding conditions.
This table shows the embryo equivalents seeded in Methocult, the number of dishes, as well as the volumes and time used for collagenase digestion for each tissue.

Tissue	ee	PBS/FCS volume/tube	Collagenase I volume/tube	Time in collagenase	Dishes seeded
AGM	0.33 (x3)	190 µl	10 µl	45min	3
Head	0.33	475 µl	25 µl	45min	1
PL	0.33	475 µl	25 µl	1h15	1
YS	0.33	475 µl	25 µl	1h15	1
FL	0.05	-	-	-	1

2.6 Transplantations

2.6.1 Primary transplantations

2.6.1.1 PDGFRβ KO and PDGF-B^{ret} transplantations

Single cell suspensions of PDGFRβ and PDGF-B^{ret} E11 AGM cells were injected in the tail vein of Ly5.1 heterozygous (CD45.1^{+}CD45.2^{+}) mice. Prior to the injections, the recipients were sub-lethally irradiated with 9.4-9.6 Gray (Gy) using a Caesium-137 Gammacell 40 Exactor. Irradiations were split in two separate doses (half and half), with a 2h break between each dose. AGMs were injected together with 20000 BM helper cells from Ly5.1 homozygous (CD45.1^{+}CD45.2^{-}) mice.

2.6.1.2 Bone marrow transplantations

To harvest the BM, the femur and tibia from both legs was taken, and the tips of the bones were carefully cut, until the BM was visible. Using a 1ml syringe and a 25G needle, the BM was washed out with PBS/10%FCS/1%PS + 2mM EDTA, and centrifuged for 10min at 2000rpm at 4ºC. Red blood cells were

lysed by re-suspending the pellets in an ammonium chloride solution (Stem Cell Technologies, 07850) for 12min (6min, mix, 6min). Cells were next washed and centrifuged. For primary BM transplantations, cells were re-suspended in 5ml PBS/10%FCS/1%PS + 2mM EDTA. 10µl of cells were taken for counting and diluted with Trypan Blue (Corning, 25-900-CI). Cells were counted using either a Bürker-Türk or a Bürker haemocytometer. To calculate the total number of cells using the Bürker-Türk (16 squares were counted), the formula below was used:

$$Cell\ number\ per\ ml = \#\ cells\ counted \times \frac{25}{16} \times dilution\ factor \times 10^4$$

To calculate the total number of cells using the Bürker haemocytometer (25 squares were counted in at least 2 different positions and the average was calculated), the formula below was used:

$$Cell\ number\ per\ ml = \#\ cells\ counted \times dilution\ factor \times 10^4$$

Between $0.5x10^6$ and $1x10^6$ cells were injected into primary recipients. For secondary BM transplantations, harvested BM cells were equally divided and injected into 2 recipients.

2.6.1.3 PDGFRβ-Cre;TdTomato transplantations

Sorted Tomato+ and Tomato- E11 AGMs, E14 FLs and adult BMs (see section 2.8.2) were injected in the tail vein of Ly5.1 heterozygous ($CD45.1^+CD45.2^+$) mice. Prior to the injections, the recipients were sub-lethally irradiated with 9 Gy using a Caesium-137 IBL 637 C irradiator (type GSR-CS137/D). Irradiations were split in two separate doses (half and half), with a 2h break between each dose. Sorted cells were injected together with 200000 spleen cells from Ly5.1 homozygous mice. These cells were injected in another animal facility, hence the difference in the helper cells injected and the irradiation dose compared to other transplantations.

2.6.2 Peripheral blood analysis

Blood was taken from the submandibular vein, 1 and 4 months after transplantation and analysed by flow cytometry to assess the level of donor chimerism (% of $CD45.1^-$ $CD45.2^+$ cells) (Table 23). At 4 months, lymphoid and myeloid reconstitution was also assessed with CD4, CD8, CD11b, CD19 and Gr1 staining (Table 23). To perform the analysis, red blood cells were lysed with an ammonium chloride solution (Stem Cell Technologies, 07850) for 12min (6min, mix, 6min) at RT, and incubated for 30min at 4°C in the dark, with the antibody mix below:

Table 23. Antibodies used for peripheral blood flow cytometry analysis

Antibody	Clone	Supplier	Cat. Number	Dilution
CD45.1 FITC	A20	Biolegend	110706	1:1000
CD45.2 Pacific Blue	104	Biolegend	109820	1:1000
CD4 PE	H129.19	Biolegend	130310	1:5000
CD8a PE	53-6.7	Biolegend	100708	1:500
CD11b/Mac-1 APC	M1/70	Biolegend	101212	1:1000
CD19 APC-Cy7	6D5	Biolegend	115530	1:1000
Gr-1/Ly-6G/C PE-Cy7	RB6-8C5	Biolegend	108416	1:2000

Cells were next washed, re-suspended in 300µl of 2% FCS in PBS and analysed by flow cytometry. Sytox AAD (Thermofisher, S10349) was used to detect dead cells.

2.6.3 Secondary transplantations

Following the 4 months analysis, successfully reconstituted mice (>4% donor chimerism) were sacrificed, and the total BM from both legs was harvested to perform secondary transplantations. Red blood cells were lysed as described above (section 2.6.1.2), and the total number of BM cells injected into two sub-lethally irradiated Ly5.1 heterozygous recipients. Blood from secondary

recipients was analysed after 1 and 4 months as described above (section 2.6.2).

2.7 Flow cytometry

All flow cytometry analyses in this thesis started with the selection of single live cells. Cells were first separated from debris or clumps of cells by forward vs. side scatter (SSC-A, FSC-A). Single cells were next separated from doublets using FSC-H vs. FSC-A correlation, and live cells were selected by the absence of Sytox staining. Occasionally, Sytox 7AAD (Thermofisher; S10349) was replaced with other live/dead markers, such as DAPI (Thermofisher Scientific; D1306), Zombie NIR (Biolegend; 423105), or Sytox Green (Thermofisher Scientific; S34860)

2.7.1 AGM cell populations analyses

AGMs were dissected and digested in collagenase type I (Sigma, C0130, 0.12% v/v), washed with PBS/2%FCS/1%PS (FACS buffer) and centrifuged at 2000rpm for 10min. Pellets were re-suspended in one of the antibody mixes described below (Table 24 andTable 25) for 30min at 4ºC. Cells were washed again, centrifuged, and pellets re-suspended in 300µl FACS buffer. All cells were analysed using BD LSR Fortessa with 4 lasers, with the exception of AGMs stained with αSMA, which were analysed using an ACEA NovoCyte flow cytometer.

2.7.1.1 PDGF-B^{ret}

PDGF-B^{ret} AGMs were stained with the antibody cocktail described below (Table 24).

Table 24. Flow cytometry antibodies used for PDGFR-B^{ret} mutant AGM analyses.

Antibody	Clone	Supplier	Cat. Number	Dilution
NG2 488	-	Millipore	ab5320a4	1:100
CD31 PE-Cy7	-	eBioscience	25-0311-82	1:4000
CD45 PerCpCy5.5	30-F11 (RUO)	BD Pharmingen	550994	1:400

cKit BV421	2B8	BD Horizon	562609	1:500
PDGFRα APC	-	Biolegend	135908	1:100
Sytox AAD	-	Thermofisher	S10349	1:10000

2.7.1.2 PDGFRβ;Runx1-IRES-GFP

PDGFRβ;Runx1-GFP mutant AGMs were stained with the antibodies below (Table 25).

Table 25. Flow cytometry antubodies used for PDGFRβ;Runx1-GFP mutant AGM analyses.

Antibody	Clone	Supplier	Cat. Number	Dilution
NG2 Cy3	-	Millipore	ab5320c3	1:100
PDGFRβ APC	APB5	eBioscience	17-1402-82	1:250
CD31 PE-Cy7	-	eBioscience	25-0311-82	1:4000
CD45 PerCpCy5.5	30-F11 (RUO)	BD Pharmingen	550994	1:400
cKit BV421	2B8	BD Horizon	562609	1:500
Sytox AAD	-	Thermofisher	S10349	1:10000

2.7.1.3 PDGFRβ analysis in all haematopoietic organs

PDGFRβ expression was assessed in E8-E11 AGM, head, FL, PL and YS by staining single cell suspensions with PDGFRβ APC antibody (1:250; eBioscience; 17-1402-82). As it is difficult to dissect the FL before E10, the whole body (excluding the organs, head, PL and YS) was analysed at E8 and E9.

2.7.1.4 αSMA expression analysis

Following collagenase digestion, E10.5 PDGFRβ mutant AGM cells were stained with Zombie NIR (Biolegend; 423105) for 30min at 4ºC. Samples were next washed and permeabilised in 200µl of 4% PFA for 30min at 4ºC, washed, and further permeabilised with 0.5% Triton X100 (Sigma; T8787-100ML) in PBS for 30min at 4ºC. αSMA-Cy3 (1:200; Sigma; C6198-.2ml) was next added to each sample and incubated for 30min at 4ºC in the dark, after which they

were washed, centrifuged, re-suspended in 300µl of FACS buffer and analysed using an ACEA NovoCyte flow cytometer.

2.7.2 LSK and LSK-SLAM analysis

BM cells from PDGF-B^{ret} mutant, PDGFRβ-Cre;TdTomato and BL6 adult mice were harvested and red blood cells were lysed as described above (section 2.6.1.2). Samples were washed with PBS/10%FCS/1%PS/2mM EDTA and centrifuged for 10min at 2000rpm. Pellets were re-suspended in an antibody mix containing haematopoietic lineage biotinylated antibodies (Lin) (Table 26) diluted in BM FACS buffer (PBS/2%FCS/1%PS/2mM EDTA) and incubated for 30min at 4ºC. Cells were next washed and centrifuged, and pellets were resuspended in a second antibody mix containing directly conjugated antibodies, and Streptavidin-PerCp to detect all Lin biotinylated antibodies (Table 27), and incubated for 30min at 4ºC. BM cells from PDGFRβ-Cre;TdTomato were not stained with CD48 nor CD150. Cells were washed and resuspended in 1ml of BM FACS buffer and analysed with a BD LSR Fortessa flow cytometer with 4 lasers. DAPI (1:500; Thermofisher Scientific, D1306) was used to distinguish between live and dead cells. Results were analysed with FlowJo X software.

Table 26. Biotinylated antibodies used for LSK and LSK-SLAM analyses.

Biotinylated antibody	Clone	Supplier	Cat. Number	Dilution
CD4	H129.19	BD Biosciences	553648	1:1600
CD5	53-7.3	BD Biosciences	553018	1:800
CD8a	53-6.7	BD Biosciences	553028	1:800
CD11b / Mac-1	M1/70	BD Biosciences	553309	1:200
CD45R / B220	RA3-6B2	BD Biosciences	553086	1:200
Gr-1 / Ly-6G/C	RB6-8C5	BD Biosciences	553125	1:100
Ter119	TER-119	BD Biosciences	553672	1:50

Table 27. Antibodies used for LSK and LSK-SLAM analyses.

Antibody	Clone	Supplier	Cat. Number	Dilution
CD117 / c-kit APC	2B8	BioLegend	105812	1:200
Sca-1 / Ly-6A/E APC-Cy7	E13-161.7	BioLegend	122514	1:200
CD48 / SLAMf2 PE	HM48-1	BioLegend	103406	1:800
CD150 / SLAMf1 PE-Cy7	TC15-12F12.2	BioLegend	115914	1:200
Streptavidin PerCp	-	BioLegend	405213	1:200

2.8 Fluorescence-activated cell sorting (FACS)

AGMs were dissected from E10 and E11 embryos, digested in collagenase type I (Sigma, C0130, 0.12% v/v) in PBS for 45 min at 37^{o}C, mechanically dissociated into single cell suspensions and washed with 10%FCS in PBS.

2.8.1 Sorting of PDGFRβ+ and PDGFRβ- cells

Cells to be sorted based on PDGFRβ expression were incubated for 30 min at 4^{o}C in the dark with PDGFRβ PE antibody (1:250; eBioscience, 136006). E11 cells were additionally stained with cKit BV421 antibody (1:500; BD Horizon; 562609) to enrich in HSPCs, as it has been reported that all progenitors are cKit+ [32]. Following the incubation, cells were washed twice in PBS/FCS and sorted using a BD FACSAria Fusion flow cytometer. Sorted cells were next seeded in methylcellulose, and colonies were counted 10-12 days later.

2.8.2 Sorting of Tomato+ and Tomato- cells

2.8.2.1 AGM

Cells to be sorted based on Tomato expression were incubated for 30 min at 4^{o}C in the dark with cKit BV421 antibody (1:500; BD Horizon; 562609), washed twice with FACS buffer and sorted using a BD FACSAria Fusion flow cytometer. Sorted cells were next seeded in methylcellulose and colonies were counted 10-12 days later.

2.8.2.2 Foetal liver and bone marrow

E14 FL and adult BMs were dissected and dissociated in PBS/FCS as described above, and single live cells were sorted based on Tomato expression using a BD FACSAria Fusion flow cytometer. Sorted cells were next seeded in methylcellulose or injected in sub-lethally irradiated recipients.

2.9 3D whole-mount immunostaining

Embryos were separated from the PL and YS, fixed in 2% PFA for 20min on ice and washed 3 times for 10min with PBS. A piece of tissue was taken for genotyping prior to the fixation. Embryos were next dehydrated twice with 50% methanol in PBS for 10min at 4ºC, twice with 75% methanol in PBS for 10min at 4ºC and once with 100% methanol for 10min at 4ºC. Embryos were then stored in 100% methanol at -20ºC until used. Before use, embryos were further dissected, removing the head, limb buds, somites, and one side of the body wall. They were then rehydrated in 75% methanol and in 50% methanol for 10min each at 4ºC. To reduce unspecific antibody binding, they were next blocked using a biotin/avidin blocking kit (ThermoFisher Scientific; 004303). Embryos were immersed in 1ml of PBS containing 3 drops of the avidin solution for 15min at RT, washed for 5min in PBS, re-immersed in 1ml of PBS containing 3 drops of the biotin solution, and washed 3 times 5min with PBS. They were additionally blocked with BSA/PBS-MT (10% (w/v) BSA, 1% (w/v) of skim milk and 0.4% (v/v) of TritonX in PBS) for 1h at 4ºC. Embryos were next incubated O/N at 4ºC on a rocking platform with the first primary antibody either unconjugated cKit (1:500; BD Bioscience; 553352), or unconjugated NG2 (1:500; Millipore; ab5320). On the second day, they were washed 4 times for 30 min to 2h with PBS-MT and incubated overnight at 4ºC with either Alexa647 (1:2500; Invitrogen; A21472) as a secondary antibody for cKit or Alexa647 (1:2500; Invitrogen; A21245) as a secondary antibody for NG2. On the third day, embryos were washed 4 times for 30 min to 2h and incubated with the second and third primary antibodies, αSMA FITC (1:500; Sigma; F3777) and CD31 biotin (1:500 BD Pharmingen; 553371) overnight at 4ºC. On the fourth day, embryos were washed as in the previous days and incubated with Streptavidin Cy3 (1:2500; Sigma; S6402) overnight at 4ºC. On the fifth

day, embryos were washed 4 times with PBS-MT and rinsed with PBST (0.4% TritonX in PBS) for 20min at 4ºC. They were next dehydrated in methanol at 4ºC (50% methanol for 10min followed by 100% methanol for 10min). Embryos were then transferred to glass containers where the methanol was replaced by 50% BABB/methanol (1 part benzyl alcohol with 2 parts benzyl benzoate in methanol) 4 times. 50% BABB/methanol was then replaced with 100% BABB until the embryos became completely clear. Embryos were next mounted on a small glass chamber and imaged using a Leica SP8 confocal microscope.

Chapter 3 Characterisation of the HSC-generating microenvironment

3.1 Introduction

Endothelial cells in the ventral aspect of the dorsal aorta rely upon signals from the sub-aortic mesenchyme to initiate the haematopoietic programme and generate HSCs. In the chick embryo, it was shown that by preventing the migration of the splanchnic mesoderm before it develops into the subaortic mesenchyme leads to the absence of Runx1 expression by ECs and subsequent formation of haematopoietic clusters [97]. This suggests that sub-aortic cells derived from the splanchnic mesoderm are required to initiate the haematopoietic programme in the dorsal aorta. In addition, several studies have shown that several murine stromal cell lines obtained from midgestation AGM support haematopoiesis and express HSC-supportive genes [125,156,178], suggesting that mesenchymal stromal cells can act as a niche for HSPCs. However, the ability to support haematopoiesis varied greatly depending on the stromal cell line, suggesting an inherent heterogeneity in AGM stromal cells. Taken together, these data suggest that the AGM microenvironment could play a role in both HSC specification and as a niche for HSCs. Characterising the microenvironment surrounding the midgestation DA both phenotypically and genetically, should provide a better insight on the cell types and signals required for HSC generation and maintenance in the AGM.

3.2 Hypothesis and aims

3.2.1 Hypothesis

The midgestation aortic microenvironment contains mesenchymal stromal cells that act as a niche for HSC generation.

3.2.2 Aims

- Phenotypic characterisation of mesenchymal stromal cell populations surrounding the aorta at the time of HSC generation.

- Establish and validate an isolation protocol for the populations defined above.
- Identification of stromal cells expressing known hematopoietic supportive genes.

3.3 Results

3.3.1 Three phenotypically distinct perivascular cell populations surround the midgestation dorsal aorta

To understand the composition of the AGM microenvironment during HSC generation, immunohistochemistry was performed on C57BL6 E11 cryosections, using different marker combinations to identify and characterise perivascular mesenchymal stromal cells that surround the dorsal aorta (Figure 8 andFigure *16*). The DA is composed of a layer of CD31+ endothelial cells, surrounded by mesenchymal stromal cells and sided by the cardinal veins (CVs). On the dorsal side of the DA, the notochord (NC) can be distinguished by its morphology (Figure 8).

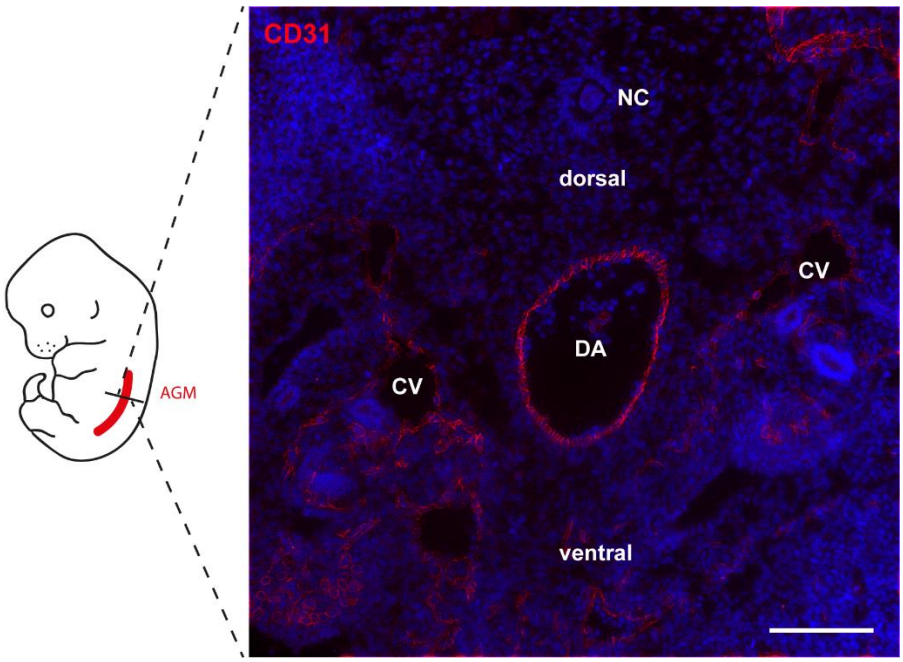

Figure 8. E11 dorsal aorta.
Cross-section of a BL6 E11 mouse embryo, showing the dorsal aorta (DA) sided by the cardinal veins (CVs). The notochord (NC) is located on the dorsal side of the DA. CD31 (red) was used to mark the endothelium and DAPI (blue) to mark the nuclei. Scale bar: 100µm.

To characterise the cells surrounding the dorsal aorta, immunohistochemistry using previously described pericyte/vascular smooth muscle cell (vSMC)

markers such as NG2, αSMA, PDGFRβ and CD146 was performed. Antibody specificity against these markers was provided by the manufacturers, confirmed in several publications and previously tested in the lab. Negative controls to test the specificity and background fluorescence levels of the secondary antibodies were performed (Figure 9). Sections were stained with only the secondary antibody and DAPI. No unspecific staining and very little background fluorescence was detected for each secondary antibody used in this study (Figure 9).

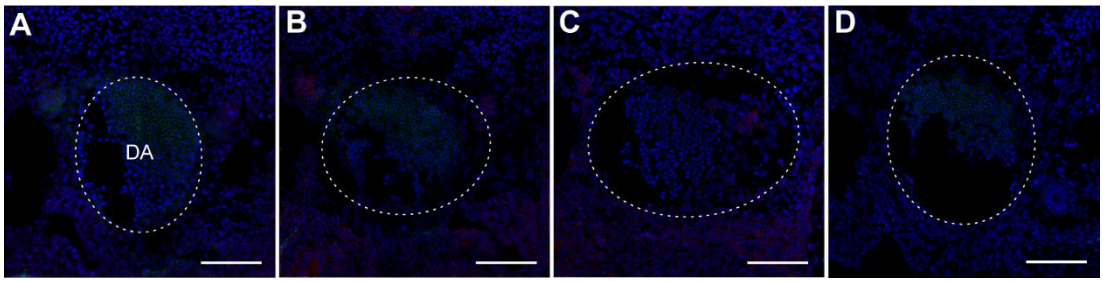

Figure 9. Negative controls.
Immunohistochemistry on frozen BL6 E11 sections stained with secondary antibodies only. (A) Goat anti-rat AF594, (B) Goat anti-rabbit AF594, (C) Goat anti-rabbit AF488, (D) Streptavidin-Cy3. Nuclei were counterstained with DAPI (blue). The dashed line delineates the DA. Scale bar: 100µm.

Immunostainings with NG2 and CD31 show one or more layers of NG2+ CD31- cells surrounding and in close contact with the CD31+ endothelium (Figure 10). The notochord is also surrounded by NG2+ CD31- cells (Figure 10). NG2 expression along the notochord varies, depending on the area in which the section was taken (Figure 10,Figure *11* and Figure *14*). As expected, all endothelial cells express CD31 (Figure 10).

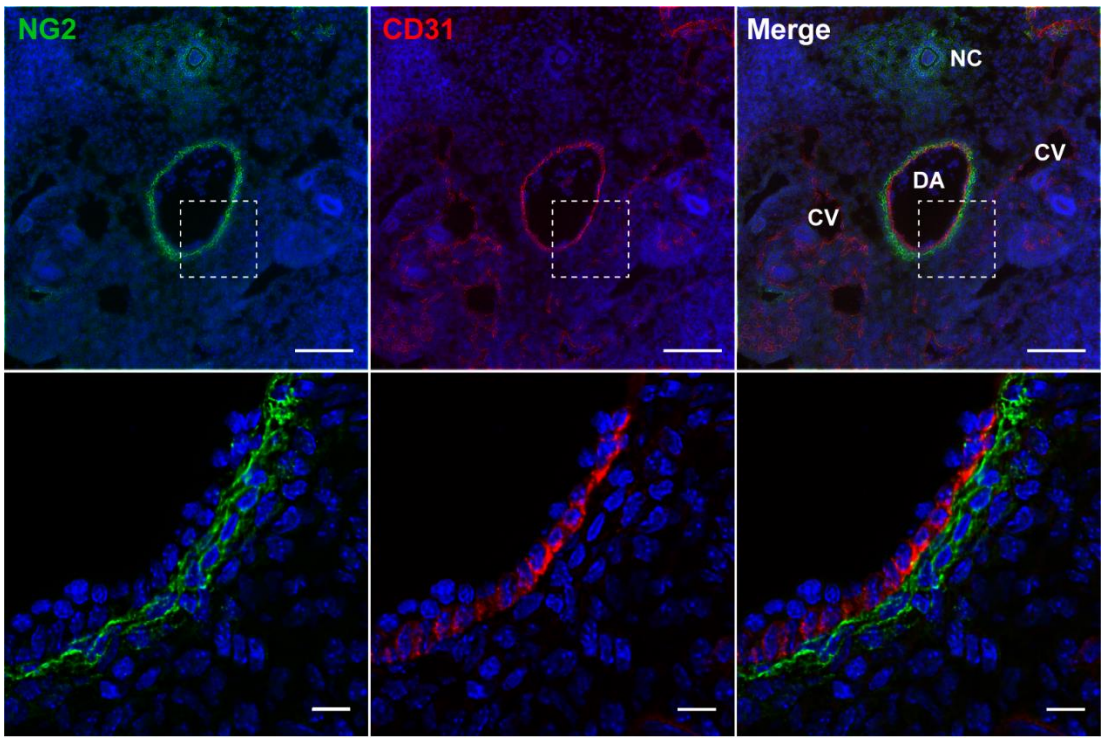

Figure 10. NG2+ cells surround the E11 DA.
Immunohistochemistry on a frozen E11 BL6 section, showing a layer of NG2+ cells (green) surrounding and in close contact with a layer of CD31+ cells (red). NG2+ CD31- cells are also found around the notochord. The bottom panel shows a higher magnification of the top panel. Nuclei were counterstained with DAPI (blue). Scale bars: upper panel: 100µm; bottom panel: 10µm.

All NG2+ cells surrounding the DA were found to express αSMA, with the exception of NG2+ cells around the notochord (Figure 11). No NG2 expression could be detected around the cardinal veins, whereas some αSMA+ cells are present (Figure 11).

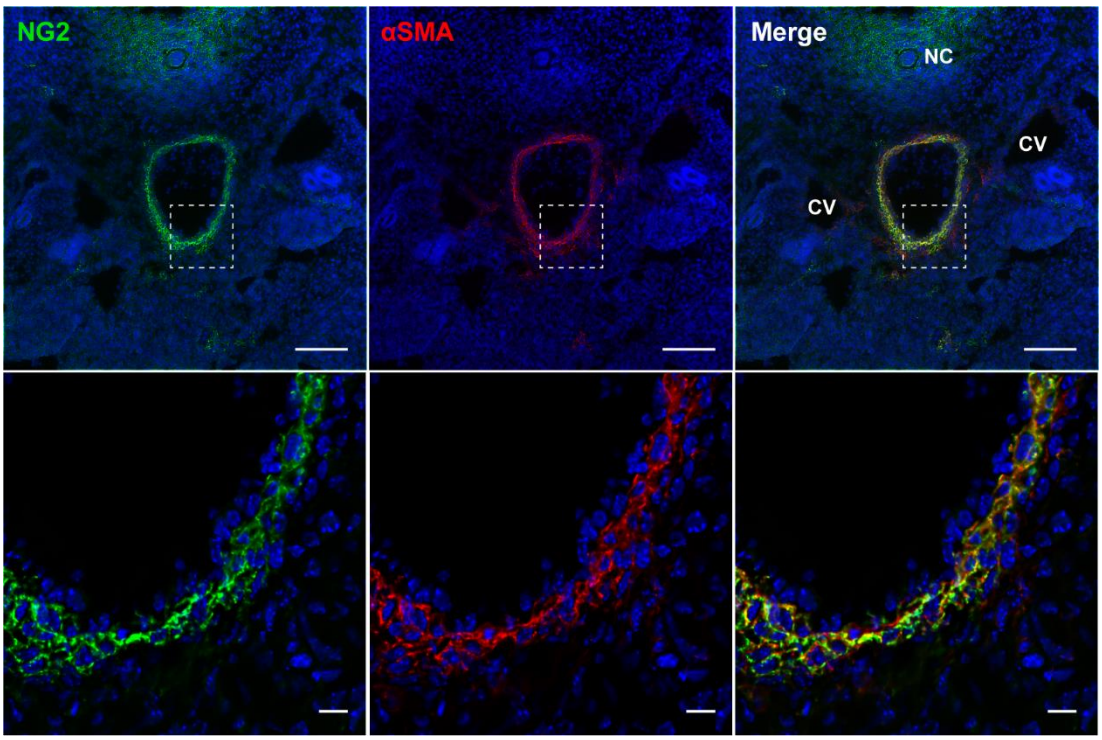

Figure 11. NG2+ perivascular cells co-express αSMA.
Immunohistochemistry on a frozen E11 C57BL6 section, showing that all NG2+ (green) cells surrounding the DA co-express αSMA (red). In contrast, NG2+ cells around the NC do not express αSMA. The bottom panel shows a higher magnification of the top panel. Nuclei were counterstained with DAPI (blue). Scale bars: upper panel: 100µm; bottom panel: 10µm.

As pericytes and vascular smooth muscle cells are embedded in a basement membrane, immunostainings with collagen IV were performed (Figure 12). NG2+ cells were found to be embedded in Collagen IV, with the exception of some NG2+ cells closer to the endothelium that only show collagen IV staining on the abluminal side, especially on the ventral side of the DA (Figure 12, middle panel). On the dorsal aspect of the DA, most NG2+ cells are fully embedded in collagen IV (Figure 12, bottom panel). The additional layers of NG2+ on the ventral aspect of the DA (Figure 12, middle panel) suggest that the section was either taken in close proximity to the vitelline artery, as shown by 3D whole mount staining in Chapter 4 (Figure 34B), or that the embryo was slightly tilted when the sections were made.

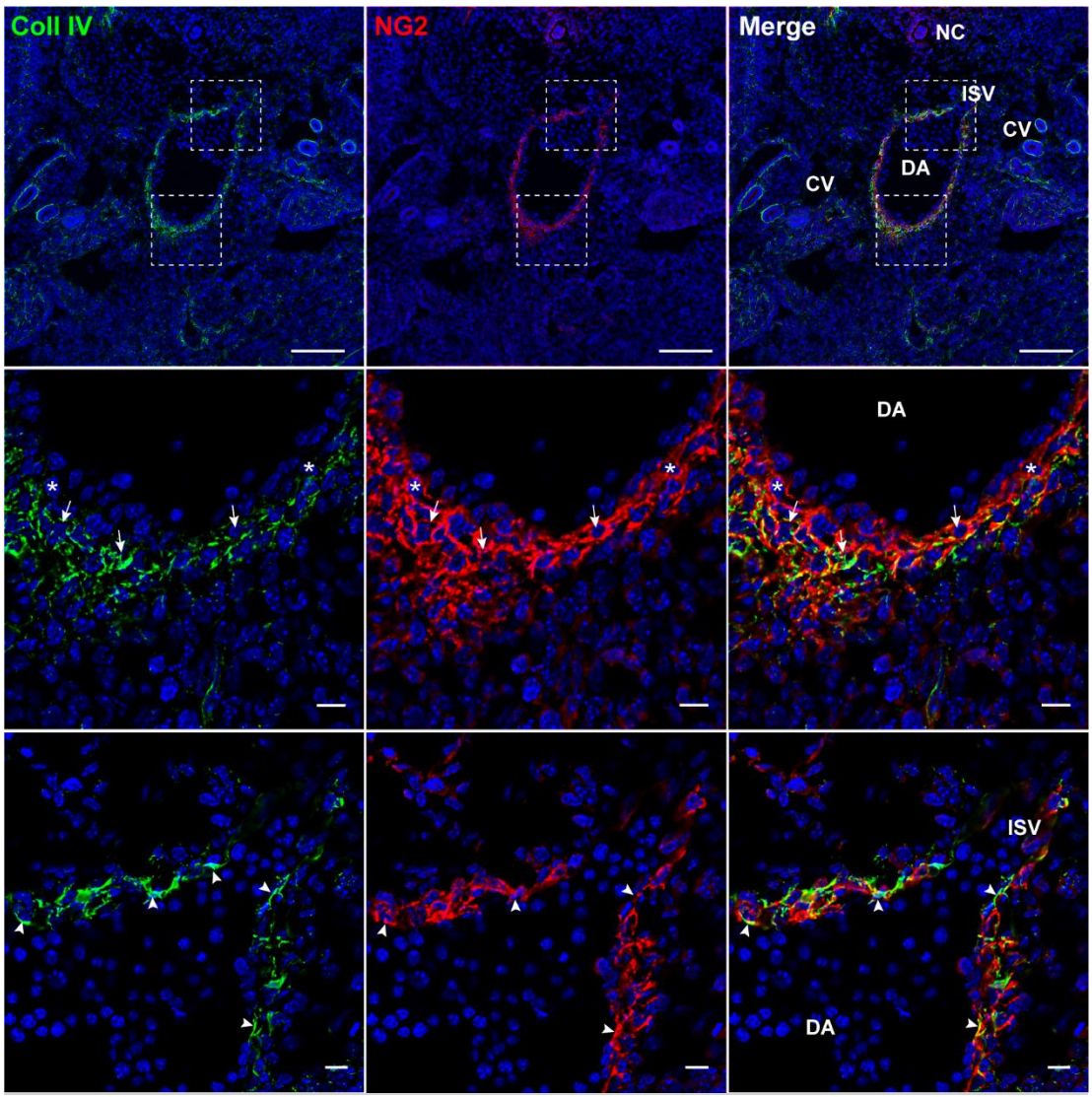

Figure 12. NG2+ perivascular cells are embedded in collagen IV.
Immunohistochemistry on a frozen E11 BL6 section, showing that NG2+ cells (red) surrounding the DA are embedded in a collagen IV+ basement membrane (green). The middle panel shows a higher magnification of the ventral aspect of the DA. Arrows: NG2+ cells fully embedded in collagen IV; asterisks: NG2+ cells partially embedded in collagen IV. The bottom panel shows a higher magnification of the dorsal aspect of the DA, and the beginning of an intersomitic vessel (ISV). Arrowheads: NG2+ cells with collagen IV on the luminal side. Nuclei were counterstained with DAPI (blue). Scale bars: upper panel: 100µm; middle and bottom panels: 10µm.

Immunostainings with PDGFRβ and CD31 showed that CD31+ ECs, as expected, do not express PDGFRβ (Figure 13) [148]. Several layers of PDGFRβ+ cells were detected around the DA and cardinal veins (CVs), and this expression was higher on the ventral aspect of the DA (Figure 13 andFigure *14*).

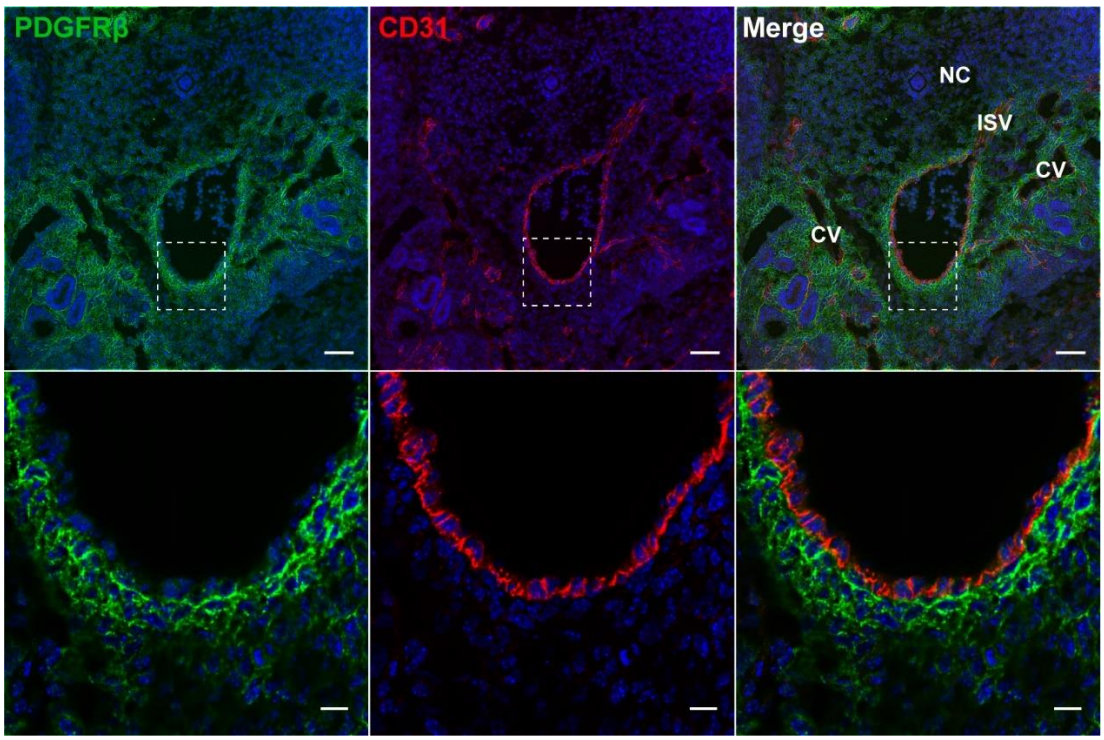

Figure 13. Several layers of PDGFRβ+ cells surround the aortic endothelium.
Immunohistochemistry on a frozen E11 C57BL6 section, showing several layers of PDGFRβ+ cells surrounding and in close contact with a layer of CD31+ (red) cells. PDGFRβ+ cells are also found surrounding the cardinal veins (CV). The bottom panel shows a higher magnification of the top panel. Nuclei were counterstained with DAPI (blue). Scale bars: upper panel: 100µm; bottom panel: 10µm.

To better understand the distribution of NG2 and PDGFRβ expressing cells, sections were stained with both markers (Figure 14). All NG2+ cells surrounding the DA co-express PDGFRβ, but not all PDGFRβ+ cells express NG2 (Figure 14). A few layers of NG2+ PDGFRβ+ cells are found next to the endothelium, and several layers of NG2- PDGFRβ+ cells are found further from the endothelium and adjacent to NG2+ PDGFRβ+ cells (Figure 14). Importantly, PDGFRβ expression was not detected around the notochord (Figure 14).

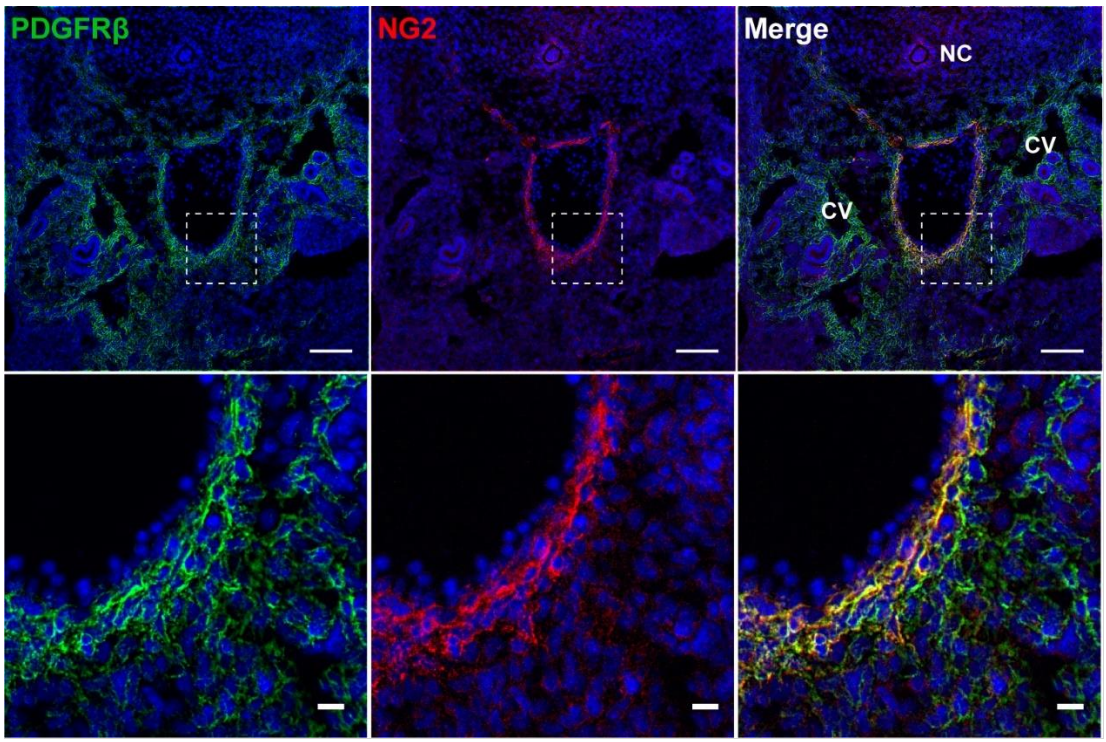

Figure 14. NG2+ cells surrounding the DA co-express PDGFRβ.
Immunohistochemistry on a BL6 E11 cryosection, showing that all NG2+ cells (red) surrounding the DA express PDGFRβ (green), but not all PDGFRβ+ cells express NG2. The bottom panel shows a higher magnification of the top panel. Nuclei were counterstained with DAPI (blue). Scale bars: upper panel: 100µm; bottom panel: 10µm.

CD146 is a marker for a subset of pericytes and endothelial cells in the mouse AGM [179]. Immunostainings against CD146 and CD31 confirmed that most ECs express CD146 (Figure 15; arrows), and few ECs (CD31+) do not express CD146 (Figure 15; arrowheads). CD146 expression was also found in perivascular cells adjacent to the endothelium (Figure 15; asterisks).

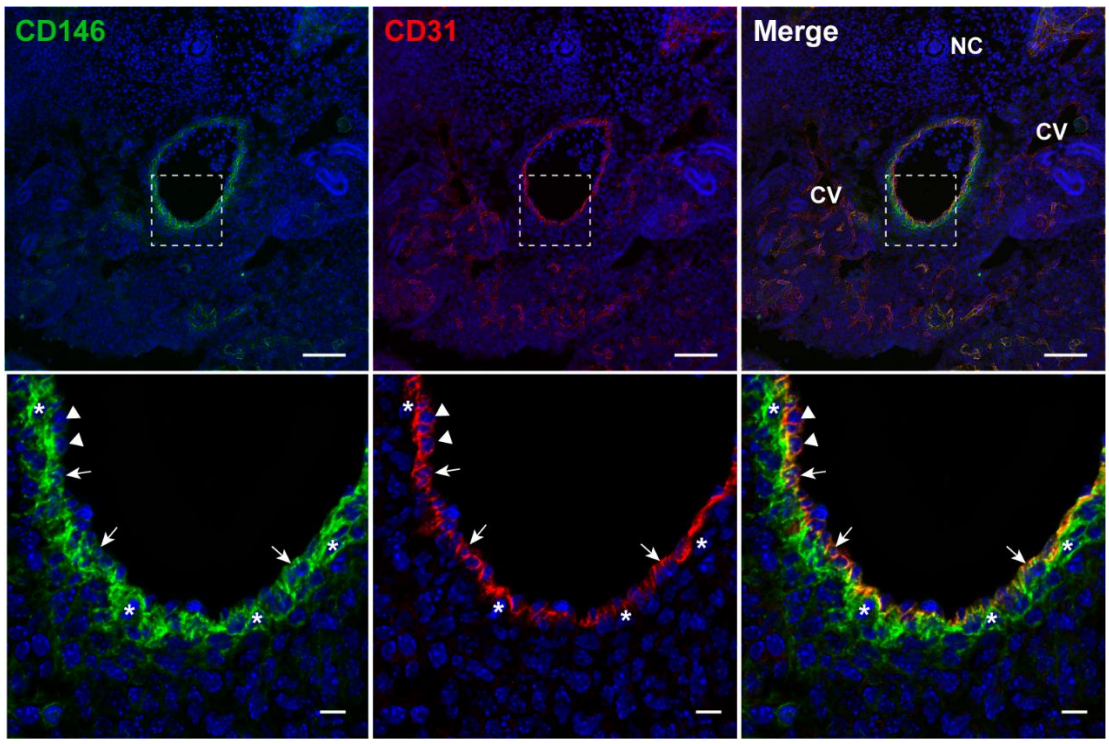

Figure 15. A subset of ECs express CD146.
Immunohistochemistry on frozen BL6 E11 sections. Most ECs express CD146 (green) and CD31 (red) (arrows), while some do not express CD146 (arrowheads). CD31- perivascular cells express CD146 (asterisks). The bottom panel shows a higher magnification of the top panel. Nuclei were counterstained with DAPI (blue). Scale bars: upper panel: 100µm; bottom panel: 10µm.

To further distinguish between CD146+ ECs and CD146+ perivascular cells, sections were co-stained with αSMA (Figure 16). As expected, on the luminal part of the DA, where the endothelium is located, CD146+ cells do not express αSMA (Figure 16; arrows). Adjacent to the endothelium, most cells co-express CD146 and αSMA. αSMA+ CD146- cells were also found next to the double positive population (Figure 16; asterisks).

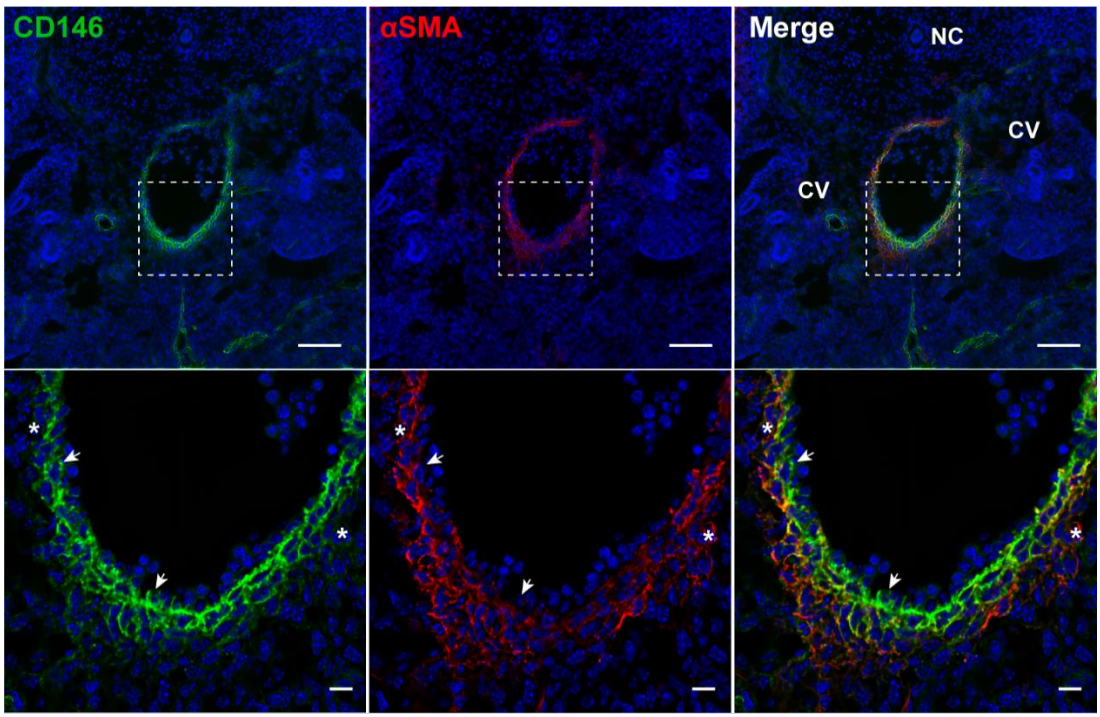

Figure 16. A subset of pericytes express CD146.
Immunohistochemistry on a BL6 E11 cryosection showing CD146 (green) and αSMA (red) expression. CD146+ αSMA- ECs can be found closest to the lumen of the DA (arrows), followed by CD146+ αSMA+ perivascular cells. Adjacent to these cells, some CD146- αSMA+ cells can be found (asterisks). The bottom panel shows a higher magnification of the top panel. Nuclei were counterstained with DAPI (blue). Scale bars: upper panel: 100μm; bottom panel: 10μm.

Based on these data, we identified three phenotypically distinct perivascular cell populations surrounding the DA at the time of HSC generation: pericytes/vascular smooth muscle cells (PCs/vSMCs), in close contact with the endothelium, which express NG2, αSMA and PDGFRβ; sub-pericytes/sub-vascular smooth muscle cells (sub-PCs/sub-vSMCs), a few layers of cells surrounding the pericytes and CVs, which express PDGFRβ but are negative for NG2 and αSMA; and the stroma, a population of cells that does not express any of these markers (Figure 17). For simplicity, PCs/vSMCs and sub-PCs/sub-vSMCs will be referred to as PCs and sub-PCs, respectively.

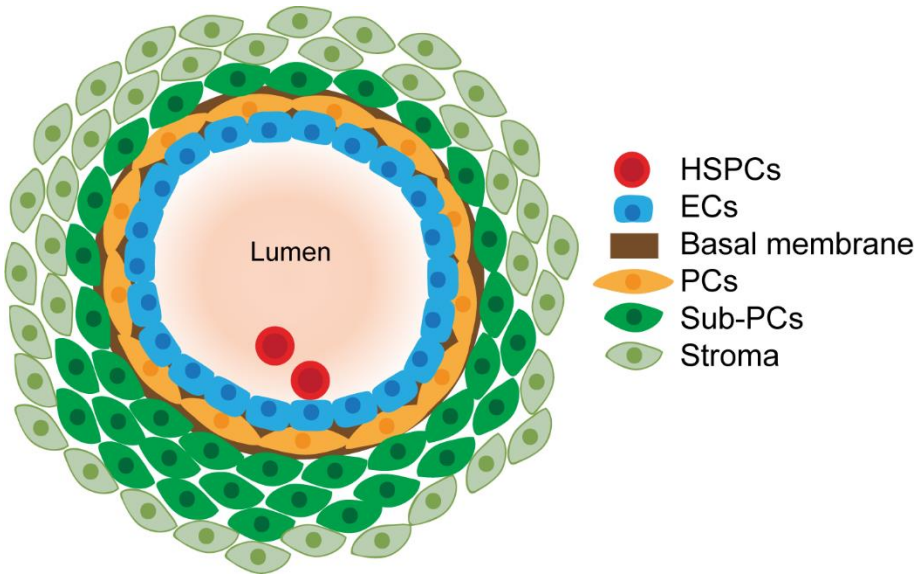

Figure 17. Scheme depicting the three perivascular cell populations surrounding the midgestation dorsal aorta.
A layer of CD31+ endothelial cells (ECs) is surrounded by NG2+ PDGFRβ+ pericytes (PCs) that are embedded in a Coll IV+ basement membrane. Several layers of NG2- PDGFRβ+ perivascular cells (sub-PCs) surround the pericytes, and are surrounded by the remaining stroma (NG2- PDGFRβ-).

3.3.2 Pericytes are found surrounding the DA at E10 but not before.

Some studies suggest that HSC specification starts between E8.5 and E10.5 [56]. As the DA is still growing and remodelling, E9 and E10 DAs were also characterised by immunohistochemistry. At E9, aortic ECs express CD31 (Figure 18). No NG2+ cells are found surrounding the paired aortae at E9 (Figure 18, upper panel), but are present around the fused aorta at E10 (Figure 18, bottom panel), suggesting that NG2 starts to be expressed between E9 and E10.

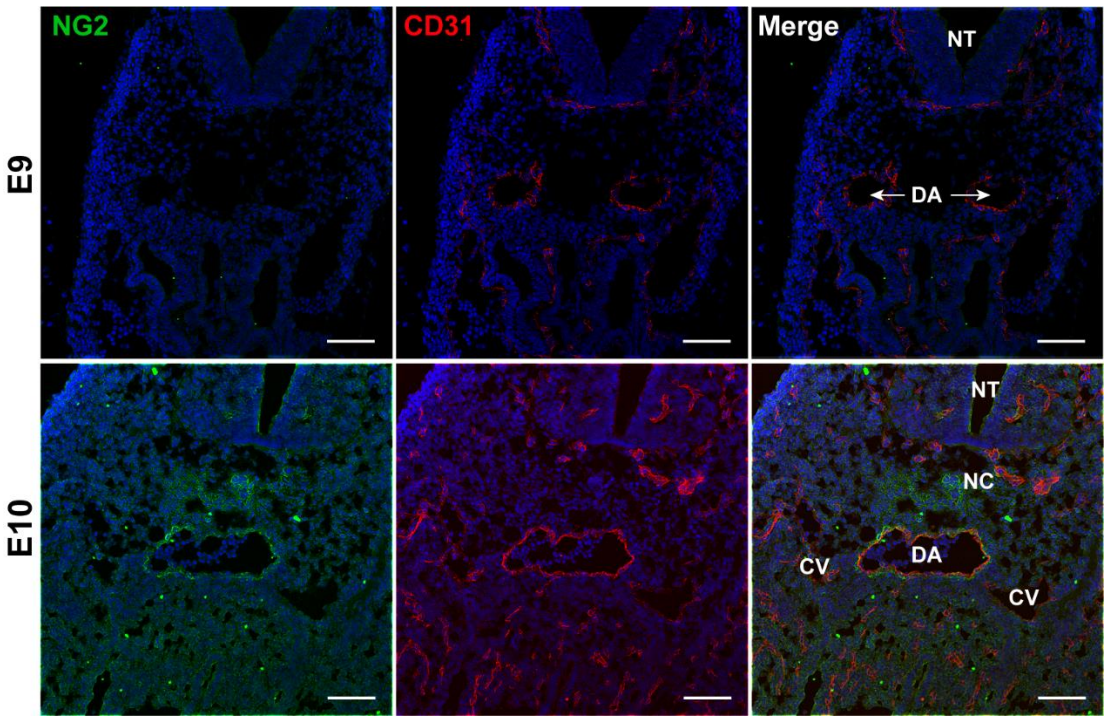

Figure 18. NG2 is expressed around the DA at E10 but not at E9.
Immunohistochemistry on BL6 E9 (upper panel) and E10 (bottom panel) cryosections showing NG2 (green) and CD31 (red) expression. No NG2+ cells are found at E9, whilst they are present around the DA endothelium at E10. Nuclei are counterstained with DAPI (blue). NT: neural tube. Scale bars: 100µm.

PDGFRβ expression was detected around the paired aortae at E9 and surrounding the fused DA and cardinal veins at E10 (Figure 19). These results were further confirmed by flow cytometry (Chapter 4, figure 30).

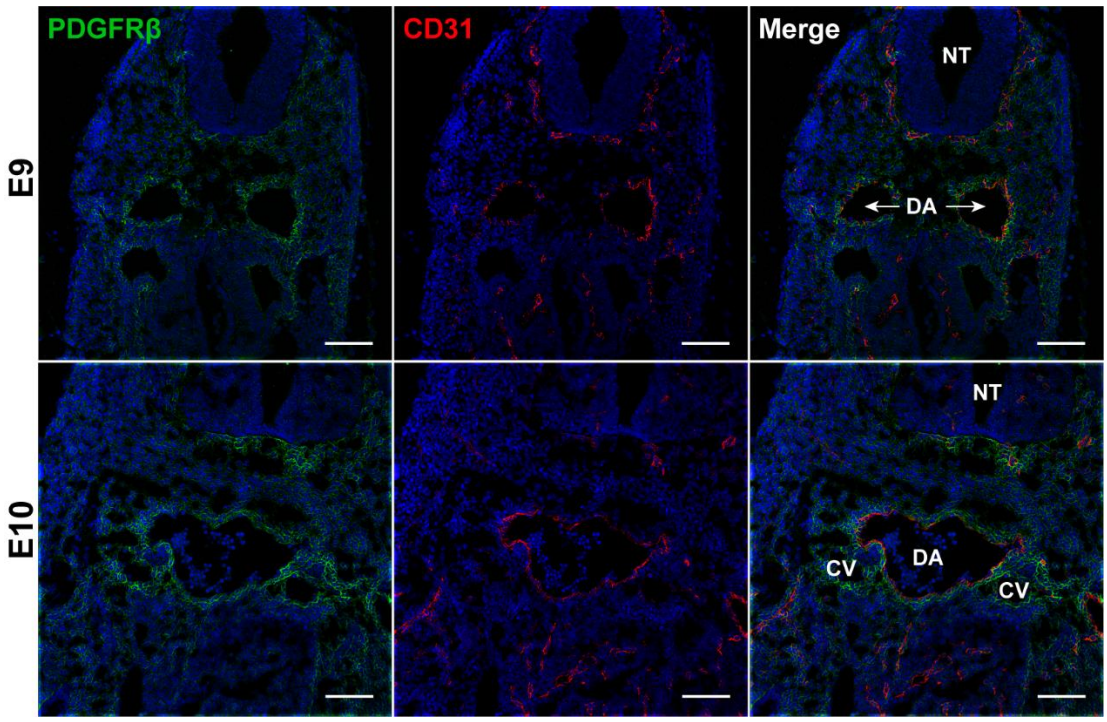

Figure 19. PDGFRβ is expressed around the DA at E9 and E10.
Immunohistochemistry on BL6 E9 (upper panel) and E10 (bottom panel) cryosections showing PDGFRβ (green) and CD31 (red) expression. PDGFRβ+ cells are found around the paired aortae at E9, and the fused aorta and cardinal veins at E10. Nuclei are counterstained with DAPI (blue). Scale bars: 100μm.

CD146 expression was detected in ECs lining the DA (αSMA- cells closer to the lumen), and a few perivascular cells (αSMA+) at both E9 and E10 (Figure 20). At E9, the paired aortae are not surrounded by αSMA+ cells, but a few αSMA+ cells can be found close to the endothelium and only between the paired aortae (Figure 20, upper panel). At E10, the DA is fully surrounded by αSMA+ cells (Figure 20, bottom panel).

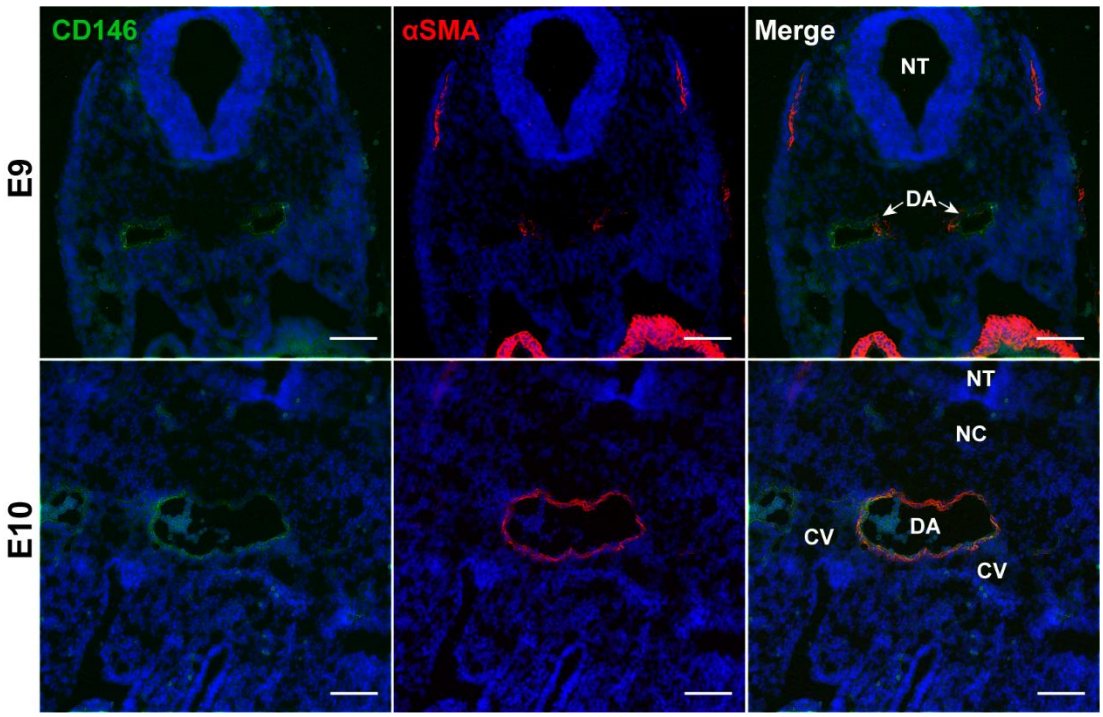

Figure 20. CD146 and αSMA are expressed around the DA at E9 and E10.
Immunohistochemistry on BL6 E9 (upper panel) and E10 (bottom panel) cryosections showing CD146 (green) and αSMA (red) expression. Few αSMA+ cells can be detected at E9, between the paired aortae, but fully surround the DA at E10. The endothelium and some αSMA+ cells express CD146 at both stages. Nuclei are counterstained with DAPI (blue). Scale bars: 100µm.

Although no NG2 expression was detected around the paired aortae at E9 (Figure 18, upper panel) and few cells express αSMA (Figure 20, upper panel), a collagen IV+ basement membrane is already present around the paired aortae at this stage (Figure 21, upper panel).

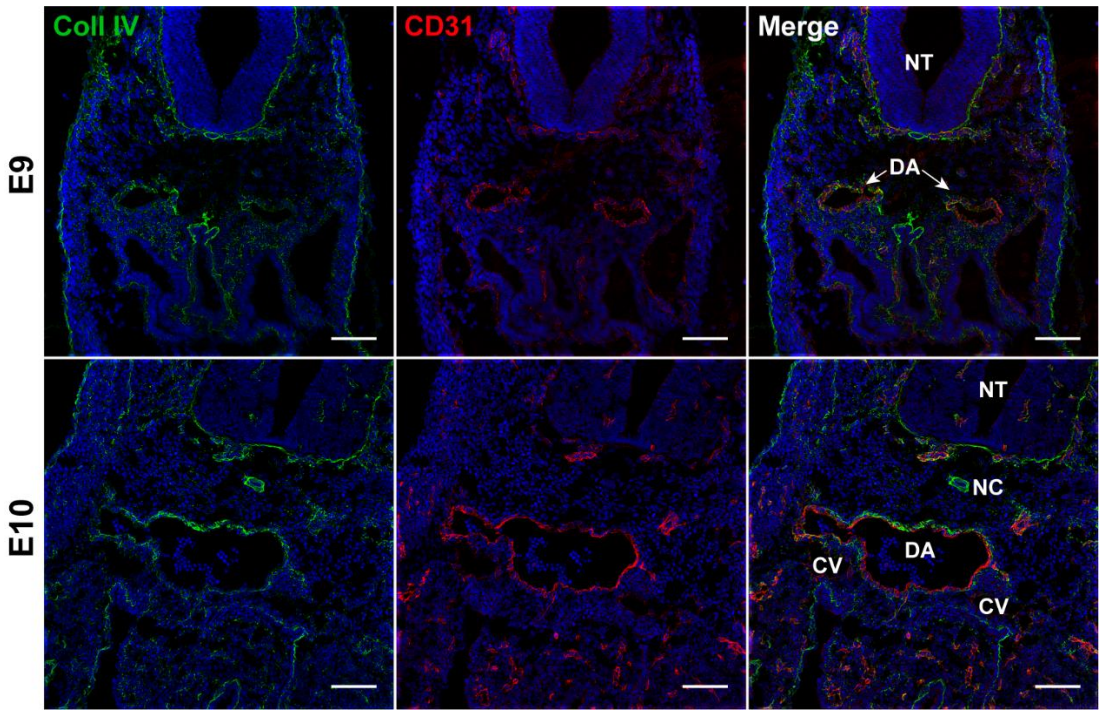

Figure 21. Collagen IV is present around the DA at E9 and E10.
Immunohistochemistry on BL6 E9 (upper panel) and E10 (bottom panel) cryosections showing collagen IV (green) and CD31 (red) expression. Collagen IV fully surrounds the CD31+ endothelium at both E9 and E10. Nuclei are counterstained with DAPI (blue). Scale bars: 100µm.

These data suggest that the same three perivascular cell populations shown to surround the DA at E11 (Figure 17) are already present at E10. E9 paired aortae on the other hand, have no NG2 expression and only a few αSMA+ cells. Interestingly, a collagen IV basement membrane is already present around the aortae at E9, even in the absence of αSMA+ cells, which suggests that either ECs or PC precursors are responsible for its production and deposition.

3.3.3 Pericytes, sub-pericytes and stromal cells surrounding the midgestation DA are genetically distinct

To understand whether the three perivascular stromal cell populations identified above are genetically different, bulk RNA sequencing was performed. Upon doublets and dead cell exclusion, E11 AGM cells were sorted

based on the absence of the haematopoietic and endothelial cell markers cKit, CD45 and CD31, and on the presence or absence of NG2 and PDGFRβ, as shown in Figure 22. Although immunohistochemistry characterisation of AGM stromal cells was not performed using CD45 and cKit, stromal cells, were sorted based on their absence to exclude all haematopoietic cells. A population of NG2+ PDGFRβ- cells were also found by flow cytometry, in line with immunohistochemistry data showing NG2+ PDGFRβ- cells surrounding the notochord (Figure 10,Figure *11* andFigure *22*).

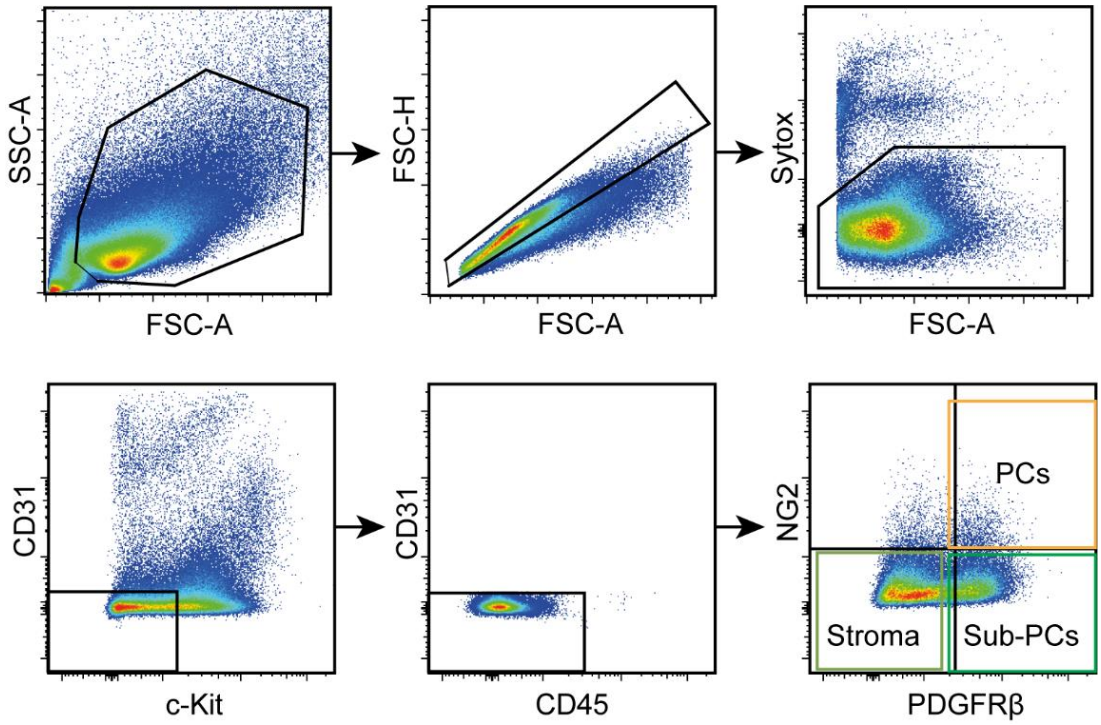

Figure 22. Gating strategy used to sort midgestation PCs, sub-PCs and stroma.
Gating strategy used to sort the three different perivascular cell populations. Haematopoietic and endothelial markers were negatively selected within the total population of single live cells. PCs (CD31- cKit- CD45- NG2+ PDGFRβ+), Sub-PCs (CD31- cKit- CD45- NG2- PDGFRβ+) and stroma (CD31- cKit- CD45- NG2- PDGFRβ-) were sorted and bulk RNA sequencing was performed.

As samples were sorted directly into a lysis buffer for RNA sequencing, it was not possible to confirm the purity of each sample after the sort. However, population purity was assessed after RNA sequencing, by plotting the FPKM (Fragments Per Kilobase of transcript per Million mapped reads) values of the

genes used for the sorting. The purity was generally good, with slight *Pdgfrb* expression in the stroma (Figure 23). This contamination of PDGFRβ+ cells in the stromal fraction might be due to the fact that there is no clear separation between PDGFRβ+ and PDGFRβ- cells and the lack of stringency in the gating strategy used to sort both populations (Figure 22).

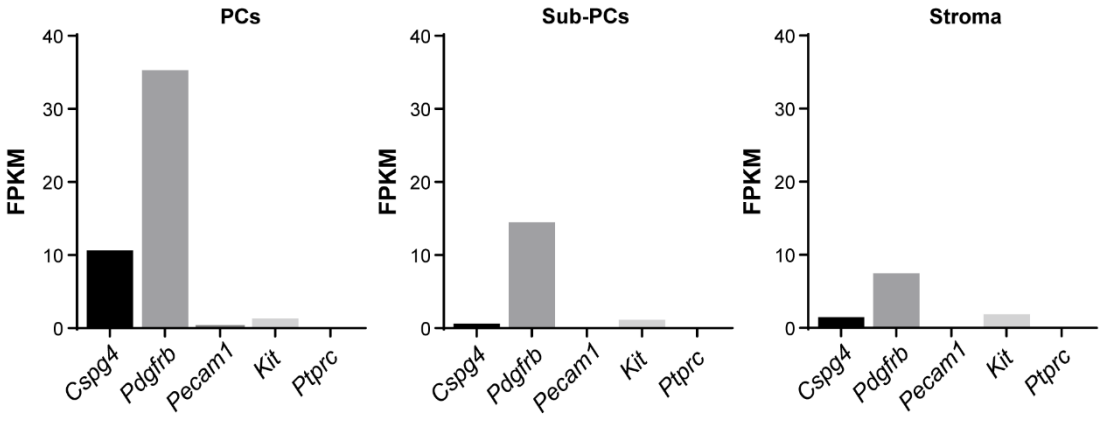

Figure 23. Post-RNA sequencing purity check.
Fragments Per Kilobase of transcript per Million mapped reads (FPKM) values of the markers used to sort each population of perivascular cells after RNA sequencing. The gene names for NG2, PDGFRβ, CD31, cKit and CD45 are *Cspg4*, *Pdgfrb*, *Pecam1*, *Kit* and *Ptprc*, respectively.

Clustering analysis was performed by our collaborator H. van de Werken, and PCs were found to be transcriptomically more distant than the sub-PCs and stroma, which cluster closer together (Figure 24A). This was confirmed by PCA analysis (Figure 24B). Dataset comparisons found 1029 differentially expressed genes (DEG) between all three populations (Figure 24C; all DEG are listed in appendix table 1). PCs and sub-PCs have a total of 791 DEGs, PCs and stromal cells have a total of 668 DEG, while sub-PCs and stroma only differ by 10 genes (Figure 24C). Comparisons between datasets are listed in appendix table 2, and DEGs common to two datasets can be found in the first table of each tab. A table containing all FPKM values can be found in appendix table 3.

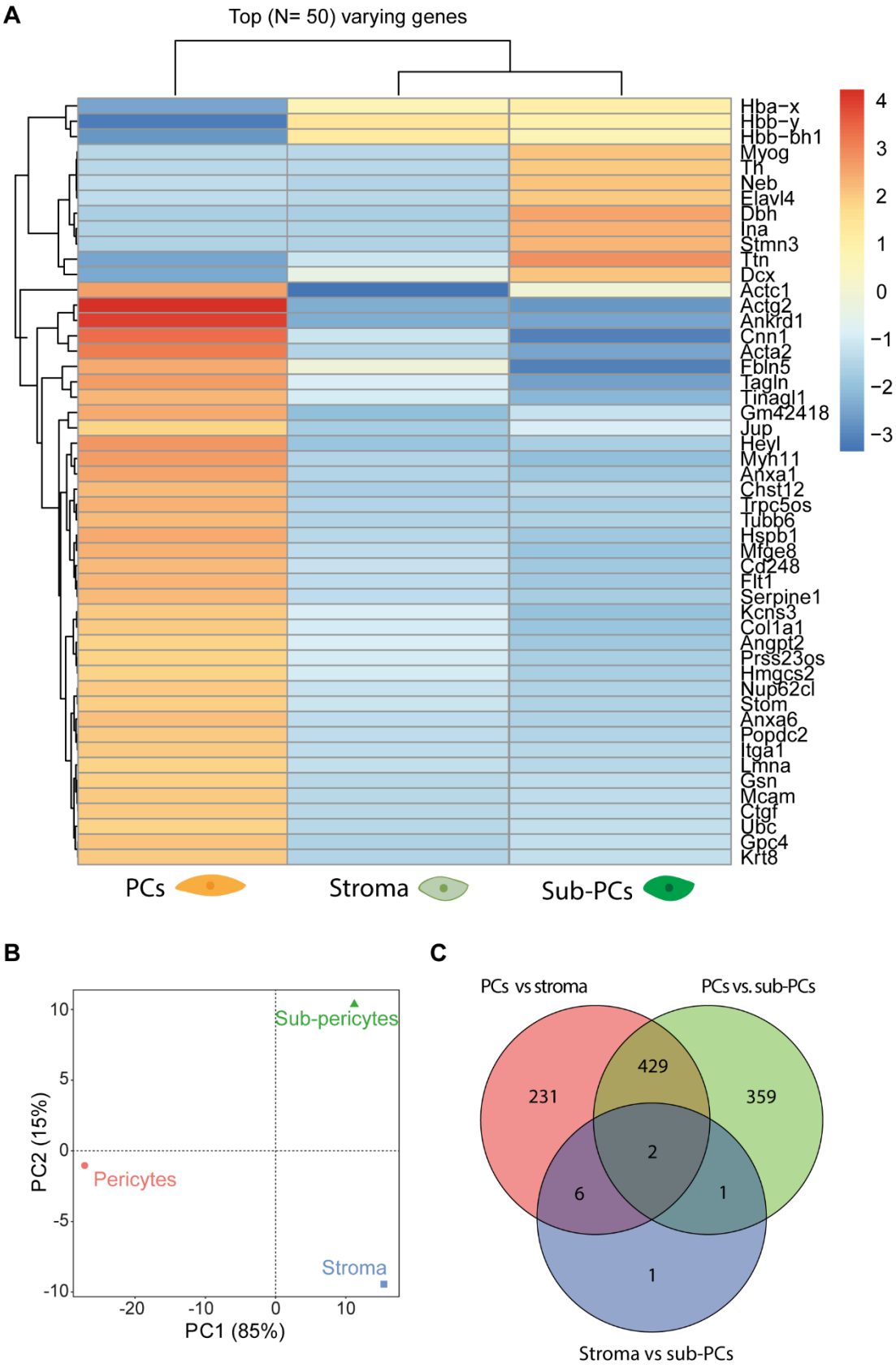

Figure 24. PCs, Sub-PCs and stroma are genetically distinct.

(A) Heatmap showing the top 50 differentially expressed genes and clustering between perivascular cell populations. (B) Principal component analysis (PCA) of gene expression, showing the two principal variance components. (C) Venn diagram showing numbers of differentially expressed genes (DEG) in comparisons of PCs vs Sub-PCs, PCs vs stroma and stroma vs sub-PCs. Total DEG is 1029 (see appendix tables 1 and 2 for gene lists). Note: these graphs were made by our collaborator H. van de Werken and adapted to this thesis by me.

3.3.4 Purified PCs from the midgestation AGM express expected genes

The isolation of perivascular cells described above was next validated by RNA sequencing analysis. An enrichment in several known pericyte-specific genes was found, as expected, in the PC population (Figure 25). Genes such as *pdgfrb*, NG2 (*Cspg4*) [180], CD146 (*Mcam*) [118,180], nestin (*nes*) [181], leptin receptor (*lepr*) [114], desmin (*Des*) and αSMA (*Acta2*) [182] were upregulated in the PC population compared to sub-PCs and stroma. Other perivascular cell marker expression, such as *Tbx18* [183] and *Gli1* [184] was higher in sub-pericytes and stromal cells than in pericytes (Figure 25).

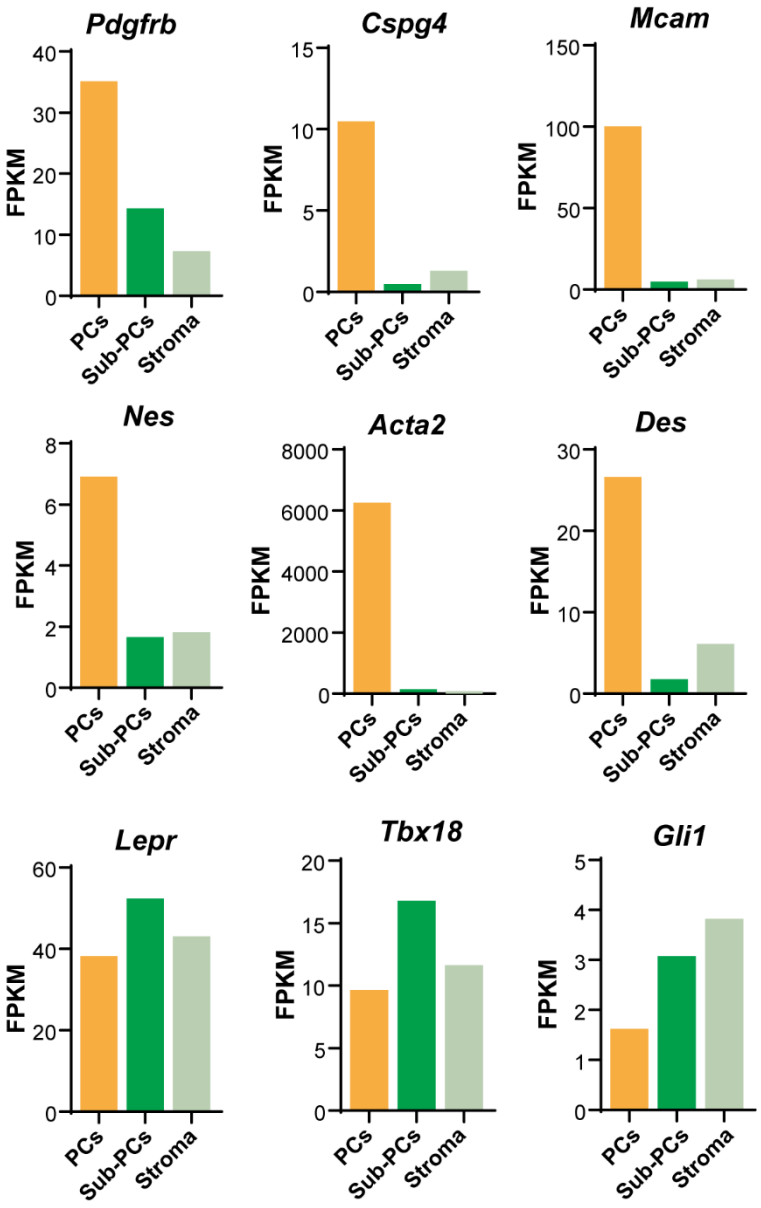

Figure 25. Pericyte-specific gene expression in E11 perivascular cells.
FPKM values for known PC/vSMC genes between the three perivascular cell populations, obtained by RNA sequencing. FPKM values were extracted from appendix table 3.

3.3.5 Midgestation PCs are enriched in genes involved in basement membrane formation

As expected, PCs were also found to express high levels of genes involved in basement membrane formation, such as calponin 1 (*Cnn1*), Collagens (*Col1a1, 4a1, 4a2*), vimentin (*Vim*), fibronectin 1 (*Fn1*) and procollagen C-endopeptidase enhancer (*Pcolce*) [185,186] (Figure 26).

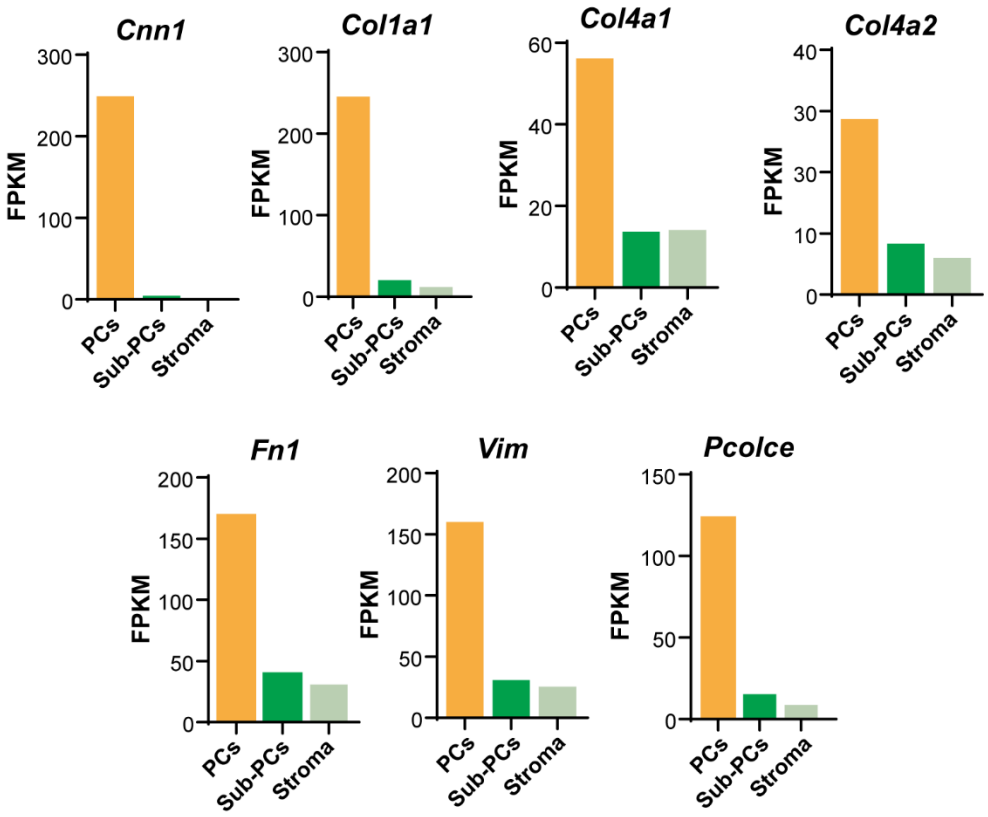

Figure 26. Basement membrane formation genes.
FPKM values for genes known to be involved in basement membrane formation between the three perivascular cell populations, obtained by RNA sequencing. FPKM values were extracted from appendix table 3.

3.3.6 DA midgestation pericytes are enriched in known HSC-niche genes

As perivascular cells were shown to support haematopoiesis in the adult BM, HSC-niche gene expression, reviewed in [107] was assessed. We found that PCs are enriched in several niche genes, such as *Cxcl12* [118,120,187], Jagged1 (*Jag1*) [117,118], N-Cadherin (*N-Cadh*) [118] (Figure 27). Other HSC-niche genes such as Angiopoietin1 (*Ang1*) [118,120] and Kit ligand or Scf (*Kitl*) [118,119] are higher in sub-pericytes and stroma than in pericytes (Figure 27), suggesting that these populations might also play a role in AGM haematopoiesis. Lastly, some genes that were also described in pericytes that support haematopoiesis in the BM, such as Adrenoceptor Beta 1 (*Adrb3*) [122] and osteopontin 3 (*Spp1*) [114,123] are lowly expressed in all three populations of perivascular stromal cells (appendix table 3).

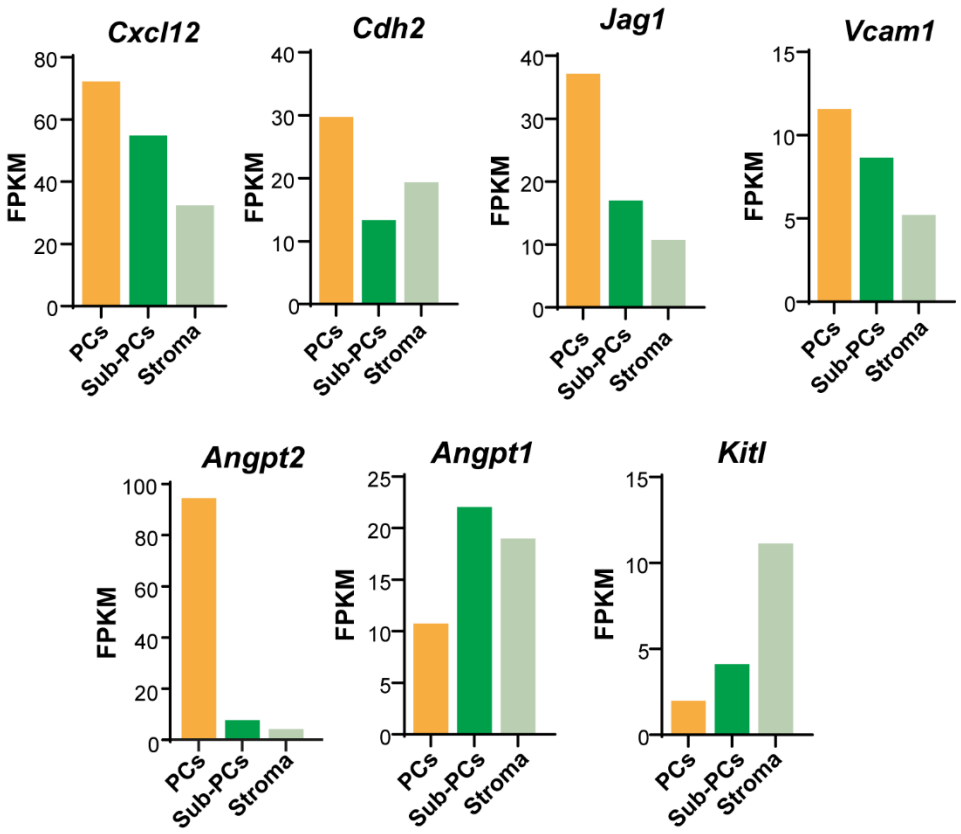

Figure 27. Adult BM HSC-niche genes.
FPKM values for known adult BM HSC-niche genes expressed by perivascular cells, obtained by RNA sequencing. FPKM values were extracted from appendix table 3.

3.4 Discussion

The main goal of this chapter was to characterise the heterogeneous HSC-generating niche both phenotypically and genetically, and to establish an isolation protocol for further analysis.

3.4.1 The midgestation HSC-generating niche is heterogeneous

HSC generation relies on signals from the AGM microenvironment. Stromal cells surrounding the dorsal aorta were shown to be required for HSC specification and generation [97], and can potentially be important for the support and maintenance of HSCs generated in this region [125,156,178]. This microenvironment is however heterogeneous, and little is known about the

types of cells present and the signals they produce. Understanding all the factors and cell types required for HSC generation in the AGM could provide important cues needed to generate and maintain HSCs in culture.

The main objective of this Chapter was to characterise the HSC-generating microenvironment, with a focus on the stromal cells surrounding the dorsal aorta. Three phenotypically distinct populations of perivascular stromal cells were defined at E10 and E11 based on immunohistochemistry by differential perivascular cell marker expression (NG2, αSMA and PDGFRβ) and absence of the endothelial marker CD31.

Pericytes (PCs) were defined as cells expressing NG2, αSMA and PDGFRβ, in close contact with the endothelium and embedded in a collagen IV+ basement membrane. Adjacent to PCs, a few layers of sub-PCs were shown to express PDGFRβ, but not NG2 nor αSMA. Surrounding sub-PCs, stromal cells that do not express any of these markers were found. NG2 and αSMA co-expression by cells surrounding the DA endothelium was previously reported between E10 and E14 [141], and more recently, PDGFRβ expression in these cells was also described [179]. Although PDGFRβ is also expressed around the cardinal veins, NG2+ αSMA+ PDGFRβ+ PCs can only be found around the DA. Interestingly, PDGFRβ was expressed in more cell layers on the aortic floor, where HSCs are born, suggesting a potential role for PDGFRβ signalling in AGM haematopoiesis. Whether NG2+ PDGFRβ+ PCs exist in other haematopoietic organs, such as the head, placenta, yolk sac and foetal liver during the two waves of embryonic haematopoietic cell generation remains to be determined.

The embryonic dorsal aorta is an organ undergoing constant growth and remodelling, and therefore, perivascular cells are continuously changing. Although the three perivascular cell populations described above were present at both E10 and E11 (time of HSC generation in the DA), at E9, NG2 expression was absent, and only a few cells were found to express αSMA, as previously reported [140,141]. After E11, the number of layers of PC/vSMCs surrounding the aorta increases as the aorta develops into a more mature

blood vessel [179]. Furthermore, although these three populations were defined based on NG2, αSMA and PDGFRβ, it is important to bear in mind that they can be even more heterogeneous. For instance, CD146, a membrane glycoprotein that mediates the interaction between pericytes and ECs [188], was found to be expressed by a subset of PCs, suggesting that PCs could be even further separated based on CD146 expression. CD146+NG2+ expression around the embryonic DA has been previously reported to mark immature vSMCs that gradually lose CD146 expression as they mature into aortic vSMCs [179]. Due to CD146 expression dynamics between E10 and E11, NG2 and PDGFRβ were preferentially used as markers to separate pericytes from sub-pericytes. It would be interesting however, to further separate PCs into CD146+ and CD146- at E10 and E11, and perform RNA sequencing to understand which, if not both populations play a role in HSC generation and/or maintenance.

A population of NG2+ cells was also detected around the notochord, which is not surprising, since NG2 (also known as neural/glial antigen 2) is a proteoglycan mainly found in cells of the developing and adult nervous system [189]. These cells did not express PDGFRβ, allowing for the separation between NG2+ cells around the notochord and those surrounding the dorsal aorta.

3.4.2 RNA sequencing analysis

Based on the expression of NG2 and PDGFRβ, and the absence of the haematopoietic and endothelial markers CD45, cKit and CD31, all three populations of perivascular cells were sorted for bulk RNA sequencing.

Clustering analysis found that PCs are transcriptomically more distinct than sub-PCs and stromal cells, with 791 DEG between PCs and Sub-PCs and 668 between PCs and stroma. Sub-PCs and stroma were only different by 10 genes. However, it is very likely that this is due to contamination of the stromal fraction by PDGFRβ+ cells, as seen by some *Pdgfrb* expression in the stromal fraction. This is probably due to the lack of stringency used on the gating

strategy to sort PDGFRβ+ and PDGFRβ- cells, as there is no clear separation between the two populations. PDGFRβ expression appears to be gradual according to flow cytometry and immunohistochemistry data, with higher PDGFRβ expression around the DA and CVs. Therefore, the differences in gene expression profile obtained between the two populations might be higher than what was obtained in this experiment. In addition, only one replicate was used for RNA sequencing, and therefore these data are only suggestive, and need to be confirmed with additional biological replicates.

3.4.2.1 Expected genes are found to be expressed in PCs

RNA sequencing data found several pericyte/vSMC-specific genes upregulated in the PC population, such as *Pdgfrb* (PDGFRβ), *Cspg4* (NG2), *Mcam* (CD146) and *Acta2* (αSMA), confirming our immunohistochemistry data and sorting strategy. Other pericyte/vSMC genes such as *Nestin* and *Desmin* were also upregulated (Figure 25). More recently, *Gli1* [184] and *Tbx18* [183] were proposed as novel pericyte markers in adult mice, but their expression was not specific to the E11 PC population, suggesting that they are not markers for AGM pericytes/vSMCs, but rather, for perivascular stromal cells around the AGM in general.

3.4.2.2 E11 PCs are enriched in basement membrane formation genes

One of the defining aspects of pericytes is their embedding in a basement membrane which is shared with the endothelium. The interaction between these two cell types was shown to regulate basement membrane assembly, which is produced by both pericytes and endothelial cells [185,186]. RNA sequencing data show that E11 PCs are highly enriched in genes involved in basement membrane formation (Figure 26). The presence of collagen IV was found surrounding the paired aortae of E9 embryos (Figure 21), before the onset of NG2, and was present in places where αSMA expression was absent, suggesting that it is either produced and deposited by ECs or PDGFRβ+ precursors of PCs that are found around the E9 aortae.

3.4.2.3 PCs are enriched in known HSC-supportive genes

In the adult BM of both mouse and human, HSCs maintenance and differentiation is controlled by the BM microenvironment [114–116], in particular by different populations of perivascular stromal cells, including pericytes. Interestingly, E11 PCs were enriched in several genes that have been described in various populations of perivascular cells that support BM haematopoiesis (reviewed in [107]).

For instance, CD146+ perivascular cells with HSC-niche activity *in vivo* and *ex vivo* were described around sinusoids and microvessels in the human adult [117,118,124] and foetal BM [117], as well as in white adipose tissue [117]. They were initially described and isolated in 2007 from human BM sinusoids, and shown to have the capacity to establish a heterotopic haematopoietic microenvironment when transplanted into immunodeficient mice [118]. These cells were shown to be osteoprogenitors, as they formed ossicles containing donor-derived bone and sinusoids upon transplantation, and recruited host-derived endothelial and haematopoietic cells. Adult BM CD146+ cells also expressed other pericyte markers such as *Cspg4*, *Acta2*, *Pdgfrb*, basement membrane formation genes, such as *Col1a1* and *Col1a2*, and haematopoietic niche-related transcripts, such as *Cxcl12* (CXC chemokine ligand, also known as SDF1), *Jagged-1* (Notch ligand), *Cdh2* (N-cadherin) and *Scf* (Kit ligand or *Kitl*). These molecules have been reported to maintain murine BM HSCs both *in vivo* and *in vitro* [119–121]. Our RNA sequencing data show that these transcripts are upregulated mainly in the PC population, (Figure 26 and*Figure 27*, Appendix table 3), with the exception of *Kitl* that was higher in the stroma than in the other two populations (but expressed in all three). *Kitl* expression has been previously reported in the entire sub-aortic mesenchyme and ECs, as well as in YS ECs and perivascular cells [155]. *Kitl* deletion was shown to reduce the numbers of YS EMP progenitors, as well as to impair the maturation and survival of pre-HSCs in the AGM [155]. Together, these data suggest that NG2- PDGFRβ- stromal cells might play a role in the maturation and maintenance of AGM HSCs via the expression of *Kitl*. This needs to be confirmed by selectively deleting *Kitl* in the different populations of perivascular

stromal cells. In addition, these CD146+ BM cells were shown to activate Notch signalling in HSPCs [118] via the expression of one of its ligands JAGGED-1, crucial for HSC generation in the AGM [190]. CXCL12 binds to CXCR4 in HSCs and promotes their homing to the BM and quiescence. Perivascular cells expressing high levels of *Cxcl12* (also known as CXCL12-abundant reticular cells, or CAR cells) were shown to be associated with quiescent HSCs in mouse BM sinusoids and endosteum [120,191]. CD146+ pericytes found in human white adipose tissue were found to differentiate into adipocytes and osteoblasts, and were shown to support HSC activity in co-cultures with cord blood HSCs through Jagged1/Notch signalling [117]. CD45+ cells taken from these co-cultures were shown to repopulate primary and secondary recipient immunodeficient mice. CD146+ pericytes were also found in foetal BM [117], and together with adipose tissue pericytes, they express *Nestin*, *Cxcl12*, and *Lepr*, which are markers that have been found in perivascular cells that have HSC niche activity in the BM [115,120,122]. These genes were upregulated in E11 AGM PCs (Figure 27), while *Lepr* was expressed by all three populations of perivascular cells (Figure 25). LepR+ cells were described around murine BM sinusoids, and were shown to be required for the maintenance of BM HSPCs and their retention in the BM [116], by secreting *Scf* [187].

Another HSC-niche population described in the adult BM with similar characteristics as E11 PCs were Nestin+ neural crest-derived MSCs found around arterioles near HSCs, adrenergic nerve fibres [114,115,122,123], and human foetal BM [123]. They were shown to express high levels of *Cxcl12*, *Adrb3* and *Agpt1* and support haematopoiesis [122]. These cells have a similar distribution to CAR cells [122]. Besides *Cxcl12* expression, E11 PCs were also enriched in *Agpt1* and *Nestin* (Figure 25 andFigure *27*). HSC numbers in the BM were shown to be reduced upon the depletion of Nestin+ cells, and their homing ability was also impaired when transplanted into Nestin+ depleted mice [122]. Within the Nestin+ MSC population, around 30% were shown to express NG2. Interestingly, deletion of *Cxcl12* from BM arteriolar NG2+ cells led to the reduction of HSCs in the BM, as well as a change in localisation [187],

suggesting that Nestin+ NG2+ MSCs are required for HSC maintenance. HSC-supporting capacity of the different perivascular cell populations needs to be further assessed, either by co-culturing AGM HSPCs with each population, or by deleting known HSC-niche genes in each population.

In addition to being components of the BM HSC niche, most of these populations showed MSC differentiation potential (osteogenic, adipogenic and chondrogenic). Interestingly, E11 AGM stromal cells were also shown to have MSC potential when cultured under different MSC conditions [127]. Other haematopoietic organs such as the YS, liver, umbilical and vitelline arteries were unable to differentiate into any of the 3 lineages [127]. It would be interesting to test the MSC potential of each individual perivascular stromal cell population described in this Chapter with differentiation assays *in vitro*.

Although the n number of this experiment was low (n=1), the data obtained by RNA sequencing was consistent with several other studies, both in embryonic and adult haematopoietic tissues, and the expression of some of these genes was confirmed by immunohistochemistry and flow cytometry.

Overall, several populations of perivascular cells with HSC niche activity have been described in the BM, many of which partially overlap. Most of the genes expressed by these cells were found to be upregulated in E11 AGM PCs, or expressed in all perivascular cell subsets identified in this Chapter, suggesting a putative role for the aortic mesenchyme in the support of HSC generation and/or maintenance in the AGM. This possible role needs to be further tested *in vitro* and *in vivo*, either by co-culturing PCs, sub-PCs and stroma together with HSPCs, or by specifically deleting certain genes such as *Kitl* or *Cxcl12* for example in perivascular cells of the AGM.

3.4.3 Nomenclature

Pericytes and vSMCs are called mural cells that function as regulators of vascular stability and blood vessel homeostasis. By definition, pericytes are cells surrounding microvessels (capillaries, postcapillary venules and terminal arterioles), although this has recently been questioned by the detection of

pericyte-like cells surrounding larger vessels [192]. The second characteristic defining pericytes, is that they are embedded in a basement membrane shared with endothelial cells. Pericytes and endothelial cells contact each other via openings in the basement membrane. It is however difficult to determine whether the basement membrane is shared by both pericytes and ECs during embryonic development, as the basement membrane is still being synthesised [193], and without the use of electron microscopy [194]. VSMCs on the other hand, surround larger vessels and arteries, are not in direct cell-cell contact with ECs, but are separated from the endothelium by a basement membrane, and in larger arteries, by the tunica intima [193]. In arterioles and venules, mural cells have intermediate properties between PCs and vSMCs. It has been suggested that vSMCs and PCs represent phenotypic variants of a continuous population of mural cells sharing the same lineage. This variation would reflect different subspecialisations in accordance with their location in the vascular system [195], as well a common origin [193,196]

Our study focuses on the embryonic aorta, where vascular remodelling takes place prior to maturation. At this stage, NG2+ αSMA+ PDGFRβ+ cells described in this chapter are similar to pericytes found in small vessels. However, due to αSMA expression and their localisation around a large vessel, it is possible that they are developing vSMCs. As the DA develops, additional αSMA+ layers can be found surrounding the endothelium from E12 onwards until it becomes a fully mature artery [179]. However, only NG2+ CD146+ cells surrounding the DA were shown to be aortic vSMC precursors (although morphologically similar to pericytes), and give rise to mature vSMCs surrounding the aorta. As only a subset of E11 PCs express CD146, it is unclear whether CD146- PCs also give rise to vSMCs in the adult aorta. The distinction between pericytes and vSMCs is often difficult, as there are currently no specific pericyte and vascular smooth muscle markers unique to each population. In addition, most markers have been described in the adult and developing brain, or at later stages in development, making it more difficult to determine the cell types present in the E10-E11 DA.

The main reason we called NG2+ PDGFRβ+ perivascular cells as pericytes, was due to their enrichment in HSC-niche genes described in pericytes and other perivascular cells in the adult BM. There have been no reports so far on vSMC support in haematopoiesis at any stage of development nor in the adult.

3.4.4 Conclusions and future work

To briefly summarise this Chapter, three phenotypically and genetically distinct populations of perivascular cells were detected around the midgestation DA: PCs, sub-PCs and stroma. All three were enriched in HSC-niche genes previously described in adult BM perivascular cells with MSC activity that are required for the maintenance of BM HSCs, suggesting a potential role in the haematopoietic AGM niche. To understand whether midgestation perivascular stromal cells support haematopoiesis, co-culture experiments of each perivascular population with HSCs need to be performed. Additionally, it would be interesting to test the differentiation potential of each population in the three MSC lineages, to better establish the relationship between AGM and BM perivascular cells, and link them to their HSC-support ability. Ideally, single cell RNA sequencing should be performed in E10 and E11 pericytes, to further dissect the heterogeneity of the HSC-generating niche. As HSC generation might not be exclusive to the AGM, it would also be interesting to determine whether these perivascular stromal cells are also present in the YS, PL and head.

Chapter 4 PDGFRβ signalling is required for AGM haematopoiesis

4.1 Introduction

In the previous chapter, PDGFRβ expression was detected in mesenchymal stromal cells surrounding the midgestation dorsal aorta, and PDGFRβ+ cells, in particular pericytes, were enriched in HSC-supportive genes previously described in the adult BM [107].

It has been suggested that during blood vessel formation and maturation, pericytes and vascular smooth muscle cells are first induced in a PDGF-B/PDGFRβ independent manner and subsequently require PDGFRβ signalling to migrate and proliferate as blood vessels develop [182]. Pericyte/vSMC induction is dependent on TGFβ signalling in mice [197], and more recently, Ando and colleagues showed that zebrafish peri-arterial naïve mesenchymal cells are induced by Notch signalling to become PDGFRβ+ mural cells [198]. Pericytes are then recruited along the developing blood vessel via PDGF-B/PDGFRβ signalling. ECs secrete PDGF-B, which binds to the extracellular matrix forming a gradient that allows pericyte/vSMC recruitment to the endothelial wall [158,199]. Morpholino knockdown of *pdgfrb* or dominant-negative *pdgfrb* expression in zebrafish was shown to reduce hematopoietic stem and progenitor cell formation in zebrafish, and PDGF-B overexpression enhanced HSPC numbers in the AGM [149]. In line with these data, it was further shown that PDGF signalling contributes to the HSC specification niche by directing neural crest cells to physically associate with HSC precursors and initiate the definitive haematopoietic programme in zebrafish [148]. Taken together, these data suggest a role for PDGFRβ in HSC specification and/or generation/maintenance. To understand whether PDGFRβ signalling plays a role in murine AGM haematopoiesis, we used a constitutive KO mouse model for PDGFRβ. PDGFRβ KO mice die at birth with haemorrhages, and show an abnormal kidney development due to the

absence of mesangial cells [157]. Some haematological defects such as thrombocytopenia and anaemia were also observed in these embryos. Interestingly, their overall development appears to be normal until E16 [142,157].

4.2 Hypothesis and aims

4.2.1 Hypothesis

PDGFRβ signalling is required for HSC generation in the dorsal aorta.

4.2.2 Aims

- Determine whether PDGFRβ deletion affects AGM haematopoiesis.
- Determine whether midgestation HSPCs are affected by PDGFRβ deletion.
- Understand whether PDGFRβ deletion affects pericyte recruitment to the dorsal aorta.
- Trace PDGFRβ-derived cells in haematopoietic organs.

4.3 Results

4.3.1 Validation of PDGFRβ KO mouse model

To validate PDGFRβ KO mouse model, immunohistochemistry was performed on E11 AGM cryosections (Figure 28). As expected, PDGFRβ expression was absent in PDGFRβ KO embryos, whereas several layers of PDGFRβ+ cells were found surrounding the WT dorsal aorta (Figure 28).

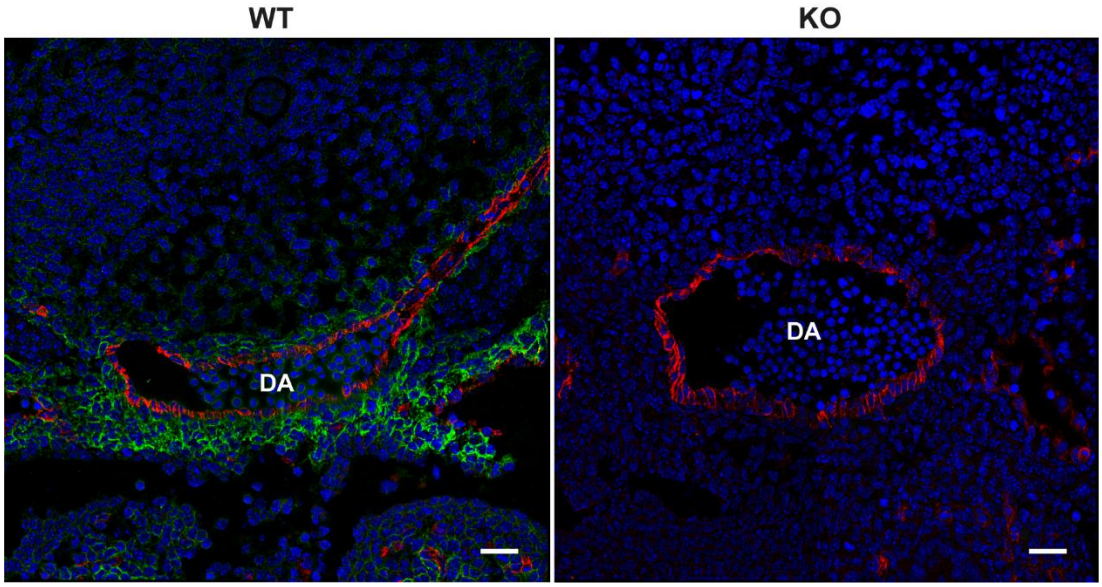

Figure 28. Validation of PDGFRβ KO mouse model.
Immunohistochemistry showing PDGFRβ+ cells (green) surrounding CD31+ endothelium (red) on an E11 WT embryo, and the absence of PDGFRβ+ cells in an E11 KO embryo. Scale bar: 20μm.

4.3.2 PDGFRβ deletion affects E11 AGM HSPCs

To understand whether PDGFRβ deletion affects midgestation haematopoiesis, haematopoietic progenitor assays (CFU-Cs) were performed on E10 and E11 mutant AGM cells. Full AGMs were dissociated and cultured in a methylcellulose medium containing factors that promote the growth of the HSPCs present in the tissue. After 10-12 days, colonies were counted and distinguished based on their morphology as shown below (Figure 29).

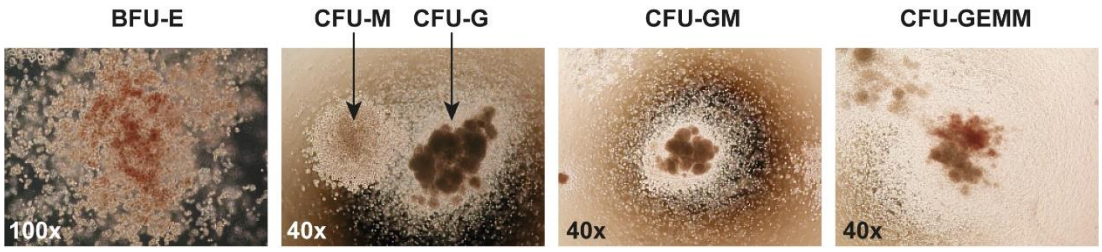

Figure 29. Haematopoietic progenitor assays.
Representative pictures of the different types of colonies found in haematopoietic progenitor assays after 10-12 days. BFU-E: burst-forming unit erythroid; CFU-G: colony-forming unit-granulocyte; CFU-M: colony-forming unit-macrophage; CFU-GM: colony-forming unit-granulocyte and macrophage; CFU-GEMM: colony-forming unit-granulocyte, erythrocyte, monocyte and megakaryocyte. Pictures adapted from

https://www.rndsystems.com/resources/protocols/mouse-colony-forming-cell-cfc-assay-using-methylcellulose-based-media.

No differences were found in the numbers of colonies at E10 (Figure 30A, Table 28). Interestingly, at E11, a significant decrease in the total number of colonies was found between WT, HET and KO embryos (Figure 30B, Table 29). The largest difference in colony numbers was found between WT and KO embryos, for all types of colonies (Table 29). Between WT and HET embryos, no differences were found in CFU-M, CFU-GM and the most immature CFU-GEMM colonies (Table 29). With the exception of the total number of colonies, there were no significant differences in individual colony numbers between HET and KO embryos (Table 29). These data suggest that PDGFRβ is required for E11 AGM haematopoiesis, but not before.

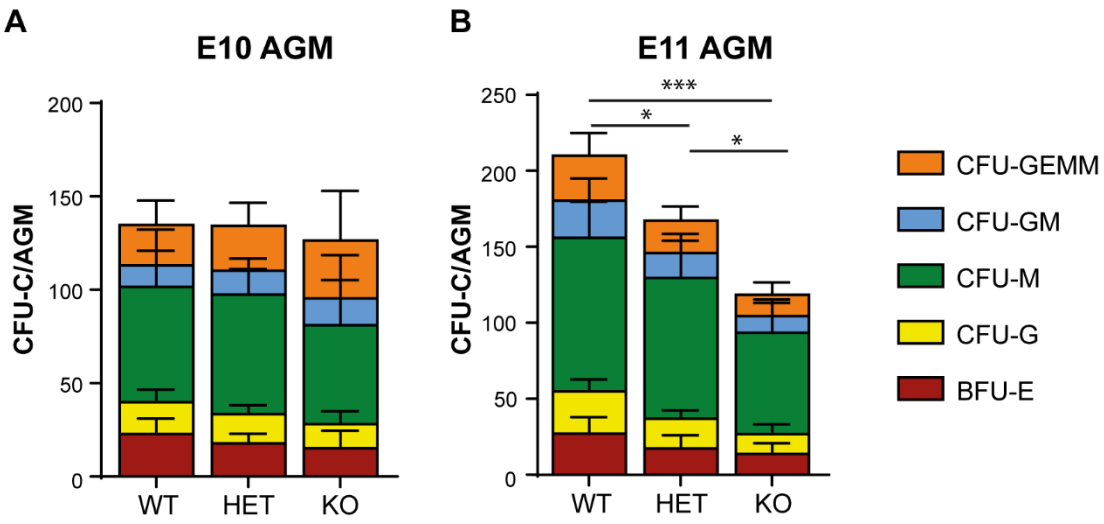

Figure 30. Haematopoietic progenitor assays in PDGFRβ mutant midgestation AGMs. Number of colonies (CFU-C) per PDGFRβ WT, HET and KO (A) E10 (29-34sp) and (B) E11 (43-45sp) AGMs. See Table 28 (E10) and Table 29 (E11) for complete CFU-C results.

The decline in HSPCs in the AGM in PDGFRβ KO embryos could be due to deficient production of HSPCs in other haematopoietic organs in the absence of PDGFRβ. To assess whether PDGFRβ is expressed in these organs, flow cytometry analysis of PDGFRβ was performed in the head, body/FL, PL and YS, from E8 to E11 (Figure 31A). PDGFRβ+ cells were detected in all organs (Figure 31). Due to the difficulty of dissecting the AGM and FL before E10, the

whole body, excluding the head, PL and YS was analysed. PDGFRβ was expressed in over 40% of the cells in the body/AGM and head between E8 and E11. Peak expression was detected in the body and AGM at E9-E10 (60.2%±2.31 and 55.3%±2.33, respectively), the head and the YS at E10 (52.4%±1.13 and 32.93%±4.83, respectively). The highest expression of PDGFRβ in the PL was found at E8 (12.67%±1.30). Foetal and maternal placenta were analysed together at this stage due to the difficulty in separating them, and therefore it is unclear whether these PDGFRβ+ cells are embryonic, maternal, or both. From E9 to E11, less than 5% of the cells in the placenta express PDGFRβ. At E10, 11.03%±1.44 of FL cells express PDGFRβ, and 22.87%±5.45 at E11 (Figure 31B).

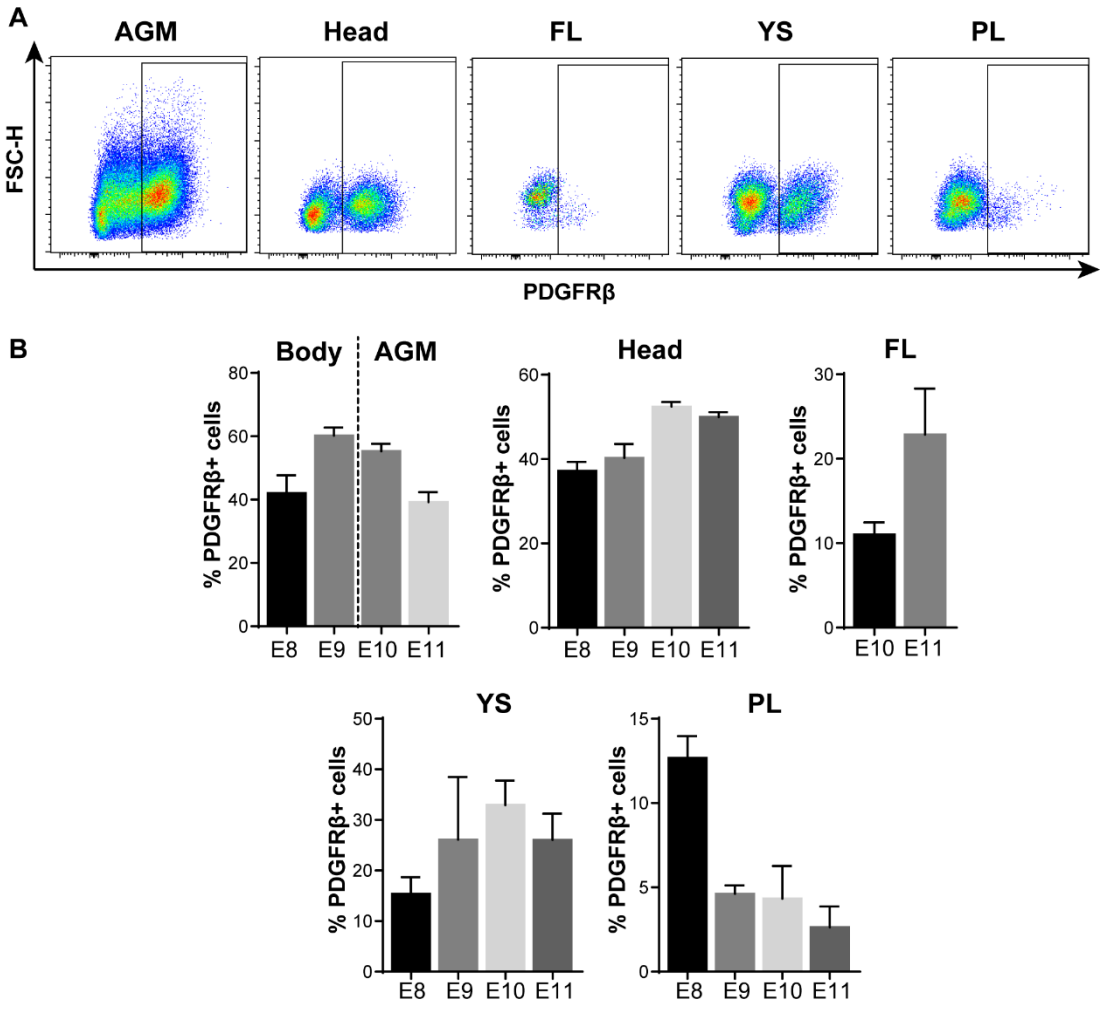

Figure 31. PDGFRβ is expressed in all E8-E11 haematopoietic organs.
(A) Example of the flow cytometry gating strategy used to analyse PDGFRβ expression in all organs. The percentage of PDGFRβ+ cells is assessed from single live cells (upper panel).

All plots shown are from E10 analyses. (B) Percentage of PDGFRβ+ cells in different BL6 haematopoietic organs from E8 to E11, determined by flow cytometry. E10 AGM, n=6; E11 AGM, n=7; n=3 for all the other organs and developmental stages.

As PDGFRβ expression was detected in all other haematopoietic organs, haematopoietic progenitor assays were also performed for E10 and E11 head, FL, PL and YS (Figure 32). Although no significant differences were detected in any of these organs (Figure 32, Table 28 andTable *29*), there seems to be a decrease in the total number of progenitors in the E10 KO head, compared to both WT and HET, as well as an increase in progenitors in the E10 PL (Figure 32, Table 28). At E11 (Figure 32, Table 29), no significant differences were found in CFU-C numbers in the head, PL, YS nor foetal liver (FL), with the exception of granulocyte progenitors (CFU-G) in the head (with a significant decrease between WT and HET, and HET and KO embryos), CFU-GM in the PL (with a significant decrease between WT and HET embryos), and in BFU-E in the YS (between WT and KO embryos). A significant difference was also detected in the number of macrophages in the FL, but the post-hoc test used is not sensitive enough to detect where the difference lies (Table 29).

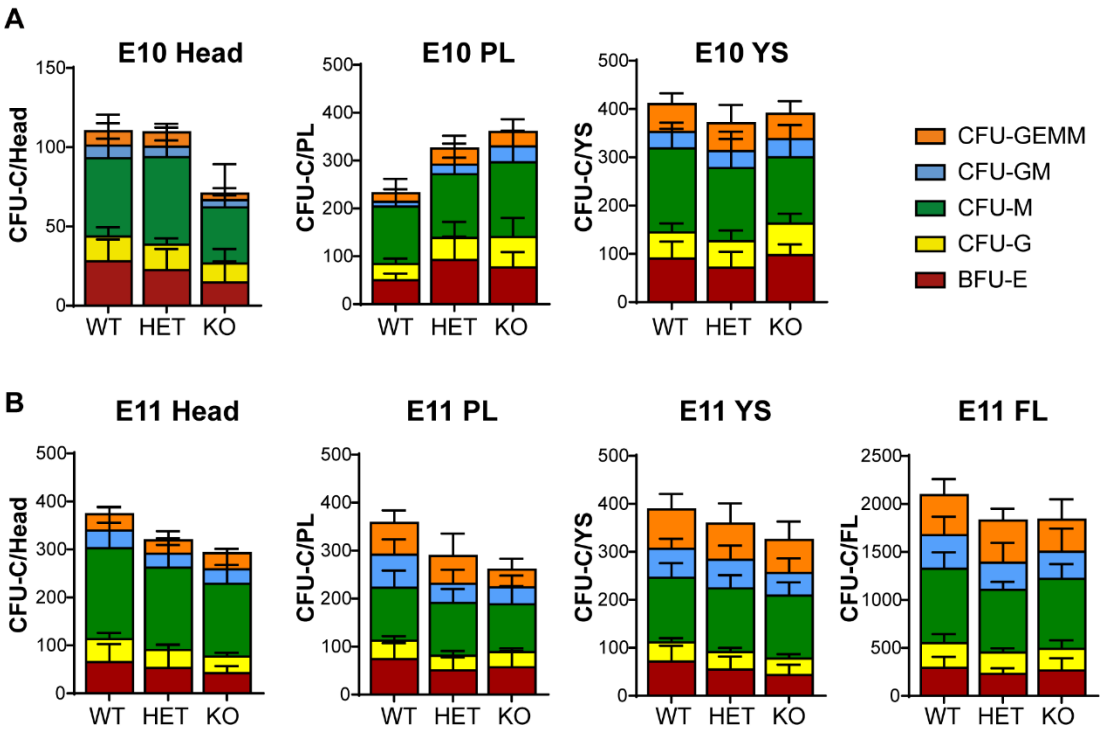

Figure 32. Haematopoietic progenitor assays in PDGFRβ mutant haematopoietic organs at midgestation.
CFU-C numbers per PDGFRβ WT, HET and KO (A) E10 (29-34sp) and (B) E11 (40-45sp) head, placenta (PL) and yolk sac (YS). See tables Table **28** (E10) and Table **29** (E11) for complete CFU-C results.

Table 28. Summary of CFU-C data for PDGFRβ WT, HET and KO E10 haematopoietic organs.
Haematopoietic progenitor assays were performed for E10 (29-34sp) AGM, head, foetal liver, placenta and yolk sac. The number of CFU-C per tissue (mean ± SD), fold changes of CFU-C numbers between WT, Het and KO mice, the statistical tests used, p values and multiple comparison tests are shown here. Ns: no significance.

				N			Average			Fold decrease							Multiple comparisons		
Tissue	Day	Somite pairs	CFU-type	WT	HET	KO	WT	HET	KO	WT vs HET	WT vs KO	HET vs KO	Statistical test	p-value		Post-hoc	WT vs HET	WT vs KO	Het vs KO
AGM	10	29-34	BFU-E	7	27	3	22.71	17.74	15.00	1.28	1.51	1.18	1-way ANOVA	0.1145	ns	Tukey's	ns	ns	ns
			CFU-G				17.00	15.59	13.00	1.09	1.31	1.20	1-way ANOVA	0.5749	ns	Tukey's	ns	ns	ns
			CFU-M				61.86	64.04	53.00	0.97	1.17	1.21	1-way ANOVA	0.6564	ns	Tukey's	ns	ns	ns
			CFU-GM				11.43	12.89	14.33	0.89	0.80	0.90	1-way ANOVA	0.815	ns	Tukey's	ns	ns	ns
			CFU-GEMM				21.71	24.00	31.00	0.90	0.70	0.77	Kruskal-Wallis	0.7387	ns	Dunn's	ns	ns	ns
			Total				134.71	134.26	126.33	1.00	1.07	1.06	1-way ANOVA	0.9569	ns	Tukey's	ns	ns	ns
Head	10	29-34	BFU-E	7	27	3	28.00	22.44	14.67	1.25	1.91	1.53	Kruskal-Wallis	0.304	ns	Dunn's	ns	ns	ns
			CFU-G				15.67	16.15	12.00	0.97	1.31	1.35	1-way ANOVA	0.373	ns	Tukey's	ns	ns	ns
			CFU-M				49.33	55.19	35.33	0.89	1.40	1.56	1-way ANOVA	0.2826	ns	Tukey's	ns	ns	ns
			CFU-GM				8.00	6.52	4.67	1.23	1.71	1.40	Kruskal-Wallis	0.4811	ns	Dunn's	ns	ns	ns
			CFU-GEMM				9.00	9.11	4.00	0.99	2.25	2.28	Kruskal-Wallis	0.2554	ns	Dunn's	ns	ns	ns
			Total				110.00	109.41	70.67	1.01	1.56	1.55	1-way ANOVA	0.2519	ns	Tukey's	ns	ns	ns
PL	10	29-34	BFU-E	5	26	3	50.00	92.31	76.67	0.54	0.65	1.20	1-way ANOVA	0.1646	ns	Tukey's	ns	ns	ns
			CFU-G				34.00	46.15	63.33	0.74	0.54	0.73	Kruskal-Wallis	0.5557	ns	Dunn's	ns	ns	ns
			CFU-M				120.00	133.08	156.67	0.90	0.77	0.85	Kruskal-Wallis	0.4175	ns	Dunn's	ns	ns	ns
			CFU-GM				10.00	20.00	33.33	0.50	0.30	0.60	Kruskal-Wallis	0.0995	ns	Dunn's	ns	ns	ns
			CFU-GEMM				18.00	33.46	30.00	0.54	0.60	1.12	Kruskal-Wallis	0.5791	ns	Dunn's	ns	ns	ns
			Total				232.00	325.00	360.00	0.71	0.64	0.90	Kruskal-Wallis	0.4289	ns	Dunn's	ns	ns	ns
YS	10	29-34	BFU-E	7	27	4	90.00	71.48	97.50	1.26	0.92	0.73	1-way ANOVA	0.1911	ns	Tukey's	ns	ns	ns
			CFU-G				54.29	55.19	65.00	0.98	0.84	0.85	1-way ANOVA	0.6748	ns	Tukey's	ns	ns	ns
			CFU-M				174.29	151.11	137.50	1.15	1.27	1.10	1-way ANOVA	0.6542	ns	Tukey's	ns	ns	ns
			CFU-GM				34.29	35.19	37.50	0.97	0.91	0.94	Kruskal-Wallis	0.97	ns	Dunn's	ns	ns	ns
			CFU-GEMM				57.14	57.78	52.50	0.99	1.09	1.10	Kruskal-Wallis	0.9716	ns	Dunn's	ns	ns	ns
			Total				410.00	370.74	390.00	1.11	1.05	0.95	1-way ANOVA	0.8235	ns	Tukey's	ns	ns	ns

Table 29. Summary of CFU-C data for PDGFRβ WT, HET and KO E11 haematopoietic organs.

Haematopoietic progenitor assays were performed for E11 (40-45sp) AGM, head, foetal liver, placenta and yolk sac. The number of CFU-C per tissue (mean ± SD), fold changes of CFU-C numbers between WT, Het and KO mice, the statistical tests used, p values and multiple comparison tests are shown here. Significant differences are indicated with asterisks: *: $p<0.05$; ** $p<0.01$; ***: $p<0.001$; ns: no significance.

				N			Average			Fold decrease							Multiple comparisons		
Tissue	Day	Somite pairs	CFU-type	WT	HET	KO	WT	HET	KO	WT vs HET	WT vs KO	HET vs KO	Statistical test	p-value		Post-hoc	WT vs HET	WT vs KO	Het vs KO
AGM	11	40-45	BFU-E	14	17	8	27.50	17.59	14.00	1.56	1.96	1.26	1-way ANOVA	0.0042	**	Tukey's	*	**	ns
			CFU-G				28.43	19.94	13.25	1.43	2.15	1.50	Kruskal-Wallis	0.0002	***	Dunn's	*	***	ns
			CFU-M				102.64	94.24	67.88	1.09	1.51	1.39	1-way ANOVA	0.0171	*	Tukey's	ns	*	ns
			CFU-GM				24.93	16.71	11.13	1.49	2.24	1.50	Kruskal-Wallis	0.0254	*	Dunn's	ns	*	ns
			CFU-GEMM				30.14	21.53	14.25	1.40	2.12	1.51	1-way ANOVA	0.0129	*	Tukey's	ns	*	ns
			Total				213.64	170.00	120.50	1.26	1.77	1.41	1-way ANOVA	0.0002	***	Tukey's	*	***	*
Head	11	40-45	BFU-E	14	18	7	65.00	53.06	42.29	1.23	1.54	1.25	Kruskal-Wallis	0.5005	ns	Dunn's	ns	ns	ns
			CFU-G				48.07	37.50	34.71	1.28	1.38	1.08	1-way ANOVA	0.013	*	Tukey's	*	*	ns
			CFU-M				189.71	171.61	151.71	1.11	1.25	1.13	1-way ANOVA	0.5263	ns	Tukey's	ns	ns	ns
			CFU-GM				36.50	28.83	30.00	1.27	1.22	0.96	1-way ANOVA	0.4112	ns	Tukey's	ns	ns	ns
			CFU-GEMM				34.14	28.11	33.43	1.21	1.02	0.84	1-way ANOVA	0.534	ns	Tukey's	ns	ns	ns
			Total				373.43	319.11	292.14	1.17	1.28	1.09	Kruskal-Wallis	0.213	ns	Dunn's	ns	ns	ns
FL	11	40-45	BFU-E	14	17	7	292.86	229.41	265.71	1,28	1.10	0.86	Kruskal-Wallis	0.3395	ns	Dunn's	ns	ns	ns
			CFU-G				258.57	224.71	225.71	1.15	1.15	1.00	Kruskal-Wallis	0.8322	ns	Dunn's	ns	ns	ns
			CFU-M				774.29	650.59	728.57	1.19	1.06	0.89	Kruskal-Wallis	0.0361	*	Dunn's	ns	ns	ns
			CFU-GM				350.00	284.71	282.86	1.23	1.24	1.01	Kruskal-Wallis	0.215	ns	Dunn's	ns	ns	ns
			CFU-GEMM				417.14	438.82	334.29	0.95	1.25	1.31	1-way ANOVA	0.3418	ns	Tukey's	ns	ns	ns
			Total				2092.86	1828.24	1837.14	1.14	1.14	1.00	Kruskal-Wallis	0.1863	ns	Dunn's	ns	ns	ns
PL	11	40-45	BFU-E	13	18	7	73.92	50.78	56.86	1.46	1.30	0.89	1-way ANOVA	0.1228	ns	Tukey's	ns	ns	ns
			CFU-G				38.23	30.33	31.57	1.26	1.21	0.96	1-way ANOVA	0.0825	ns	Tukey's	ns	ns	ns
			CFU-M				110.38	109.89	99.71	1.00	1.11	1.10	1-way ANOVA	0.7581	ns	Tukey's	ns	ns	ns
			CFU-GM				69.00	39.89	35.43	1.73	1.95	1.13	Kruskal-Wallis	0.0291	*	Dunn's	*	ns	ns
			CFU-GEMM				66.23	58.06	37.14	1.14	1.78	1.56	1-way ANOVA	0.2594	ns	Tukey's	ns	ns	ns
			Total				357.77	288.94	281.14	1.24	1.27	1.03	Kruskal-Wallis	0.1231	ns	Dunn's	ns	ns	ns
YS	11	40-45	BFU-E	7	27	4	71.36	54.83	43.63	1.30	1.64	1.26	Kruskal-Wallis	0.0428	*	Dunn's	ns	*	ns
			CFU-G				40.21	36.39	33.88	1.11	1.19	1.07	Kruskal-Wallis	0.2351	ns	Dunn's	ns	ns	ns
			CFU-M				134.29	132.67	131.38	1.01	1.02	1.01	1-way ANOVA	0.9724	ns	Tukey's	ns	ns	ns
			CFU-GM				60.79	59.50	47.00	1.02	1.29	1.27	1-way ANOVA	0.4766	ns	Tukey's	ns	ns	ns
			CFU-GEMM				81.93	75.56	68.88	1.08	1.19	1.10	1-way ANOVA	0.7383	ns	Tukey's	ns	ns	ns
			Total				388.57	358.94	324.75	1.08	1.20	1.11	1-way ANOVA	0.0934	ns	Tukey's	ns	ns	ns

Although HSPCs are affected in the E11 AGM, transplantations need to be performed to understand whether HSCs are affected. For this, E11 WT, HET and KO AGMs were transplanted into sub-lethally irradiated recipients, together with BM helper cells (Figure 33A). To detect and distinguish cells from donors and recipients, the Ly5.1 (CD45.1) and Ly5.2 (CD45.2) isoform system was used. AGM cells express the Ly5.2 isoform, BM helper cells express Ly5.1, and the recipients' blood cells express both Ly.1 and Ly.2 on their surface (Figure 33B).

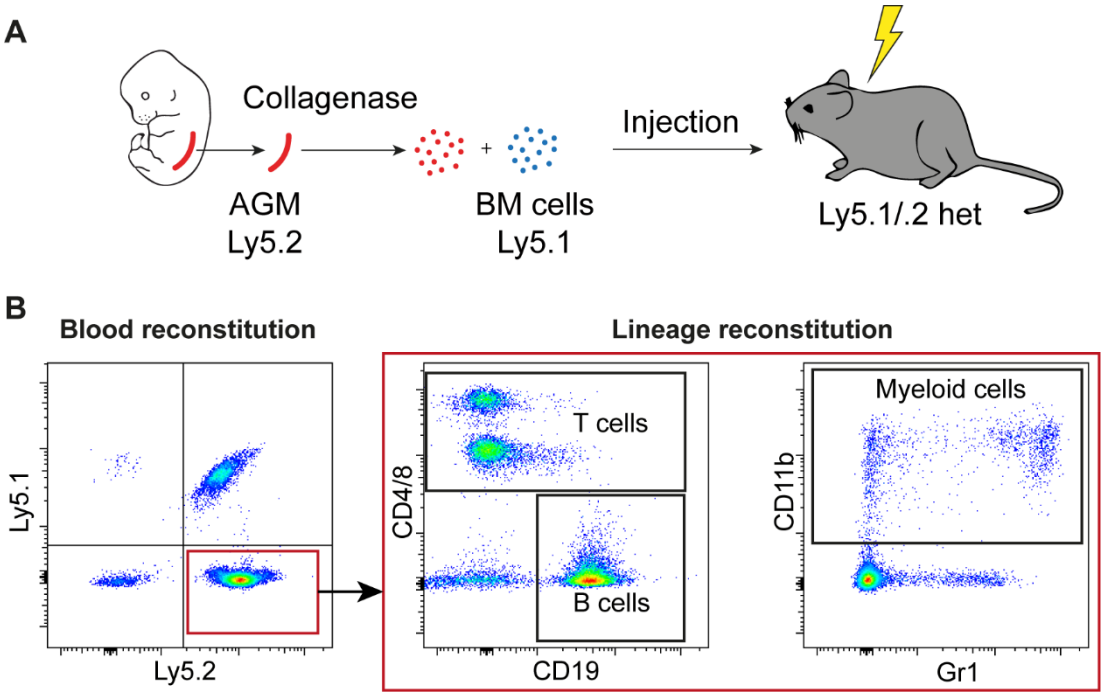

Figure 33. AGM transplantations and peripheral blood analysis.
(A) Schematic representation of the transplantation procedure for mutant AGMs. AGMs (Ly5.2) cells were injected together with Ly5.1 homozygous BM helper cells into sub-lethally irradiated Ly5.1/.2 heterozygous recipients. (B) Gating strategy used to assess the level of reconstitution 4 months after transplantation. After selecting for single live cells, the percentage of donor cells could be assessed by the expression of Ly5.2 and absence of Ly5.1. From Ly5.1- Ly5.2+ donor cells, lymphoid (CD4/8+ T cells, CD19+ B cells) and myeloid (CD11b+ and Gr1) reconstitution was also assessed.

Peripheral blood was analysed for the presence of donor Ly5.1- Ly5.2+ cells at 4 months, and mice were considered positively reconstituted, when the percentage of donor chimerism was above 4%. Although the number of reconstituted mice was generally low after 4 months in the control group (1

mouse reconstituted/ 5 transplanted) (Figure 34), KO AGMs failed to reconstitute primary recipients, suggesting that the deletion of PDGFRβ affects HSCs. Lineage reconstitution was assessed among positively reconstituted mice, and no differences were found in lineage reconstitution potential (not shown).

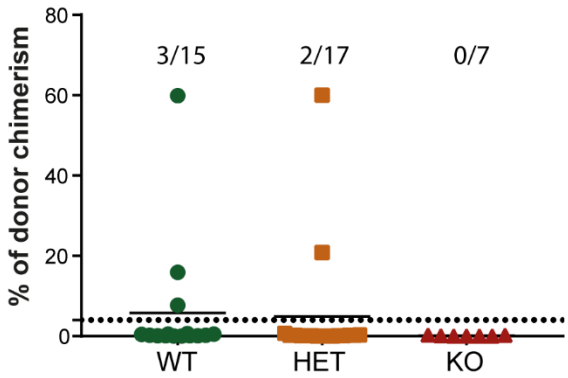

Figure 34. Blood reconstitution analysis 16 weeks after primary transplantations.
Analysis of long-term reconstitution potential 4 months after E11 AGM transplantation into sub-lethally irradiated recipients. Each data point represents one mouse injected with 1 embryo equivalent. Mice are reconstituted when >4% donor cells are found in the host peripheral blood. Numbers of reconstituted mice/number of transplanted mice are given for each group.

4.3.3 PDGFRβ deletion alters pericyte phenotype but does not affect DA integrity

One possible explanation for the reduction in HSPC numbers in the AGM of PDGFRβ KO embryos is a leakage in the dorsal aorta (DA), as PDGF-B/PDGFRβ signalling is required for blood vessel integrity via the recruitment of pericytes to the endothelial wall [182]. No morphological differences were observed between WT and KO whole E10.5 embryos (Figure 35A). Whole-mount immunostainings for CD31, αSMA, NG2 and cKit were next performed on E10.5 WT and KO DAs (Figure 35B, C). The integrity of the DA was not impaired, as seen by normal aortic morphology and CD31 expression in the KO compared to the WT (Figure 35B, C). NG2+ αSMA+ perivascular cells are still present around the endothelium, suggesting that PDGF-B/PDGFRβ signalling is not required for pericyte recruitment to the DA. Interestingly, NG2

expression is lower in the KO DA compared to the WT, while αSMA expression is higher, especially near the vitelline artery (VA). These results suggest that pericytes are differentiating towards more mature vSMCs and possibly proliferating (Figure 35B). Although cKit+ haematopoietic clusters were detected in both WT and KO DAs, clusters appear to be larger in the KO. Importantly, no leakage of cKit+ cells from the DA was observed in KO embryos (Figure 35C).

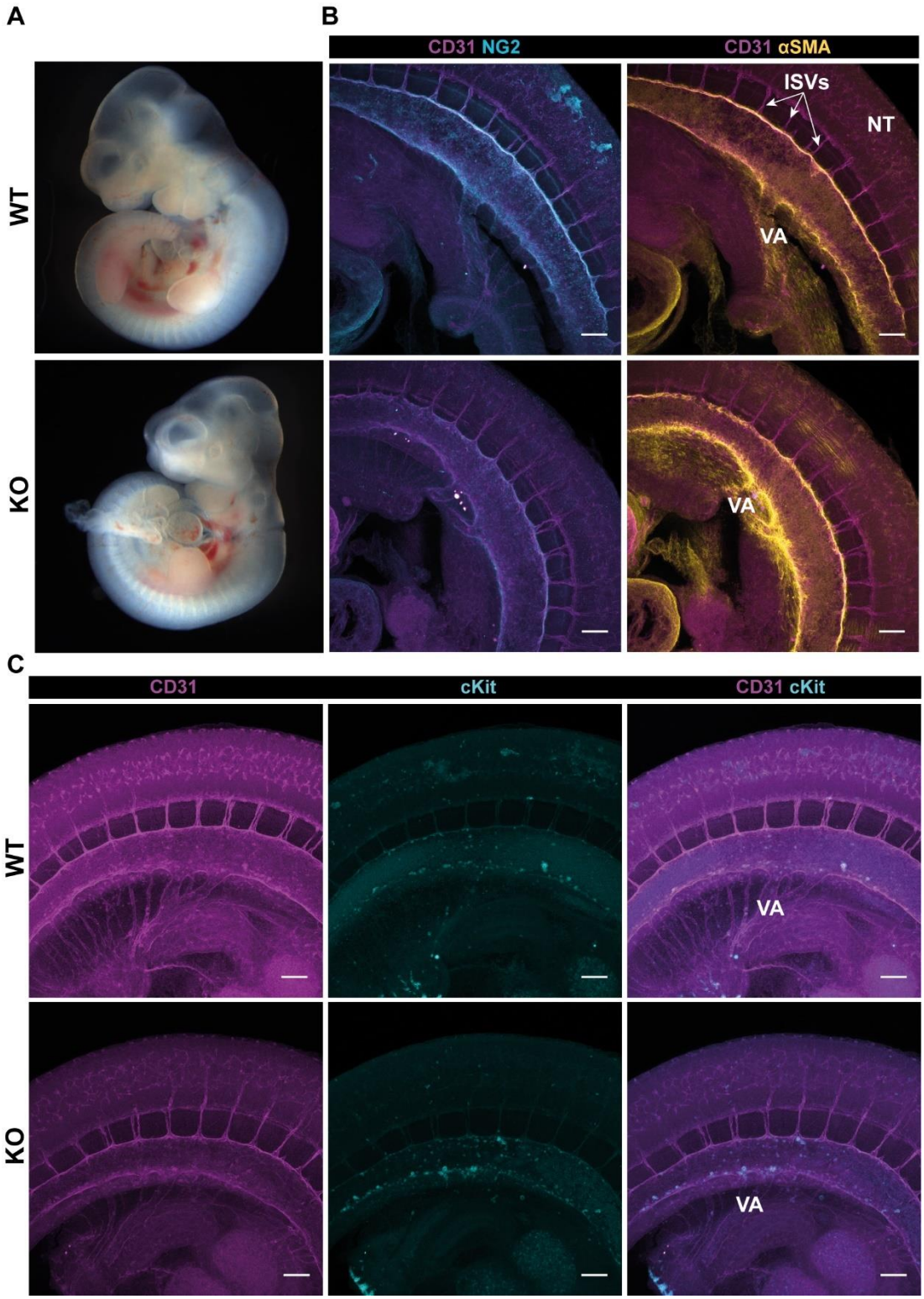

Figure 35. PDGFRβ deletion leads to phenotypic changes in pericytes.
(A) Brightfield images of WT and KO E10.5 embryos. (B, C) Confocal images of whole-mount immunostainings of WT and KO E10.5 DAs stained with (B) NG2 (cyan), αSMA (yellow) and CD31 (magenta), and (C) cKit (cyan) and CD31 (magenta). ISV: intersomitic vessels; NT: neural tube; VA: vitelline artery. Scale bars: 100µm.

Immunohistochemistry was also performed on PDGFRβ WT and KO cryosections, to see whether PDGFRβ deletion leads to changes in the presence or cell distribution of the different populations of perivascular cells (Figure 36-Figure *38*). Confirming the 3D-whole mount immunostaining data (Figure 35B), NG2+ cells are still present around the CD31+ endothelium in both PDGFRβ WT and KO DAs, and NG2 expression is lower in the KO than in the WT. NG2 expression around the notochord appears to be unchanged (Figure 36).

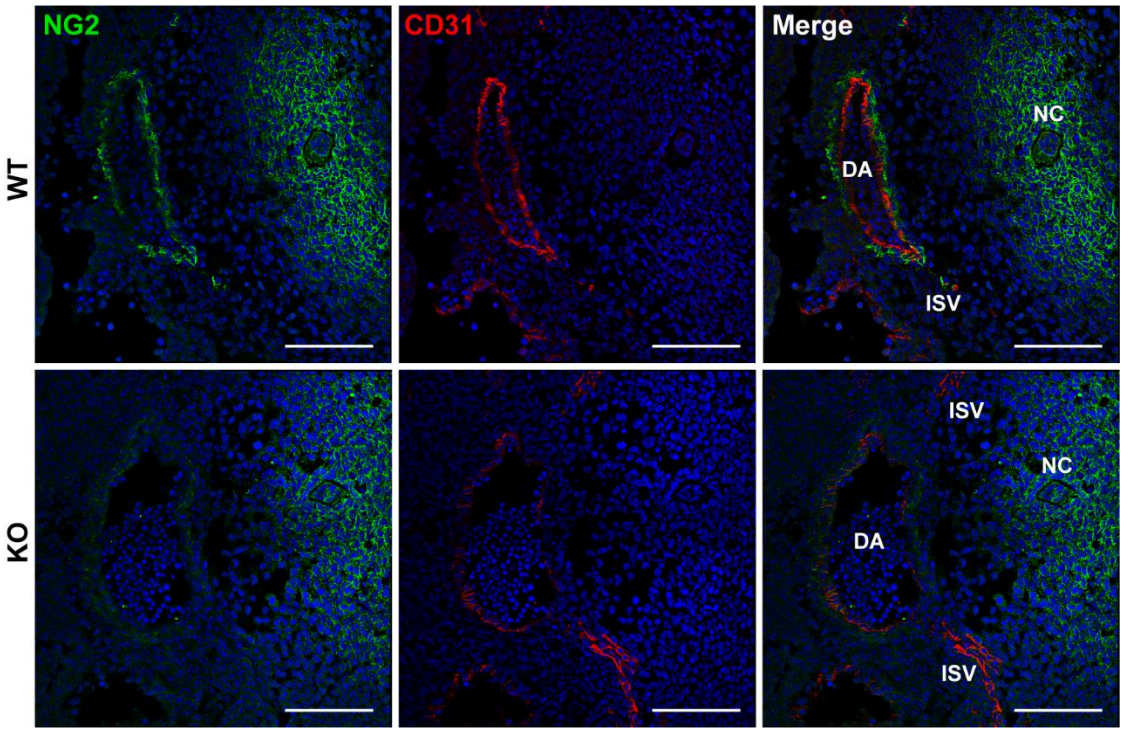

Figure 36. NG2 expression is reduced in PDGFRβ KO embryos.
Immunohistochemistry on PDGFRβ WT and KO E11 cryosections, stained with NG2 (green) and CD31 (red). Nuclei were counterstained with DAPI. ISV: intersomitic vessel; NC: notochord. The dorsal side of the DA is on the right, and the ventral on the left. Scale bars: 100µm.

Immunostaining with αSMA and NG2 in E11 PDGFRβ WT and KO embryos shows a higher number of αSMA+ cell layers around the aorta in KO embryos (Figure 37), confirming the data obtained by whole mount immunostaining (Figure 35B).

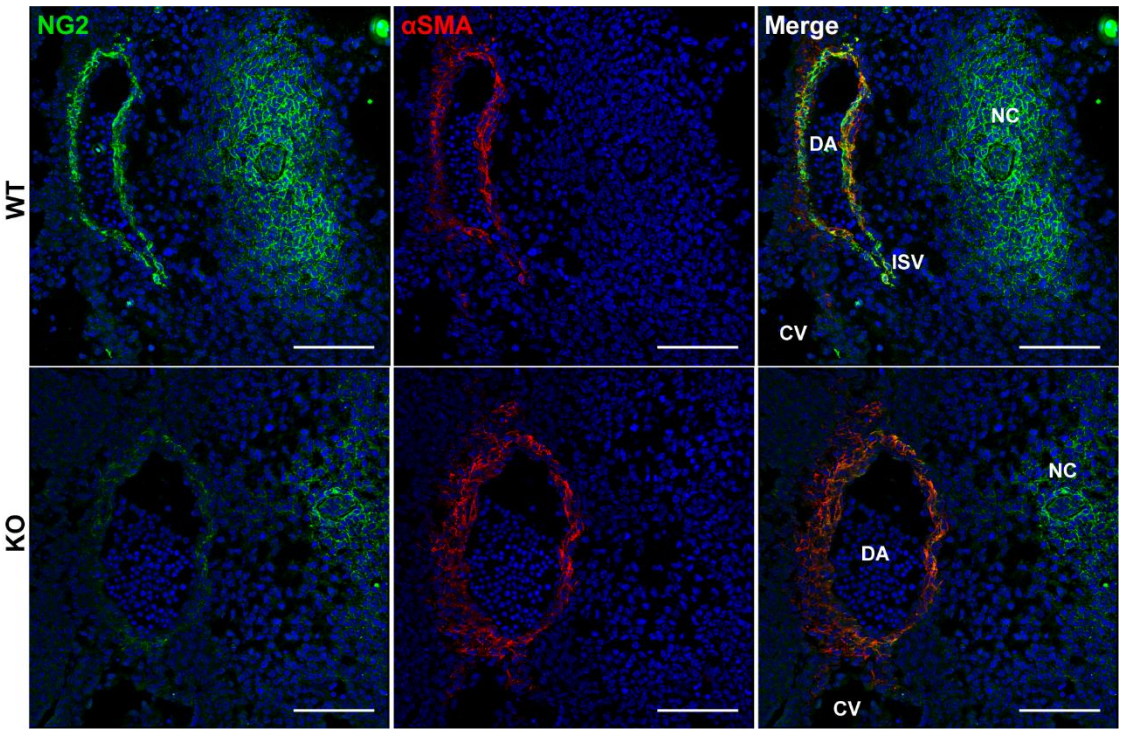

Figure 37. Increase in the number of αSMA+ layers surrounding the DA of PDGFRβ KO embryos.
Immunohistochemistry on PDGFRβ WT and KO E11 cryosections stained with NG2 (green) and αSMA (red). Nuclei were counterstained with DAPI. ISV: intersomitic vessel; NC: notochord. The dorsal side of the DA is on the right, and the ventral on the left.

No differences were found in CD146 expression between PDGFRβ WT and KO E11 embryos, with both the endothelial and pericyte layers expressing CD146 (Figure 38).

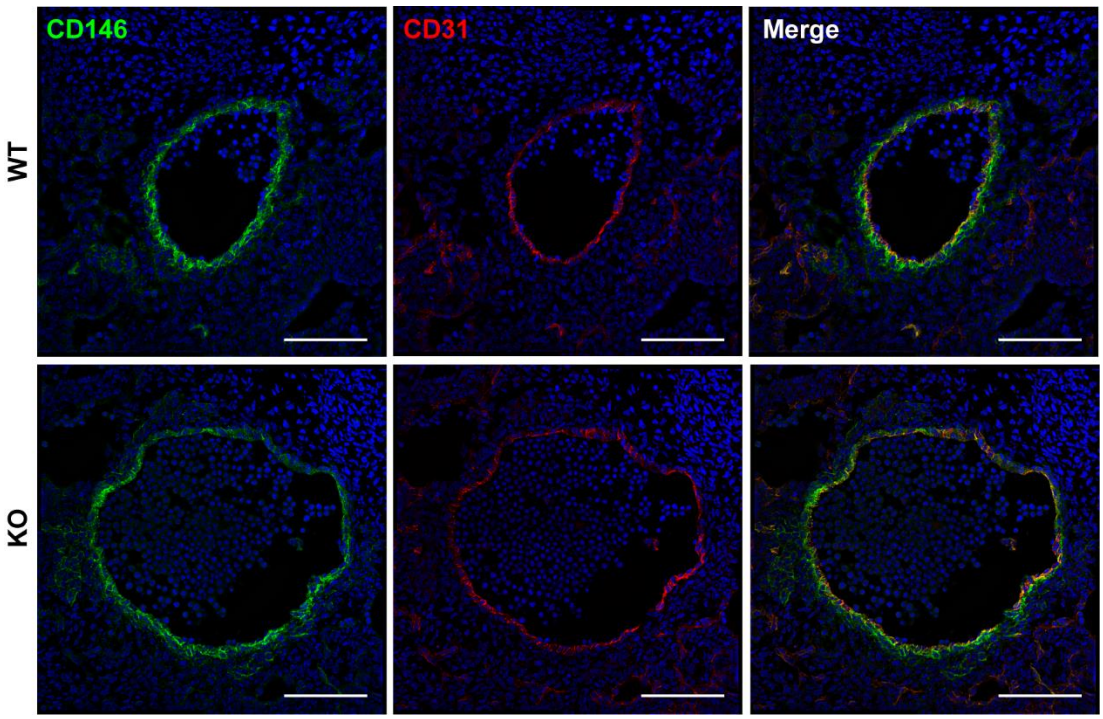

Figure 38. CD146+ cells distribution is not affected by PDGFRβ deletion.
Immunohistochemistry on PDGFRβ WT and KO E11 cryosections, stained with CD146 (green) and CD31 (red). Nuclei were counterstained with DAPI. ISV: intersomitic vessel; NC: notochord.

4.3.4 Characterisation of AGM cell populations in PDGFRβ mutants by flow cytometry.

Flow cytometry analyses were next performed on PDGFRβ;Runx1-IRES-GFP E10 and E11 AGMs, to determine whether the percentages of different cell populations in the AGM, including HECs (ECs expressing Runx1) were altered upon PDGFRβ deletion (Figure 39-Figure *42*). Single live cells were analysed for the expression of different markers such as αSMA, NG2, CD31, CD45, cKit, PDGFRβ and Runx1-GFP at E10 (Figure 39) and E11 (Figure 40). At E10, no significant differences were found in αSMA expression between PDGFRβ WT and KO embryos, although an increase can be observed in the KO (Figure 39A). In addition, a significant decrease in NG2 expression was detected in NG2+ cells (Figure 39B). Together, these results support the observations made in the E10.5 whole-mounts (Figure 39B). As expected, no PDGFRβ+ cells were found in KO embryos. In addition, no differences were found in CD31+, CD45+, cKit+ nor Runx1-GFP+ cell percentages in mutant embryos.

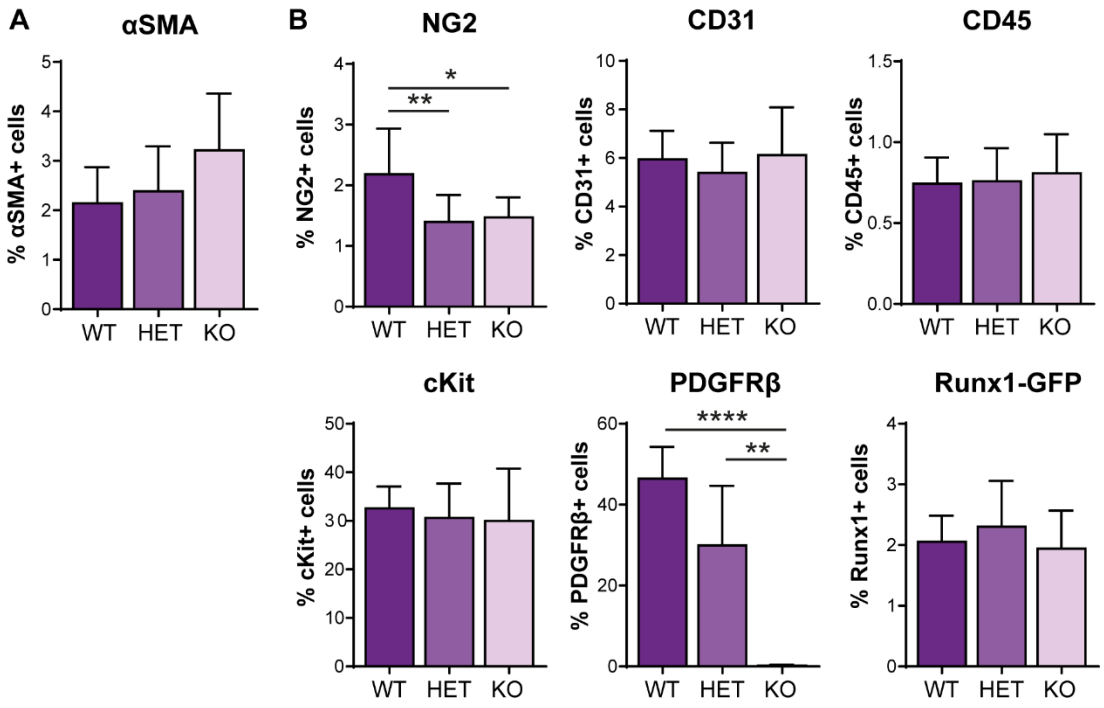

Figure 39. Flow cytometry analysis of single AGM cell populations in E10 PDGFRβ mutants.
(A) Percentage of αSMA+ single viable cells in PDGFRβ WT(n=4), HET (n=7), KO (n=5) E10 (31-34sp) AGMs (B) Percentage of NG2+, CD31+, CD45+, cKit+, PDGFRβ+ and Runx1-GFP+ single viable cells in WT (n=6), HET (n=17) and KO (n=8) PDGFRβ;Runx1-GFP per E10 AGM (33-36sp). Error bars: SD. * p<0.05; ** p<0.01; **** p<0.0001.

At E11, no differences were found in any single population of cells, with the exception of PDGFRβ (Figure 40). The decrease in NG2+ cells at E10 (Figure 39B) was not observed at E11.

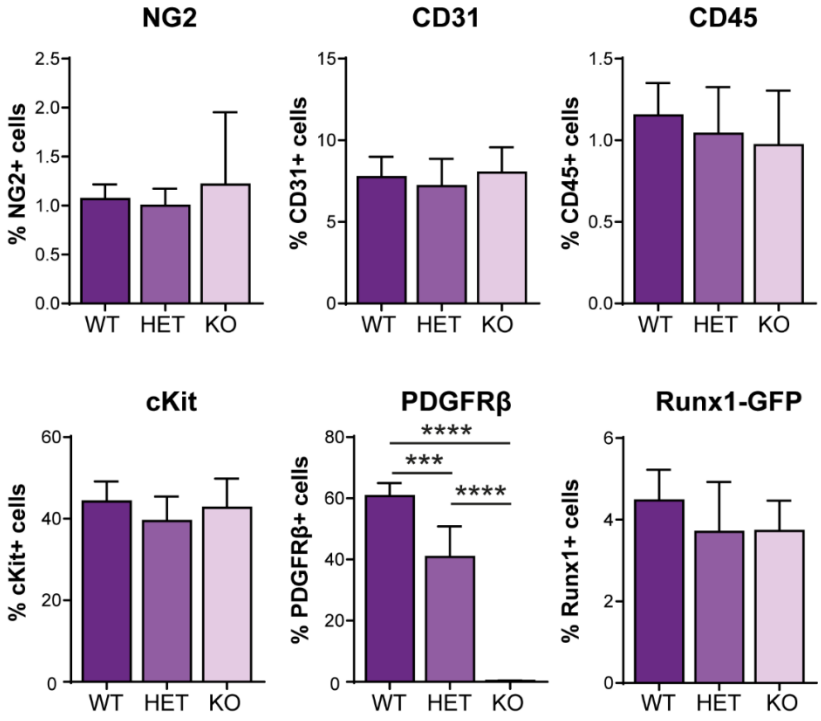

Figure 40. Flow cytometry analysis of NG2, CD31, cKit, PDGFRβ and Runx1-GFP populations from mutant E11 PDGFRβ;Runx1-GFP AGMs.
Percentage of NG2, CD31, CD45, cKit, PDGFRβ and Runx1-GFP single viable cells in WT (n=5), HET (n=7) and KO (n=7) PDGFRβ;Runx1-GFP per E11 AGM (43-46sp). Error bars: SD. *** p<0.001; **** p<0.0001.

To determine whether ECs and HECs were affected by the deletion of PDGFRβ, flow cytometric analysis was performed on E10 and E11 PDGFRβ;Runx1-GFP AGMs (Figure 41). The percentage of ECs was determined by the exclusion of cKit+ and CD45+ cells, and expression of CD31 (Figure 41A). CD31+ ECs were next gated on Runx1+ cells to obtain the percentage of HECs (Figure 41A). No differences were found at either stage in the percentage of ECs (Figure 41B, C). However, at E10, but not at E11, the percentage of HECs was significantly reduced in KO embryos (Figure 41B, C).

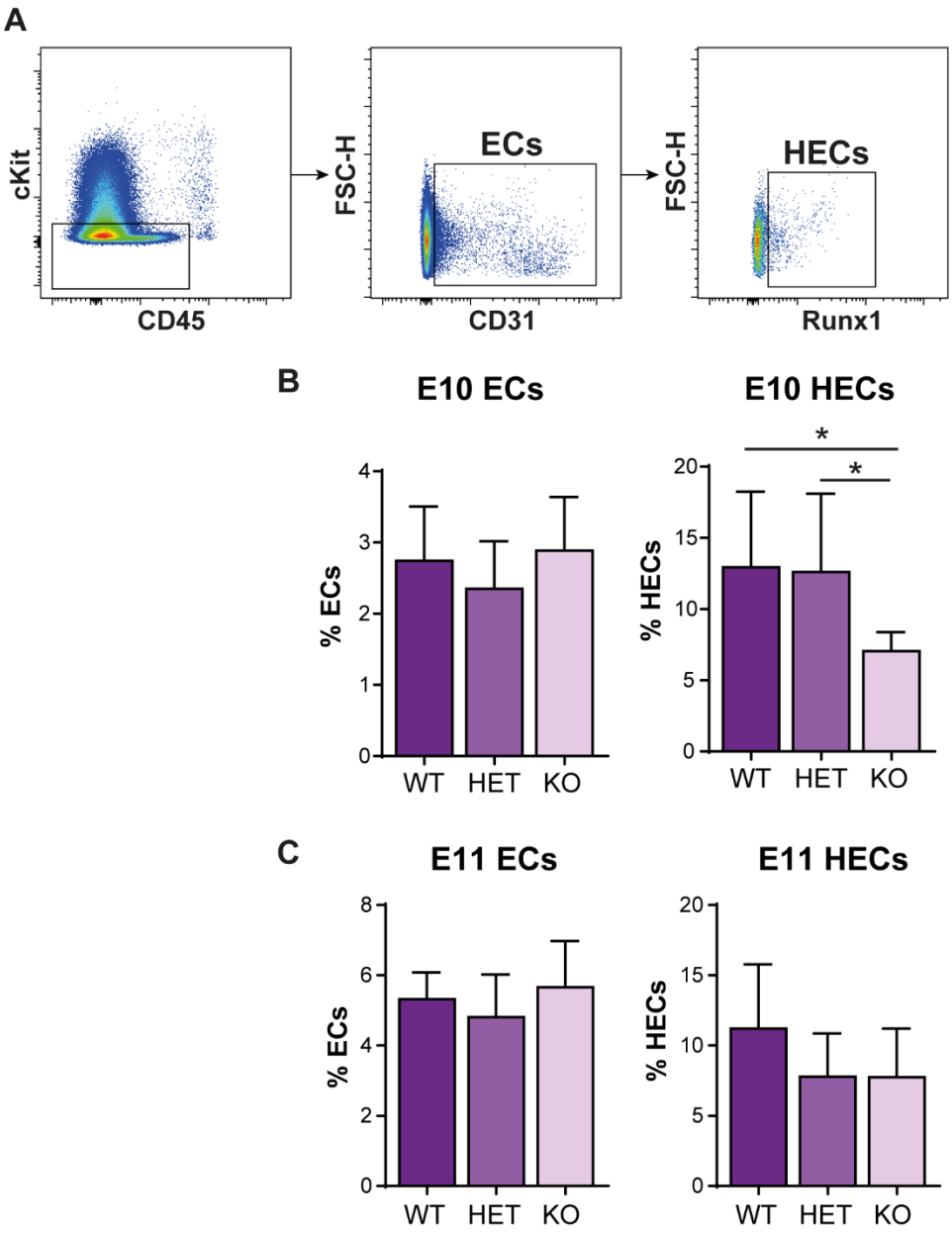

Figure 41. HECs are significantly decreased in PDGFRβ KO embryos.
(A) Gating strategy used to analyse ECs (CD31+ CD45- cKit-) and HECs (CD31+ Runx1+ CD45- cKit-) AGM cells by flow cytometry, based on the absence of cKit and CD45 expression. (B,C) Percentage of ECs and HECs in mutant PDGFRβ;Runx1-GFP AGMs at (B) E10 (33-36sp) and (C) E11 (43-46sp). Error bars: SD. * $p<0.05$.

HSPCs were next analysed by selecting single CD31+ cKit+ cells. No changes in the percentages of HSPCs and Runx1+ HSPCs were found in PDGFRβ;Runx1-GFP embryos (Figure 42).

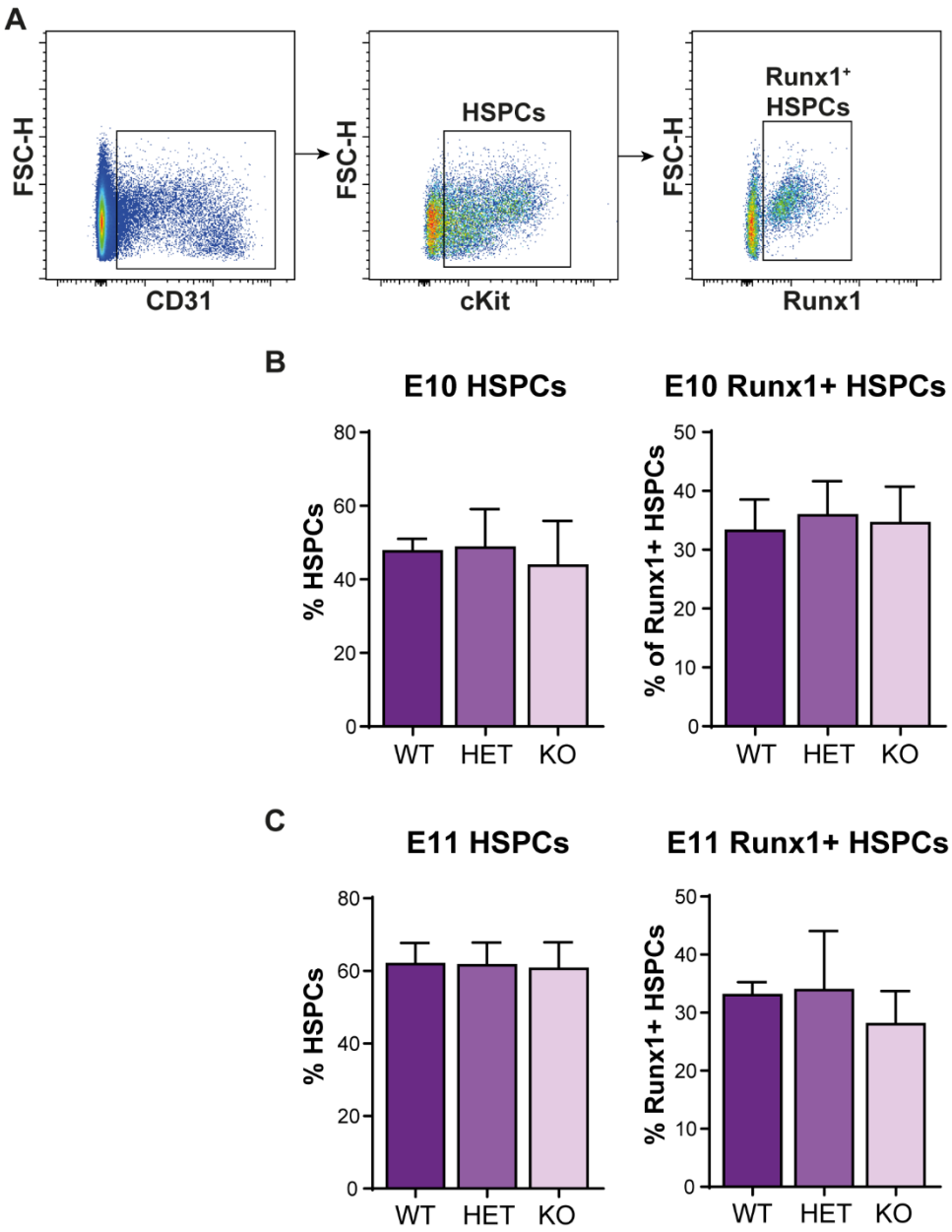

Figure 42. Percentages of AGM HSPCs and Runx1+ HSPCs are not affected in PDGFRβ KO mutants.
(A) Gating strategy used to analyse HSPCs (CD31+ cKit+) and Runx1+ HSPCs (CD31+ cKit+ Runx1+) AGM cells by flow cytometry. (B,C) Percentage of HSPCs and Runx1+ HSPCs in mutant PDGFRβ;Runx1-GFP AGMs at (B) E10 (33-36sp) and (C) E11 (43-46sp). Error bars: SD.

As some stromal cells also express Runx1, we analysed the percentages of Runx1 expressing cells in PDGFRβ mutant embryos at E10 and E11 (Figure 43). Stromal cells were analysed based on the absence of the endothelial and hematopoietic markers CD31, cKit and CD45 (Figure 43A). The percentage of

stromal cells was not altered upon PDGFRβ deletion at either time points (Figure 43A, B). At E10, no differences were observed in the percentage of Runx1-expressing stromal cells (Figure 43A), but at E11 a significant decrease was detected in KO embryos compared to WT (Figure 43B). These data suggest PDGFRβ deletion also affects Runx1 expression in the stroma, in addition to HECs.

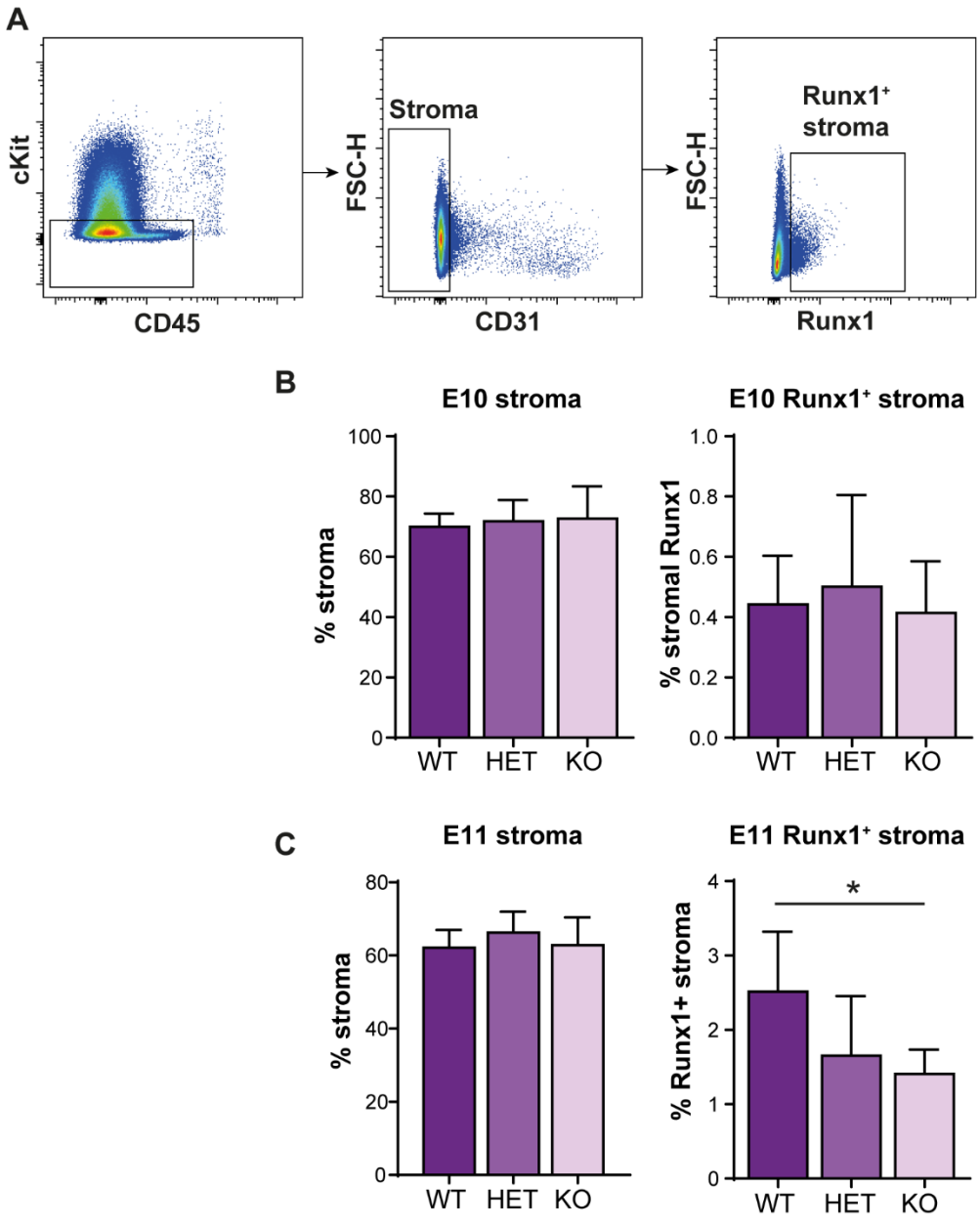

Figure 43. Runx1 expression in stromal cells is reduced in PDGFRβ KO mutants.
(A) Gating strategy used to analyse AGM stromal cells by flow cytometry, based on the absence of cKit, CD45 and CD31 expression. (B,C) Percentage of stromal cells and Runx1+

stromal cells in mutant PDGFRβ;Runx1-GFP AGMs at (B) E10 (33-36sp) and (C) E11 (43-46sp). Error bars: SD. * p<0.05.

4.3.5 Functional AGM HSPCs do not express PDGFRβ

Whether midgestation functional HSPCs express PDGFRβ is not known. E10 and E11 BL6 AGMs were sorted into PDGFRβ+ and PDGFRβ- populations (Figure 44A, C) and seeded in methylcellulose. Post-sort purity checks were conducted, and all samples were found to be highly purified (Figure 44B, D)

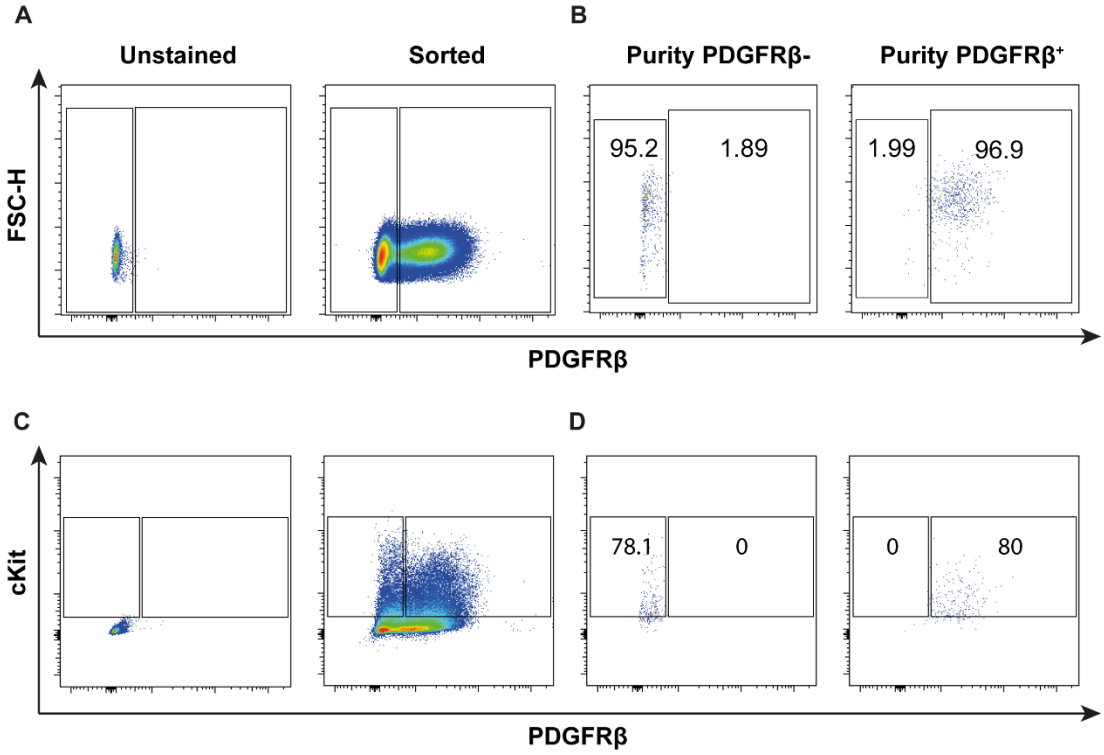

Figure 44. Gating strategy and post-sort purity of PDGFRβ+ and PDGFRβ- E10 and E11 AGM cells.
(A) Representative FACS plots of PDGFRβ+ and PDGFRβ- E10 AGM sorts. Gates are based on the unstained sample and PDGFRβ staining. (B) Post-sort purity of PDGFRβ+ and PDGFRβ- cells shows negligible contamination of PDGFRβ+ in the PDGFRβ- population and vice-versa. (C) Representative FACS plots of PDGFRβ+ and PDGFRβ- E11 AGM sorts. Gates are based on the unstained sample and cKit and PDGFRβ staining. (D) Post-sort purity of PDGFRβ+ and PDGFRβ- cells shows no contamination in either sorted population. (B, D) Numbers in the gates correspond to the percentage of the total number of cells found inside each gate.

Haematopoietic progenitor activity was only detected in the PDGFRβ- population at both stages (Figure 45), suggesting that functional HSPCs do

not express PDGFRβ and therefore, the deletion of PDGFRβ does not directly affect HSPC function.

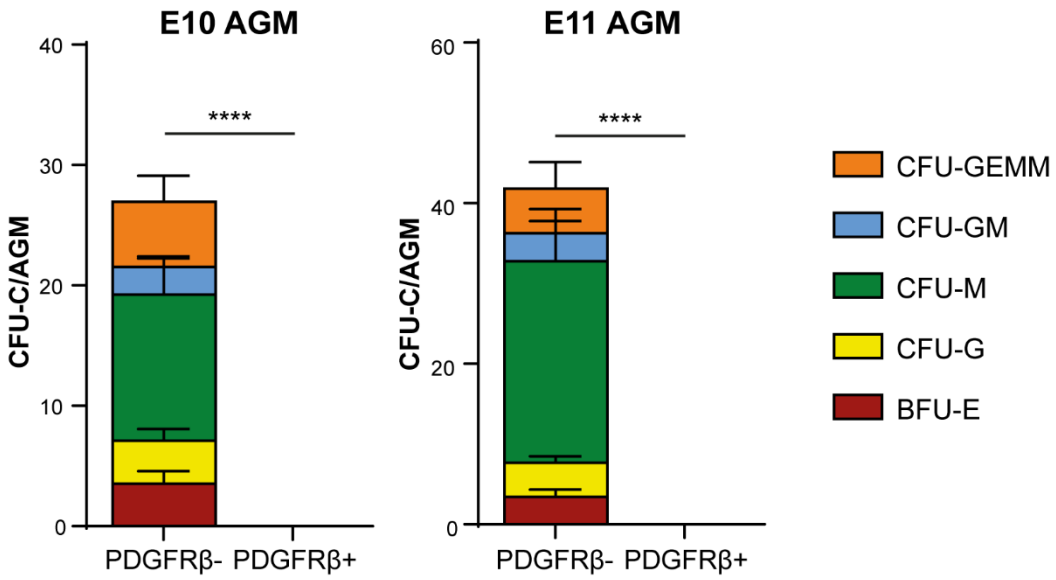

Figure 45. PDGFRβ+ E10 and E11 AGM cells are not haematopoietic.
CFU-C numbers of sorted BL6 PDGFRβ- and PDGFRβ+ cells at E10 (26-33sp; n=8) and E11 (40-45sp; n=6). Error bars: SD; ****: p<0.0001.

4.3.6 PDGFRβ-Cre marks a subset of HSPC precursors

Another possibility to explain the phenotype observed in PDGFRβ KO embryos is that HSPCs derive from PDGFRβ precursors. To test this, PDGFRβ-Cre mice were crossed with R26;TdTomato mice [161]. Upon PDGFRβ expression, Cre recombinase excises a stop cassette, allowing for TdTomato expression. Thus, PDGFRβ+ cells and their progeny will express TdTomato. E10 and E11 AGM cells from PDGFRβ-Cre;TdTomato were sorted into Tomato+ and Tomato- populations, and seeded in methylcellulose (Figure 46A). As all AGM HSPCs were reported to express cKit [32], Tomato- cells were enriched in cKit expression (Figure 46A). No contamination was detected in either population after sorting (Figure 46B).

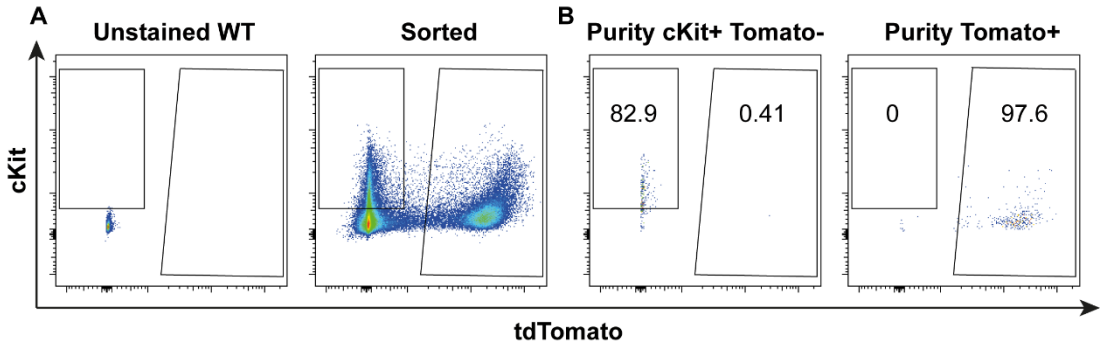

Figure 46. Gating strategy and post-sort purity of cKit+Tomato- and Tomato+ AGM cells. (A) Representative FACS plots of cKit+Tomato- and Tomato+ E10 and E11 AGM sorts. Gates were based on the unstained sample, cKit staining and Tomato endogenous expression. E10 AGM cells were sorted only based on Tomato expression (B) Post-sort purity of cKit+Tomato- and Tomato+ cells shows no or very little contamination in either sorted population. Numbers in the gates correspond to the percentage of cells inside the gate.

At E10, very few colonies were found in the Tomato+ fraction compared to the Tomato- fraction. At E11, this number increased in the Tomato+ fraction, suggesting that some AGM HSPCs derive from PDGFRβ precursors (Figure 47). Tomato- and Tomato+ E11 AGM cell transplantations were also performed, but no reconstitution was detected in either fraction, suggesting that something did not work in the experimental procedure (data not shown).

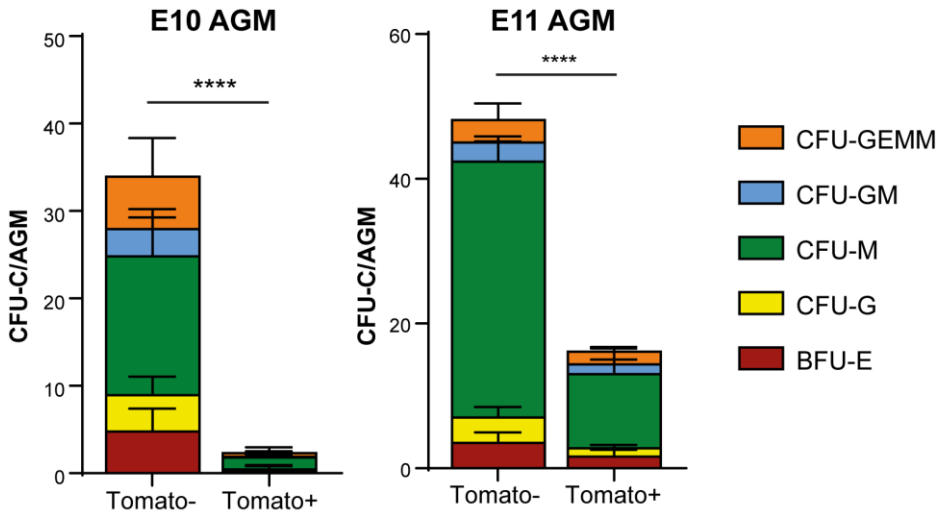

Figure 47. PDGFRβ-Cre;TdTomato+ cells are haematopoietic.
CFU-C numbers of sorted Tomato- and Tomato+ from PDGFRβ-Cre;TdTomato E10 (33-34sp; n=6) and E11 (44-45sp; n=4) AGMs.

To understand whether PDGFRβ-Cre;TdTomato-derived HSPCs persisted at later stages, haematopoietic progenitor assays were performed on Tomato- and Tomato+ sorted E14 FL and adult BM cells (Figure 48A, C). Post-sort purity was relatively high, with less than 6% contamination of Tomato- cells into the Tomato+ E14 FL fraction (Figure 48B), and less than 4% in the Tomato+ BM fraction (Figure 48D).

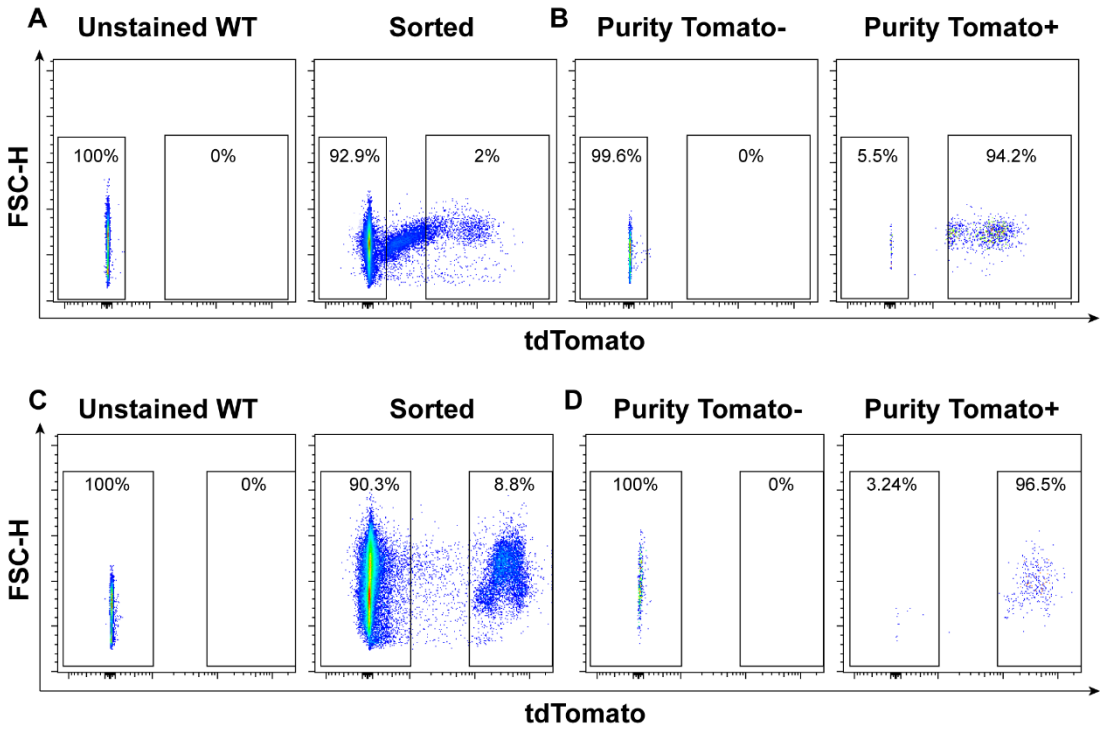

Figure 48. Gating strategy and post-sort purity of Tomato- and Tomato+ E14 FL and adult BM cells.
(A) Representative FACS plot of Tomato- and Tomato+ E14 FL cell sorts. An unstained WT E14 FL control was used to set the gates for tomato expression. (B) Post-sort purity of E14 FL Tomato- and Tomato+ cells. (C) Representative FACS plot of Tomato- and Tomato+ adult BM cell sorts. An unstained WT BM control was used to set the gates for tomato expression. (D) Post-sort purity of BM Tomato- and Tomato+ cells.

HSPCs were found in both Tomato- and Tomato+ fractions of the E14 FL and adult BM (Figure 49). Since the same number of cells was seeded in methylcellulose from Tomato- and Tomato+ cells and the percentage of Tomato+ cells in each population was different, higher frequencies in HSPCs were observed in the Tomato+ E14 FL CFU-Cs and similar frequencies were

found in the Tomato+ BM CFU-Cs (not shown). However, this is not representative of the total number of HSPCs in each fraction. Therefore, CFU-C numbers obtained were re-calculated per organ, taking into account the percentage of Tomato+ and Tomato- cells and the absolute number of CFU-C is shown in Figure 49.

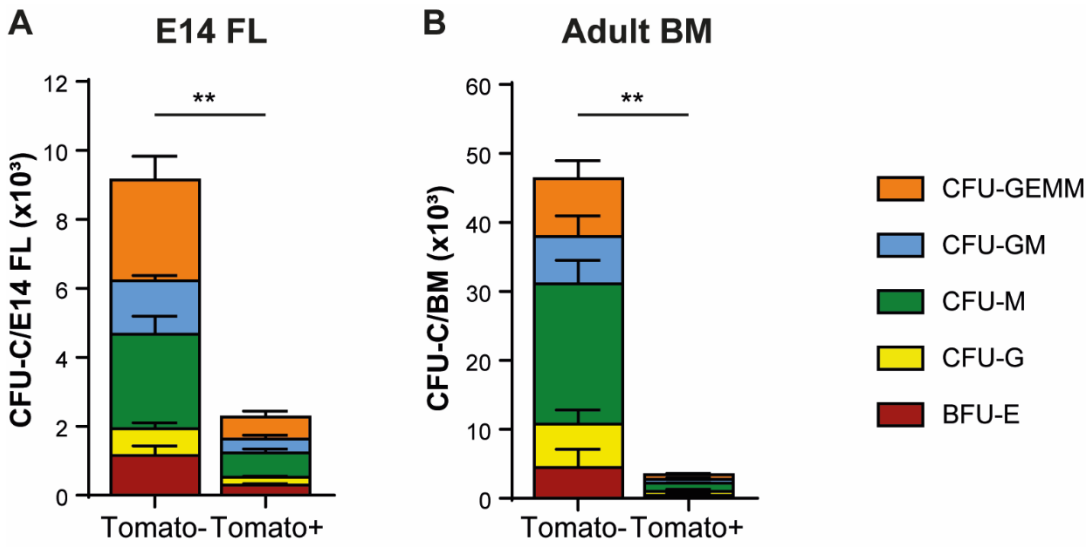

Figure 49. E14 FL and adult BM Tomato+ and Tomato- populations contain HSPCs. CFU-C absolute number of sorted Tomato- and Tomato+ from PDGFRβ-Cre;TdTomato (A) E14 FL (n=5) and (B) adult BM (n=4). Error bars: SD; **: $p<0.01$. An unpaired t-test was used for the E14 FL data, and an unpaired t-test with Welch's correction was used for the adult BM data.

Flow cytometry analyses were next performed on PDGFRβ-Cre;TdTomato E14 FL and adult BM cells to understand whether LSKs (immature progenitors and HSCs) were present in both fractions, and at what proportion (Figure 50). LSK cells are by definition negative for all haematopoietic lineage markers (Lin-: CD4, CD5, CD8a, CD11b, CD45R, Gr-1 and Ter119), and positive for cKit and Sca1 [200].

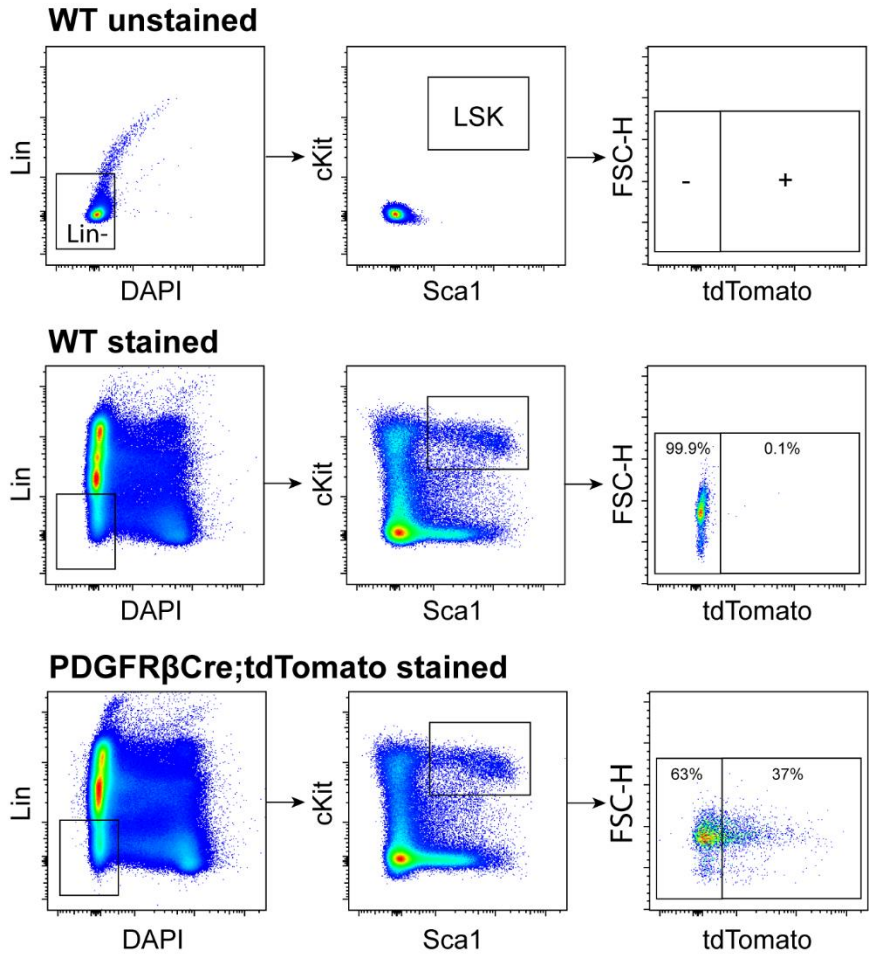

Figure 50. LSK gating strategy for PDGFRβ-Cre;TdTomato BM cells.
Gating strategy for LSK (Lin- Sca1+ cKit+) cells from single live cells. From the LSK population, percentages of Tomato- and Tomato+ cells was assessed. A WT BM control was used to set the gates separating Tomato- and Tomato+ cells.

Within all LSK cells detected in the E14 FL and adult BM, around 1/10 FL cells and 3/10 BM cells derived from PDGFRβ-Cre precursors (Figure 51).

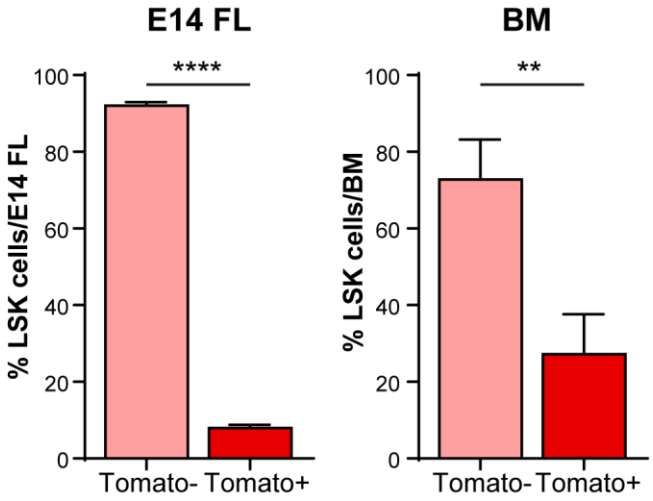

Figure 51. Tomato- and Tomato+ LSKs are found in both E14 FL and adult BM.
Percentages of Tomato- and Tomato+ LSK cells detected in the E14 FL (n=5) and adult BM (n=3) determined by flow cytometry analysis. Error bars: SD; **: p<0.01; ****: p<0.0001. An unpaired t-test was used in both analyses.

To determine whether both Tomato+ and Tomato- fractions contain bona fide HSCs, transplantations with Tomato+ and Tomato- sorted cells from PDGFRβ-Cre;tdTomato E14 FL and adult BM were performed into sub-lethally irradiated recipients. After 4 months, 2/4 mice injected with Tomato- and 3/3 mice injected with Tomato+ E14 FL cells were successfully reconstituted (Figure 52A, left graph). Adult BM Tomato- cells reconstituted 4/5 recipients, while 2/5 mice were reconstituted by Tomato+ (Figure 52B, left graph). Secondary transplantations show that HSCs derived from both fractions were able to self-renew. Together, these data demonstrate that some HSCs derive from PDGFRβ-Cre precursors and persist into adulthood.

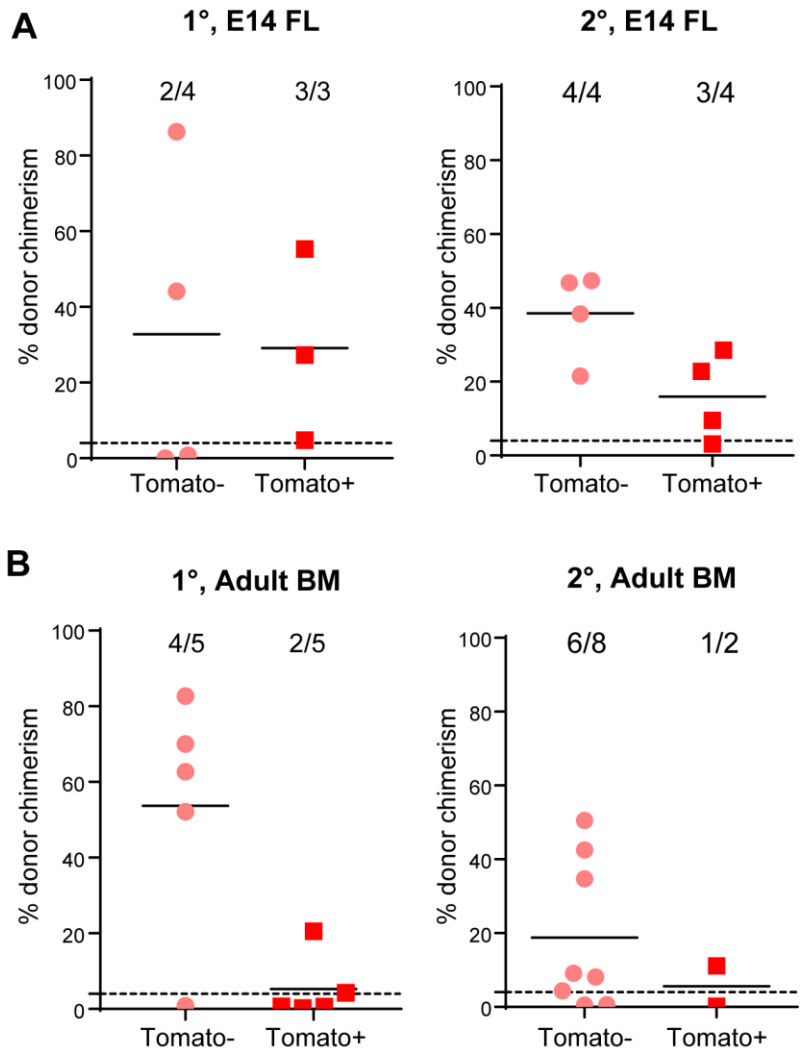

Figure 52. Tomato- and Tomato+ E14FL and adult BM cells contain long-term, self-renewing HSCs.
Analysis of long-term reconstitution potential of Tomato- and Tomato+ cells from (A) E14 FL (n=4 injected with Tomato-, and n=3 injected with Tomato+ cells) and (B) adult BM (n=5) into sub-lethally irradiated recipients 4 months after primary (1^o) transplantations and 1 month after secondary (2^o) transplantations. BM of mice reconstituted in primary transplantations were injected into 2 mice in secondary transplantations. Each data point represents one mouse. Mice are reconstituted when >4% donor cells (dashed line) are found in the host peripheral blood. Numbers of reconstituted mice/number of transplanted mice are given in each group.

To confirm the data obtained with PDGFRβ-Cre;TdTomato mice, a second model was tested. PDGFRβ-Cre;mTmG mice were used by crossing PDGFRβ-Cre with R26-mTmG mice (Figure 53). PDGFRβ-Cre mice [160], have a sequence encoding the Cre recombinase under PDGFRβ promoter. R26-mTmG mice contain a sequence encoding TdTomato and a stop cassette

flanked by two loxp sites, followed by a sequence encoding Gfp, both under the Rosa26 promoter (Figure 53A) [163]. Upon PDGFRβ expression, Cre recombinase is expressed and excises the sequence containing TdTomato and the stop cassette, activating GFP expression. GFP+ cells are mainly found in the head of PDGFRβ-Cre;mTmG E11 embryos, as well as in the trunk, namely in the AGM and neural tube regions (Figure 53B).

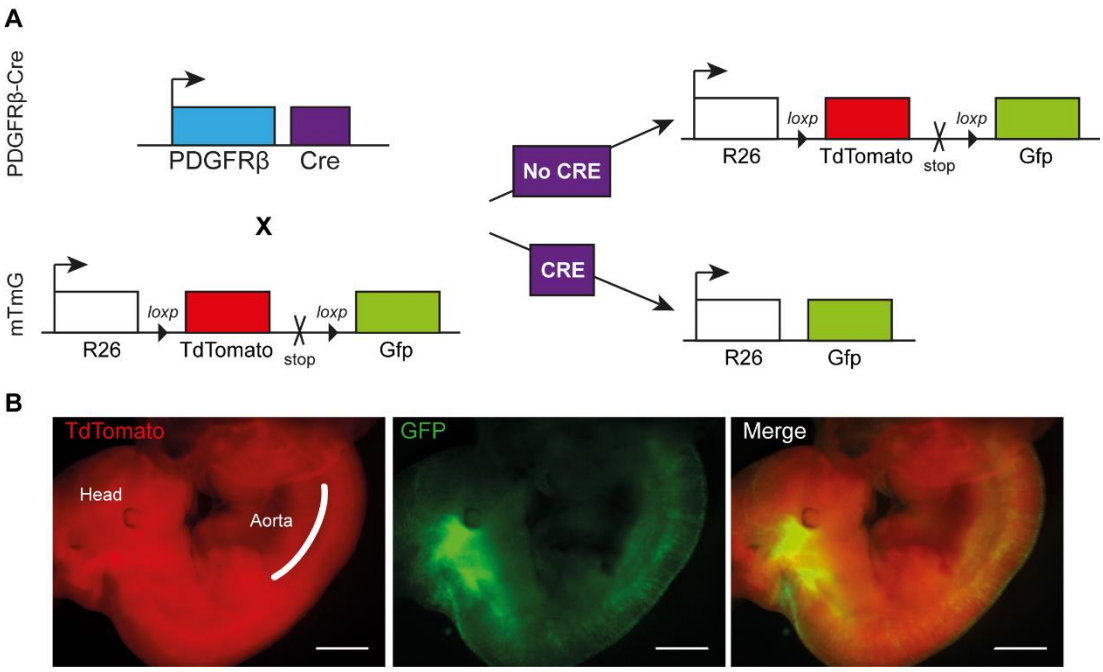

Figure 53. PDGFRβ-Cre;mTmG mouse model.
(A) Schematic representation of PDGFRβ-Cre;mTmG mechanism. (B) PDGFRβ-Cre;mTmG E11 embryos, showing Cre+ cells by GFP expression and Cre- cells by TdTomato expression. Scale bar: 1mm.

GFP+ and GFP- cells were sorted from E11 AGM and E14 FLs from PDGFRβ-Cre;mTmG embryos (Figure 54A). Unfortunately, AGM cells (both GFP+ and GFP-) failed to generate colonies in methylcellulose, suggesting an underlying technical problem, and rendering the experiment unusable (not shown). E14 FL CFU-Cs were successful, and the post-sort purity for both populations was high (Figure 54B,C). Although the frequency of colonies was higher in the GFP fraction (not shown), results were re-calculated pre organ, taking into account the percentage of sorted cells for each fraction.

Both fractions contained HSPCs, and more colonies were found on the GFP- fraction compared to GFP+ fraction (Figure 54). Interestingly, the numbers of colonies obtained in the GFP+ fraction was much higher than the ones obtained using cells sorted from PDGFRβ-Cre;tdTomato (Figure 49). This difference is likely due to the larger stringency used to sort Tomato+ cells (excluding a Tomato intermediate population), compared to the gate used to sort GFP+ cells.

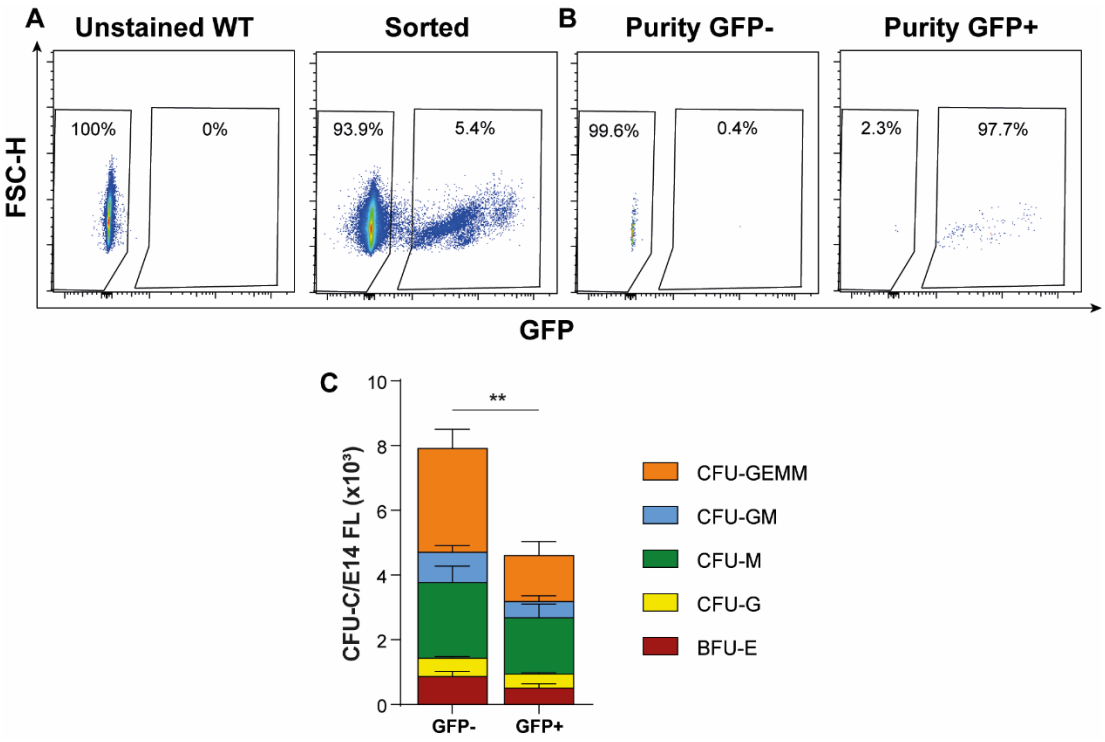

Figure 54. E14 FL GFP+ and GFP- populations contain HSPCs.
(A) Representative FACS plot of GFP- and GFP+ E14 FL cell sorts. An unstained WT E14 FL control was used to set the gates for tomato expression. (B) Post-sort purity of E14 FL Tomato- and Tomato+ cells. (C) CFU-C numbers of sorted GFP- and GFP+ from PDGFRβ-Cre;mTmG E14 FL (n=5). Error bars: SD; **: p<0.01. A Mann Whitney test was used.

To better understand which cells derive from PDGFRβ progenitors, immunohistochemistry was performed on PDGFRβ-Cre;mTmG E11 AGM cryosections. As expected, PDGFRβ-Cre (GFP+) was co-expressed by NG2+ cells surrounding the DA (Figure 55, upper panel). Several CD31+ cells were also found to express GFP (Figure 55, bottom panel), showing that some ECs derive from PDGFRβ-Cre precursors.

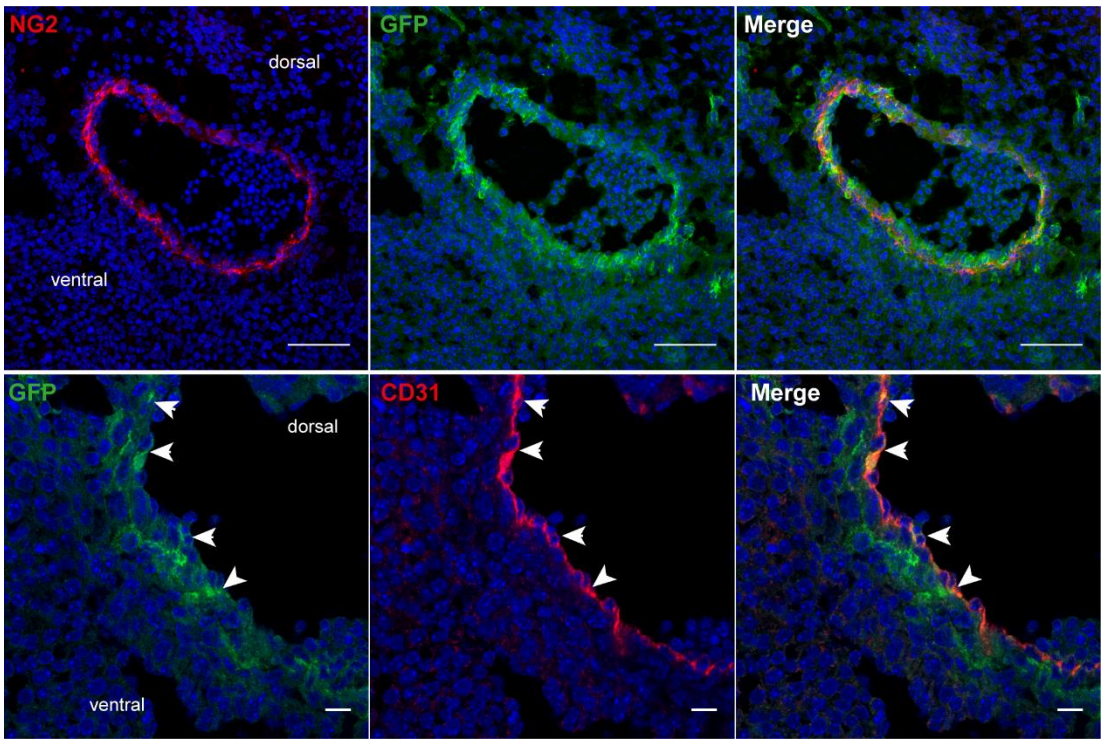

Figure 55. PDGFRβ-Cre expression is detected in PCs and ECs around the E11 DA. Immunohistochemistry of PDGFRβ-Cre;mTmG E11 sections stained in red with NG2 (upper panel) and CD31 (bottom panel), and PDGFRβ-Cre is expressed by GFP (green). Scale bars: upper panel: 50µm; bottom panel: 10µm.

4.4 Discussion

The main objective of this chapter was to determine whether PDGFRβ signalling is required for HSC generation in the AGM.

4.4.1 PDGFRβ is required for HSPC generation in the AGM

In Chapter 3, we described PDGFRβ+ cells surrounding the endothelium between E9 and E11, during the time of HSC specification and generation, that expressed high levels of HSC-niche genes required for HSC maintenance in the adult BM. We therefore sought to determine whether PDGFRβ is required for HSC generation and/or maintenance in the midgestation AGM.

Using a constitutive PDGFRβ KO mouse model [157], we assessed HSPC numbers in the AGM slightly before HSC generation (E10) and slightly after HSC generation has started in this region (E11). No differences were found in the number of HSPC at E10, but a significant decrease was detected at E11

between PDGFRβ WT, HET and KO embryos (Figure 30). These data suggest that PDGFRβ deletion affects AGM haematopoiesis after the onset of HSC generation in the AGM (E10.5). However, the AGM region not only harbours AGM-derived HSPCs, but also circulating HSPCs from other organs. Therefore, the differences detected by CFU-C could be due to defects in HSPC production before HSC generation. Importantly, we found that PDGFRβ KO AGMs were unable to reconstitute primary sub-lethally irradiated recipients, suggesting an underlying defect in HSC generation in the absence of PDGFRβ.

Since PDGFRβ expression was detected in the head, PL, YS and FL from E8 to E11 (Figure 31), we performed haematopoietic progenitor assays in these organs at E10 and E11 to determine whether any similar defects to the AGM could be found at these stages. No significant differences were found in any of the organs analysed, suggesting that PDGFRβ deletion does not affect haematopoiesis in these organs at E10 and E11. This does not exclude the possibility PDGFRβ plays a role in primitive haematopoiesis at earlier time-points, and therefore, additional haematopoietic progenitor assays need to be conducted at E8 and E9, to determine whether HSPC production in other organs is altered before the onset of AGM haematopoiesis.

We next looked at whether HSCs were affected in the AGM of PDGFRβ KO embryos. Primary transplantations of E11 PDGFRβ KO AGMs led to no reconstitution of irradiated recipients in primary transplantations, suggesting that the deletion of PDGFRβ affects the generation or maintenance of AGM HSCs. Overall reconstitution both in WT and HET mice was low, most likely because embryos harvested for injections were under 46sp, and optimal reconstitution at E11 occurs with embryos closer to E12. Interestingly, transplantations of PDGFRβ KO and PDGF-B KO E14 FLs were shown to reconstitute irradiated recipients [201], suggesting that HSCs are present in these embryos, although the cellularity of mutant FLs was decreased. This could be explained by the generation of HSCs in other haematopoietic organs that compensate for the defects HSC generation in the AGM. It would therefore

be interesting to perform YS and PL transplantations at E11 to see whether they contain HSCs, which would prove their generation outside the AGM.

4.4.2 PDGFRβ deletion affects the phenotype of PCs but not their recruitment to the DA

Since PDGF-B/PDGFRβ signalling is required for PC/vSMC recruitment and blood vessel stabilisation, we hypothesised that the reduction of the number of AGM HSPCs could be due to defects in DA integrity and leakage of HSPCs. Immunohistochemistry and 3D whole mount immunostaining data at E10 and E11 (Figure 35 andFigure *38*) suggest that the integrity of the DA is not compromised by PDGFRβ deletion, as seen by a continuous CD31 expression and no leakage of cKit+ cells to the surrounding mesenchyme. Interestingly, although no expression of PDGFRβ was detected in KO embryos, NG2+ αSMA+ perivascular cells were still present, suggesting that pericyte/vSMC recruitment around the aorta is independent of PDGF-B/PDGFRβ signalling. The presence of these cells in the absence of PDGFRβ signalling also suggests that rather than being recruited, their differentiation into PC/vSMCs is induced instead, most likely via TGFβ signalling [197], and possibly through Notch signalling as well [197]. Although NG2+ αSMA+ perivascular cells are detected around the aorta of mutant embryos, we found a significant decrease in NG2 expression at E10.5 and an increase in the percentage of αSMA+ cells and αSMA intensity around the DA (Figure 35 andFigure *37*). These results were further confirmed by flow cytometry. Such changes in NG2 and αSMA expression have been reported at later time-points in WT dorsal aorta. As the blood vessel matures, developing vSMCs lose NG2 expression and αSMA expression increases [179]. Moreover, it was recently shown that inhibiting VEGFR/PDGFR with axitinib led to the induction of αSMA expression and a pro-fibrotic phenotype in human placental pericytes [202]. These data suggest that PDGFRβ deletion leads to a premature differentiation of PCs into a more mature vSMC phenotype, marked by an increase in αSMA expression and αSMA+ cells around the aorta, coupled with a decrease in NG2 expression.

4.4.3 PDGFRβ deletion affects IAHC size

Another interesting observation in E10.5 PDGFRβ KO DAs was that cKit+ clusters are larger than WT clusters. Recently, large sized clusters were found in the E10.5 DA of mice constitutively lacking the Notch ligand Dll4 [203]. Although the perivascular cell populations around the AGM do not express any notch ligand (see *Dll1*, *3*, *4* and *Jag2* in appendix table 3) with the exception of Jagged1, PDGFRβ+ cells could play a role in the regulation of Notch signalling. It would be interesting to see whether the Notch signalling pathway is altered in the AGMs of PDGFRβ KO embryos. Another similar phenotype has been reported in Drosophila when the PDGF/VEGF receptor is deleted, and haemocytes undergo apoptosis and are phagocytosed by the remaining blood cells [152]. It would be interesting to examine the expression of apoptotic markers in the murine PDGFRB KO aorta to determine whether IAHCs contain more apoptotic cells.

4.4.4 Collagen IV deposition is not affected by the absence of PDGFRβ

No differences were found in collagen IV nor CD146 expression around the dorsal aorta of PDGFRβ KO E11 embryos by immunohistochemistry. Basement membrane assembly was shown to rely on the interaction between pericytes and endothelial cells, and therefore, on pericyte recruitment to the blood vessel wall [185,186,204]. Although the blockage of PDGF-BB *in vitro* was shown to impair pericyte recruitment to EC tubes and decrease collagen IV deposition [186], collagen IV expression around the DA was normal. This is not surprising, given that NG2+ αSMA+ cells are still present around the aorta of mutant embryos. However, the basement membrane is complex, and many other proteins are involved in the basement membrane synthesis, such as laminins and integrins [204], and PDGFs were shown to play a role in the production of extracellular matrix components [144,145]. It would therefore be interesting to determine whether other components of the basement membrane are affected in these embryos.

4.4.5 E10 AGM haemogenic endothelial cells are affected by PDGFRβ deletion

As HSCs were not detected in the AGM of PDGFRβ KO embryos, we sought to determine whether haemogenic endothelial cells were affected by PDGFRβ deletion. For this purpose, PDGFRβ mutant mice were crossed with Runx1-IRES-GFP mice, and F2 embryos were analysed by flow cytometry. A significant decrease in the percentage of HECs was detected at E10. This decrease could still be observed at E11, but was not statistically significant. Runx1 expression by ECs was shown to be essential for endothelial to haematopoietic transition, but not afterwards [79]. These data suggest that PDGFRβ is important either for the specification of HECs and/or as HEC precursors. In the chick embryo, it was shown that the presence of a splanchnopleura-derived sub-aortic mesenchyme (where PDGFRβ is expressed in the mouse) was required for the induction of Runx1 expression by endothelial cells, and subsequent HSPC formation [97]. PDGFRβ signalling could therefore be required to signal endothelial cells to express Runx1 and initiate aortic haematopoiesis. In zebrafish for instance, PDGFR signalling (mainly PDGFRα but also PDGFRβ) was shown to be necessary for the migration of neural crest cells to the ventral aspect of the DA. Morpholino knock down of *pdgfra* and *pdgfrb* halted this migration, which in turn led to a reduction of Runx1-expressing cells [148]. Understanding whether this niche effect is conserved in mice would bring additional cues to understanding this reduction in HECs.

As Runx1 is also expressed in mesenchymal and haematopoietic cells [47], Runx1 expression by these cells was also assessed by flow cytometry. The percentages of Runx1+ HSPCs were similar in WT, HET and KO at both E10 and E11 suggesting that PDGFRβ deletion only affects HECs and not HSPCs (Figure 42). The percentage of Runx1+ stromal cells was unchanged between WT, HET and KO E10 AGMs, but a marked decrease was observed in the stroma at E11 (Figure 43). The role of stromal cell expressing Runx1 is however unknown. Our unpublished observations show that the deletion of

Runx1 in stromal cells impairs AGM haematopoiesis (*Gonzalez et al, In Preparation*).

4.4.6 Midgestation PDGFRβ+ cells are not haematopoietic, but a subset of HSPCs derives from PDGFRβ-Cre precursors

As AGM HSPCs were affected by the deletion of PDGFRβ, we sought to determine whether midgestation HSPCs express this marker. Haematopoietic progenitor assays with AGM PDGFRβ- and PDGFRβ+ sorted cells showed no colony formation in the PDGFRβ+ fraction (Figure 45). We can therefore conclude that PDGFRβ deletion does not affect HSPCs directly, as they do not express PDGFRβ.

Another possible explanation for the effect of PDGFRβ deletion in the AGM is that PDGFRβ+ cells are precursors of AGM HSPCs. To test this possibility, PDGFRβ-Cre mice were crossed with TdTomato mice, AGM cells were sorted based on Tomato expression and seeded in methylcellulose. At E10, a small fraction of Tomato+ cells were able to form colonies, and this number increased at E11, suggesting that PDGFRβ-Cre marks some HSPC (Figure 47). As their numbers increase between E10 and E11, the period in which AGM HSCs are generated, it is plausible to postulate that these cells could be generated by the AGM. To confirm this possibility, CFU-Cs will need to be performed with Tomato+ and Tomato- cells sorted from other haematopoietic organs before the onset of AGM haematopoiesis. Interestingly, the deletion of PDGFRβ led to a decrease in nearly half of haematopoietic progenitors in the AGM (Figure 32), which could be explained by the finding that about 1/3 of AGM HSPCs derive from PDGFRβ-Cre precursors (Figure 47). These data do not exclude the possibility that PDGFRβ-Cre-derived HSPCs are produced in other haematopoietic organs. Tracing experiments using the same PDGFRβ-Cre mouse line as the one used in this study showed that although PDGFRβ-Cre is expressed in YS ECs, it does not target cKit+ E9 and E10 YS-derived EMPs, suggesting that PDGFRβ precursors do not contribute to YS haematopoietic cells [205]. Ongoing experiments in the lab aim to confirm

these data and address this question in other haematopoietic organs before HSC generation in the AGM.

To understand whether PDGFRβ-Cre-derived HSPCs persist during development and in the adult, CFU-Cs were performed with sorted Tomato cells from the E14 FL and adult BM. Tomato+-derived colonies were detected in both tissues, although in lower numbers than in the Tomato- fraction (Figure 49), suggesting that PDGFRβ-Cre-derived HSCs persist into adulthood. It would also be possible that PDGFRβ-Cre-derived HSCs are generated *de novo* after AGM haematopoiesis. To rule out this possibility, it would be important to trace PDGFRβ-Cre-derived cells after AGM haematopoiesis, using for example PDGFRβ-P2A-CreERT2;mTmG [206] embryos injected with tamoxifen after E12 and determine whether GFP+ HSCs are present in both, the E14 FL and in the adult BM.

LSK analysis was also performed in these organs to determine the percentage of immature HSPCs in each fraction. Unfortunately, LSK-SLAM analysis could not be performed due to a spectral overlap of the CD48 (Slamf2) PE antibody with TdTomato to see whether any of the fractions was more enriched in specific types of HSPCs. On average, $1/10^{th}$ of FL LSKs were found in the tomato+ fraction, and this number increased to $1/4^{th}$ in the adult BM (Figure 51), suggesting that PDGFRβ-Cre cells give rise to immature haematopoietic progenitors. To test whether both fractions contained bona fide HSCs, sorted Tomato+ and Tomato- cells from E14 FL and adult BM were injected into irradiated recipients. Both fractions were found to reconstitute primary recipients after 4 months and secondary recipients after 1 month, suggesting that both fractions contain long-term reconstituting HSCs (LTR-HSCs).

4.4.7 A subset of aortic ECs derives from PDGFRβ-Cre precursors

The existence of PDGFRβ-Cre-derived HSCs suggests that some HECs derive from PDGFRβ-Cre precursors. We looked at CD31 expression in PDGFRβ-Cre;mTmG E11 AGM sections and found that most, if not all CD31+ cells at this stage also express GFP (Figure 55). PDGFRβ-Cre expression in

ECs of the dorsal aorta has already been reported at E13.5 [205]. These results are not surprising, as both ECs and SMCs in the murine dorsal aorta were shown to derive from common precursors from the lateral plate mesoderm before HSC generation [139,207]. Although in the chick embryo aortic ECs were shown to be replaced by somite-derived ECs following HSC generation [137], in the mouse this does not seem to be the case, and ECs from the lateral plate mesoderm are maintained in the DA after E11.5 [139]. This might explain why GFP+ ECs are still present in the DA at E11.5. To confirm these data, analysis of PDGFRβ-P2A-CreERT2 E11 embryos born from females injected with tamoxifen at either E7, E8 or E9 is underway.

Whether HECs derive from PDGFRβ precursors is still under investigation. We crossed PDGFRβ-Cre;tdTomato with Runx1-GFP mice to determine the percentage of tdTomato+ HECs. Unfortunately, an unknown biological effect occurs with this crossing and the presence of Runx1-GFP induces tdTomato expression in almost 100% of the cells (not shown). Flow cytometry analysis of PDGFRβ-Cre;tdTomato using CD41 as HEC marker, together with immunohistochemistry with Runx1 antibody staining will be performed instead, to determine PDGFRβ contribution to the haemogenic endothelium. If all AGM HECs derive from PDGFRβ-Cre precursors, it will confirm that there are other sites for the generation of HSCs that persist into adulthood.

4.4.8 Conclusions and future work

In this chapter we have shown that PDGFRβ is required for HSC generation in the AGM. Deletion of PDGFRβ led to a reduction of HECs and a change in the phenotype of PCs surrounding the DA. Single cell RNA sequencing analysis is currently underway in E11 PDGFRβ WT and KO embryos, to determine if there are any signalling pathways affected by PDGFRβ deletion that could impair HSC generation and/or maintenance in the AGM.

We have also shown that a subset of HSCs that persist into adulthood derive from PDGFRβ-Cre precursors, while others do not, suggesting a dual origin for HSCs. Ongoing experiments investigating the presence of PDGFRB-

derived HPSCs in other organs will allow us to determine whether PDGFRβ is only required for HSC generation in the AGM or could also play a role in other haematopoietic organs. If PDGFRβ-Cre only marks AGM haematopoietic cells, this study will prove that adult-type HSCs can also be produced outside the AGM.

It would also be interesting in the future to analyse the BM of PDGFRβ-Cre;TdTomato mice and determine whether PDGFRβ-Cre-derived HSCs and HSCs from another origin are genetically distinct. For instance, previous work showed that a subset of FL and BM HSCs is BMP-activated and another subset is not [208]. It would therefore be interesting to investigate whether PDGFRβ-derived HSCs are BMP-dependent or BMP-independent.

Chapter 5 PDGF-B^{ret} mutation in haematopoiesis

5.1 Introduction

PDGF-B signalling via PDGFR-β is critically involved in the recruitment of pericytes and vascular smooth muscle cells to blood vessels [182,209]. PDGF-B is expressed by endothelial cells, and once released, binds to the extracellular matrix surrounding the endothelium, creating a gradient required for the proper recruitment and investment of pericytes to blood vessel walls [158]. Interestingly, overexpression of PDGF-B in zebrafish was shown to lead to an increase in AGM HSPC production [149]. Similarly to PDGFRβ KO embryos [157], PDGF-B KO embryos also die perinatally [210]. These embryos have abnormal kidney glomeruli due to a defect in mesangial cell development, heart and blood vessel dilation, anaemia, thrombocytopenia and are thought to die of haemorrhages [210].

As PDGF-B/PDGFRβ signalling is required for important developmental processes and we found that PDGFRβ+ cells are precursors to a subset of HSCs in Chapter 4, we sought to determine whether proper PDGF-B/PDGFRβ signalling between endothelial cells and pericytes is required for embryonic and adult haematopoiesis. As both PDGFRβ and PDGF-B KO embryos die perinatally [157,209], we used a mouse model called PDGF-B^{ret} that survives into adulthood, with a milder phenotype than the ones of PDGFRβ and PDGF-B mice [158]. In this model, PDGF-B has a mutation in its retention domain and cannot bind to the extracellular matrix surrounding ECs. Therefore, PDGF-B does not accumulate and create a gradient necessary for proper pericyte investment to the blood vessel wall [158]. As a result, PDGF-B^{ret} KO mice have defective PDGF-B/PDGFRβ signalling between pericytes and endothelial cells, and pericytes are deficiently recruited to the blood vessel wall. As a consequence, pericytes and vSMCs are found around blood vessels, but in lower numbers, and their processes detach from the endothelium. PDGF-B^{ret} KO mice have defects in mesangial cells in the kidneys which leads to glomerulosclerosis, proteinuria, and severe deterioration of the retina [158]. As

PDGF-B^{ret} KO mice survive into adulthood, the role of PDGF-B/PDGFRβ signalling can also be studied in adult haematopoiesis.

5.2 Hypothesis and aims

5.2.1 Hypothesis

PDGF-B retention motif deletion affects haematopoiesis either due to defects in PDGF-B/PDGFRβ signalling or pericyte/vSMC recruitment to the midgestation dorsal aorta.

5.2.2 Aims

- Determine whether PDGF-B retention motif deletion affects AGM HSPCs.
- Determine whether PDGF-B retention motif deletion affects HSPCs in other haematopoietic organs.
- Determine whether PDGF-B retention motif deletion affects the recruitment of pericytes to the dorsal aorta or the interaction between PCs and ECs.
- Understand whether perivascular cell populations surrounding the dorsal aorta are affected by a deficient PDGF-B/PDGFRβ signalling in the dorsal aorta.
- Determine whether adult haematopoiesis is affected in PDGF-B^{ret} KO mice.

5.3 Results

5.3.1 PDGF-B^{ret} mutation during embryonic development

5.3.1.1 AGM HSPCs

To understand whether a deletion of PDGF-B retention motif affects AGM haematopoiesis, haematopoietic progenitor assays were performed with E11 PDGF-B^{ret} mutant AGMs. Due to large deviations in the number of colonies obtained from early E11 (40-43sp) embryos compared to late E11 (44-46sp) embryos, results were plotted separately. No significant differences were found in PDGF-B^{ret} mutants at early E11 (Figure 56, Table 30). In late E11 mutants, differences were found between HET and KO embryos, with a

significant decrease in the number of KO BFU-E, CFU-G, CFU-GEMM (Table 30) and in the total number of CFU-C compared to heterozygous mice (Figure 56, Table 30).

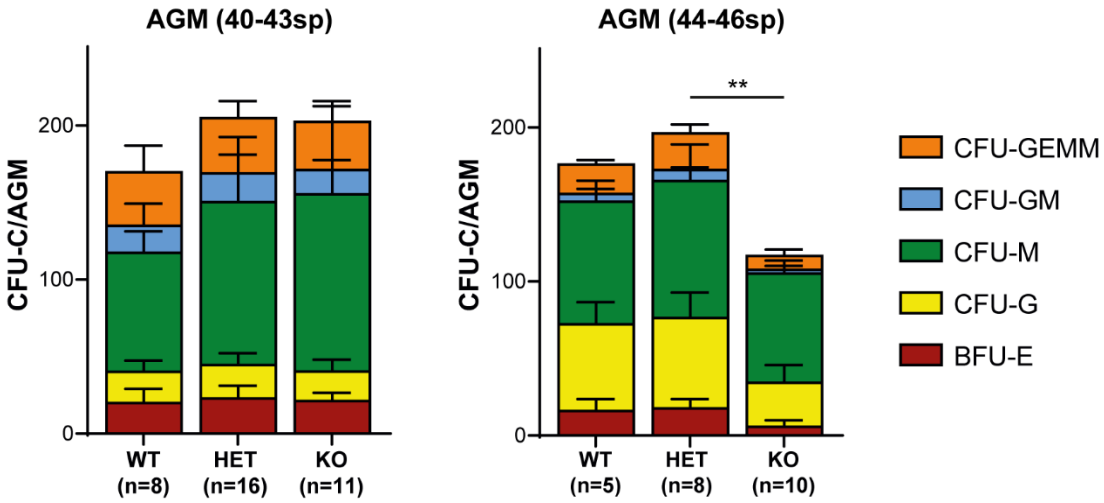

Figure 56. Total HSPC numbers decrease between PDGF-B^{ret} HET and KO late E11 embryos.
Number of colonies (CFU-C) per PDGF-B^{ret} WT, HET and KO early E11 (40-43sp) and late E11 (44-46sp) AGMs. **: p<0.01.

Table 30. Summary of CFU-C data for PDGF-B^{ret} WT, HET and KO E11 AGMs.
Haematopoietic progenitor assays were performed for PDGF-Bret WT, HET and KO early E11 (40-43sp) and late E11 (44-46sp) AGMs. The number of embryos, CFU-C per tissue (mean ± SD), fold changes in CFU-C numbers between WT, HET and KO mice, the statistical tests used, p values and multiple comparison tests are shown here. Significant differences are indicated with asterisks: * p<0.05; ** p<0.01; ns: no significance.

			N				Average			Fold decrease			Statistics				Multiple comparisons		
Tissue	Day	Somite pairs	WT	HET	KO	CFU-type	WT	HET	KO	WT vs HET	WT vs KO	HET vs KO	Statistical test	Post-hoc	p-value		WT vs HET	WT vs KO	Het vs KO
AGM	11	40-43	8	16	11	BFU-E	18.88	22.75	21.09	0.83	0.89	1.08	1 way ANOVA	Tukey's test	0.6724	ns	ns	ns	ns
						CFU-G	20.31	21.69	19.18	0.94	1.06	1.13	1 way ANOVA	Tukey's test	0.6974	ns	ns	ns	ns
						CFU-M	77.19	105.94	115.00	0.73	0.67	0.92	1 way ANOVA	Tukey's test	0.1923	ns	ns	ns	ns
						CFU-GM	17.44	18.75	15.91	0.93	1.10	1.18	1 way ANOVA	Tukey's test	0.8128	ns	ns	ns	ns
						CFU-GEMM	34.94	35.69	31.27	0.98	1.12	1.14	1 way ANOVA	Tukey's test	0.6526	ns	ns	ns	ns
						Total	169.75	204.81	202.46	0.83	0.84	1.01	1 way ANOVA	Tukey's test	0.4629	ns	ns	ns	ns
AGM	11	44-46	5	8	10	BFU-E	16	17.67	5.75	0.91	2.78	3.07	1 way ANOVA	Tukey's test	0.0276	*	ns	ns	*
						CFU-G	56.25	58.67	28.5	0.96	1.97	2.06	Kruskal-Wallis	Dunn's test	0.0196	*	ns	ns	*
						CFU-M	79.5	89.00	70.75	0.89	1.12	1.26	1 way ANOVA	Tukey's test	0.3251	ns	ns	ns	ns
						CFU-GM	5	7.00	2.5	0.71	2.00	2.80	Kruskal-Wallis	Dunn's test	0.0844	ns	ns	ns	ns
						CFU-GEMM	19.25	23.83	9	0.81	2.14	2.65	Kruskal-Wallis	Dunn's test	0.0016	**	ns	ns	**
						Total	176	197.33	116	0.89	1.52	1.70	1 way ANOVA	Tukey's test	0.0175	*	ns	ns	**

5.3.1.2 HSPCs in other haematopoietic organs

To determine whether HSPCs are affected by PDGF-B^{ret} deletion in other haematopoietic organs at the time of HSC generation, haematopoietic progenitor assays were performed in E11 embryos (40-43sp) (Figure 57, Table 31). No significant differences were found in the total number of colonies in PDGF-B^{ret} mutant E11 head, PL and FL, with the exception of the YS, where differences were detected, however post-hoc test was not sensitive enough to find where the difference lies (Figure 57, Table 31). KO BFU-Es in both the FL and the PL were also significantly reduced compared to WT BFU-Es, and there was a significant increase between HET and KO CFU-GEMM in the head (Table 31). No other differences were found in HSPCs of E11 haematopoietic organs, although there seems to be a trend increase between WT and KO YS CFU-Cs.

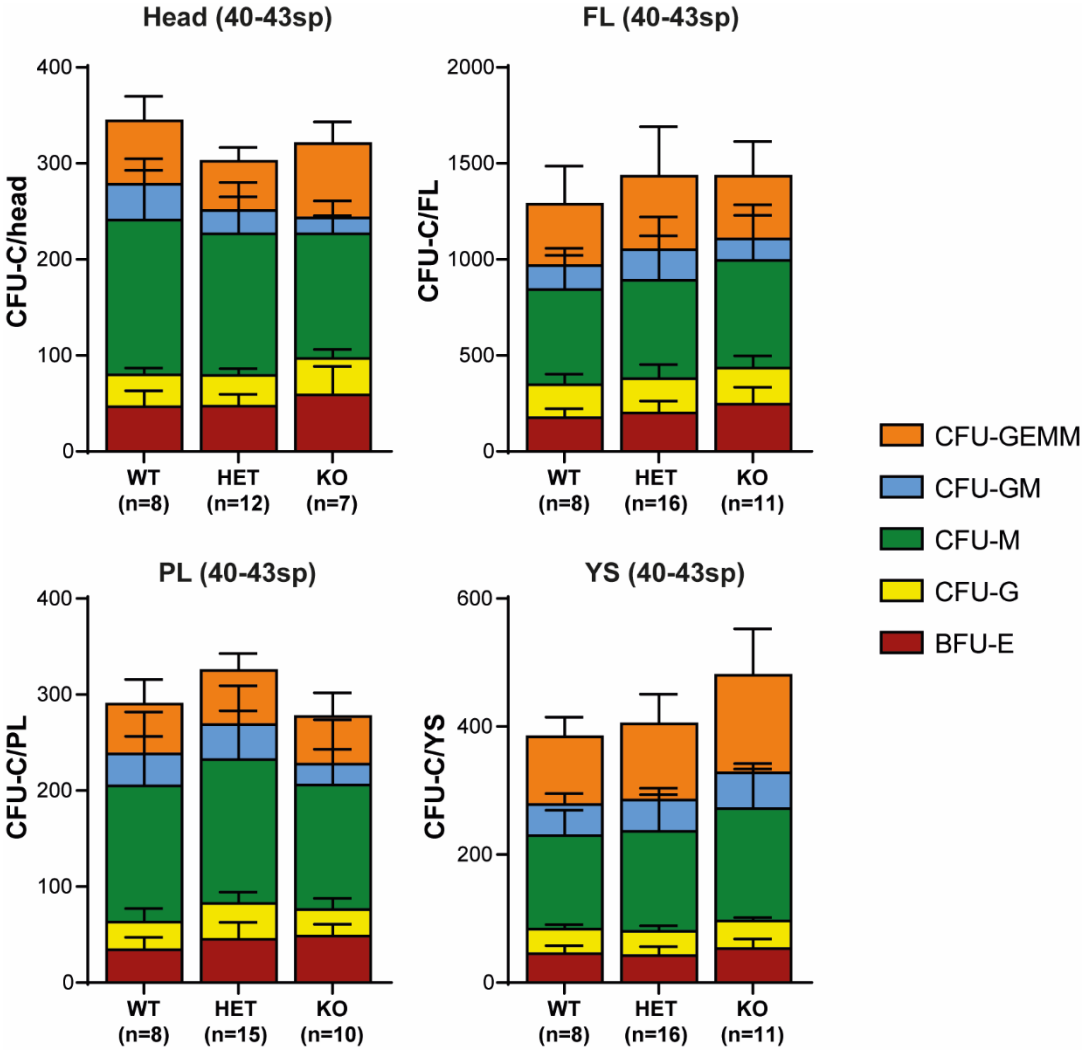

Figure 57. HSPCs in the head, foetal liver, placenta and yolk sac are not affected in E11 PDGF-B^{ret} mutants.
CFU-C numbers per PDGF-B^{ret} WT, HET and KO E11 (40-43sp) head, FL, PL and YS.

Table 31. Summary of CFU-C data for PDGF-B^{ret} WT, HET and KO E11 haematopoietic organs.
Haematopoietic progenitor assays were performed for PDGF-Bret WT, HET and KO early E11 (40-43sp) head, FL, PL and YS. The number of embryos, CFU-C per tissue (mean ± SD), fold changes in CFU-C numbers between WT, HET and KO mice, the statistical tests used, p values and multiple comparison tests are shown here. Significant differences are indicated with asterisks: * p<0.05; ** p<0.01; *** p<0.001 ns: no significance.

			N				Average			Fold decrease			Statistics				Multiple comparisons		
Tissue	Day	Somite pairs	WT	HET	KO	CFU-type	WT	HET	KO	WT vs HET	WT vs KO	HET vs KO	Statistical test	Post-hoc	p-value		WT vs HET	WT vs KO	Het vs KO
Head	11	40-43	8	12	7	BFU-E	46.59	47.22	58.87	0.99	0.79	0.80	Kruskal-Wallis	Dunn's test	0.7723	ns	ns	ns	ns
						CFU-G	33.33	31.82	38.10	1.05	0.88	0.84	1 way ANOVA	Tukey's test	0.243	ns	ns	ns	ns
						CFU-M	160.98	147.47	129.44	1.09	1.24	1.14	1 way ANOVA	Tukey's test	0.4401	ns	ns	ns	ns
						CFU-GM	37.12	24.24	16.88	1.53	2.20	1.44	Kruskal-Wallis	Dunn's test	0.1621	ns	ns	ns	ns
						CFU-GEMM	66.29	51.26	77.06	1.29	0.86	0.67	Kruskal-Wallis	Dunn's test	0.0316	*	ns	ns	*
						Total	344.32	302.02	480.44	1.14	0.72	0.63	Kruskal-Wallis	Dunn's test	0.5195	ns	ns	ns	ns
FL	11	40-43	8	16	11	BFU-E	175.00	200.00	245.45	0.88	0.71	0.81	Kruskal-Wallis	Dunn's test	0.023	*	ns	*	ns
						CFU-G	172.50	178.75	189.09	0.97	0.91	0.95	1 way ANOVA	Tukey's test	0.8575	ns	ns	ns	ns
						CFU-M	495.00	512.50	560.00	0.97	0.88	0.92	Kruskal-Wallis	Dunn's test	0.8772	ns	ns	ns	ns
						CFU-GM	125.00	158.75	110.91	0.79	1.13	1.43	Kruskal-Wallis	Dunn's test	0.8366	ns	ns	ns	ns
						CFU-GEMM	320.00	382.50	327.27	0.84	0.98	1.17	Kruskal-Wallis	Dunn's test	0.9195	ns	ns	ns	ns
						Total	1287.50	1432.50	1432.73	0.90	0.90	1.00	1 way ANOVA	Tukey's test	0.8178	ns	ns	ns	ns
PL	11	40-43	8	15	10	BFU-E	34.20	45.25	48.48	0.76	0.71	0.93	Kruskal-Wallis	Dunn's test	0.0413	*	ns	*	ns
						CFU-G	29.00	37.37	27.61	0.78	1.05	1.35	1 way ANOVA	Tukey's test	0.1226	ns	ns	ns	ns
						CFU-M	141.56	149.49	129.63	0.95	1.09	1.15	Kruskal-Wallis	Dunn's test	0.8407	ns	ns	ns	ns
						CFU-GM	33.33	36.57	21.89	0.91	1.52	1.67	1 way ANOVA	Tukey's test	0.0986	ns	ns	ns	ns
						CFU-GEMM	51.95	56.57	49.49	0.92	1.05	1.14	1 way ANOVA	Tukey's test	0.7276	ns	ns	ns	ns
						Total	290.04	325.25	277.10	0.89	1.05	1.17	Kruskal-Wallis	Dunn's test	0.305	ns	ns	ns	ns
YS	11	40-43	8	16	11	BFU-E	45.45	42.23	53.44	1.08	0.85	0.79	1 way ANOVA	Tukey's test	0.131	ns	ns	ns	ns
						CFU-G	38.26	38.07	42.70	1.00	0.90	0.89	1 way ANOVA	Tukey's test	0.2519	ns	ns	ns	ns
						CFU-M	146.21	155.87	175.48	0.94	0.83	0.89	Kruskal-Wallis	Dunn's test	0.556	ns	ns	ns	ns
						CFU-GM	48.48	49.05	55.92	0.99	0.87	0.88	1 way ANOVA	Tukey's test	0.5291	ns	ns	ns	ns
						CFU-GEMM	106.06	119.13	152.89	0.89	0.69	0.78	1 way ANOVA	Tukey's test	0.1404	ns	ns	ns	ns
						Total	384.47	404.36	480.44	0.95	0.80	0.84	Kruskal-Wallis	Dunn's test	0.0247	*	ns	ns	ns

5.3.1.3 HSCs from PDGF-Bret KO embryos fail to reconstitute secondary recipients

Although few differences were detected in haematopoietic progenitor assays, HSCs could still be affected in PDGF-B^{ret} KO embryos. E11 AGMs were therefore injected into sub-lethally irradiated recipients, and the percentage of donor chimerism assessed in the peripheral blood of transplanted mice after 4 months. Positive reconstitution was detected in 4/21 mice injected with PDGF-B^{ret} WT AGM cells, 8/28 with HET AGM cells and 4/19 with KO AGM cells (Figure 59A). This suggests that the deletion of PDGF-B retention motif does not affect long-term reconstitution potential. To test whether these cells self-renew, secondary transplantations were performed. The whole BM of positively reconstituted recipients was injected into two sub-lethally irradiated recipients (Figure 58), and peripheral blood was analysed after 1 and 4 months following transplantation (Figure 59B). Whereas WT and HET donor HSCs were found to self-renew, KO donor cells did not. No difference in lineage reconstitution was detected between positively reconstituted mutants in both primary and secondary transplantations (not shown).

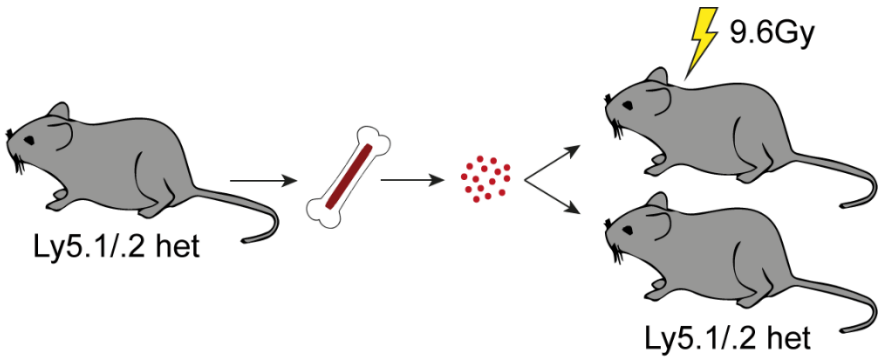

Figure 58. Secondary transplantations.
Schematic representation of secondary transplantation procedure. Whole BM cells from a successfully reconstituted recipient were injected into two sub-lethally irradiated Ly5.1/.2 heterozygous recipient mice.

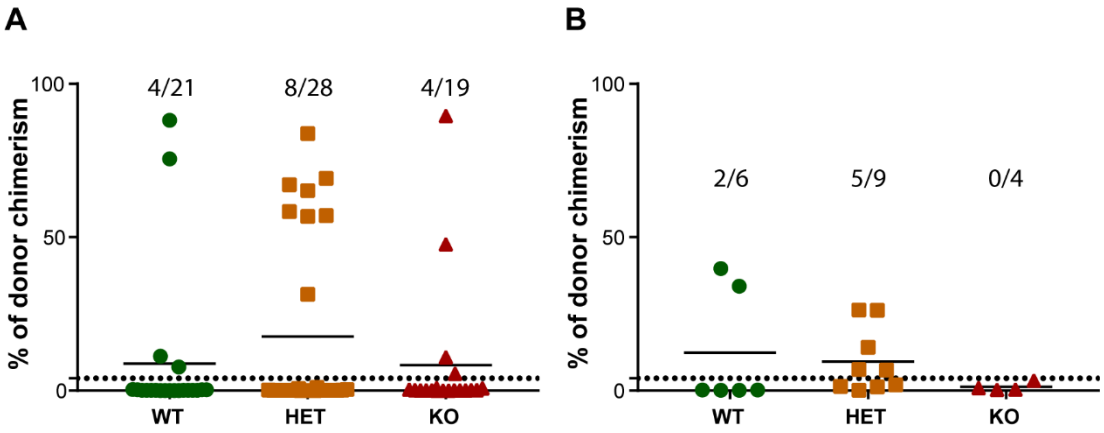

Figure 59. Self-renewal of PDGF-B^{ret} KO E11 HSCs is impaired.
(A) Percentages of donor chimerism is shown after 4 months following primary transplantations, and (B) 4 months following secondary transplantations into sub-lethally irradiated recipients. BM of mice reconstituted in primary transplantations were injected into 2 mice in secondary transplantations. Each dot represents one transplanted mouse. Mice are reconstituted when >4% donor cells are found in the host peripheral blood (dotted line). Number of reconstituted mice/number of transplanted mice are given in each group. A two proportion Z-test was used to test for significance.

5.3.1.4 The dorsal aorta is properly formed in PDGF-B^{ret} KO midgestation embryos

To understand whether PDGF-B retention is important for the formation and integrity of the dorsal aorta, 3D-whole mount immunostainings were performed on E10.5 PDGF-B^{ret} mutant embryos (Figure 60). cKit expression was detected in haematopoietic clusters of both PDGF-B^{ret} WT and KO embryos, as expected, with no visible differences in the size of clusters between WT and KO. No differences were observed in DA morphology, and its integrity was not affected (Figure 60). A slight increase in αSMA expression was detected around the KO aorta (Figure 60).

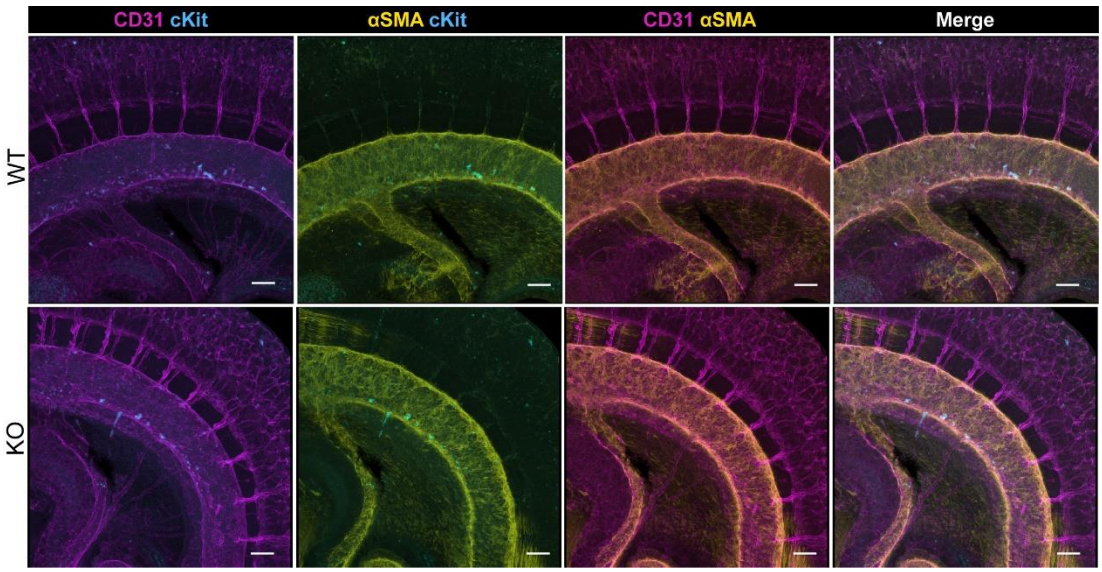

Figure 60. DA is properly formed in PDGF-B^{ret} KO E10.5 embryos.
Confocal images of whole-mount immunostainings of PDGF-B^{ret} WT and KO E10.5 DAs stained with cKit (cyan), αSMA (yellow) and CD31 (magenta). Scale bars: 100µm.

To understand whether the distribution of the different perivascular cell populations surrounding the DA was altered by the lack of PDGF-B retention motif, immunohistochemistry analysis was performed in PDGF-B^{ret} WT and KO embryos. E11 cryosections were first stained with PDGFRβ and CD31. No differences in PDGFRβ expression and distribution were detected in the KO embryos (Figure 61). CD31 expression appeared normal, confirming the whole mount immunostaining data (Figure 60 andFigure *61*).

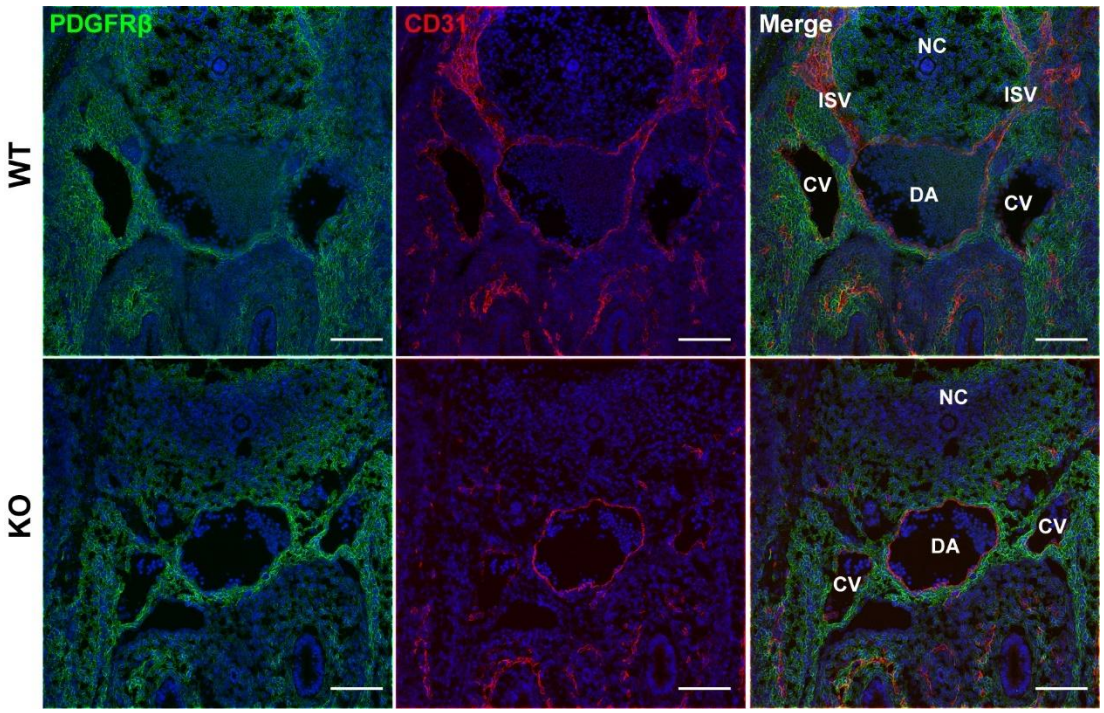

Figure 61. PDGB-B^{ret} KO does not affect PDGFRβ expression around the DA and CVs. Immunohistochemistry on PDGF-Bret WT and KO E11 cryosections stained with PDGFRβ (green) and CD31 (red). Nuclei were counterstained with DAPI. Scale bars: 100µm.

Sections were next stained with NG2 and CD31. NG2 expression appeared to be normal both around the DA as well as around the notochord in PDGF-B^{ret} KO E11 embryos. In the WT sections, NG2 expression was absent near and around the ISVs (Figure 62). This is in line with the data obtained by 3D-whole mount immunostaining in Chapter 4 (Chapter 4, Figure 35B), suggesting that only the dorsal aorta and umbilical and vitelline arteries are surrounded by NG2+ PCs.

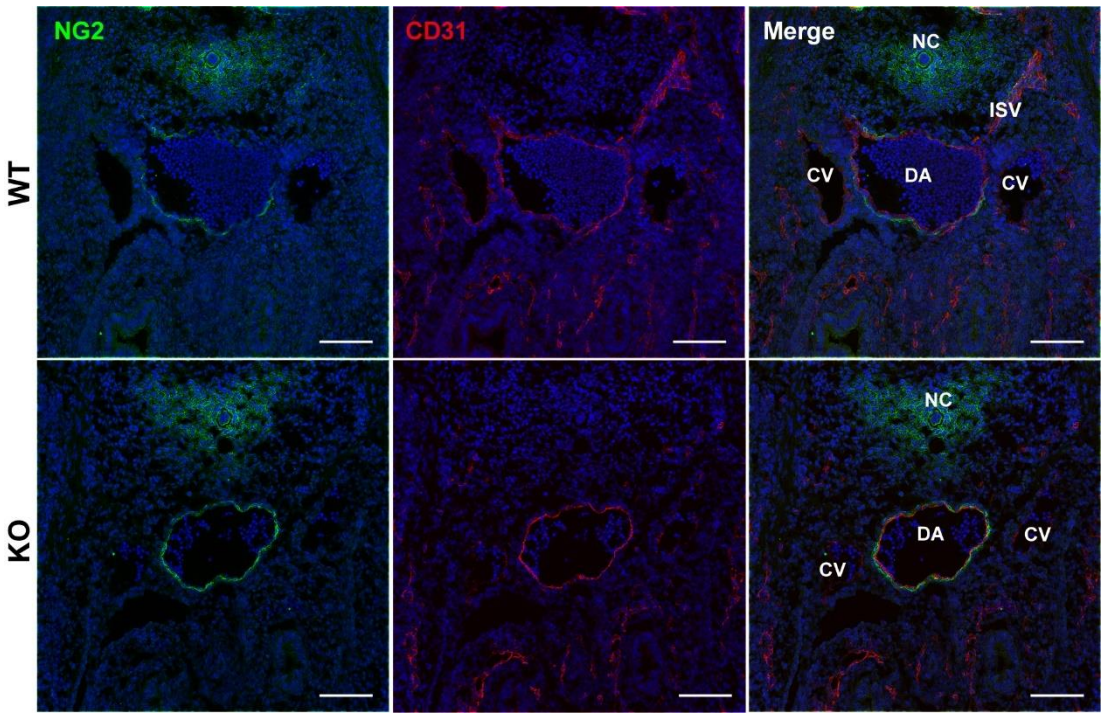

Figure 62. PDGB-B^{ret} KO does not affect NG2 expression around the DA and NC. Immunohistochemistry on PDGF-Bret WT and KO E11 cryosections stained with NG2 (green) and CD31 (red). Nuclei were counterstained with DAPI. Scale bars: 100µm.

Double staining with NG2 and PDGFRβ was next performed. PCs and sub-PCs were detected in both PDGF-B^{ret} WT and KO, suggesting that deletion in PDGF-B retention motif does not affect their recruitment to the DA (Figure 63).

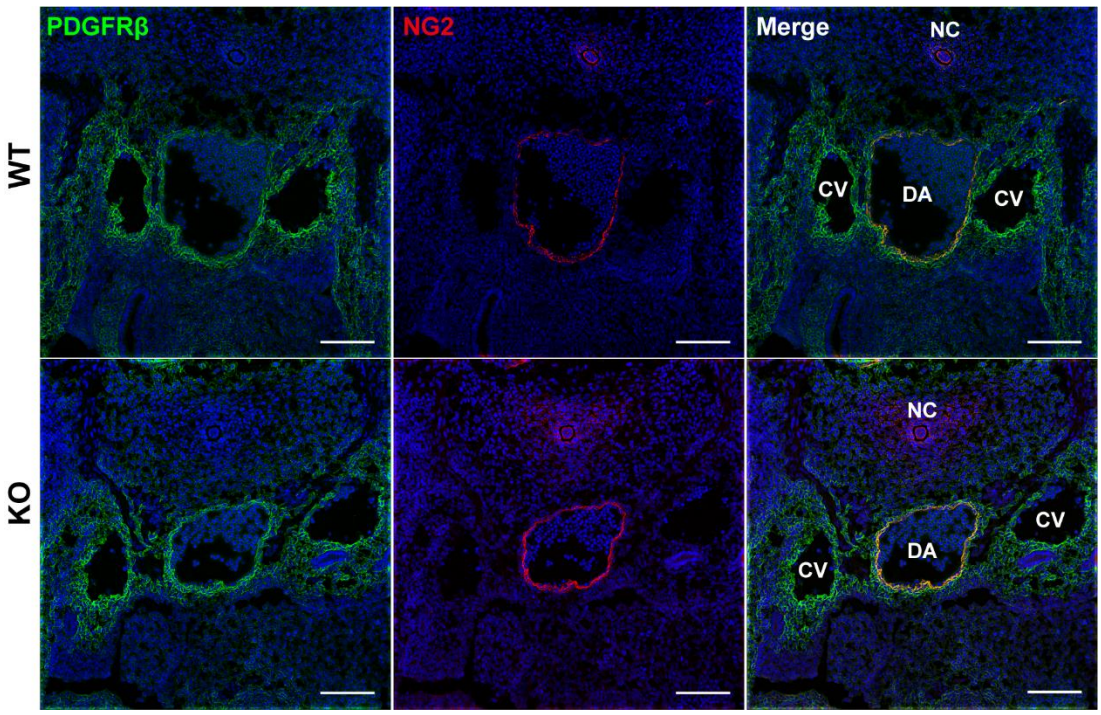

Figure 63. NG2+ PDGFRβ+ PCs are unaffected in PDGF-Bret KO E11 embryos.
Immunohistochemistry on PDGF-Bret WT and KO E11 cryosections stained with PDGFRβ (green) and NG2 (red). Nuclei were counterstained with DAPI. Scale bars: 100µm.

Staining with αSMA was also performed, and no difference was detected in the distribution of αSMA+ cells in the KO embryos. However, αSMA expression in PDGF-Bret KO appeared slightly higher than in the WT (Figure 64), in line with the observations made on the whole-mount data (Figure 60).

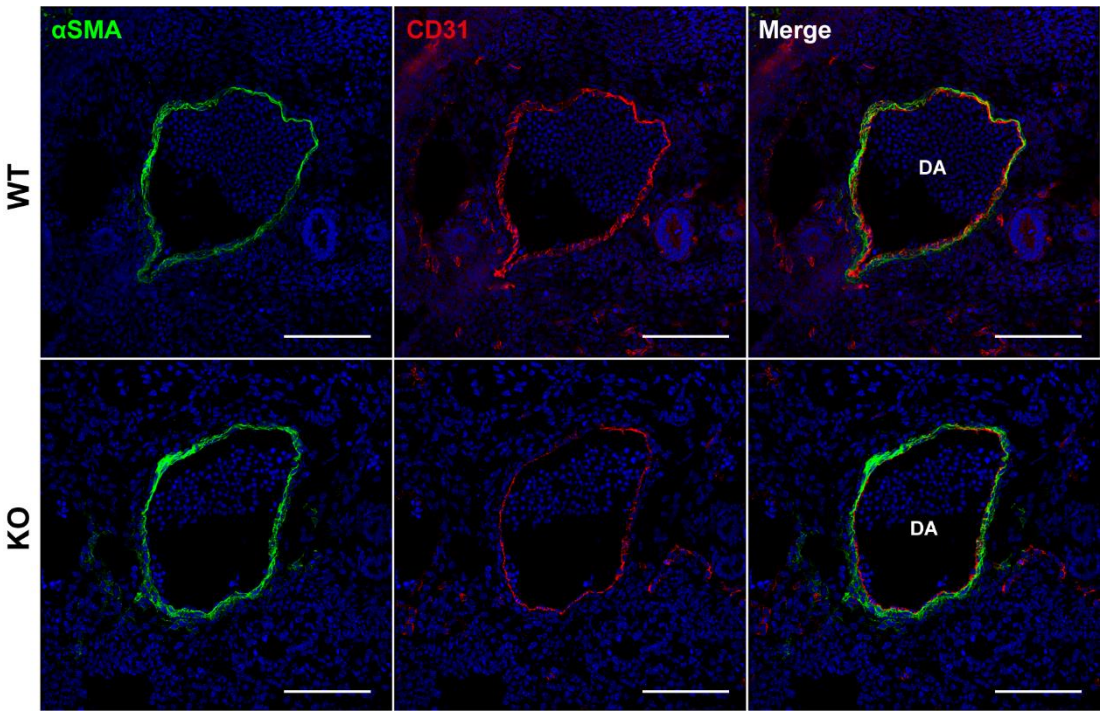

Figure 64. αSMA expression is slightly increased around PDGF-B^{ret} KO E11 DA. Immunohistochemistry on PDGF-Bret WT and KO E11 cryosections stained with αSMA (green) and CD31 (red). Nuclei were counterstained with DAPI. Scale bars: 100µm.

CD146 expression was also assessed, and no differences were found in PDGF-B^{ret} KO embryos compared to WT (Figure 65).

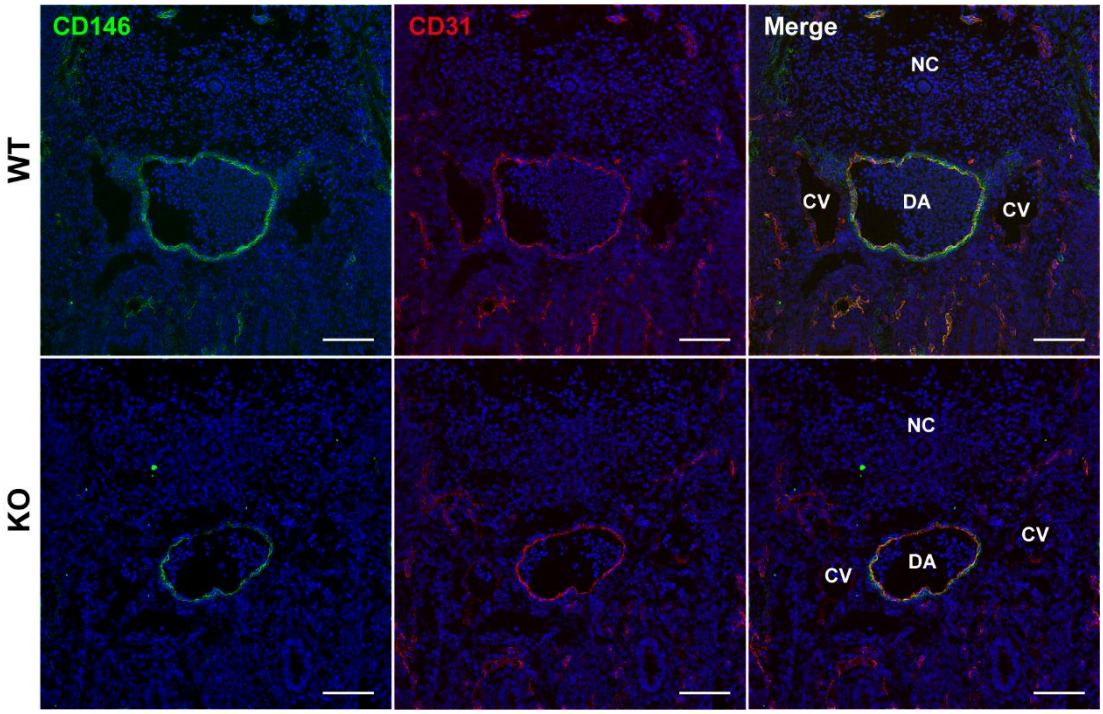

Figure 65. CD146 expression was not altered in PDGF-B^{ret} KO E11 embryos.
Immunohistochemistry on PDGF-Bret WT and KO E11 cryosections stained with CD146 (green) and CD31 (red). Nuclei were counterstained with DAPI. Scale bars: 100µm.

Lastly, Collagen IV staining was also performed, and no differences in Collagen IV expression were detected between PDGF-B^{ret} WT and KO embryos (Figure 66).

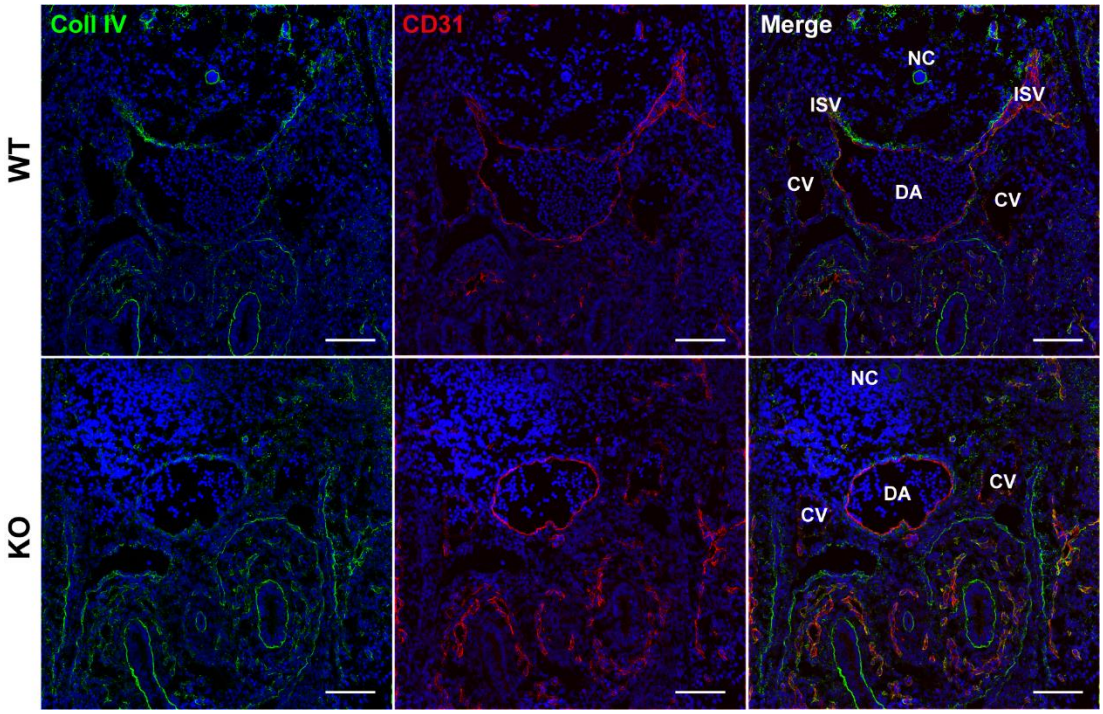

Figure 66. Collagen IV expression is not affected in PDGF-B^{ret} KO E11 embyros.
Immunohistochemistry on PDGF-Bret WT and KO E11 cryosections stained with Collagen IV (green) and CD31 (red). Nuclei were counterstained with DAPI. Scale bars: 100µm.

5.3.1.5 PDGF-B^{ret} mutation does not affect the cellular composition of the midgestation AGM

To understand whether PDGF-B^{ret} mutation affects the normal composition of cells in the AGM, E11 embryos were analysed by flow cytometry. Single live AGM cells were analysed for the expression of different markers (Figure 67). No differences were found in the percentages of any of the markers analysed (CD31, CD45, cKit, NG2, PDGFRβ and PDGFRα) (Figure 67).

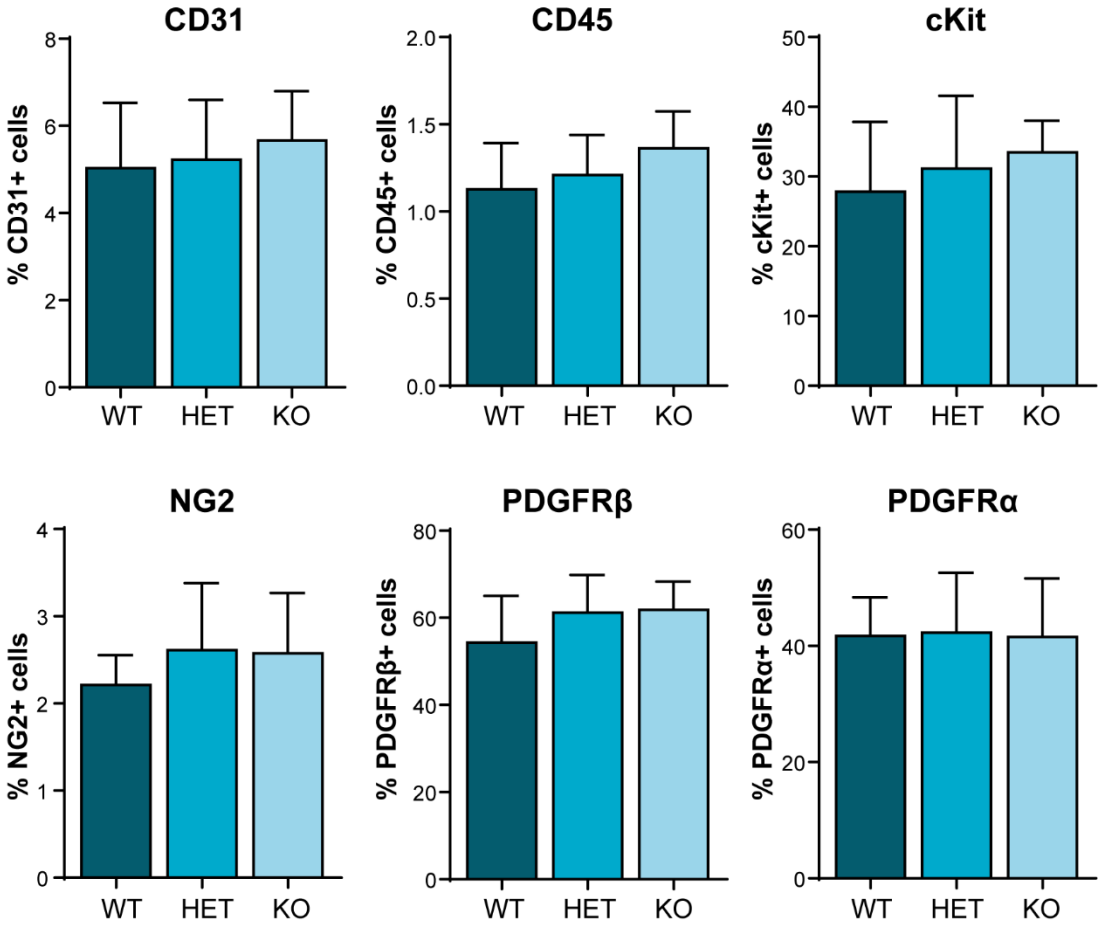

Figure 67. No differences in percentages of E11 AGM cell populations were found in PDGF-B^{ret} mutants.
Percentage of CD31+, CD45+, cKit+, NG2+, PDGFRβ+ and PDGFRα+ single viable cells in PDGF-B^{ret} analysed by flow cytometry. 9 WT, 15 HET and 5 KO embryos were analysed.

The percentages of endothelial cells (CD31+ cKit- CD45-) and HSPCs (CD31+ cKit+ NG2- PDGFRβ-) were also assessed (Figure 68). HSPCs were analysed based on the absence of the perivascular cell markers PDGFRβ and NG2, because we found in the previous chapter that PDGFRβ+ cells are not haematopoietic (Chapter 4, Figure 17), nor are NG2+ cells (*Gonzalez et al., In Preparation*). Deletion of PDGF-B retention motif did not affect the percentages of ECs not HSPCs (Figure 68).

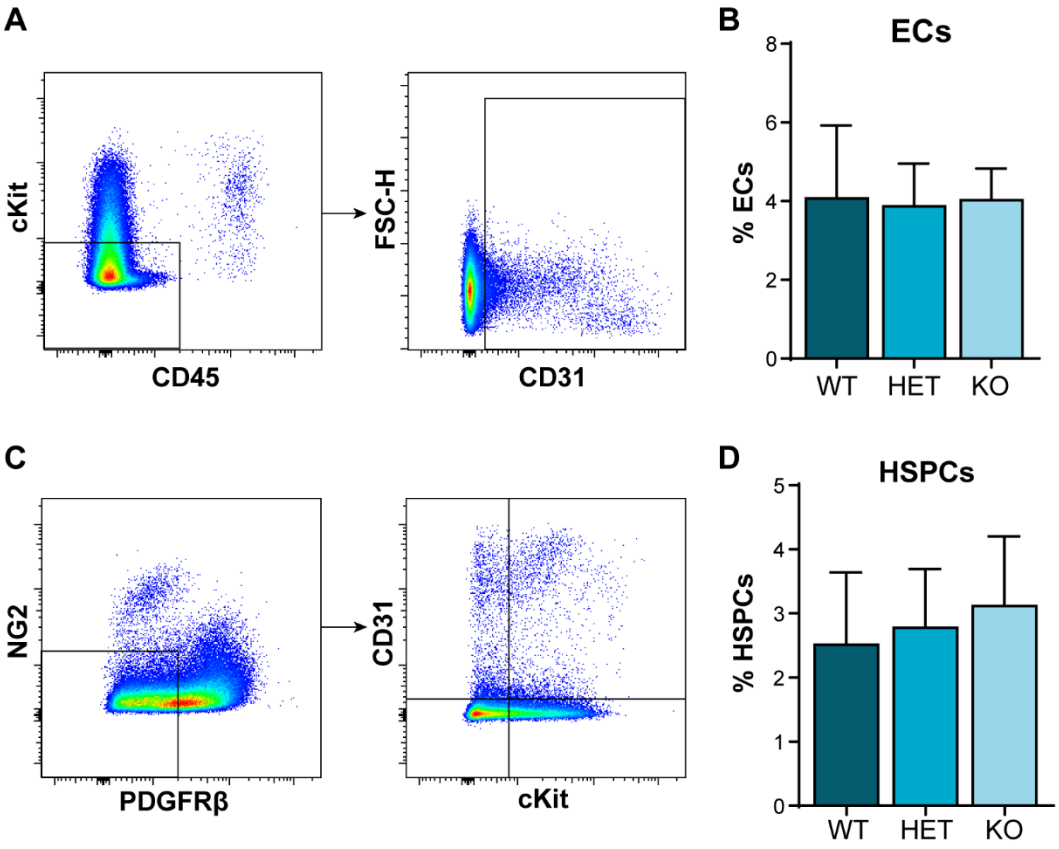

Figure 68. Flow cytometry analysis of ECs and HSPCs from E11 PDGF-B^{ret} mutants. (A) Gating strategy used to analyse ECs (CD31+ CD45- cKit- single live cells). (B) Percentages of ECs in PDGF-B^{ret} WT, HET and KO E11 embryos. (C) Gating strategy used to analyse HSPCs (CD31+ cKit+ NG2- PDGFRβ- single live cells). (D) Percentages of HSPCs in PDGF-B^{ret} WT, HET and KO embryos. 9 WT, 15 HET and 5 KO embryos were analysed.

Perivascular cell percentages were next assessed to understand whether PDGF-B^{ret} mutation affected their numbers. No differences were found in any of the populations of perivascular cells in PDGF-B^{ret} mutants compared to WT (Figure 69).

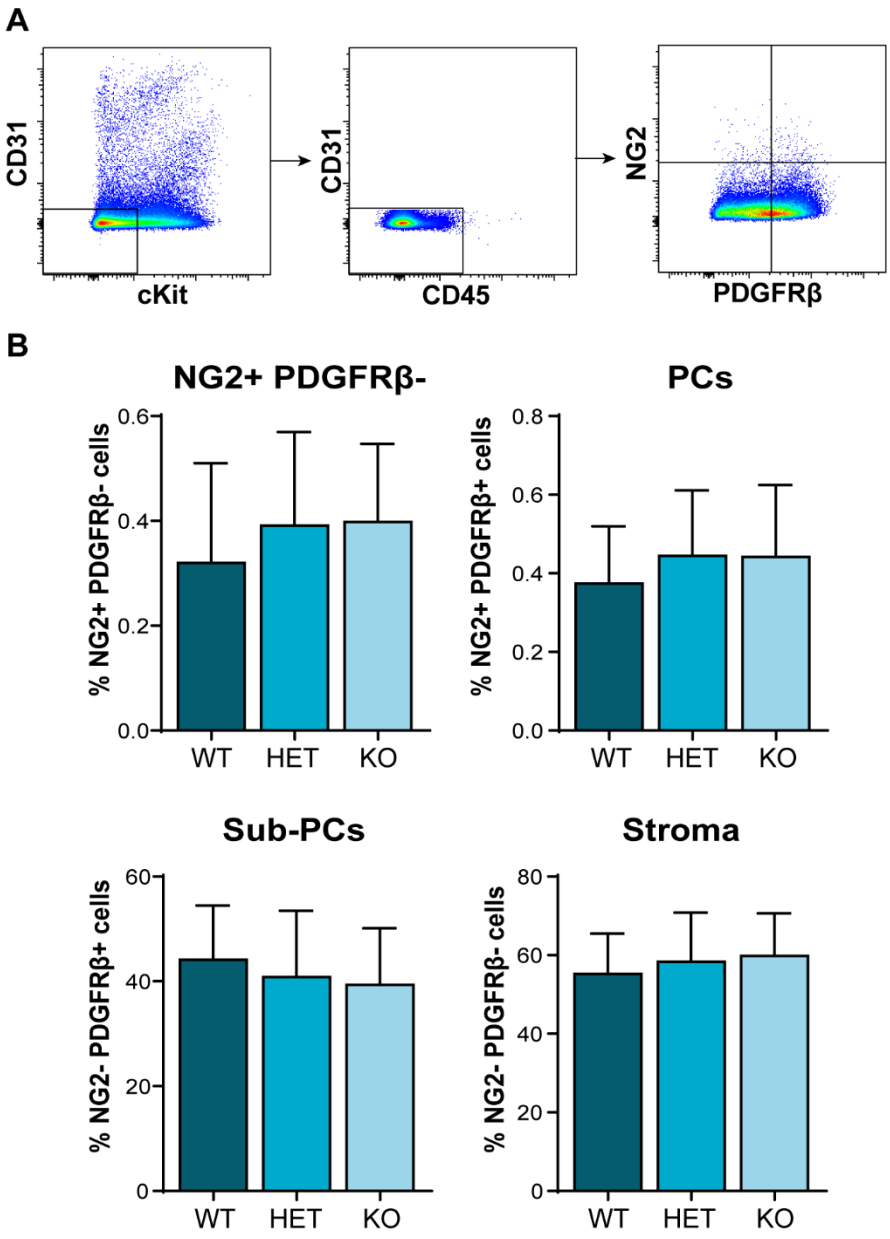

Figure 69. Flow cytometry analysis of the three perivascular cell populations in PDGF-B^{ret} WT, HET and KO E11 AGMs.
(A) Gating strategy used to analyse the percentages of the three perivascular cell populations described in Chapter 3 by flow cytometry. (B) Percentages of NG2+ PDGFRβ- notochord cells, PCs, sub-PCs and stroma in E11 PDGF-B^{ret} mutants. 9 WT, 15 HET and 5 KO embryos were analysed.

Because PDGF-B is also a ligand of PDGFRα, a mutation in PDGF-B retention motif could potentially lead to an increase in PDGFRα expression in the AGM to compensate for the diffusion of PDGF-B. Therefore, PDGFRα expression was analysed in HSPCs, ECs and perivascular cells by flow cytometry. No

changes were detected in PDGFRα expression in any population analysed. We also found that PDGFRα was highly expressed in PCs and sub-PCs (in approximately 80% of cells) (Figure 70). These data suggest that there is no PDGFRα compensation around the DA due to the PDGF-B^{ret} mutation.

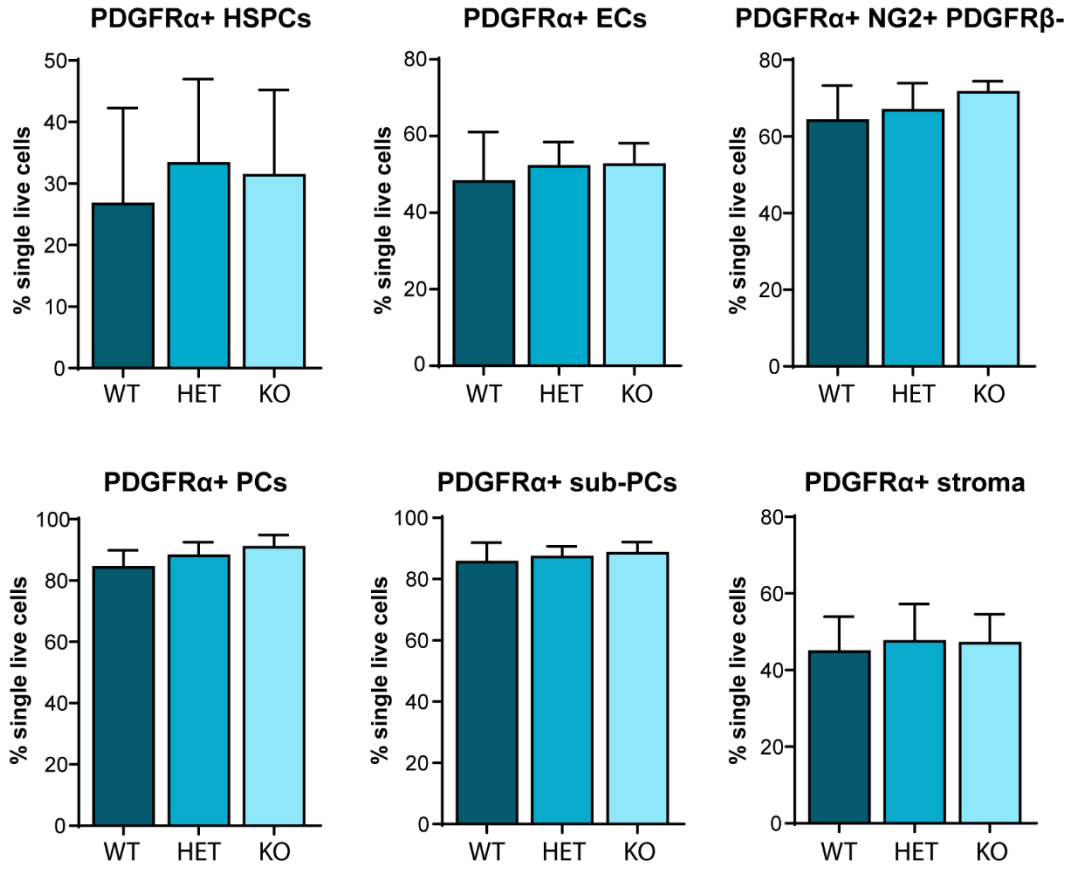

Figure 70. PDGFRα expression in PDGF-B^{ret} E11 mutant HSPCs, ECs, and perivascular cells.
Flow cytometry analyses of PDGFRα+ HSPCs, ECs, NG2+ PDGFRβ- notochord cells, PCs, sub-PCs and stroma. 9 WT, 15 HET and 5 KO embryos were analysed.

5.3.2 PDGF-B^{ret} adult BM haematopoiesis

5.3.2.1 Haematopoietic progenitors are not affected by the deletion of PDGF-B retention motif.

To understand whether PDGF-B retention defects affect adult haematopoiesis, haematopoietic progenitor assays were performed on BM cells of PDGF-B^{ret} WT, Het and KO adult mice. No significant differences in the number of progenitors between PDGF-B^{ret} WT, HET and KO were found (Figure 71),

suggesting that PDGF-B^{ret} mutation does not affect HSPC homeostasis in the adult BM.

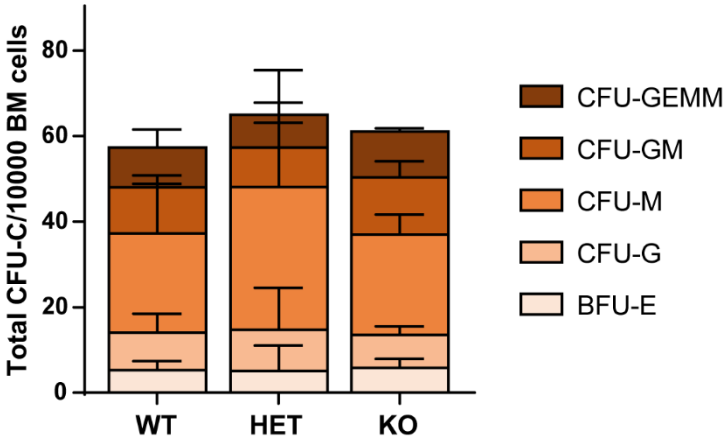

Figure 71. Haematopoietic progenitor assays.
CFU-Cs per 10000 cells of PDGF-B^{ret} adult BM seeded. WT: n=8; HET: n=7; KO: n=3.

5.3.2.2 No significant differences in LSK-SLAM populations in the adult BM of PDGF-B^{ret} mutants

LSK-SLAM analysis was performed on PDGF-B^{ret} mutant BM cells to determine whether there are any differences in the most immature haematopoietic progenitors and HSCs due to the deletion of PDGF-B retention motif (Figure 72). LSK (Lin- Sca1+ cKit+) HSCs [211–213] were selected by the absence of lineage surface markers (Lin-) and presence of Sca1 and cKit, and further purified into four populations based on the expression of the SLAM family markers CD48 and CD150 [212,213] (Figure 72A). Within the LSK population, CD48+CD150- (HPC1) and CD48+CD150+ (HPC2) cells are restricted progenitors, while CD48-CD150- cells (MPPs) are non-self-renewing or transiently reconstituting multipotent progenitors, and CD150+CD48- cells are HSCs. No differences were found in PDGF-B^{ret} mutant BMs in any of the populations analysed (Figure 72B), suggesting that PDGF-B^{ret} mutation does not alter the frequency of immature haematopoietic progenitors and stem cells in the BM.

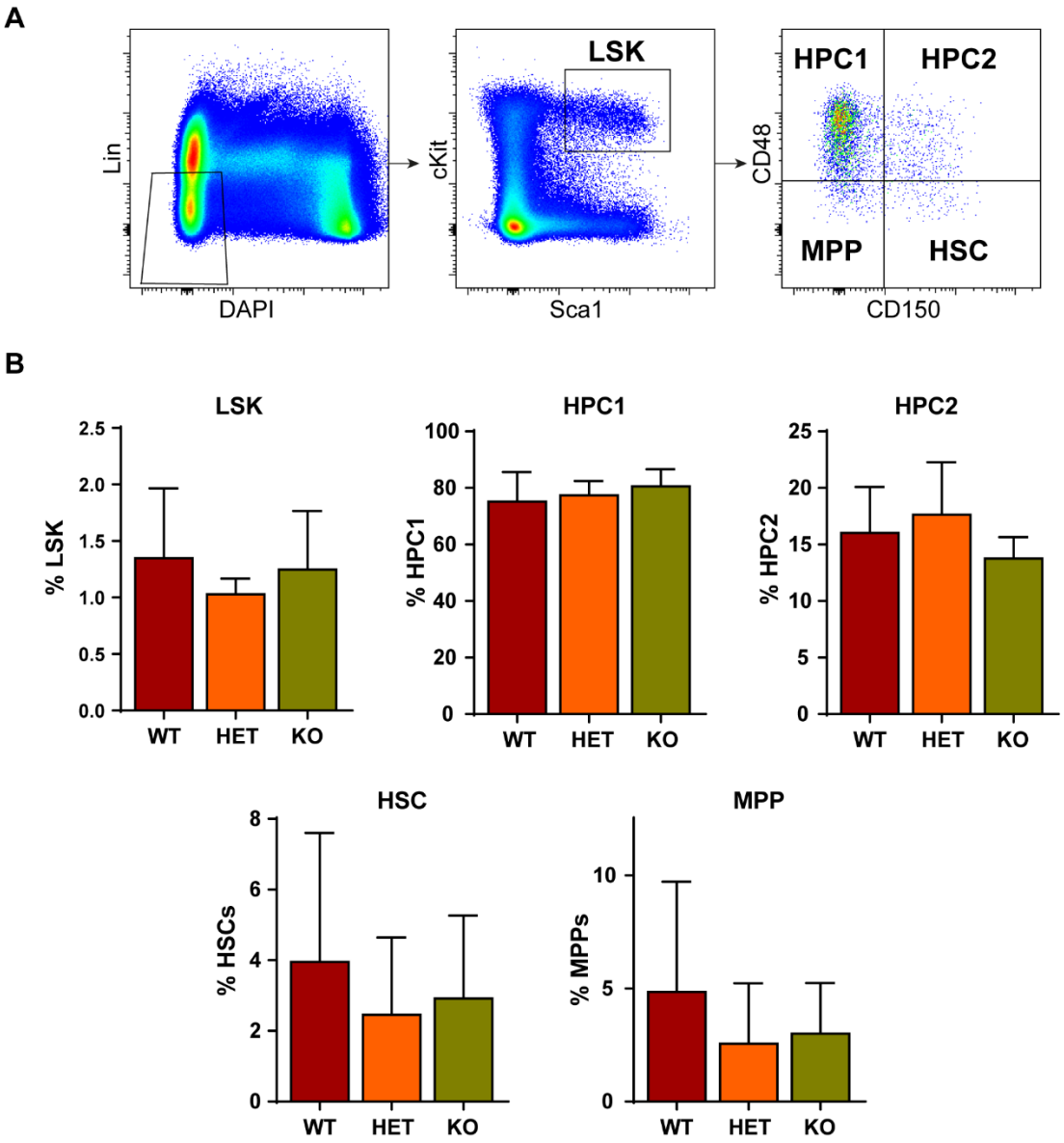

Figure 72. LSK-SLAM analysis of PDGF-Bret adult BM.
(A) Gating strategy for LSK cells from single live cells and the expression of the SLAM family markers CD150 (Slamf1) and CD48 (Slamf2) within the LSK population in PDGF-B^{ret} WT, HET and KO adult BM. Within LSK HSPCs, HPC1 (CD48+ CD150-) and HPC2 (CD48+ CD150+) contain restricted progenitors; MPPs (CD48- CD150-) contain non-self-renewing or transiently reconstituting multipotent progenitors. The CD150+ CD48- fraction contains highly purified HSCs. (B) Percentages of the different populations of LSK-SLAM obtained by flow cytometry. WT: n=4; HET: n=5; KO: n=3.

5.3.2.3 Self-renewing haematopoietic stem cells are present in the BM of PDGF-B mutants.

To understand whether BM HSCs are affected, BM cells from PDGF-B^{ret} WT, Het and KO mice were transplanted into sub-lethally irradiated recipients. No

significant differences in reconstitution were found after 4 months between WT, HET and KO BM cells both in primary (Figure 73) and secondary transplantations (Figure 73). In addition, there were no differences in lineage reconstitution (lymphoid and myeloid) between mutants (not shown). Together, these data suggest that adult HSCs are not affected by the deletion of PDGF-B retention motif.

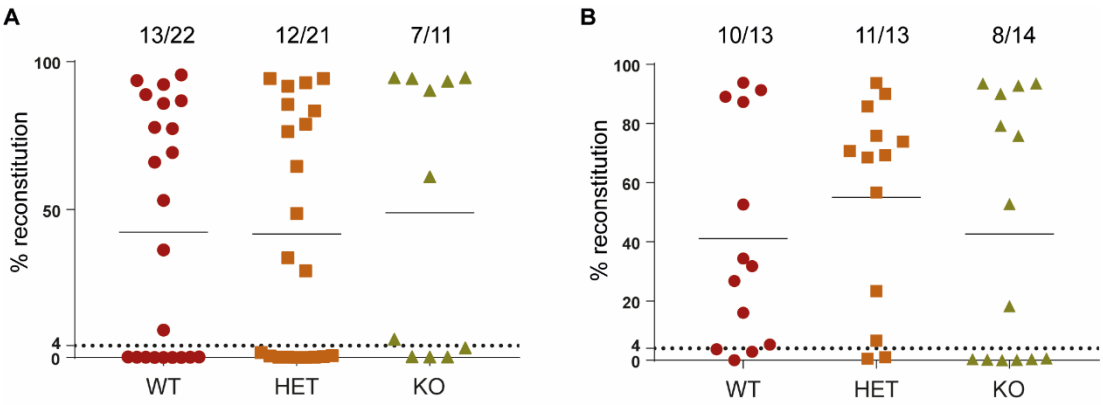

Figure 73. PDGF-B^{ret} BM contain self-renewing HSCs.
Percentages of donor chimerism 4 months after (A) primary transplantations and (B) secondary transplantations with PDGF-Bret adult BMs. Each dot represents one transplanted mouse. Mice are reconstituted when >4% donor cells are found in the host peripheral blood (dotted line). Numbers on the graph represent the number of mice that was reconstituted per number of mice injected.

5.4 Discussion

Since PDGF-B and PDGFRβ KO embryos die perinatally, we sought to determine whether defective PDGF-B/PDGFRβ signalling affects murine embryonic and adult haematopoiesis with the use of PDGF-B^{ret} mutant mice.

5.4.1 PDGF-B^{ret} AGM-derived HSCs fail to reconstitute secondary recipients

PDGF-B overexpression in zebrafish was shown to increase the percentage of HSPCs in the dorsal aorta [149]. We therefore hypothesised that defects in PDGF-B retention around the endothelium would decrease the number of HSPCs found in the AGM, due to a defective PDGF-B/PDGFRβ signalling between pericytes and endothelial cells.

Although no differences were detected between WT and KO AGM HSPCs, we sought to determine whether HSCs were affected by PDGF-B mutation. PDGF-B^{ret} KO embryos appear to contain HSCs that reconstitute primary recipients but fail to reconstitute secondary recipients (Figure 59), suggesting that PDGF-B^{ret} KO AGMs fail to generate long-term reconstituting HSCs. Due to the low number of reconstituted mice and the low number of mice injected in secondary transplantations, these results remain inconclusive. Additional secondary transplantations from PDGF-B^{ret} KO reconstituted primary recipients should be performed to confirm these results. If these data are confirmed, it would support the hypothesis that HSCs generated in other haematopoietic organs during development are able to take over FL and adult haematopoiesis, as was proposed in Chapter 4. This would further suggest that a proper ECs communication with adjacent perivascular cells is required to maintain HSCs immature.

5.4.2 PDGF-B^{ret} KO midgestation embryos exhibit an apparently normal dorsal aorta and surrounding perivascular cells

PDGF-B retention to the extracellular matrix was shown to be required for the proper investment of pericytes to the blood vessel wall, as it creates a PDGF-B gradient required for PDGFRβ+ pericytes/vSMCs recruitment [158,159,199]. PDGF-B^{ret} KO embryos exhibit a partial detachment of pericytes from the endothelium and have a leaky vasculature [158]. Whether this mutation also affects large vessels, has not been reported. To address this question, immunohistochemistry in both DA whole-mounts and cryosections of mutant AGMs was performed. The dorsal aorta of KO embryos was properly formed and the perivascular cell coverage appeared unchanged. A slight increase in αSMA expression was detected in the PDGF-B^{ret} KO whole-mount (Figure 60), but not as striking as the one detected in PDGFRβ KO embryos. This slight increase needs to be further confirmed with additional whole-mounts and by flow cytometry.

Immunohistochemistry was performed with different combinations of perivascular and endothelial markers, to determine whether PDGF-B^{ret} KO

affected perivascular cell distribution around the DA. It is important to note that the expression levels of the different markers between WT and KO embryos cannot be compared. At the time of the analysis of these data, the 64GB RAM computer that was used to analyse and mount the pictures for Chapter 4 was broken. As a consequence, these files had to be analysed by a 16GB RAM computer that could not open the WT and KO files simultaneously, and therefore brightness and contrast could not be equally matched in FIJI/ImageJ. Despite the technical difficulties in the analysis, presence of the different perivascular cells can be seen, and no differences were detected in the distribution of PCs, sub-PCs and stromal cells. In addition, PDGFRβ expression was present in both WT and KO embryos, suggesting that PDGF-B^{ret} mutation does not affect PDGFRβ expression, nor pericyte/vSMC recruitment to the dorsal aorta. A new analysis of αSMA, NG2 and PDGFRβ levels should be performed again, matching the brightness/contrast changes between WT and KO embryos to determine whether expression levels vary upon PDGF-B retention motif deletion.

Recent RNA sequencing analysis on E11 AGM endothelial cells in our lab found high expression of *pdgfb* in these cells (not shown). Antibody staining against PDGF-B was therefore tested to determine the pattern of PDGF-B expression around the aortic endothelium, but the antibodies did not work on frozen and paraffin sections (not shown). We could therefore not validate the presence of pdgfb in the dorsal aorta at the protein level. The best visualisation of PDGF-B has so far been achieved by *in situ* hybridisation (ISH) [182]. It would be important to perform ISH in the dorsal aorta to assess PDGF-B expression. Some studies found that it is only expressed in tip cells during angiogenesis [182,209], however, not much data is available on PDGF-B expression during vasculogenesis and whether it is normally expressed around the dorsal aorta at the time of HSC generation. Indeed, the presence of PDGFRβ around the aorta was found already at E9 (see Chapter 4) and is expected to be present even earlier. Thus, PDGF-B/PDGFRβ signalling may have started at early developmental time points with mRNA expression persisting at later stages. Although PDGF-B role in the recruitment,

proliferation and differentiation of pericytes and vSMCs has mainly been reported in angiogenic sprouts [182,209], it is believed that it might also play a role in aortic and venous PCs/vSMCs [193]. Characterisation of PDGF-B expression in the developing DA needs to be performed to conclude whether in fact, PDGF-B diffuses in PDGF-B retention motif KO AGMs compared to WT, and to what extent PDGF-B/PDGFRβ signalling is affected. It would be interesting to perform western blotting analysis on the level of PDGFRβ phosphorylation (which marks activated PDGFRβ) in WT and KO AGMs.

In addition, although no differences in collagen IV expression were detected between PDGF-Bret WT and KO embryos, it would be interesting to determine whether other extracellular matrix proteins are affected in mutant embryos, as PDGFs have been implicated in the formation of the extracellular matrix (Owen, Geyer and Antoniades, 1982; Majack, Cook and Bornstein, 1985).

5.4.3 No PDGFR compensation occurs due to the reduction of PDGF-B/PDGFRβ signalling between PCs and ECs

Although no differences in the distribution of perivascular cells was detected in PDGF-B^{ret} mutant aortas, we looked at whether the percentages of different populations of endothelial, haematopoietic and perivascular cells were altered in these mutants by flow cytometry. We found no differences in the populations of cells analysed, including PDGFRβ+ perivascular cells, suggesting that PDGF-B^{ret} mutation does not affect the cell composition of the AGM nor induces a compensation by increasing PDGFRβ expression. As PDGF-B is also a ligand for PDGFRα [143], we also analysed PDGFRα expression in mutant embryos to determine whether there was a compensation for the reduced PDGF-B/PDGFRβ signalling. PDGFRα expression was not altered in any of the populations analysed. These data indicate that PDGF-B retention motif deletion and consequent reduction in PDGF-B/PDGFRβ signalling is not compensated by an increase in PDGF-B receptors. PDGF-B binding to PDGFRα was shown to activate similar downstream signalling transduction pathways as its binding to PDGFRβ *in vitro*, this might not be the case during embryonic development *in vivo* [143]. Indeed, a study showed that when the

intracellular domain of PDGFRβ is interchanged with the one of PDGFRα, the vascular defects and retinopathy occurring in PDGFRβ and PDGF-B KO embryos as well as PDGF-B^{ret} KO embryos persist, suggesting that PDGFRα signalling has different biological functions to PDGFRβ and cannot compensate for the lack of PDGF-B/PDGFRβ signalling *in vivo* [214].

We also sought to determine whether the haemogenic endothelium was affected by PDGF-B^{ret} mutation by crossing mutant mice with Runx1-IRES-GFP mice. However, these data could not be used, as Runx1-GFP mice were heterozygous for GFP and differences in Runx1-GFP expression were later found between Runx1$^{GFP/GFP}$ compared to Runx1$^{GFP/+}$ AGMs analysed by flow cytometry. Unfortunately PDGF-B^{ret};Runx1-GFP mice were not genotyped for Runx1-GFP, and therefore we could not determine whether embryos were GFP/+ or GFP/GFP (data not shown). It would be interesting to repeat these experiments using Runx1$^{GFP/GFP}$ mice to determine whether HECs are affected in PDGF-B^{ret} mutants.

5.4.4 Adult haematopoiesis is not affected by PDGF-B retention motif deletion

As PDGF-Bret KO mice survive into adulthood and E11 AGMs seem to be unable to produce LTR-HSCs, we looked at adult haematopoiesis in these mutants. No differences in BM HSPC numbers were detected in PDGF-Bret KO mice, suggesting that the deletion of PDGF-B retention motif does not affect adult haematopoiesis. Furthermore, LSK-SLAM analysis showed no significant differences in the percentages of LSK, HPC1, HPC2, HSCs and MPPs (Figure 72), which is not surprising, since no defects were detected in the number and types of HSPC colonies obtained in PDGF-B^{ret} mutants (Figure 71). A slight, albeit not significant decrease in the number of HSCs and MPPs could be detected. There was however a high variation between biological replicates, and the number of samples was low (4 WT, 5 HET and 3 KO BMs). Therefore, no conclusions can be drawn on whether this is a real trend. In addition, BM from both PDGF-Bret HET and KO mice could reconstitute both primary and secondary irradiated recipients (Figure 73),

suggesting that HSCs are not affected by this mutation. Nonetheless, it would be important to add a few additional samples to confirm the LSK-SLAM data.

5.4.5 Conclusions and future work

In this Chapter, PDGF-B retention motif KO was shown to have no consequences for adult haematopoiesis, as mutant BMs were able to reconstitute irradiated recipients in both primary and secondary transplantations. However, PDGF-B^{ret} KO AGMs failed to reconstitute secondary recipients, suggesting that these AGMs are unable to produce self-renewing HSCs. These data need to be confirmed with further secondary transplantation analysis, as the number of animals transplanted was low (n=2 into 4 irradiated recipients), and reconstitution levels of primary recipients were also generally low.

Overall, the effects of PDGF-B^{ret} mutation appear to be milder than in PDGFRβ KO AGMs, with a lower increase in αSMA expression in mutant aortas, as well as no changes in AGM HSPCs. This is in line with previous reports that the retention deletion has less severe effects in mice compared to a full KO of PDGF-B or PDGFRβ [157,158,210]. As expected, following the results obtained in Chapter 4, pericyte/vSMC recruitment to the DA is not affected in the absence/reduction of PDGF-B/PDGFRβ signalling.

To conclude, it remains unclear how defective retention of PDGF-B affects the dorsal aorta, and whether and how PDGF-B/PDGFRβ signalling is affected. As PDGF-B is still produced and functional, at least a certain level of PDGF-B/PDGFRβ signalling is bound to occur between aortic pericytes and endothelial cells. A better characterisation of this mouse model needs to be conducted in order to make any conclusions of the effects of a possible defect in PDGF-B/PDGFRβ signalling in haematopoiesis.

Chapter 6 Conclusions and future considerations

Haematopoietic stem cells have been widely used to treat haematological malignancies and other blood/immune diseases, and have the potential to treat a broader range of genetic disorders, such as metabolic disorders, where patients lack the production of certain enzymes. Unfortunately, such therapies still rely on the availability of compatible donors, as it has yet not been possible to generate and expand these cells *in vitro*. Understanding how HSC generation, maintenance and expansion occurs *in vivo* could provide the cues necessary for their culture *in vitro*.

In the last decades, much has been discovered regarding HSC generation during embryonic development. HSCs have been shown to arise from haemogenic endothelial cells and require signals from the microenvironment for this process to occur. However, the signals and cells involved in HSC generation are still poorly understood. This thesis has shed a new light on the cells composing the HSC-generating microenvironment and the signals they produce, and uncovered possible multiple origins for embryonic HSCs.

6.1 Perivascular cells surrounding the midgestation dorsal aorta might act as a niche for HSC generation and/or maintenance

In Chapter 1, three perivascular cell populations were defined and separated based on the expression of the perivascular cell surface markers NG2 and PDGFRβ. Pericytes/vSMCs, in closer contact with the aortic endothelium express both markers, while a few layers of cells surrounding them only express PDGFRβ. The remaining mesenchyme, further from the DA does not express any of these markers. Using bulk RNA sequencing analysis of these three populations we found that the PC/vSMC population is enriched in HSC niche related transcripts that were previously described in perivascular cells of the adult BM. In the next several months, the ability for each of these stromal cell populations to support HPSCs will be tested with co-culture experiments.

As a subset of PCs was shown to express CD146, it would also be interesting to further separate them into CD146+ and CD146- PCs, perform RNA sequencing and test their ability to support haematopoiesis and determine whether they differ in their niche potential. Recent data in our lab found that the deletion of Runx1 from PC/vSMCs impairs aortic haematopoiesis, with the failure to generate HSCs. Interestingly, recent single cell RNA sequencing in our lab showed that most Runx1+ PC/vSMCs also express CD146. One study showed that CD146+ but not CD146- human perivascular cells support cord blood CD34+ HPSCs [117]. It would be interesting to test whether CD146+ PCs/vSMCs in the AGM support HSCs better than their CD146- counterpart.

6.2 PDGFRβ signalling is required for AGM haematopoiesis

As the two closest populations of perivascular cells to the aortic endothelium express PDGFRβ, and since PDGFRβ was shown to be required for HSC specification [148], Chapters 4 and 5 looked at the role of PDGF-B/PDGFRβ signalling in midgestation haematopoiesis. We found that the germline KO of PDGFRβ leads to the complete absence of HSCs in the AGM and reduced HSPC numbers. HSPCs in other haematopoietic organs at midgestation were not affected. As injections of PDGFRβ KO E14 FL were shown to reconstitute irradiated recipients [201], our data suggest that not all HSCs are generated in the AGM region, or that they do not become fully functional before migrating to the FL. We also found that PDGF-B^{ret} KO AGM transplantations fail to reconstitute secondary recipients, suggesting that a defective PDGF-B/PDGFRβ signalling affects HSCs self-renewal capacity. However, it remains unclear how PDGF-B^{ret} mutation affects PDGF-B/PDGFRβ signalling in these mice.

We are currently performing single cell RNA sequencing in E11 WT and KO AGMs to investigate how gene expression and signalling pathways are altered in different populations of AGM cells upon PDGFRβ KO deletion.

6.3 Pericytes/vSMC recruitment to the DA is not affected by defects in PDGF-B/PDGFRβ signalling

As PDGF-B/PDGFRβ signalling was shown to be required for the recruitment of pericytes/vSMCs to the endothelial wall of small blood vessels, we investigated whether aortic perivascular cells were also absent or their numbers reduced in the DA of PDGFRβ KO and PDGF-B^{ret} KO embryos. We found that PDGF-B/PDGFRβ signalling is not responsible for the proper investment of the aortic endothelium by PCs/vSMCs, as these populations were still present and with a similar distribution in both mutant lines (in PDGFRβ KO embryos, NG2+ αSMA+ were present in the same location as PC/vSMCs but did not express PDGFRβ). Interestingly, the phenotype of this population was altered in PDGFRβ KO embryos, with a significant decrease in NG2 expression and an increase in αSMA expression. Expression levels of NG2 and αSMA need to be further tested on PDGF-B^{ret} KO embryos, as it remains unclear if this mutation affects PC/vSMC phenotype.

To test whether these phenotypic changes alter the niche for HSC generation/maintenance, co-culture experiments will be performed to compare the HSC supportive capacity of stromal cells from PDGFRβ WT and KO embryos.

6.4 Possible multiple origins for developing HSCs

Since PDGFRβ KO affects AGM HSPCs and we found that midgestation HSPCs do not express PDGFRβ, we hypothesised that PDGFRβ could mark haematopoietic cell precursors, and its disruption could affect HSC generation. Using PDGFRβ-Cre;TdTomato or PDGFRβ-Cre;mTmG mice, we found that a subset of embryonic HSPCs derive from PDGFRβ precursors. This subset contained bona fide HSCs that were able to reconstitute irradiated recipients, and were still present in the adult BM. As HSCs are absent in PDGFRβ KO AGM, it is likely that PDGFRβ-derived HSCs come from the AGM region. To test this, immunohistochemistry was performed on PDGFRβ-Cre;mTmG cryosections, and we found that endothelial cells and some hematopoietic cluster cells express GFP, demonstrating a developmental link between

PDGFRβ and haematopoiesis. To further understand at which stage these precursors appear and validate the findings obtained with the PDGFRβ-Cre mouse line, we established a collaboration with H. Grajal Cuervo at the University of Illinois, Chicago, whose lab works with PDGFRβ-P2A-CreERT2;mTmG mice. Pregnant dams were injected with tamoxifen at E7, E8 and E9, and embryos were harvested at E11. Analysis of these embryos is currently underway, but we have been able to confirm that GFP expression is found in E11 ECs from all the three different tamoxifen injection timepoints (not shown).

In addition, we are currently performing haematopoietic progenitor assays in other haematopoietic organs at stages that precede AGM haematopoiesis (E8-E9) up to E11 to test whether PDGFRβ+ precursors only give rise to definitive haematopoiesis. If this is the case, HP colonies will be only found in tissues after E10.5.

6.5 Conclusions

Overall, this study has found that there are at least two origins of HSCs in the embryo, one of which, derives from PDGFRβ+ precursor cells, that give rise to fully functional HSCs in the AGM. Defects in PDGFRβ signalling appear to either impair the maturation or the maintenance of PDGFRβ-derived HSCs, as haematological defects can only be detected at E11.5, but not before. Importantly, PDGFRβ-derived HSCs are still present in the adult. Finally, Whether PDGFRβ signalling plays a role in the niche for HSC generation remains to be tested.

References

1. Till, J.E., and McCulloch, E.A. (1961). A Direct Measurement of the Radiation Sensitivity of Normal Mouse Bone Marrow Cells. Radiat. Res. *14*, 213.

2. Becker, A.J., Mcculloch, E.A., and Till, J.E. (1963). Spleen Colonies Derived From Transplanted Mouse Marrow Cells. Nature *197*, 452–454.

3. Crisan, M., and Dzierzak, E. (2016). The many faces of hematopoietic stem cell heterogeneity. Development *143*, 4571–4581.

4. Muller-Sieburg, C.E., Sieburg, H.B., Bernitz, J.M., and Cattarossi, G. (2012). Stem cell heterogeneity: Implications for aging and regenerative medicine. Blood *119*, 3900–3907.

5. Ema, H., Morita, Y., and Suda, T. (2014). Heterogeneity and hierarchy of hematopoietic stem cells. Exp. Hematol. *42*, 74–82.

6. Benz, C., Copley, M.R., Kent, D.G., Wohrer, S., Cortes, A., Aghaeepour, N., Ma, E., Mader, H., Rowe, K., Day, C., *et al.* (2012). Hematopoietic stem cell subtypes expand differentially during development and display distinct lymphopoietic programs. Cell Stem Cell *10*, 273–283.

7. Dykstra, B., Kent, D., Bowie, M., McCaffrey, L., Hamilton, M., Lyons, K., Lee, S.J., Brinkman, R., and Eaves, C. (2007). Long-Term Propagation of Distinct Hematopoietic Differentiation Programs In Vivo. Cell Stem Cell *1*, 218–229.

8. Wilson, A., Laurenti, E., Oser, G., van der Wath, R.C., Blanco-Bose, W., Jaworski, M., Offner, S., Dunant, C.F., Eshkind, L., Bockamp, E., *et al.* (2008). Hematopoietic Stem Cells Reversibly Switch from Dormancy to Self-Renewal during Homeostasis and Repair. Cell *135*, 1118–1129.

9. Ema, H., Sudo, K., Seita, J., Matsubara, A., Morita, Y., Osawa, M., Takatsu, K., Takaki, S., and Nakauchi, H. (2005). Quantification of self-

renewal capacity in single hematopoietic stem cells from normal and Lnk-deficient mice. Dev. Cell *8*, 907–914.

10. Chabannon, C., Kubal, J., Bondanza, A., Dazzi, F., Pedrazzoli, P., Toubert, A., Ruggeri, A., Fleischhauer, K., and Bonini, C. (2018). Hematopoietic stem cell transplantation in its 60s: A platform for cellular therapies. Sci. Transl. Med. *10*, 1–11.

11. Slatter, M.A., and Gennery, A.R. (2018). Hematopoietic cell transplantation in primary immunodeficiency – conventional and emerging indications. Expert Rev. Clin. Immunol. *14*, 103–114.

12. Laberko, A., and Gennery, A.R. (2018). Clinical considerations in the hematopoietic stem cell transplant management of primary immunodeficiencies. Expert Rev. Clin. Immunol. *14*, 297–306.

13. Gratwohl, A., Baldomero, H., Aljurf, M., Pasquini, M.C., Bouzas, L.F., Yoshimi, A., Szer, J., Lipton, J., Schwendener, A., Gratwohl, M., *et al.* (2010). Hematopoietic Stem Cell Transplantation: A Global Perspective. JAMA *303*, 1617–1624.

14. Mamcarz, E., Zhou, S., Lockey, T., Abdelsamed, H., Cross, S.J., Kang, G., Ma, Z., Condori, J., Dowdy, J., Triplett, B., *et al.* (2019). Lentiviral gene therapy combined with low-dose busulfan in infants with SCID-X1. N. Engl. J. Med. *380*, 1525–1534.

15. Visigalli, I., Delai, S., Politi, L.S., Di Domenico, C., Cerri, F., Mrak, E., D'Isa, R., Ungaro, D., Stok, M., Sanvito, F., *et al.* (2010). Gene therapy augments the efficacy of hematopoietic cell transplantation and fully corrects mucopolysaccharidosis type I phenotype in the mouse model. Blood *116*, 5130–5139.

16. Sugimura, R., Jha, D.K., Han, A., Soria-Valles, C., da Rocha, E.L., Lu, Y., Goettel, J.A., Serrao, E., Rowe, R.G., Malleshaiah, M., *et al.* (2017). Haematopoietic stem and progenitor cells from human pluripotent stem

cells. Nature *545*, 432–438.

17. Kim, S.J., Jung, J.W., Ha, H.Y., Koo, S.K., Kim, E.G., and Kim, J.H. (2017). Generation of hematopoietic stem cells from human embryonic stem cells using a defined, stepwise, serum-free, and serum replacement-free monolayer culture method. Blood Res. *52*, 37–43.

18. Sykes, S.M., and Scadden, D.T. (2013). Modeling human hematopoietic stem cell biology in the mouse. Semin. Hematol. *50*, 92–100.

19. Choi, K., Kennedy, M., Kazarov, A., Papadimitriou, J.C., and Keller, G. (1998). A common precursor for hematopoietic and endothelial cells. Development *125*, 725–732.

20. Fehling, H.J., Lacaud, G., Kubo, A., Kennedy, M., Robertson, S., Keller, G., and Kouskoff, V. (2003). Tracking mesoderm induction and its specification to the hemangioblast during embryonic stem cell differentiation. Development *130*, 4217–4227.

21. Huber, T.L., Kouskoff, V., Fehling, H.J., Palis, J., and Keller, G. (2004). Haemangioblast commitment is initiated in the primitive streak of the mouse embryo. Nature *432*, 625–630.

22. Ferkowicz, M.J., and Yoder, M.C. (2005). Blood island formation: Longstanding observations and modern interpretations. Exp. Hematol. *33*, 1041–1047.

23. Ueno, H., and Weissman, I.L. (2006). Clonal Analysis of Mouse Development Reveals a Polyclonal Origin for Yolk Sac Blood Islands. Dev. Cell *11*, 519–533.

24. Palis, J., Robertson, S., Kennedy, M., Wall, C., and Keller, G. (1999). Development of erythroid and myeloid progenitors in the yolk sac and embryo proper of the mouse. Development *126*, 5073–5084.

25. Lux, C.T., Yoshimoto, M., McGrath, K., Conway, S.J., Palis, J., and

Yoder, M.C. (2008). All primitive and definitive hematopoietic progenitor cells emerging before E10 in the mouse embryo are products of the yolk sac. Blood *111*, 3435–3438.

26. Tober, J., Koniski, A., McGrath, K.E., Vemishetti, R., Emerson, R., De Mesy-Bentley, K.K.L., Waugh, R., and Palis, J. (2007). The megakaryocyte lineage originates from hemangioblast precursors and is an integral component both of primitive and of definitive hematopoiesis. Blood *109*, 1433–1441.

27. Bertrand, J.Y., Jalil, A., Klaine, M., Jung, S., Cumano, A., and Godin, I. (2005). Three pathways to mature macrophages in the early mouse yolk sac. Blood *106*, 3004–3011.

28. Kauts, M.L., Vink, C.S., and Dzierzak, E. (2016). Hematopoietic (stem) cell development — how divergent are the roads taken? FEBS Lett. *590*, 3975–3986.

29. Ferkowicz, M.J., Starr, M., Xie, X., Li, W., Johnson, S.A., Shelley, W.C., Morrison, P.R., and Yoder, M.C. (2003). CD41 expression defines the onset of primitive and definitive hematopoiesis in the murine embryo. Development *130*, 4393–4403.

30. McGrath, K.E., Frame, J.M., Fegan, K.H., Bowen, J.R., Conway, S.J., Catherman, S.C., Kingsley, P.D., Koniski, A.D., and Palis, J. (2015). Distinct Sources of Hematopoietic Progenitors Emerge before HSCs and Provide Functional Blood Cells in the Mammalian Embryo. Cell Rep. *11*, 1892–1904.

31. Alvarez-Silva, M., Belo-Diabangouaya, P., Salaün, J., and Dieterlen-Lièvre, F. (2003). Mouse placenta is a major hematopoietic organ. Development *130*, 5437–5444.

32. Sánchez, M.J., Holmes, A., Miles, C., and Dzierzak, E. (1996). Characterization of the first definitive hematopoietic stem cells in the

AGM and liver of the mouse embryo. Immunity *5*, 513–525.

33. Gomez Perdiguero, E., Klapproth, K., Schulz, C., Busch, K., Azzoni, E., Crozet, L., Garner, H., Trouillet, C., De Bruijn, M.F., Geissmann, F., *et al.* (2015). Tissue-resident macrophages originate from yolk-sac-derived erythro-myeloid progenitors. Nature *518*, 547–551.

34. Godin, I., Dieterlen-Lièvre, F., and Cumano, A. (1995). Emergence of multipotent hemopoietic cells in the yolk sac and paraaortic splanchnopleura in mouse embryos, beginning at 8.5 days postcoitus. Proc. Natl. Acad. Sci. *92*, 773 LP – 777.

35. Yokota, T., Huang, J., Tavian, M., Nagai, Y., Hirose, J., Zúñiga-Pflücker, J.C., Péault, B., and Kincade, P.W. (2006). Tracing the first waves of lymphopoiesis in mice. Development *133*, 2041–2051.

36. Yoshimoto, M., Porayette, P., Glosson, N.L., Conway, S.J., Carlesso, N., Cardoso, A.A., Kaplan, M.H., and Yoder, M.C. (2012). Autonomous murine T-cell progenitor production in the extra-embryonic yolk sac before HSC emergence. Blood *119*, 5706–5714.

37. Böiers, C., Carrelha, J., Lutteropp, M., Luc, S., Green, J.C.A., Azzoni, E., Woll, P.S., Mead, A.J., Hultquist, A., Swiers, G., *et al.* (2013). Lymphomyeloid contribution of an immune-restricted progenitor emerging prior to definitive hematopoietic stem cells. Cell Stem Cell *13*, 535–548.

38. Sonoda, T., Hayashi, C., and Kitamura, Y. (1983). Presence of mast cell precursors in the yolk sac of mice. Dev. Biol. *97*, 89–94.

39. Yoder, M.C., Hiatt, K., and Mukherjee, P. (1997). In vivo repopulating hematopoietic stem cells are present in the murine yolk sac at day 9.0 postcoitus. Proc. Natl. Acad. Sci. U. S. A. *94*, 6776–80.

40. Travnickova, J., Chau, V.T., Julien, E., Mateos-Langerak, J., Gonzalez, C., Lelièvre, E., Lutfalla, G., Tavian, M., and Kissa, K. (2015). Primitive

macrophages control HSPC mobilization and definitive haematopoiesis. Nat. Commun. *6*, 1–9.

41. Espín-Palazón, R., Stachura, D.L., Campbell, C.A., García-Moreno, D., Del Cid, N., Kim, A.D., Candel, S., Meseguer, J., Mulero, V., and Traver, D. (2014). Proinflammatory signaling regulates hematopoietic stem cell emergence. Cell *159*, 1070–1085.

42. Mariani, S.A., Li, Z., Rice, S., Krieg, C., Fragkogianni, S., Robinson, M., Vink, C.S., Pollard, J.W., and Dzierzak, E. (2019). Pro-inflammatory Aorta-Associated Macrophages Are Involved in Embryonic Development of Hematopoietic Stem Cells. Immunity *50*, 1439-1452.e5.

43. Li, Y., Esain, V., Teng, L., Xu, J., Kwan, W., Frost, I.M., Yzaguirre, A.D., Cai, X., Cortes, M., Maijenburg, M.W., *et al.* (2014). Inflammatory signaling regulates embryonic hematopoietic stem and progenitor cell production. Genes Dev. *28*, 2597–2612.

44. Medvinsky, A., and Dzierzak, E. (1996). Definitive hematopoiesis is autonomously initiated by the AGM region. Cell *86*, 897–906.

45. Müller, A.M., Medvinsky, A., Strouboulis, J., Grosveld, F., and Dzierzakt, E. (1994). Development of hematopoietic stem cell activity in the mouse embryo. Immunity *1*, 291–301.

46. Taoudi, S., and Medvinsky, A. (2007). Functional identification of the hematopoietic stem cell niche in the ventral domain of the embryonic dorsal aorta. Proc. Natl. Acad. Sci. *104*, 9399–9403.

47. North, T.E., De Bruijn, M.F.T.R., Stacy, T., Talebian, L., Lind, E., Robin, C., Binder, M., Dzierzak, E., and Speck, N.A. (2002). Runx1 expression marks long-term repopulating hematopoietic stem cells in the midgestation mouse embryo. Immunity *16*, 661–672.

48. de Bruijn, M.F.T.R., Ma, X., Robin, C., Ottersbach, K., Sanchez, M.-J., and Dzierzak, E. (2002). Hematopoietic stem cells localize to the

endothelial cell layer in the midgestation mouse aorta. Immunity *16*, 673–683.

49. Tavian, M., Coulombel, L., Luton, D., Clemente, H.S., Dieterlen-Lièvre, F., and Péault, B. (1996). Aorta-associated CD34+ hematopoietic cells in the early human embryo. Blood *87*, 67–72.

50. North, T., Gu, T.L., Stacy, T., Wang, Q., Howard, L., Binder, M., Marín-Padilla, M., and Speck, N.A. (1999). Cbfa2 is required for the formation of intra-aortic hematopoietic clusters. Development *126*, 2563–75.

51. Thompson, M.A., Ransom, D.G., Pratt, S.J., MacLennan, H., Kieran, M.W., Detrich, H.W., Vail, B., Huber, T.L., Paw, B., Brownlie, A.J., *et al.* (1998). The cloche and spadetail genes differentially affect hematopoiesis and vasculogenesis. Dev. Biol. *197*, 248–269.

52. Jaffredo, T., Gautier, R., Eichmann, A., and Dieterlen-Lievre, F. (1998). Intraaortic hemopoietic cells are derived from endothelial cells during ontogeny. Development *125*, 4575 LP – 4583.

53. Kumaravelu, P., Hook, L., Morrison, A.M., Ure, J., Zhao, S., Zuyev, S., Ansell, J., and Medvinsky, A. (2002). Quantitative developmental anatomy of definite haematopoietic stem cells/long-term repopulating units (HSC/RUs): Role of the aorta-gonad-mesonephros (AGM) region and the yolk sac in colonisation of the mouse embryonic liver. Development *129*, 4891–4899.

54. Medvinsky, A., Rybtsov, S., and Taoudi, S. (2011). Embryonic origin of the adult hematopoietic system: Advances and questions. Development *138*, 1017–1031.

55. Henninger, J., Santoso, B., Hans, S., Durand, E., Moore, J., Mosimann, C., Brand, M., Traver, D., and Zon, L. (2017). Clonal fate mapping quantifies the number of haematopoietic stem cells that arise during development. Nat. Cell Biol. *19*, 17–27.

56. Ganuza, M., Hall, T., Finkelstein, D., Chabot, A., Kang, G., and McKinney-Freeman, S. (2017). Lifelong haematopoiesis is established by hundreds of precursors throughout mammalian ontogeny. Nat. Cell Biol. *19*, 1153–1163.

57. Sánchez, M.J., Bockamp, E.O., Miller, J., Gambardella, L., and Green, A.R. (2001). Selective rescue of early haematopoietic progenitors in Scl-/-mice by expressing Scl under the control of a stem cell enhancer. Development *128*, 4815–4827.

58. Ling, K.W., Ottersbach, K., Van Hamburg, J.P., Oziemlak, A., Tsai, F.Y., Orkin, S.H., Ploemacher, R., Hendriks, R.W., and Dzierzak, E. (2004). GATA-2 plays two functionally distinct roles during the ontogeny of hematopoietic stem cells. J. Exp. Med. *200*, 871–882.

59. Minegishi, N., Ohta, J., Yamagiwa, H., Suzuki, N., Kawauchi, S., Zhou, Y., Takahashi, S., Hayashi, N., Engel, J.D., and Yamamoto, M. (1999). The mouse GATA-2 gene is expressed in the para-aortic splanchnopleura and aorta-gonads and mesonephros region. Blood *93*, 4196–4207.

60. de Bruijn, M.F.T.R. (2000). Definitive hematopoietic stem cells first develop within the major arterial regions of the mouse embryo. EMBO J. *19*, 2465–2474.

61. Li, Z., Lan, Y., He, W., Chen, D., Wang, J., Zhou, F., Wang, Y., Sun, H., Chen, X., Xu, C., *et al.* (2012). Mouse embryonic head as a site for hematopoietic stem cell development. Cell Stem Cell *11*, 663–675.

62. Gekas, C., Dieterlen-Lièvre, F., Orkin, S.H., and Mikkola, H.K.A. (2005). The placenta is a niche for hematopoietic stem cells. Dev. Cell *8*, 365–375.

63. Ottersbach, K., and Dzierzak, E. (2005). The murine placenta contains hematopoietic stem cells within the vascular labyrinth region. Dev. Cell

8, 377–387.

64. Johnson, G.R., and Moore, M.A.S. (1975). Role of stem cell migration in initiation of mouse foetal liver haemopoiesis. Nature *258*, 726–728.

65. Houssaint, E. (1981). Differentiation of the mouse hepatic primordium. II. Extrinsic origin of the haemopoietic cell line. Cell Differ. *10*, 243–252.

66. Takeuchi, M., Sekiguchi, T., Hara, T., Kinoshita, T., and Miyajima, A. (2002). Cultivation of aorta-gonad-mesonephros-derived hematopoietic stem cells in the fetal liver microenvironment amplifies long-term repopulating activity and enhances engraftment to the bone marrow. Blood *99*, 1190–1196.

67. Ciriza, J., Thompson, H., Petrosian, R., Manilay, J.O., and García-Ojeda, M.E. (2013). The migration of hematopoietic progenitors from the fetal liver to the fetal bone marrow: Lessons learned and possible clinical applications. Exp. Hematol. *41*, 411–423.

68. Rhodes, K.E., Gekas, C., Wang, Y., Lux, C.T., Francis, C.S., Chan, D.N., Conway, S., Orkin, S.H., Yoder, M.C., and Mikkola, H.K.A. (2008). The emergence of hematopoietic stem cells is initiated in the placental vasculature in the absence of circulation. Cell Stem Cell *2*, 252–263.

69. Matsuoka, S., Tsuji, K., Hisakawa, H., Xu, M., Ebihara, Y., Ishii, T., Sugiyama, D., Manabe, A., Tanaka, R., Ikeda, Y., *et al.* (2001). Generation of definitive hematopoietic stem cells from murine early yolk sac and paraaortic splanchnopleures by aorta-gonad-mesonephros region–derived stromal cells. Blood *98*, 6–12.

70. McGrath, K.E., Koniski, A.D., Malik, J., and Palis, J. (2003). Circulation is established in a stepwise pattern in the mammalian embryo. Blood *101*, 1669–1676.

71. Ottersbach, K. (2019). Endothelial-to-haematopoietic transition: An update on the process of making blood. Biochem. Soc. Trans. *47*, 591–

601.

72. Young, P.E., Baumhueter, S., and Lasky, L.A. (1995). The sialomucin CD34 is expressed on hematopoietic cells and blood vessels during murine development. Blood *85*, 96–105.

73. Hsu, H.C., Ema, H., Osawa, M., Nakamura, Y., Suda, T., and Nakauchi, H. (2000). Hematopoietic stem cells express Tie-2 receptor in the murine fetal liver. Blood *96*, 3757–3762.

74. Sabin, F.R. (1920). Studies on the origin of blood-vessels and of red blood-corpuscles as seen in the living blastoderm of chicks during the second day of incubation. 213–262.

75. Hirschi, K.K. (2012). Hemogenic endothelium during development and beyond. Blood *119*, 4823–4837.

76. Kissa, K., and Herbomel, P. (2010). Blood stem cells emerge from aortic endothelium by a novel type of cell transition. Nature *464*, 112–115.

77. Boisset, J.-C., van Cappellen, W., Andrieu-Soler, C., Galjart, N., Dzierzak, E., and Robin, C. (2010). In vivo imaging of haematopoietic cells emerging from the mouse aortic endothelium. Nature *464*, 116–20.

78. Bertrand, J.Y., Chi, N.C., Santoso, B., Teng, S., Stainier, D.Y.R., and Traver, D. (2010). Haematopoietic stem cells derive directly from aortic endothelium during development. Nature *464*, 108–111.

79. Chen, M.J., Yokomizo, T., Zeigler, B., Dzierzak, E., and Speck, A. (2009). Runx1 is required for the endothelial to hematopoietic cell transition but not thereafter. Nature *457*, 887–891.

80. Tavian, M., and Péault, B. (2005). Embryonic development of the human hematopoietic system. Int. J. Dev. Biol. *49*, 243–250.

81. Clements, W.K., and Traver, D. (2013). Signalling pathways that control

vertebrate haematopoietic stem cell specification. Nat. Rev. Immunol. *13*, 336–48.

82. Yvernogeau, L., Gautier, R., Petit, L., Khoury, H., Relaix, F., Ribes, V., Sang, H., Charbord, P., Souyri, M., Robin, C., *et al.* (2019). In vivo generation of haematopoietic stem/progenitor cells from bone marrow-derived haemogenic endothelium. Nat. Cell Biol. *21*, 1334–1345.

83. Li, Z., Vink, C.S., Mariani, S.A., and Dzierzak, E. (2016). Subregional localization and characterization of Ly6aGFP-expressing hematopoietic cells in the mouse embryonic head. Dev. Biol. *416*, 34–41. Available at: http://dx.doi.org/10.1016/j.ydbio.2016.05.031.

84. Swiers, G., Rode, C., Azzoni, E., and De Bruijn, M.F.T.R. (2013). A short history of hemogenic endothelium. Blood Cells, Mol. Dis. *51*, 206–212.

85. Rybtsov, S., Sobiesiak, M., Taoudi, S., Souilhol, C., Senserrich, J., Liakhovitskaia, A., Ivanovs, A., Frampton, J., Zhao, S., and Medvinsky, A. (2011). Hierarchical organization and early hematopoietic specification of the developing HSC lineage in the AGM region. J. Exp. Med. *208*, 1305–1315.

86. Rybtsov, S., Batsivari, A., Bilotkach, K., Paruzina, D., Senserrich, J., Nerushev, O., and Medvinsky, A. (2014). Tracing the origin of the HSC hierarchy reveals an SCF-dependent, IL-3-independent CD43- embryonic precursor. Stem Cell Reports *3*, 489–501.

87. Taoudi, S., Gonneau, C., Moore, K., Sheridan, J.M., Blackburn, C.C., Taylor, E., and Medvinsky, A. (2008). Extensive hematopoietic stem cell generation in the AGM region via maturation of VE-Cadherin+CD45+ pre-definitive HSCs. Cell Stem Cell *3*, 99–108.

88. Baron, C.S., Kester, L., Klaus, A., Boisset, J.C., Thambyrajah, R., Yvernogeau, L., Kouskoff, V., Lacaud, G., Van Oudenaarden, A., and Robin, C. (2018). Single-cell transcriptomics reveal the dynamic of

haematopoietic stem cell production in the aorta. Nat. Commun. *9*.

89. Tsai, F.Y., Keller, G., Kuo, F.C., Weiss, M., Chen, J., Rosenblatt, M., Alt, F.W., and Orkin, S.H. (1994). An early haematopoietic defect in mice lacking the transcription factor GATA-2. Nature *371*, 221–226.

90. Gao, X., Johnson, K.D., Chang, Y.I., Boyer, M.E., Dewey, C.N., Zhang, J., and Bresnick, E.H. (2013). Gata2 cis-element is required for hematopoietic stem cell generation in the mammalian embryo. J. Exp. Med. *210*, 2833–2842.

91. de Pater, E., Kaimakis, P., Vink, C.S., Yokomizo, T., Yamada-Inagawa, T., van der Linden, R., Kartalaei, P.S., Camper, S.A., Speck, N., and Dzierzak, E. (2013). Gata2 is required for HSC generation and survival. J. Exp. Med. *210*, 2843–2850.

92. Okuda, T., Van Deursen, J., Hiebert, S.W., Grosveld, G., and Downing, J.R. (1996). AML1, the target of multiple chromosomal translocations in human leukemia, is essential for normal fetal liver hematopoiesis. Cell *84*, 321–330.

93. Wang, Q., Stacy, T., Binder, M., Marín-Padilla, M., Sharpe, A.H., and Speck, N.A. (1996). Disruption of the Cbfa2 gene causes necrosis and hemorrhaging in the central nervous system and blocks definitive hematopoiesis. Proc. Natl. Acad. Sci. U. S. A. *93*, 3444–3449.

94. Kaimakis, P., Pater, E. De, Eich, C., Kartalaei, P.S., Kauts, M., Vink, C.S., Linden, R. Van Der, Jaegle, M., Yokomizo, T., Meijer, D., *et al.* (2016). Functional and molecular characterization of mouse Gata2-independent hematopoietic progenitors. Blood *127*, 1426–1438.

95. Iizuka, K., Yokomizo, T., Watanabe, N., Tanaka, Y., Osato, M., Takaku, T., and Komatsu, N. (2016). Lack of Phenotypical and Morphological Evidences of Endothelial to Hematopoietic Transition in the Murine Embryonic Head during Hematopoietic Stem Cell Emergence. PLoS

One *11*, e0156427.

96. Lam, E.Y.N., Hall, C.J., Crosier, P.S., Crosier, K.E., and Flores, M.V. (2010). Live imaging of Runx1 expression in the dorsal aorta tracks the emergence of blood progenitors from endothelial cells. Blood *116*, 909–914.

97. Richard, C., Drevon, C., Canto, P.Y., Villain, G., Bollérot, K., Lempereur, A., Teillet, M.A., Vincent, C., Rosselló Castillo, C., Torres, M., *et al.* (2013). Endothelio-Mesenchymal Interaction Controls runx1 Expression and Modulates the notch Pathway to Initiate Aortic Hematopoiesis. Dev. Cell *24*, 600–611.

98. Guiu, J., Shimizu, R., D'Altri, T., Fraser, S.T., Hatakeyama, J., Bresnick, E.H., Kageyama, R., Dzierzak, E., Yamamoto, M., Espinosa, L., *et al.* (2013). Hes repressors are essential regulators of hematopoietic stem cell development downstream of notch signaling. J. Exp. Med. *210*, 71–84.

99. Maeno, B.M., Mead, P.E., Kelley, C., Xu, R., Kung, H., Suzuki, A., Ueno, N., and Zon, L.I. (1996). The Role of BMP-4 and GATA-2 in the Induction and Differentiation of Hematopoietic Mesoderm in Xenopus Laevis. *88*, 1965–1972.

100. Lempereur, A., Canto, P.Y., Richard, C., Martin, S., Thalgott, J., Raymond, K., Lebrin, F., Drevon, C., and Jaffredo, T. (2018). The TGFβ pathway is a key player for the endothelial-to-hematopoietic transition in the embryonic aorta. Dev. Biol. *434*, 292–303.

101. Rybtsov, S., Ivanovs, A., Zhao, S., and Medvinsky, A. (2016). Concealed expansion of immature precursors underpins acute burst of adult HSC activity in foetal liver. Development *143*, 1284–9.

102. Ganuza, M., Chabot, A., Finkelstein, D., and McKinney-Freeman, S. (2019). Clonal dynamics of embryonic and early-post-birth blood

precursors. Exp. Hematol. *76*, S66.

103. Godin, I., Garcia-Porrero, J.A., Dieterlen-Lièvre, F., and Cumano, A. (1999). Stem cell emergence and hemopoietic activity are incompatible in mouse intraembryonic sites. J. Exp. Med. *190*, 43–52.

104. Morrison, S.J., Hemmati, H.D., Wandycz, A.M., and Weissman, I.L. (1995). The purification and characterization of fetal liver hematopoietic stem cells. Proc. Natl. Acad. Sci. *92*, 10302–10306.

105. Christensen, J.L., Wright, D.E., Wagers, A.J., and Weissman, I.L. (2004). Circulation and chemotaxis of fetal hematopoietic stem cells. PLoS Biol. *2*, 368–377.

106. Schofield, R. (1978). The relationship between the spleen colony-forming cell and the haemopoietic stem cell. Blood Cells *4*, 7–25.

107. Sá da Bandeira, D., Casamitjana, J., and Crisan, M. (2017). Pericytes, integral components of adult hematopoietic stem cell niches. Pharmacol. Ther. *171*, 104–113.

108. Zhang, J., Niu, C., Ye, L., Huang, H., He, X., Tong, W.-G., Ross, J., Haug, J., Johnson, T., Feng, J.Q., *et al.* (2003). Identification of the haematopoietic stem cell niche and control of the niche size. Nature *425*, 836–841.

109. Calvi, L.M., Adams, G.B., Weibrecht, K.W., Weber, J.M., Olson, D.P., Knight, M.C., Martin, R.P., Schipani, E., Divieti, P., Bringhurst, F.R., *et al.* (2003). Osteoblastic cells regulate the haematopoietic stem cell niche. Nature *425*, 841–846.

110. Dennis, J.E., and Charbord, P. (2002). Origin and Differentiation of Human and Murine Stroma. Stem Cells *20*, 205–214.

111. Devine, S.M., and Hoffman, R. (2000). Role of mesenchymal stem cells in hematopoietic stem cell transplantation. Curr. Opin. Hematol. *7*.

112. Almeida-Porada, G., Brown, R.L., MacKintosh, F.R., and Zanjani, E.D. (2000). Evaluation of Serum-Free Culture Conditions Able to Support the Ex Vivo Expansion and Engraftment of Human Hematopoietic Stem Cells in the Human-to-Sheep Xenograft Model. J. Hematother. Stem Cell Res. *9*, 683–693.

113. Almeida-Porada, G., Porada, C.D., Tran, N., and Zanjani, E.D. (2000). Cotransplantation of human stromal cell progenitors into preimmune fetal sheep results in early appearance of human donor cells in circulation and boosts cell levels in bone marrow at later time points after transplantation. Blood *95*, 3620–3627.

114. Kunisaki, Y., Bruns, I., Scheiermann, C., Ahmed, J., Pinho, S., Zhang, D., Mizoguchi, T., Wei, Q., Lucas, D., Ito, K., *et al.* (2013). Arteriolar niches maintain haematopoietic stem cell quiescence. Nature *502*, 637–643.

115. Ding, L., Saunders, T.L., Enikolopov, G., and Morrison, S.J. (2012). Endothelial and perivascular cells maintain haematopoietic stem cells. Nature *481*, 457–62.

116. Ding, L., and Morrison, S.J. (2013). Haematopoietic stem cells and early lymphoid progenitors occupy distinct bone marrow niches. Nature *495*, 231–5.

117. Corselli, M., Chin, C.J., Parekh, C., Sahaghian, A., Wang, W., Ge, S., Evseenko, D., Wang, X., Montelatici, E., Lazzari, L., *et al.* (2013). Perivascular support of human hematopoietic stem/progenitor cells. Blood *121*, 2891–2901.

118. Sacchetti, B., Funari, A., Michienzi, S., Di Cesare, S., Piersanti, S., Saggio, I., Tagliafico, E., Ferrari, S., Robey, P.G., Riminucci, M., *et al.* (2007). Self-Renewing Osteoprogenitors in Bone Marrow Sinusoids Can Organize a Hematopoietic Microenvironment. Cell *131*, 324–336.

119. Duncan, A.W., Rattis, F.M., DiMascio, L.N., Congdon, K.L., Pazianos, G., Zhao, C., Yoon, K., Cook, J.M., Willert, K., Gaiano, N., *et al.* (2005). Integration of Notch and Wnt signaling in hematopoietic stem cell maintenance. Nat. Immunol. *6*, 314–322.

120. Sugiyama, T., Kohara, H., Noda, M., and Nagasawa, T. (2006). Maintenance of the Hematopoietic Stem Cell Pool by CXCL12-CXCR4 Chemokine Signaling in Bone Marrow Stromal Cell Niches. Immunity *25*, 977–988.

121. Wilson, A., and Trumpp, A. (2006). Bone-marrow haematopoietic-stem-cell niches. Nat. Rev. Immunol. *6*, 93–106.

122. Mendez-Ferrer, S., Michurina, T. V, Ferraro, F., Mazloom, A.R., MacArthur, B.D., Lira, S.A., Scadden, D.T., Ma/'ayan, A., Enikolopov, G.N., and Frenette, P.S. (2010). Mesenchymal and haematopoietic stem cells form a unique bone marrow niche. Nature *466*, 829–834.

123. Pinho, S., Lacombe, J., Hanoun, M., Mizoguchi, T., Bruns, I., Kunisaki, Y., and Frenette, P.S. (2013). PDGFRα and CD51 mark human Nestin(+) sphere-forming mesenchymal stem cells capable of hematopoietic progenitor cell expansion. J. Exp. Med. *210*, 1351–1367.

124. Isern, J., Martin-Antonio, B., Ghazanfari, R., Martin, A.M., Lopez, J.A., del Toro, R., Sanchez-Aguilera, A., Arranz, L., Martin-Perez, D., Suarez-Lledo, M., *et al.* (2013). Self-renewing human bone marrow mesenspheres promote hematopoietic stem cell expansion. Cell Rep. *3*, 1714–1724.

125. Oostendorp, R.A.J., Harvey, K.N., Kusadasi, N., de Bruijn, M.F.T.R., Saris, C., Ploemacher, R.E., Medvinsky, A.L., and Dzierzak, E.A. (2002). Stromal cell lines from mouse aorta-gonads-mesonephros subregions are potent supporters of hematopoietic stem cell activity. Blood *99*, 1183–1189.

126. Durand, C., Robin, C., and Dzierzak, E. (2006). Mesenchymal lineage potentials of aorta-gonad-mesonephros stromal clones. Haematologica *91*, 1172–1179.

127. Mendes, S. C.; Robin, C., and Dzierzak, E. (2005). Mesenchymal progenitor cells localize within hematopoietic sites throughout ontogeny. Development *132*, 1127–1136.

128. Durand, C., Robin, C., Bollerot, K., Baron, M.H., Ottersbach, K., and Dzierzak, E. (2007). Embryonic stromal clones reveal developmental regulators of definitive hematopoietic stem cells. Proc. Natl. Acad. Sci. U. S. A. *104*, 20838–43.

129. Marshall, C.J., Kinnon, C., and Thrasher, a J. (2000). Polarized expression of bone morphogenetic protein-4 in the human aorta-gonad-mesonephros region. Blood *96*, 1591–1593.

130. Souilhol, C., Gonneau, C., Lendinez, J.G., Batsivari, A., Rybtsov, S., Wilson, H., Morgado-Palacin, L., Hills, D., Taoudi, S., Antonchuk, J., *et al.* (2016). Inductive interactions mediated by interplay of asymmetric signalling underlie development of adult haematopoietic stem cells. Nat. Commun. *7*, 10784.

131. McGarvey, A.C., Rybtsov, S., Souilhol, C., Tamagno, S., Rice, R., Hills, D., Godwin, D., Rice, D., Tomlinson, S.R., and Medvinsky, A. (2017). A molecular roadmap of the AGM region reveals BMP ER as a novel regulator of HSC maturation. J. Exp. Med. *214*, 3731–3751.

132. Peeters, M., Ottersbach, K., Bollerot, K., Orelino, C., de Bruijn, M., Wijgerde, M., and Dzierzak, E. (2009). Ventral embryonic tissues and Hedgehog proteins induce early AGM hematopoietic stem cell development. Development *136*, 2613–2621.

133. Mendez-Ferrer, S., Lucas, D., Battista, M., and Frenette, P.S. (2008). Haematopoietic stem cell release is regulated by circadian oscillations.

Nature *452*, 442–447.

134. Fitch, S.R., Kimber, G.M., Wilson, N.K., Parker, A., Mirshekar-Syahkal, B., Göttgens, B., Medvinsky, A., Dzierzak, E., and Ottersbach, K. (2012). Signaling from the sympathetic nervous system regulates hematopoietic stem cell emergence during embryogenesis. Cell Stem Cell *11*, 554–566.

135. Strilić, B., Kučera, T., Eglinger, J., Hughes, M.R., McNagny, K.M., Tsukita, S., Dejana, E., Ferrara, N., and Lammert, E. (2009). The Molecular Basis of Vascular Lumen Formation in the Developing Mouse Aorta. Dev. Cell *17*, 505–515.

136. Sato, Y. (2013). Dorsal aorta formation: Separate origins, lateral-to-medial migration, and remodeling. Dev. Growth Differ. *55*, 113–129.

137. Pouget, C., Gautier, R., Teillet, M.-A., and Jaffredo, T. (2006). Somite-derived cells replace ventral aortic hemangioblasts and provide aortic smooth muscle cells of the trunk. Development *133*, 1013–1022.

138. Pardanaud, L., Luton, D., Prigent, M., Bourcheix, L.M., Catala, M., and Dieterlen-Lievre, F. (1996). Two distinct endothelial lineages in ontogeny, one of them related to hemopoiesis. Development *122*, 1363–1371.

139. Wasteson, P., Johansson, B.R., Jukkola, T., Breuer, S., Akyürek, L.M., Partanen, J., and Lindahl, P. (2008). Developmental origin of smooth muscle cells in the descending aorta in mice. Development *135*, 1823–32.

140. Takahashi, Y., Imanaka, T., and Takano, T. (1996). Spatial and temporal pattern of smooth muscle cell differentiation during development of the vascular system in the mouse embryo. Anat. Embryol. (Berl). *194*, 515–526.

141. Ozerdem, U., Grako, K.A., Dahlin-Huppe, K., Monosov, E., and Stallcup,

W.B. (2001). NG2 proteoglycan is expressed exclusively by mural cells during vascular morphogenesis. Dev. Dyn. *222*, 218–227.

142. Betsholtz, C., Karlsson, L., and Lindahl, P. (2001). Developmental roles of platelet-derived growth factors. BioEssays *23*, 494–507.

143. Betsholtz, C. (2003). Biology of Platelet-Derived Growth Factors in Development. Birth Defects Res. Part C - Embryo Today Rev. *69*, 272–285.

144. Owen, A.J., Geyer, R.P., and Antoniades, H.N. (1982). Human platelet-derived growth factor stimulates amino acid transport and protein synthesis by human diploid fibroblasts in plasma-free media. Proc. Natl. Acad. Sci. *79*, 3203 LP – 3207.

145. Majack, R.A., Cook, S.C., and Bornstein, P. (1985). Platelet-derived growth factor and heparin-like glycosaminoglycans regulate thrombospondin synthesis and deposition in the matrix by smooth muscle cells. J. Cell Biol. *101*, 1059–1070.

146. Berk, B.C., Alexander, R.W., Brock, T.A., Gimbrone, M.A., and Webb, R.C. (1986). Vasoconstriction: a new activity for platelet-derived growth factor. Science (80-.). *232*, 87 LP – 90.

147. Gullberg, D., Tingström, A., Thuresson, A.C., Olsson, L., Terracio, L., Borg, T.K., and Rubin, K. (1990). β1 Integrin-mediated collagen gel contraction is stimulated by PDGF. Exp. Cell Res. *186*, 264–272.

148. Damm, E.W., and Clements, W.K. (2017). Pdgf Signalling Guides Neural Crest Contribution to the Haematopietic Stem Cell Specification Niche. Nat. Cell Biol. *19*.

149. Lim, S.E., Esain, V., Kwan, W., Theodore, L.N., Cortes, M., Frost, I.M., Liu, S.Y., and North, T.E. (2017). HIF1α-induced PDGFRβ signaling promotes developmental HSC production via IL-6 activation. Exp. Hematol. *46*, 83-95.e6.

150. Harris, J.M., Esain, V., Frechette, G.M., Harris, L.J., Cox, A.G., Cortes, M., Garnaas, M.K., Carroll, K.J., Cutting, C.C., Khan, T., *et al.* (2013). Glucose metabolism impacts the spatiotemporal onset and magnitude of HSC induction in vivo. Blood *121*, 2483–2493.

151. Imanirad, P., Solaimani Kartalaei, P., Crisan, M., Vink, C., Yamada-Inagawa, T., de Pater, E., Kurek, D., Kaimakis, P., van der Linden, R., Speck, N., *et al.* (2014). HIF1a is a regulator of hematopoietic progenitor and stem cell development in hypoxic sites of the mouse embryo. Stem Cell Res. *12*, 24–35.

152. Brückner, K., Kockel, L., Duchek, P., Luque, C.M., Rørth, P., and Perrimon, N. (2004). The PDGF/VEGF receptor controls blood cell survival in Drosophila. Dev. Cell *7*, 73–84.

153. Rolny, C., Nilsson, I., Magnusson, P., Armulik, A., Jakobsson, L., Wentzel, P., Lindblom, P., Norlin, J., Betsholtz, C., Heuchel, R., *et al.* (2006). Platelet-derived growth factor receptor-B promotes early endothelial cell differentiation. Development *108*, 1877–1886.

154. Chhabra, A., Lechner, A.J., Ueno, M., Acharya, A., Handel, B. Van, Wang, Y., Iruela-arispe, M.L., Tallquist, M.D., and Mikkola, H.K.A. (2012). Trophoblasts Regulate the Placental Hematopoietic Niche through PDGF-B Signaling. Dev. Cell *22*, 651–659.

155. Azzoni, E., Frontera, V., McGrath, K.E., Harman, J., Carrelha, J., Nerlov, C., Palis, J., Jacobsen, S.E.W., and de Bruijn, M.F.T.R. (2018). Kit ligand has a critical role in mouse yolk sac and aorta–gonad–mesonephros hematopoiesis. EMBO Rep. *19*, e45477.

156. Charbord, P., Pouget, C., Binder, H., Dumont, F., Stik, G., Levy, P., Allain, F., Marchal, C., Richter, J., Uzan, B., *et al.* (2014). A systems biology approach for defining the molecular framework of the hematopoietic stem cell Niche. Cell Stem Cell *15*, 376–391.

157. Soriano, P. (1994). Abnormal kidney development and hematological disorders in PDGF beta-receptor mutant mice. Genes Dev. *8*, 1888–1896.

158. Lindblom, P., Gerhardt, H., Liebner, S., Abramsson, A., Enge, M., Hellström, M., Bäckström, G., Fredriksson, S., Landegren, U., Nyström, H.C., *et al.* (2003). Endothelial PDGF-B retention is required for proper investment of pericytes in the microvessel wall. Genes Dev. *17*, 1835–1840.

159. Abramsson, A., Lindblom, P., and Betsholtz, C. (2003). Endothelial and nonendothelial sources of PDGF-B regulate pericyte recruitment and influence vascular pattern formation in tumors. J. Clin. Invest. *112*, 1142–1151.

160. Foo, S.S., Turner, C.J., Adams, S., Compagni, A., Aubyn, D., Kogata, N., Lindblom, P., Shani, M., Zicha, D., and Adams, R.H. (2006). Ephrin-B2 controls cell motility and adhesion during blood-vessel-wall assembly. Cell *124*, 161–173.

161. Madisen, L., Zwingman, T.A., Sunkin, S.M., Oh, S.W., Zariwala, H.A., Gu, H., Ng, L.L., Palmiter, R.D., Hawrylycz, M.J., Jones, A.R., *et al.* (2009). A robust and high-throughput Cre reporting and characterization system for the whole mouse brain. Nat. Neurosci. *13*, 133.

162. Lorsbach, R.B., Moore, J., Ang, S.O., Sun, W., Lenny, N., and Downing, J.R. (2004). Role of RUNX1 in adult hematopoiesis: Analysis of RUNX1-IRES-GFP knock-in mice reveals differential lineage expression. Blood *103*, 2522–2529.

163. Muzumdar, M.D., Tasic, B., Miyamichi, K., Li, L., and Luo, L. (2007). A global Double-Fluorescent Cre Reporter Mouse. Genesis *605*, 593–605.

164. Ostman, A., Bäckström, G., Fong, N., Betsholtz, C., Wernstedt, C., Hellman, U., Westermark, B., Valenzuela, P., and Heldin, C.-H. (1989).

Expression of three recombinant homodimeric isoforms of PDGF in Saccharomyces cerevisiae: evidence for difference in receptor binding and functional activities. Growth Factors *1*, 271–81.

165. Song, W.-J., Sullivan, M.G., Legare, R.D., Hutchings, S., Tan, X., Kufrin, D., Ratajczak, J., Resende, I.C., Haworth, C., Hock, R., *et al.* (1999). Haploinsufficiency of CBFA2 causes familial thrombocytopenia with propensity to develop acute myelogenous leukaemia. Nat. Genet. *23*, 166–175.

166. Cai, Z., de Bruijn, M., Ma, X., Dortland, B., Luteijn, T., Downing, R.J., and Dzierzak, E. (2000). Haploinsufficiency of AML1 affects the temporal and spatial generation of hematopoietic stem cells in the mouse embryo. Immunity *13*, 423–431.

167. Sabu, A., Naoko, K., Reinhard, F., and H., A.R. (2008). Integrin β1 Subunit Controls Mural Cell Adhesion, Spreading, and Blood Vessel Wall Stability. Circ. Res. *102*, 562–570.

168. Kogata, N., Tribe, R.M., Fässler, R., Way, M., and Adams, R.H. (2009). Integrin-linked kinase controls vascular wall formation by negatively regulating Rho/ROCK-mediated vascular smooth muscle cell contraction. Genes Dev. *23*, 2278–2283.

169. Gieseck, R.L., Ramalingam, T.R., Hart, K.M., Vannella, K.M., Cantu, D.A., Lu, W.-Y., Ferreira-González, S., Forbes, S.J., Vallier, L., and Wynn, T.A. (2016). Interleukin-13 Activates Distinct Cellular Pathways Leading to Ductular Reaction, Steatosis, and Fibrosis. Immunity *45*, 145–158.

170. Bartlett, C.S., Scott, R.P., Carota, I.A., Wnuk, M.L., Kanwar, Y.S., Miner, J.H., and Quaggin, S.E. (2017). Glomerular mesangial cell recruitment and function require the co-receptor neuropilin-1. Am. J. Physiol. Physiol. *313*, F1232–F1242.

171. Kim, D., Pertea, G., Trapnell, C., Pimentel, H., Kelley, R., and Salzberg, S.L. (2013). TopHat2: accurate alignment of transcriptomes in the presence of insertions, deletions and gene fusions. Genome Biol. *14*, R36.

172. Harrow, J., Frankish, A., Gonzalez, J.M., Tapanari, E., Diekhans, M., Kokocinski, F., Aken, B.L., Barrell, D., Zadissa, A., Searle, S., *et al.* (2012). GENCODE: The reference human genome annotation for The ENCODE Project. Genome Res. *22*, 1760–1774.

173. Gentleman, R.C., Carey, V.J., Bates, D.M., Bolstad, B., Dettling, M., Dudoit, S., Ellis, B., Gautier, L., Ge, Y., Gentry, J., *et al.* (2004). Bioconductor: open software development for computational biology and bioinformatics. Genome Biol. *5*, R80.

174. Love, M.I., Huber, W., and Anders, S. (2014). Moderated estimation of fold change and dispersion for RNA-seq data with DESeq2. Genome Biol. *15*, 550.

175. Meinders, M., Kulu, D.I., van de Werken, H.J.G., Hoogenboezem, M., Janssen, H., Brouwer, R.W.W., van Ijcken, W.F.J., Rijkers, E.-J., Demmers, J.A.A., Krüger, I., *et al.* (2015). Sp1/Sp3 transcription factors regulate hallmarks of megakaryocyte maturation and platelet formation and function. Blood *125*, 1957 LP – 1967.

176. Yu, G., and He, Q.-Y. (2016). ReactomePA: an R/Bioconductor package for reactome pathway analysis and visualization. Mol. Biosyst. *12*, 477–479.

177. R Core Team (2018). R: A language and environment for statistical computing. R Foundation for Statistical Computing, Vienna, Austria.

178. Oostendorp, R.A.J., Medvinsky, A.J., Kusadasi, N., Nakayama, N., Harvey, K., Orelio, C., Ottersbach, K., Covey, T., Ploemacher, R.E., Saris, C., *et al.* (2002). Embryonal subregion-derived stromal cell lines

from novel temperature-sensitive SV40 T antigen transgenic mice support hematopoiesis. J. Cell Sci. *115*, 2099–2108.

179. Roostalu, U., Aldeiri, B., Albertini, A., Humphreys, N., Simonsen-Jackson, M., Wong, J.K.F., and Cossu, G. (2018). Distinct cellular mechanisms underlie smooth muscle turnover in vascular development and repair. Circ. Res. *122*, 267–281.

180. Crisan, M., Yap, S., Casteilla, L., Chen, C.-W., Corselli, M., Park, T.S., Andriolo, G., Sun, B., Zheng, B., Zhang, L., *et al.* (2008). A Perivascular Origin for Mesenchymal Stem Cells in Multiple Human Organs. Cell Stem Cell *3*, 301–313.

181. Alliot, F., Rutin, J., Leenen, P.J., and Pessac, B. (1999). Pericytes and periendothelial cells of brain parenchyma vessels co-express aminopeptidase N, aminopeptidase A, and nestin. J. Neurosci. Res. *58*, 367–378.

182. Hellstrom, M., Kalen, M., Lindahl, P., Abramsson, A., and Betsholtz, C. (1999). Role of PDGF-B and PDGFR-beta in recruitment of vascular smooth muscle cells and pericytes during embryonic blood vessel formation in the mouse. Development *126*, 3047–3055.

183. Guimaraes-Camboa, N., Cattaneo, P., Sun, Y., Moore-Morris, T., Gu, Y., Dalton, N.D., Rockenstein, E., Masliah, E., Peterson, K.L., Stallcup, W.B., *et al.* (2017). Pericytes of Multiple Organs Do Not Behave as Mesenchymal Stem Cells In Vivo. Cell Stem Cell *20*, 345-359.e5.

184. Kramann, R., Schneider, R.K., Dirocco, D.P., Machado, F., Fleig, S., Bondzie, P.A., Henderson, J.M., Ebert, B.L., and Humphreys, B.D. (2015). Perivascular Gli1+ progenitors are key contributors to injury-induced organ fibrosis. Cell Stem Cell *16*, 51–66.

185. Stratman, A.N., Malotte, K.M., Mahan, R.D., Davis, M.J., and Davis, G.E. (2009). Pericyte recruitment during vasculogenic tube assembly

stimulates endothelial basement membrane matrix formation. Blood *114*, 5091–5101.

186. Stratman, A.N., Schwindt, A.E., Malotte, K.M., and Davis, G.E. (2010). Endothelial-derived PDGF-BB and HB-EGF coordinately regulate pericyte recruitment during vasculogenic tube assembly and stabilization. Blood *116*, 4720–4730.

187. Asada, N., Kunisaki, Y., Pierce, H., Wang, Z., Fernandez, N.F., Birbrair, A., Ma'ayan, A., and Frenette, P.S. (2017). Differential cytokine contributions of perivascular haematopoietic stem cell niches. Nat. Cell Biol. *19*, 214–223.

188. Ishikawa, T., Wondimu, Z., Oikawa, Y., Gentilcore, G., Kiessling, R., Egyhazi Brage, S., Hansson, J., and Patarroyo, M. (2014). Laminins 411 and 421 differentially promote tumor cell migration via alpha6beta1 integrin and MCAM (CD146). Matrix Biol. *38*, 69–83.

189. Sakry, D., and Trotter, J. (2016). The role of the NG2 proteoglycan in OPC and CNS network function. Brain Res. *1638*, 161–166.

190. Bigas, A., Robert-Moreno, A., and Espinosa, L. (2010). The Notch pathway in the developing hematopoietic system. Int. J. Dev. Biol. *54*, 1175–1188.

191. Omatsu, Y., Sugiyama, T., Kohara, H., Kondoh, G., Fujii, N., Kohno, K., and Nagasawa, T. (2010). The essential functions of adipo-osteogenic progenitors as the hematopoietic stem and progenitor cell niche. Immunity *33*, 387–399.

192. Diaz-flores, L., Gutiérrez, R., Madrid, J., Varela, H., Valladares, F., Acosta, E., and Martín-Vasallo, P. (2009). Pericytes. Morphofunction, interactions and pathology in a quiescent and activated mesenchymal cell niche. Histol. Histopathol. *24*, 909–969.

193. Armulik, A., Genové, G., and Betsholtz, C. (2011). Pericytes:

Developmental, Physiological, and Pathological Perspectives, Problems, and Promises. Dev. Cell *21*, 193–215.

194. Sims, D.E. (1986). The pericyte - a review. Tissue Cell *18*.

195. Sims, D.E. (2000). Diversity within pericytes. Clin. Exp. Pharmacol. Physiol. *27*, 842–846.

196. Nehls, V., and Drenckhahn, D. (1993). The versatility of microvascular pericytes: from mesenchyme to smooth muscle. Histochemistry *99*, 1–12.

197. Armulik, A., Abramsson, A., and Betsholtz, C. (2005). Endothelial/pericyte interactions. Circ. Res. *97*, 512–523.

198. Ando, K., Wang, W., Peng, D., Chiba, A., Lagendijk, A., Barske, L., Crump, J.G., Stainier, D.Y.R., Lendahl, U., Koltowska, K., *et al.* (2019). Peri-arterial specification of vascular mural cells from naïve mesenchyme requires Notch signaling. Development *146*.

199. Stenzel, D., Nye, E., Nisancioglu, M., Adams, R.H., Yamaguchi, Y., and Gerhardt, H. (2009). Peripheral mural cell recruitment requires cell-autonomous heparan sulfate. Blood *114*, 915–924.

200. Chen, J., Ellison, F.M., Keyvanfar, K., Omokaro, S.O., Desierto, M.J., Eckhaus, M.A., and Young, N.S. (2008). Enrichment of hematopoietic stem cells with SLAM and LSK markers for the detection of hematopoietic stem cell function in normal and Trp53 null mice. Exp. Hematol. *36*, 1236–1243.

201. Kaminski, W.E., Lindahl, P., Lin, N.L., Broudy, V.C., Crosby, J.R., Hellstrom, M., Swolin, B., Bowen-Pope, D.F., Martin, P.J., Ross, R., *et al.* (2001). Basis of hematopoietic defects in platelet-derived growth factor (PDGF)- B and PDGF beta-receptor null mice. Blood *97*, 1990–1998.

202. Siedlecki, J., Asani, B., Wertheimer, C., Hillenmayer, A., Ohlmann, A., Priglinger, C., Priglinger, S., Wolf, A., and Eibl-Lindner, K. (2018). Combined VEGF/PDGF inhibition using axitinib induces αSMA expression and a pro-fibrotic phenotype in human pericytes. Graefe's Arch. Clin. Exp. Ophthalmol. *256*, 1141–1149.

203. Porcheri, C., Golan, O., Calero-Nieto, F.J., Thambyrajah, R., Ruiz-Herguido, C., Wang, X., Catto, F., Guillen, Y., Sinha, R., González, J., *et al.* (2019). Notch ligand Dll4 impairs cell recruitment into aortic clusters and limits hematopoietic stem cells. bioRxiv, 2019.12.16.877407.

204. Stratman, A.N., and Davis, G.E. (2012). Endothelial cell-pericyte interactions stimulate basement membrane matrix assembly: influence on vascular tube remodeling, maturation, and stabilization. Microsc. Microanal. *18*, 68–80.

205. Ulvmar, M.H., Martinez-Corral, I., Stanczuk, L., and Mäkinen, T. (2016). Pdgfrb-Cre targets lymphatic endothelial cells of both venous and non-venous origins. Genesis *54*, 350–358.

206. Cuervo, H., Pereira, B., Nadeem, T., Lin, M., Lee, F., Kitajewski, J., and Lin, C.S. (2017). PDGFRβ-P2A-CreERT2 mice: a genetic tool to target pericytes in angiogenesis. Angiogenesis *20*, 655–662.

207. Zovein, A.C., Hofmann, J.J., Lynch, M., French, W.J., Turlo, K.A., Yang, Y., Becker, M.S., Zanetta, L., Dejana, E., Gasson, J.C., *et al.* (2008). Fate Tracing Reveals the Endothelial Origin of Hematopoietic Stem Cells. Cell Stem Cell *3*, 625–636.

208. Crisan, M., Kartalaei, P.S., Vink, C.S., Yamada-Inagawa, T., Bollerot, K., van IJcken, W., van der Linden, R., de Sousa Lopes, S.M.C., Monteiro, R., Mummery, C., *et al.* (2015). BMP signalling differentially regulates distinct haematopoietic stem cell types. Nat. Commun. *6*, 8040.

209. Lindahl, P., Johansson, B.R., Leveen, P., and Betsholtz, C. (1997).

Pericyte loss and microaneurysm formation in PDGF-B-deficient mice. Science *277*, 242–245.

210. Levéen, P., Pekny, M., Gebre-Medhin, S., Swolin, B., Larsson, E., and Betsholtz, C. (1994). Mice deficient for PDGF B show renal, cardiovascular, and hematological abnormalities. Genes Dev. *8*, 1875–1887.

211. Spangrude, G.J., Heimfeld, S., and Weissman, I.L. (1988). Purification and Characterization of Mouse Hematopoietic Stem Cells. Science (80-.). *241*, 58–62.

212. Kiel, M.J., Yilmaz, Ö.H., Iwashita, T., Yilmaz, O.H., Terhorst, C., and Morrison, S.J. (2005). SLAM family receptors distinguish hematopoietic stem and progenitor cells and reveal endothelial niches for stem cells. Cell *121*, 1109–1121.

213. Oguro, H., Ding, L., and Morrison, S.J. (2013). SLAM family markers resolve functionally distinct subpopulations of hematopoietic stem cells and multipotent progenitors. Cell Stem Cell *13*, 102–116.

214. Klinghoffer, R.A., Mueting-Nelsen, P.F., Faerman, A., Shani, M., and Soriano, P. (2001). The two PDGF receptors maintain conserved signaling in vivo despite divergent embryological functions. Mol. Cell *7*, 343–354.